NTNU – Trondheim
Norwegian University of
Science and Technology

Changes in Lipid Composition Induced by Environmental and Genetic Manipulation in *Synechocystis* sp. PCC 6803

Kristin Forfang

Biotechnology (5 year)
Submission date: June 2014
Supervisor: Martin Frank Hohmann-Marriott, IBT
Co-supervisor: Rahmi Lale, IBT

Norwegian University of Science and Technology
Department of Biotechnology

Abstract

The objective of this research was to investigate the photosynthetic lipids synthesized by the cyanobacterium *Synechocystis* sp. PCC 6803 and to develop methods to extract, separate and characterize them. A particular focus has been directed towards the function of isoprenoid quinones and specifically the biosynthesis of plastoquinone, an essential component in photosynthetic and respiratory electron transport chains of cyanobacteria. This pathway differs from that in plants and algae and candidate genes assumed to be involved in this unresolved pathway were identified through *in silico* analyses. The gene deletion strain Δ*sll1653* was constructed and characterized to assess whether *sll1653* is involved in plastoquinone synthesis or if a shift in the utilization of quinones can be initiated upon depletion of oxygen. The mutant strain had similar growth characteristics to the wild-type but failed to grow on glucose under high light. Spectroscopic and mass spectrometry analyses revealed accumulation of phycobilins and photoprotective carotenoids and tocopherols in the mutant strain. This strain was impaired in phylloquinone synthesis but a significant decrease in plastoquinone levels could not be observed. When the wild-type and mutant strain were subjected to limiting oxygen concentrations, both a state transition from PS II to PS I and an increase in F_0 could be observed. Still, anaerobic conditions did not induce the replacement of plastoquinone by phylloquinone in the PQ-pool. The results obtained in this study indicate that the *sll1653* gene, encoding a methyltransferase, is not directly involved in the biosynthesis of plastoquinone in *Synechocystis* sp. PCC 6803.

Sammendrag

Formålet med denne masteroppgaven var å utforske, samt utvikle metoder for ekstraksjon, separasjon og karakterisering av fotosyntetiske lipider i cyanobakterien *Synechocystis* sp. PCC 6803. Et spesielt fokus har vært rettet mot funksjonen av isoprenoid kinoner og syntesen av plastokinon, en essensiell komponent i fotosyntetisk- og respiratorisk elektrontransport hos cyanobakterier. Syntesesporet for plastokinon varierer fra det i planter og alger, og genkandidater som kan tenkes å være involvert ble identifisert gjennom bioinformatiske tilnærminger. Kandidaten *sll1653* ble genetisk slettet fra *Synechocystis* 6803 og den resulterende fenotypen ble karakterisert for å vurdere genets rolle i plastokinon-syntese og hvorvidt plastokinon kan erstattes av fyllokinon under anaerobe forhold. Den mutante stammen hadde like vekstkarakteristikker som villtypen, men kunne ikke vokse på glukose under store lysmengder. Spektroskopiske- og massespektrometriske teknikker avslørte akkumulering av fykobiliner og fotoprotektive karotenoider og tokoferoler i den mutante stammen. Denne stammen kunne ikke produsere fyllokinon, mens nivået av plastokinon var omtrent det samme som i villtypen. Når villtype og mutant stamme ble utsatt for begrensede oksygenforhold ble det observert en overgang av lys-høstende fykobilisomer fra fotosystem II til fotosystem I samt en økning i minimal fluorescens (F_0). Overgangen til anaerobe forhold induserte ikke erstatningen av plastokinon med fyllokinon i elektrontransportkjeden og resultatene indikerer også at *sll1653* genet, som koder for en metyltransferase, ikke er involvert i biosyntesen av plastokinon i *Synechocystis* sp. PCC 6803.

Acknowledgements

The completion of a Master Thesis demands for more than one person to be involved and I needed, as the Beatles so neatly describes it, “A Little Help from My Friends”. I would therefore like to thank the people who contributed to my work in any means.

I would like to thank my family who has, with their tremendous support and encouragement, motivated me to gain my education. Additionally, I owe a great thanks to Vegard for keeping out with me even on my grumpy days.

Thereafter, I would like to thank the staff at Institute of Biotechnology, fellow students and lab members of PhotoSynLab. Some have of course contributed more to this research than others. I would like to thank Kåre Kristiansen for all his help in the MS-lab and Thor Bernt Melø for interesting conversations and perspectives on spectroscopy. Also, I am forever grateful and owe a huge thank-you to Jake Lamb for all his help in the lab, without his contribution none of this would have been possible. And to my advisor, Associate Professor Martin Hohmann-Marriott, thank you for giving me this research opportunity. You taught me the most important aspects of being a researcher – dedication and curiosity.

Contents

ABSTRACT **I**

SAMMENDRAG **III**

ACKNOWLEDGEMENTS **V**

CONTENTS **VII**

LIST OF FIGURES **XIII**

LIST OF TABLES **XV**

ABBREVIATIONS **XVI**

CHAPTER 1: INTRODUCTION **1**

1. Photosynthesis and Respiration **1**

1.1. Oxygenic Photosynthesis 3

1.1.1. Light Harvesting 5

1.1.2. Electron Transport 6

1.2. Aerobic Respiration 9

1.3. Anaerobic Respiration 10

2. Photosynthetic Lipids **10**

2.1. Chlorophylls 11

2.2. Carotenoids 11

2.3. Isoprenoid Quinones 11

3. Biosynthesis of Quinones **12**

3.1. Biosynthesis of Quinones in Bacteria and Archaea 14

3.2. Biosynthesis of Quinones in Plants and Algae 17

3.3. Changes in Quinone Composition under Variable Environmental Conditions 18

4. *Synechocystis* sp. PCC 6803 as a Model System **19**

4.1. Intertwined Electron Transport Chains 20

5. Techniques Utilized for Phenotypic Characterization of *Synechocystis* 6803 21
5.1. SLIC Cloning 22
5.1.1. BioBricks™ as a Cloning Tool 23
5.2. Spectroscopic Techniques 24
5.2.1. *In Vivo* Absorption 24
5.2.2. 77K Fluorescence 25
5.2.3. Pulse Amplitude Modulation Fluorescence 27
5.3. Analysis of Photosynthetic Lipids 28
5.3.1. Thin-Layer Chromatography 29
5.3.2. Liquid Chromatography – Mass Spectrometry 29

6. Aims of Research 30

CHAPTER 2: MATERIALS AND METHODS 33

1. Bacterial Strains and Growth conditions 33
1.1. General Techniques 33
1.2. *Synechocystis* sp. PCC 6803 Strains 33
1.2.1. Growth and Maintenance 33

2. Optimization of Lipid Extraction, Separation and Characterization 36
2.1. Lipid Extraction 36
2.2. Separation by TLC 37
2.3. Characterization of Lipids by LC-MS 37

3. BioBrick Cloning and *Synechocystis* 6803 Mutagenesis 39
3.1. Polymerase Chain Reaction 39
3.1.1. Touchdown PCR 39
3.1.2. Primer Sequences 41
3.2. Restriction Cutting 42
3.3. Separation of DNA Fragments by Gel Electrophoresis 42
3.4. DNA Ligation 42
3.4.1. Restriction Based Cloning 43
3.4.2. Gibson Cloning 43
3.5. Making Competent *E. coli* cells 43
3.6. Heat-Shock Transformation of Competent *E. coli* cells 44
3.7. Small-Scale Plasmid Isolation 45
3.8. Transformation of *Synechocystis* 6803 45

4. Phenotypic Characterizations 46
4.1. Growth Curve 46
4.1.1. Plate-Imager 47
4.1.2. Calculation of Cell Density Values 47
4.2. Oxygen Evolution 48
4.3. Respiration Rate 49
4.4. Absorption and Fluorescence Spectroscopy 49
4.4.1. Chlorophyll Concentration 50
4.4.2. *In Vivo* Absorption 50
4.4.3. 77 K Fluorescence 50
4.4.4. PAM Fluorescence 51
4.5. Lipid Analysis 51

CHAPTER 3: RESULTS 53

1. Introduction 53

2. Optimization of Lipid Extraction, Separation and Characterization 54
2.1. Extraction of Photosynthetic Lipids 54
2.2. Separation by TLC 58
2.3. Characterization by LC-MS 60

3. *In Silico* Analysis of Cyanobacterial Plastoquinone Synthesis 62
3.1. Identification of Candidate Genes in *Synechocystis* 6803 62
3.2. Identification of Homologs in Other Cyanobacterial Species 64

4. Production of a Novel BioBrick 66

5. Generation of the *Synechocystis* Δ*sll1653* Strain 69

6. Phenotypic Characterization of the Δ*sll1653* Mutant 72
6.1. Growth Curves 72
6.2. Oxygen Evolution 75
6.3. Respiration Rates 77
6.4. Pigment Composition 78
6.5. Photosystems and Light-Harvesting Antennas 80
6.6. Photosynthetic Lipid Composition 82
6.6.1. Chlorophylls 83

6.6.2. Carotenoids 84
6.6.3. Isoprenoid quinones 84

7. Transition from Aerobic to Anaerobic Conditions 88
7.1. State 1 – State 2 Transition 88
7.2. Functioning of the Electron Transport Chain 90
7.3. Quinone Composition 95

CHAPTER 4: DISCUSSION 97

1. Introduction 97

2. Analysis of Photosynthetic Lipids in *Synechocystis* 6803 98
2.1. Development of Methods for Photosynthetic Lipid Analysis 98
2.1.1. Extraction of Photosynthetic Lipids 98
2.1.2. Separation by TLC 99
2.1.3. Characterization by LC-MS 100
2.2. Analysis of Lipids Extracted from *Synechocystis* 6803 101

3. BioBrick Cloning 103

4. Biosynthetic Pathway of Plastoquinone in Cyanobacteria 104
4.1. Candidate Genes 104
4.1.1. Decarboxylases 104
4.1.2. Hydroxylases 105
4.1.3. Methyltransferases 105
4.2. The Δ*sll1653* Deletion Strain 106
4.2.1. The Strain Does Not Grow on Glucose under High Light Conditions 106
4.2.2. Decreased Respiratory Capacity 107
4.2.3. The Strain is More Protected against Photoinhibition 108
4.2.4. Methylation of PQ is Not Solely Dependent on the *sll1653* Gene 109

5. Effects of Oxygen Depletion in *Synechocystis* 6803 109
5.1. Glucose Oxidase Affects State Transition from PS II to PS I 110
5.2. Depletion of Oxygen Causes an Increase in F_0 110
5.2.1. Q_A^- Can Still Be Rescued in the Presence of DBMIB 111
5.3. PQ is Not Replaced by PhQ under Anaerobic Conditions 112

CHAPTER 5: CONCLUSIONS 113

FUTURE RESEARCH **115**

REFERENCES **117**

APPENDIX **125**

1. Photosynthetic Lipids in *Synechocystis* 6803 **127**

2. Identification of Genes Involved in Plastoquinone Synthesis in Cyanobacteria **141**

3. Lipid Analysis **147**

List of Figures

Figure 1.1 – Photosynthesis and Respiration 2
Figure 1.2 – Overview of Oxygenic Photosynthesis 4
Figure 1.3 – Z-scheme of Oxygenic Photosynthesis 7
Figure 1.4 – Electron Transport in Aerobic Respiration 9
Figure 1.5 – Redox Reactions of the Quinone Ring 12
Figure 1.6 – Quinone Structures 13
Figure 1.7 – Biosynthesis of Menaquinone 15
Figure 1.8 – Ubiquinone Biosynthesis 16
Figure 1.9 – Biosynthesis of Plastoquinone in Plants and Algae 17
Figure 1.10 – Intertwined Electron Transport Chains in Cyanobacteria 21
Figure 1.11 – SLIC Cloning 22
Figure 1.12 – BioBricks ™ 23
Figure 1.13 – Absorption Spectra of Cyanobacterial Pigments and Whole Cells 24
Figure 1.14 – 77K Fluorescence Emission Spectra 26
Figure 1.15 – PAM Fluorescence Traces upon Depletion of Oxygen 28

Figure 2.1 – Culture Flask 34
Figure 2.2 – Agar Plate for Generation of Growth Curve 46
Figure 2.3 – Plate-Imager 47

Figure 3.1 – Lipid Extracts and Pellets 55
Figure 3.2 – Absorption Spectra of Lipid Extracts 56
Figure 3.3 – Comparison between Extraction Solvent Systems 57
Figure 3.4 – TLC Separation of Extracts by Hexane-Acetone 58
Figure 3.5 – Thin-layer Chromatogram for Plastoquinone 60
Figure 3.6 – Hypothesized Pathway for Plastoquinone Synthesis in Cyanobacteria 63
Figure 3.7 – BioBrick Plasmids 67
Figure 3.8 – *E. coli* Transformed with the Constructed BioBrick Plasmid 68
Figure 3.9 – BioBrick Digest 68
Figure 3.10 – PCR Amplification of Fragments for Construction of *sll1653*-Deletion Construct 69
Figure 3.11 – *sll1653*-Deletion Plasmid 70
Figure 3.12 – Construction of Δ*sll1653* Strain 71

Figure 3.13 – Growth Curves 74
Figure 3.14 – Oxygen Evolution 76
Figure 3.15 – Photosynthetic Efficiency and Oxygen Evolution Rates at Different Light Intensities 77
Figure 3.16 – Oxygen Consumption 78
Figure 3.17 – *In Vivo* Absorption Spectra 79
Figure 3.18 – 77 K Fluorescence Emission Spectra of Wild-Type and Δ*sll1653* Mutant Strain 81
Figure 3.19 – Chlorophylls in the Wild-Type. 83
Figure 3.20 – Chromatogram for Oxidized and Reduced Plastoquinone 85
Figure 3.21 – Chromatogram for Identification of Phylloquinone 86
Figure 3.22 – Relative Abundance of Phylloquinone in the Mutant and Wild-Type 87
Figure 3.23 – State Transition Induced by Depletion of Oxygen 89
Figure 3.24 – PAM Fluorescence Traces upon Oxygen Depletion 92
Figure 3.25 – Single Peak PAM Fluorescence Traces 93
Figure 3.26 – PAM Fluorescence Traces upon Depletion of Oxygen and Treatment with DBMIB 94
Figure 3.27 – Relative Abundance of Quinones under Aerobic and Anaerobic conditions 96

List of Tables

Table 2.1 – BG11 Medium Stock Solutions 35
Table 2.2 – Additions for BG11 Medium 35
Table 2.3 – 50 µL Reaction for PCR using Phusion HF DNA Polymerase 40
Table 2.4 – Thermocycler Conditions for Touchdown PCR using Phusion Polymerase 40
Table 2.5 – Reagents for Making Competent *E. coli* DH5α Cells 44
Table 2.6 – Medium and Antibiotic Additions for *E. coli* Growth 45
Table 2.7 – Light Curve Conditions for Measuring Oxygen Evolution 49
Table 3.1 – Pigments Separated by TLC using Hexane-Acetone as Development System 59
Table 3.2 – Retention Times and Masses of Standards Detected by UPLC-APCI/ESI-qTOF-MS 61
Table 3.3 – Doubling times for Wild-type and Δ*sll1653* 75
Table 3.4 – Respiration Rates 77
Table 3.5 – Relative Ratios of Carotenoids and Phycobiliproteins to Chlorophyll *a* Determined by *In Vivo* Absorption Spectroscopy 80
Table 3.6 – Photosynthetic Lipids Detected by UPLC-qTOF-MS 82

Abbreviations

A_0	Primary electron acceptor of PS I
A_1	Phylloquinone molecule
APC	Allophycocyanin
APCI	Atmospheric-pressure chemical ionization
ATP	Adenosine triphosphate
BHT	Butylated hydroxytoluene
BLAST	Basic local alignment search tool
BPI	Base peak intensity
$CHCl_3$	Chloroform
Chl	Chlorophyll
Chl *a*	Chlorophyll *a*
Cyt b_6f	Cytochrome b_6f complex
Cyt c_6	Cytochrom c_6 complex
DAD	Diode array detector
DBMIB	2,5-dibromo-3-methyl-6-isopropyl-*p*-benzoquinone
DCM	Dichloromethane
DCMU	3-(3,4-dichlorophenyl)-1,1-dimethylurea
DHNA	1,4-dihydroxy-2-naphthoate
DMK	Demethyl-menaquinone
DXP	1-deoxy-D-xylulose-5-phosphate
ESI	Electrospray ionization
ETC	Electron transport chain
F_0	Minimal fluorescence
Fd	Ferredoxin
F_M	Maximal fluorescence
GT	Glucose-tolerant
HGA	Homogenisate
HL	High light
HPLC	High performance liquid chromatography
HPPD	4-hydroxyphenylpyruvate dioxygenase
IPA	Isopropanol
KEGG	Kyoto Encyclopedia of genes and genomes
LC	Liquid chromatography
LC-MS	Liquid chromatography-mass spectrometry
m/z	Mass-to-charge ratio
MeOH	Methanol
MK	Menaquinone
MS	Mass spectrometry
MVA	Mevalonate
NADPH	Nicotinamide adenine dinucleotide phosphate

NDH	NAD(P)H dehydrogenase
NL	Normal light
PAM	Pulse amplitude modulation
PAR	Photosynthetically active radiation
PBP	Phycobiliproteins
PC	Plastocyanin
PHB	4-hydroxybenzoate
PHC	Phycocyanin
Pheo	Pheophytin
PhQ	Phylloquinone
PQ	Plastoquinone
PQH_2	Plastoquinol
PRT	Prenyltransferase
PS I	Photosystem I
PS II	Photosystem II
Q	Quadrupole
Q_A	First plastoquinone electron acceptor of PS II
Q_B	Second electron acceptor of PS II
ROS	Reactive oxygen species
SLIC	Sequence and ligation independent cloning
THF	Tetrahydrofuran
TLC	Thin-layer chromatography
TOF	Time-of-flight
UPLC	Ultra-performance liquid chromatography
UQ	Ubiquinone

Chapter 1: Introduction

1. Photosynthesis and Respiration

Photosynthesis is arguably the most fundamental biological process on Earth. Photosynthesis produces oxygen and consumes carbon dioxide, fulfills our food requirements either directly or indirectly and provides a basis for both wood and fossil fuel reserves. Life as we know it ultimately depends upon this process. Scientific research into photosynthesis becomes an important topic as the current challenges of increased demand for food, fuels, and a healthier atmosphere, become more apparent. Gaining a thorough understanding of photosynthesis can improve crop yields of food, fuel, wood and fiber, and can also be used to design adapted systems which provide more efficient ways to harvest and utilize solar energy.

Photosynthesis and respiration are processes that provide energy equivalents to supply the energy requirements of an organism. In these processes, electron donors transfer their electrons to electron acceptors through different components in what is known as the electron transport chain (ETC). During photosynthesis, two water molecules can be split into four H^+ atoms and an O_2 molecule, liberating four electrons. This reaction is driven by light energy and thus is known as the light reaction. Ultimately, electron transport leads to the reduction of CO_2 to produce organic molecules for cellular storage, a process that does not require light, known as the dark reaction. These energy-rich compounds can in turn used as the energy source for growth and reproduction through the process of respiration. Oxidation of the organic molecules recombines electrons with O_2 and protons, generating water molecules and energy equivalents (Fig. 1.1) - making respiration essentially the reverse reaction of photosynthesis (Nelson and Cox, 2008).

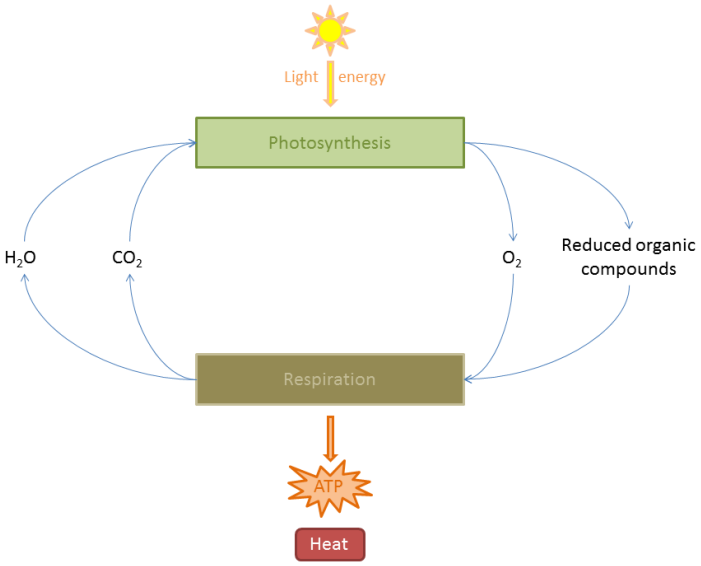

Figure 1.1 – Photosynthesis and Respiration. Photosynthetic organisms use light energy to fix CO_2 for production of reduced organic compounds and release O_2 as a byproduct. This organic matter can be broken down by photosynthetic or other organisms as food for energy release in the process of respiration.

A wide range of organisms are able to perform photosynthesis. Some derive all their cellular energy from light (autotrophs), whereas others only use light as part of their energy source (mixotrophs). Many organisms including plants, algae, cyanobacteria and certain other species of bacteria transform and store solar energy using photosynthetic machinery, although the molecular mechanisms for doing so differ between species. Most of these organisms possess separate compartments for photosynthetic and respiratory machinery; however, cyanobacteria are among the very few groups that perform photosynthesis and respiration using the same compartment. To this extent, cyanobacterial ETCs do in fact intersect, utilizing some of the same components (Vermaas, 2001), although the reason for such arrangement remains unclear.

1.1. Oxygenic Photosynthesis

During the course of evolution, two types of photosynthetic organisms have evolved, displaying variations in the nature of the electron donor utilized to produce reduced organic compounds. Anoxygenic photosynthetic organisms take advantage of other electron donors than water, resulting in a lack of oxygen evolution. Organisms that are able to perform this type of photosynthesis belong to clades such as Purple bacteria, Green sulfur bacteria, Green non-sulfur bacteria and Heliobacteria. In contrast, oxygenic photosynthesis is performed by cyanobacteria, algae and higher plants. These organisms use water as the electron donor and light as the source of energy, culminating in the evolution of oxygen as a byproduct. The net process of photosynthesis can be expressed as:

$$6\ CO_2 + 6\ H_2O + \text{light energy} \rightarrow C_6H_{12}O_6 + 6\ O_2$$

The reactions of oxygenic photosynthesis take place in protein complexes embedded in a membrane referred to as the thylakoid membrane (Fig 1.2). In cyanobacteria these membranes are located in the bacterial cytosol whereas in photosynthetic eukaryotes they are arranged within intracellular compartments called chloroplasts. Chloroplasts are believed to have evolved from an ancient cyanobacteria engulfed through endosymbiosis, indicated by the existence of DNA and bacteria-like ribosomes within this organelle (Weeden, 1981).

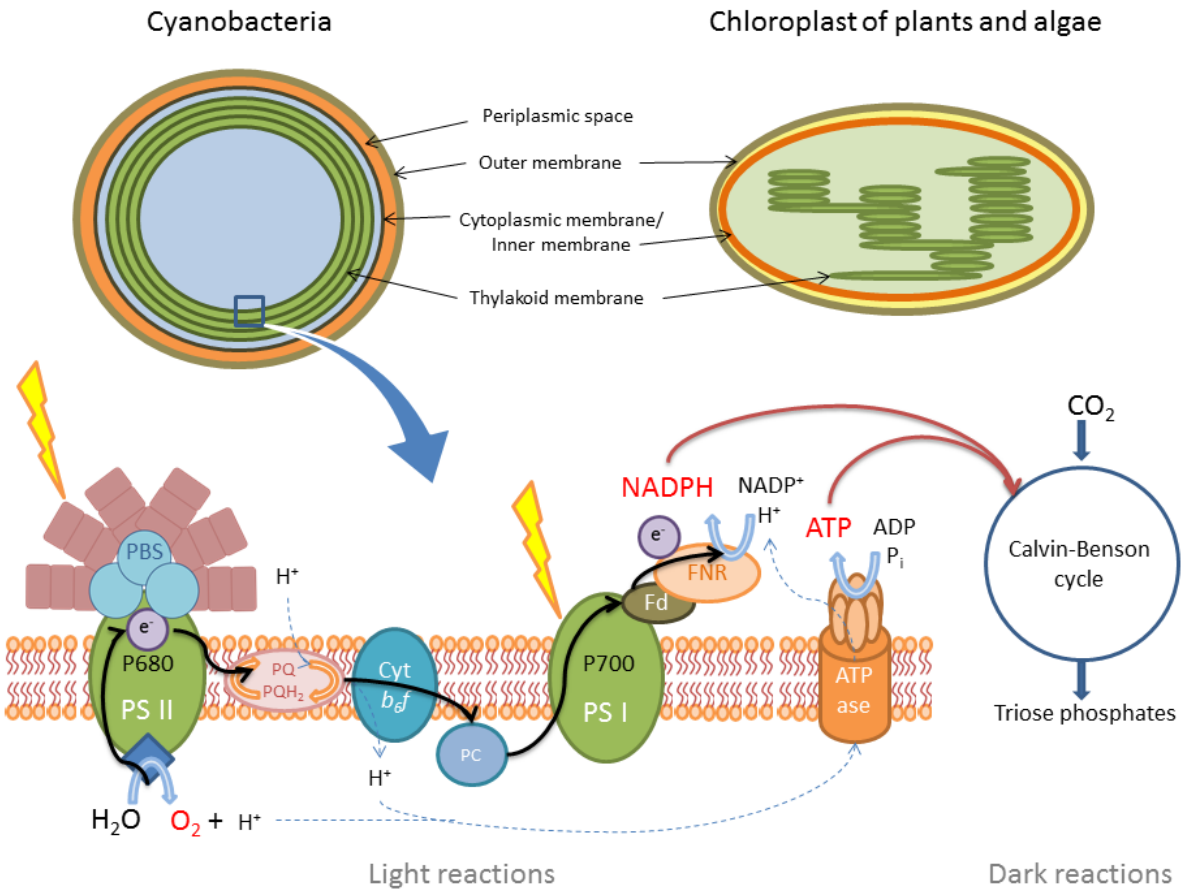

Figure 1.2 – Overview of Oxygenic Photosynthesis. Oxygenic photosynthesis takes place in the thylakoid membranes located in chloroplasts of plants and algae and in the cytosol of cyanobacteria. Electrons generated from the splitting of water in PS II are transferred through a chain of electron transport, eventually reaching $NADP^+$ (solid line). During electron transport, protons translocate across the membrane to generate an electrochemical gradient for synthesis of ATP (dotted line). NADPH and ATP are used for fixation of CO_2 in the Calvin-Benson cycle. Abbreviations: PBS, the light harvesting complex in cyanobacteria called phycobilisome; PS II, photosystem II; PQ, the lipid-soluble electron carrier plastoquinone; Cyt b_6f, the cytochrome b_6f complex; PC, the water-soluble electron carrier plastocyanin; PS I, photosystem I; Fd, ferredoxin; FNR, ferredoxin:$NADP^+$ oxidoreductase; NADPH, nicotinamide adenine dinucleotide phosphate; ATP, adenosine triphosphate.

Oxygenic photosynthesis is a series of redox-coupled reactions resulting in the production of chemical energy and reducing power in the form of adenosine triphosphate (ATP) and nicotinamide adenine dinucleotide phosphate (NADPH), respectively. NADPH is produced by the reduction of $NADP^+$ using electrons originating from the splitting of water molecules. Electrons flow through two distinct, but interconnected, protein complexes in the thylakoid membrane called photosystem II (PS II) and photosystem I (PS I), eventually reaching $NADP^+$. Generation of an electrochemical membrane potential drives the synthesis of ATP. Both ATP and NADPH are utilized to power the reduction of CO_2 into organic compounds. One can divide photosynthesis into two main reactions: the light reaction and the dark reaction. The light reaction comprises the absorption of light energy (light harvesting) and the conservation of this energy as ATP and NADPH (electron transport). Although the nomenclature is somewhat misleading, the dark reactions are indirectly driven by light, fixing CO_2 into simple carbohydrates through the Calvin-Benson cycle (Calvin and Benson, 1948).

1.1.1. Light Harvesting

The input of light energy is required to drive the oxidation of water, a very poor electron donor with a redox potential of +0.8 V. To be able to harvest light energy, photosynthetic organisms synthesize different pigments which can absorb a quantum of light (a photon) causing an excited state that can be transferred to neighboring pigment molecules. This transferred excitation energy is known as the exciton. The initial pigment then returns back to its ground state ready to absorb another photon. This type of energy transfer is referred to as Förster resonance energy transfer (Förster, 1965). There are three main groups of light harvesting pigments utilized by photosynthetic organisms: chlorophylls, carotenoids and phycobilins. The photosynthetic pigments and proteins are arranged in a three-dimensional fashion in light-gathering antenna systems.

In cyanobacteria, chlorophylls, carotenoids and phycobilins participate in light capture and charge separation. The main light-harvesting antenna consists of phycobiliproteins and is known as phycobilisomes. Chlorophylls and carotenoids also function as antennas, collecting light and delivering it to the special pair of chlorophyll *a* molecules in the reaction center of PS I or PS II, where charge separation takes place. This reaction is known as the photochemical reaction of photosynthesis. The transition of light harvesting into electron

transport occurs when the special pair of chlorophylls absorbs an exciton and donated an electron to an electron carrier.

1.1.2. Electron Transport

Both photosystems contain a special pair of chlorophylls, although they are slightly different from each other. Upon excitation of the reaction center in PS I, a bleaching occurs at 700 nm in the absorbance difference spectra (Witt *et al.*, 1963; Döring *et al.*, 1968). The primary donor of PS I was therefore named P700. Similarly, the primary donor of the PS II reaction center obtained the label P680 (Döring *et al.*, 1967; Döring *et al.*, 1969). In the pathway of electron transfer from water to $NADP^+$, electrons are carried from P680 in PS II via the cytochrome b_6f complex and the soluble protein plastocyanin to P700 of PS I (Fig 1.2).

The electron transport in oxygenic photosynthesis is often displayed in a Z-scheme, as originally proposed by Hill and Bendall (1960). The standard reduction potential of the various electron carriers are plotted vertically, displaying thermodynamically favorable reactions downhill on the diagram (Fig. 1.3). In accordance with this scheme, the absorption of eight photons is generally accepted as the minimum photon requirement per molecule of O_2 evolved during photosynthesis; however, a number of determinations are not in agreement with this general conclusion (Osborne and Geider, 1987).

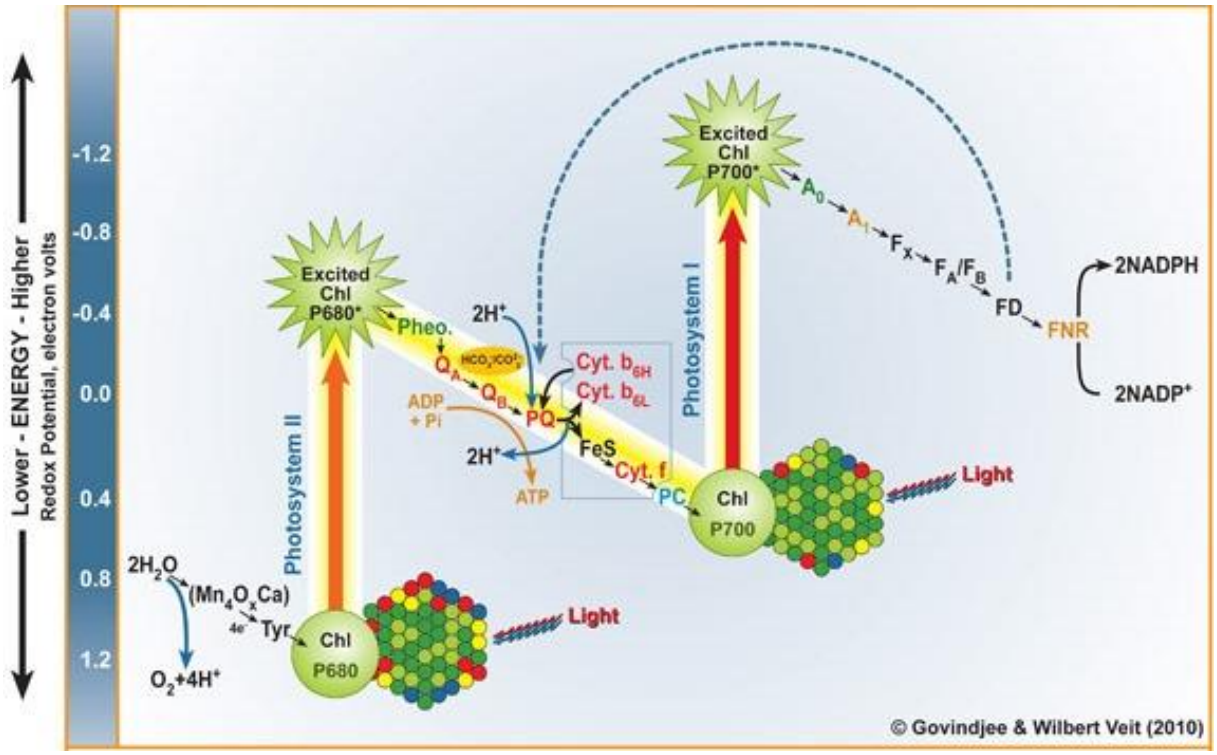

Figure 1.3 – Z-scheme of Oxygenic Photosynthesis. Electrons are transferred from H_2O to $NADP^+$ via the following components (from left to right): Mn_4O_xCa, the manganese cluster which participates in the splitting of water molecules; Tyr, redox-active tyrosine molecule in the D1 protein; Chl P680, primary electron donor of PS II; Pheo, pheophytin – primary electron acceptor of PS II; Q_A, first plastoquinone electron acceptor of PS II; Q_B, second plastoquinone electron acceptor of PS II; PQ, plastoquinone pool; FeS, the Rieske iron-sulfur protein of the cytochrome b_6f complex; Cyt *f*, cytochrome *f* of Cyt b_6f complex; Cyt b_6H/Cyt b_6L, cytochrome b_6 molecules of Cyt b_6f; PC, plastocyanin; Chl P700, primary electron donor of PS I; A_0, a special Chl molecule that is the primary electron acceptor of PS I; A_1, a phylloquinone molecule; F_X, F_A and F_B, separate immobile iron-sulfur protein centers; FD, ferredoxin; FNR, the enzyme ferredoxin-NADP-oxidoreductase. From Govindjee and Veit (2010).

Upon absorption of an exciton in PS II, the redox potential of the special chlorophylls is shifted, converting the pair into a strong electron donor, assigned P680*. Within picoseconds, one electron is donated to its immediate electron acceptor – pheophytin. The loss of an electron transforms P680* into a radical cation, assigned $P680^{+}$. The removed electron is replaced with an electron obtained from the oxidation of water, carried out at the oxygen-evolving complex embedded in PS II. The reduced pheophytin ($Pheo^{-}$) rapidly passes the extra electron to a protein-bound plastoquinone (Q_A), which in turn passes the electron to a more loosely bound plastoquinone (Q_B). Q_A can only pass on one electron at a time and as soon as Q_B has acquired two electrons, Q_B^{2-} picks up two protons (H^{+}) from the cytosol forming PQH_2 (plastoquinol). The reduced plastoquinol contains hydroxyl groups which make the molecule more polar, enabling the detachment from PS II and the diffusion through the polar, interphase region of the membrane (Nowicka and Kruk, 2010). Plastoquinol docks to the cytochrome *b_6f* complex (Cyt *b_6f*) where the electrons are passed on to a water-soluble electron carrier called plastocyanin (PC), at the same time producing the proton gradient essential for synthesis of ATP.

As in PS II, the excitation of the reaction center in PS I, P700, produces a radical cation ($P700^{+}$) upon donation of an electron to its immediate electron acceptor, A_0. This electron acceptor is believed to be a special form of chlorophyll which passes its electron through a chain of electron carriers, eventually reaching $NADP^{+}$. $P700^{+}$ quickly acquires an electron from plastocyanin, a soluble electron carrying protein that connects PS II and PS I. A_0^{-} is a strong reducing agent that passes an electron on to phylloquinone (A_1). From phylloquinone, the electron is transferred to an iron-sulfur protein via three iron-sulfur clusters in PS I. Ferredoxin (Fd), another iron-sulfur protein, then accepts the electron and is further oxidized by ferredoxin:$NADP^{+}$ oxidoreductase. This flavoprotein transfers electrons from reduced ferredoxin to $NADP^{+}$, producing NADPH that can then be used as reducing power in the dark reactions.

1.2. Aerobic Respiration

Aerobic respiration is the cellular process that generates energy by the full oxidation of nutrients, using oxygen as the final electron acceptor. Electrons from NADH (and related energy equivalents) produced during oxidation of carbohydrates, are transferred through membrane-bound protein complexes in an ETC, finally reaching O_2 (Fig. 1.4). The free energy released during electron transport is utilized to actively drive proton translocation across the membrane, generating an electrochemical gradient for synthesis of ATP from ADP and P_i via ATP-synthase.

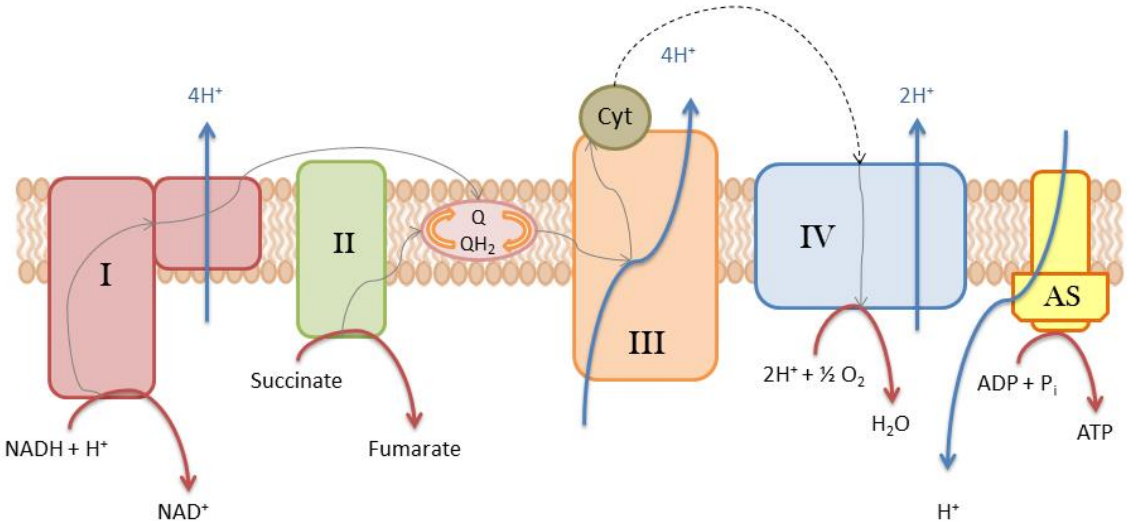

Figure 1.4 – Electron Transport in Aerobic Respiration. Electrons from reduced energy equivalents generated from the degradation of organic molecules are transferred through four protein complexes, eventually reaching O_2. Free energy released during electron transport is utilized to drive the synthesis of ATP by ATP-synthase (AS). Complex I catalyzes electron transfer to the quinone (Q) pool from NADH, whereas Complex II transfers electrons to the Q-pool from succinate. Complex III in bacteria and mitochondria, which is equivalent to the cytochrome b_6f complex in cyanobacteria and chloroplasts, catalyzes electron transfer from the Q-pool to a cytochrome. Complex IV completes the ETC by driving the reduction of O_2 into H_2O.

The electron carriers of the respiratory chain are organized into membrane-embedded supramolecular complexes. Complex I and II catalyze electron transfer to a quinone in the membrane from two different electron donors; NADH and succinate, respectively. Complex III, (cytochrome *bc1* complex) within many bacteria and all mitochondria or the cytochrome b_6f complex in cyanobacteria, carries electrons from the reduced quinol to a cytochrome, another mobile connecting link. The sequence is completed by Complex IV (a terminal oxidase) which transfers electrons from the cytochrome to O_2. Electron flow through Complexes I, III and IV is accompanied by proton translocation across the membrane. Although the general pathway of electron transfer is similar in virtually all organisms, the utilization of related quinones, cytochromes, flavoproteins and iron-sulfur proteins is highly variable between species.

1.3. Anaerobic Respiration

Anaerobic respiration is an important means for an organism to generate energy in the absence of oxygen. A respiratory electron chain is still used, but instead of oxygen, other less-oxidizing substances are used as terminal electron acceptors. Alternative electron acceptors can be nitrate (NO_3^-), sulfate (SO_4^{2-}), sulfur (S_0) or fumarate. When oxygen becomes depleted, the respiratory system can no longer shuttle electrons into H_2O, and as a result, electrons accumulate within the cell. To maintain electron homeostasis, electrons need to be donated to exogenous electron acceptors in order for the ETC to function and uphold the electrochemical gradient for ATP synthesis.

2. Photosynthetic Lipids

The structure of secondary metabolites from microorganisms provides a useful tool for characterization and chemotaxonomic classification. Several microorganisms synthesize pigments and lipids as secondary metabolites, in which the composition of these compounds within the organism varies between species and environmental conditions they grow in. Photosynthetic organisms synthesize a range of lipids that function in light harvesting, photoprotection and electron transport. Chlorophylls, carotenoids and phycobilins are the

major groups of pigments involved in light harvesting. In addition, carotenoids also function in photoprotection, a mechanism which prevents the formation of excess reactive oxygen species (ROS) under high light conditions. Both photosynthetic and other living organisms synthesize isoprenoid quinones, lipids involved in electron transport.

2.1. Chlorophylls

The major pigments utilized by the reaction centers are chlorophylls (Chls) - porphyrin-based pigments with a polycyclic, planar structure resembling the protoporphyrin of hemoglobin (Blankenship, 2002). In contrast to the heme group, a magnesium atom occupies the center of the porphyrin ring of chlorophylls instead of an iron. Also, a long-chained alcohol is attached to the porphyrin ring and several specific substitutions can be made to form chlorophyll derivatives.

2.2. Carotenoids

Carotenoids are extended molecules with alternating single and double bonds providing a delocalized system of π-electrons (Lohr, 2011). These include pure hydrocarbons and oxygenated structures, and the structural diversity within this group is fairly large. Ring structures are usually found at each end in carotenoids originating from oxygenic organisms, and the majority of carotenoids also contain oxygen atoms as part of hydroxyl or epoxide groups (Blankenship, 2002).

2.3. Isoprenoid Quinones

Quinones constitute a class of oxidized organic structures derived from aromatic compounds by introducing an even number of carbonyl groups. The quinone ring structure can undergo a two-step reversible reduction forming a quinol, a feature that enables quinones to function as electron and proton carriers (Fig. 1.5). Isoprenoid quinones are one of the most important groups of compounds occurring in membranes of living organisms. These redox-active lipids

are composed of a hydrophilic head group (the quinone ring) and an apolar isoprenoid side chain, which anchors them in membrane lipid bilayers.

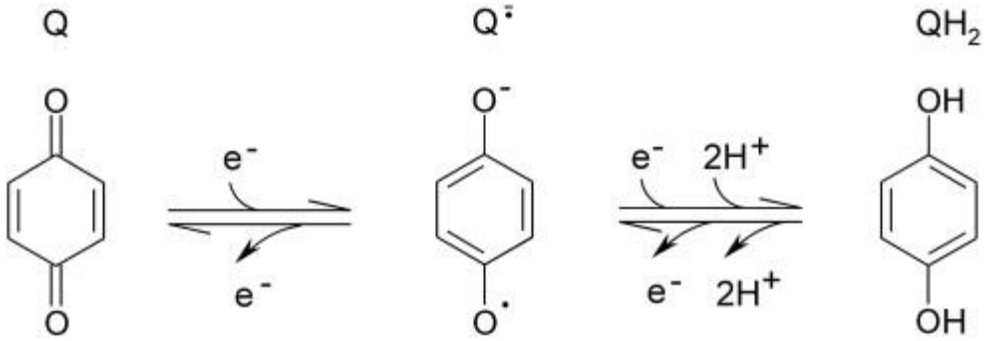

Figure 1.5 – Redox Reactions of the Quinone Ring. Electron and proton transfer reactions of the quinone molecule. Abbreviations: Q, oxidized form; $Q^{\cdot -}$, charged, semiquinone radical; QH_2, non-charged hydroquinone. From Nowicka and Kruk (2010).

The ability of reversible reduction and the lipid-soluble character of isoprenoid quinones make them ideal candidates for electron transport-mediated hydrogen shuttling across biological membranes (Nowicka and Kruk, 2010). Quinones function in ETCs as mobile hydrogen and electron carriers associated with membranes or as electron carriers within protein complexes. Compared to other redox components in electron transfer systems, quinones are usually present in a several-fold excess (Nohl, 1986). This creates a pool of oxidized quinones and reduced quinols in the hydrophobic phase of the membrane, which functionally links quinone reductases (such as reaction centers) with quinol oxidases (e.g. Cyt b_6f complex). The redox state of the quinone molecule varies with electron flux to or from the quinone pool, which is equally accessible to reductases and oxidases (Ian Ragan and Cottingham, 1985).

3. Biosynthesis of Quinones

The majority of naturally occurring quinones are divided into two groups based on the chemical nature of the polar head group – naphthoquinones and benzoquinones. Plastoquinone (the bound cofactor of PS II in plants, algae and cyanobacteria) and ubiquinone (the cofactor in the aerobic respiratory ETC of eukaryotes and some bacteria), both represent

benzoquinones. Phylloquinone, present in PS I of oxygenic phototrophs, and menaquinone (which functions in respiratory and photosynthetic ETCs of bacteria), are classified as naphthoquinones. The chemical structures of these quinones are displayed in Figure 1.6.

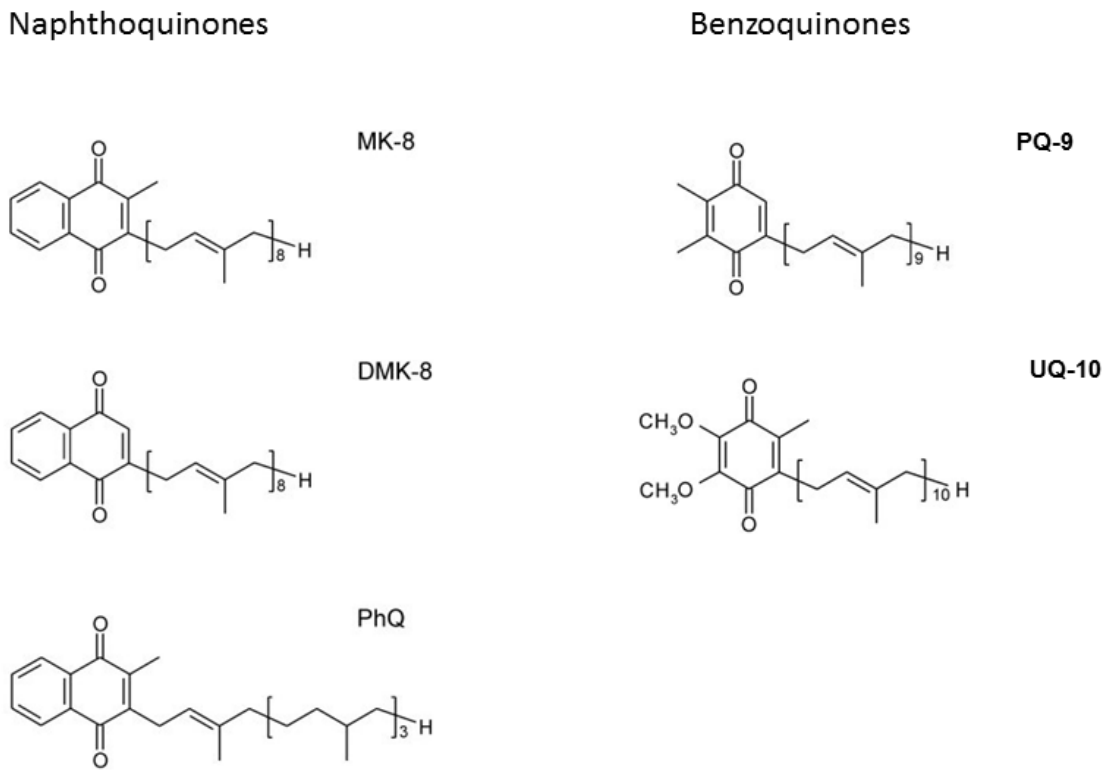

Figure 1.6 – Quinone Structures. Chemical structures of common isoprenoid naphthoquinones and benzoquinones in electron transport chains. Both the isoprenoid chain length and degree of saturation can be highly variable between different taxonomic groups of organisms. Numbers represents isoprenoid units present in the side chain. Abbreviations: MK-8, menaquinone-8; DMK-8, dimethyl-menaquinone-8; PhQ, phylloquinone; PQ-9, plastoquinone-9; UQ-10, ubiquinone-10.

During biosynthesis of quinones, the head group precursor and the isoprenoid side chain are synthesized separately before the precursors are condensed together. This condensation reaction is catalyzed by an enzyme belonging to the prenyltransferase (PRT) family (Nowicka and Kruk, 2010). The aromatic ring of the hydrophilic head group undergoes several modifications after the condensation reaction to produce the quinone of interest.

To synthesize the isoprenoid side chain of quinones, two primary precursors are utilized: dimetylallyl diphosphate and isopentenyl diphosphate. Archaea take advantage of the mevalonate (MVA) pathway, whereas most bacteria utilize the 1-deoxy-D-xylulose-5-

phosphate (DXP) pathway to synthesize these precursors (Lange *et al.*, 2000). Higher plants utilize the DXP pathway for synthesis of the prenyl chains of phylloquinone, plastoquinone and tocopherolquinone, whereas the MVA pathway provides these precursors for ubiquinone synthesis (Lichtenthaler, 1999; Szkopińska, 2000). A series of condensation reactions carried out by a specific prenyl diphosphate synthase take place to generate the isoprenoid side chain from the precursors, where the isoprenoid chain length varies with the specific enzyme used.

3.1. Biosynthesis of Quinones in Bacteria and Archaea

As mentioned above, the majority of bacteria and archaea synthesize menaquinone (MK) and ubiquinone (UQ), where menaquinone functions in anaerobic and ubiquinone is utilized in aerobic respiratory electron chains, respectively. The precursor for the MK head group in bacteria and archaea is 1,4-dihydroxy-2-naphthoate (DHNA), which is derived from chorismate produced via the shikimate pathway (Bentley and Meganathan, 1982). Two known pathways for synthesis of DHNA exist, but the condensation reaction that links the head group to the isoprenoid side chain is carried out by DHNA prenyltransferase in both pathways. After condensation, the naphthoate group is methylated to yield menaquinone (Fig. 1.7)

The precursor for the head group of UQ is 4-hydroxybenzoate (PHB), which can be formed from chorismate via the shikimate pathway (Meganathan, 2001). PHB prenyltransferase catalyzes condensation of PHB with the prenyl side chain. This enzyme shows a broad specificity for the polyprenyl side chain, leaving the determination of the chain length to the specific prenyl diphosphate synthase (Clarke, 2000). After the condensation reaction, the benzoate head group undergoes decarboxylation, hydroxylations and methylations to produce ubiquinone (Fig. 1.8).

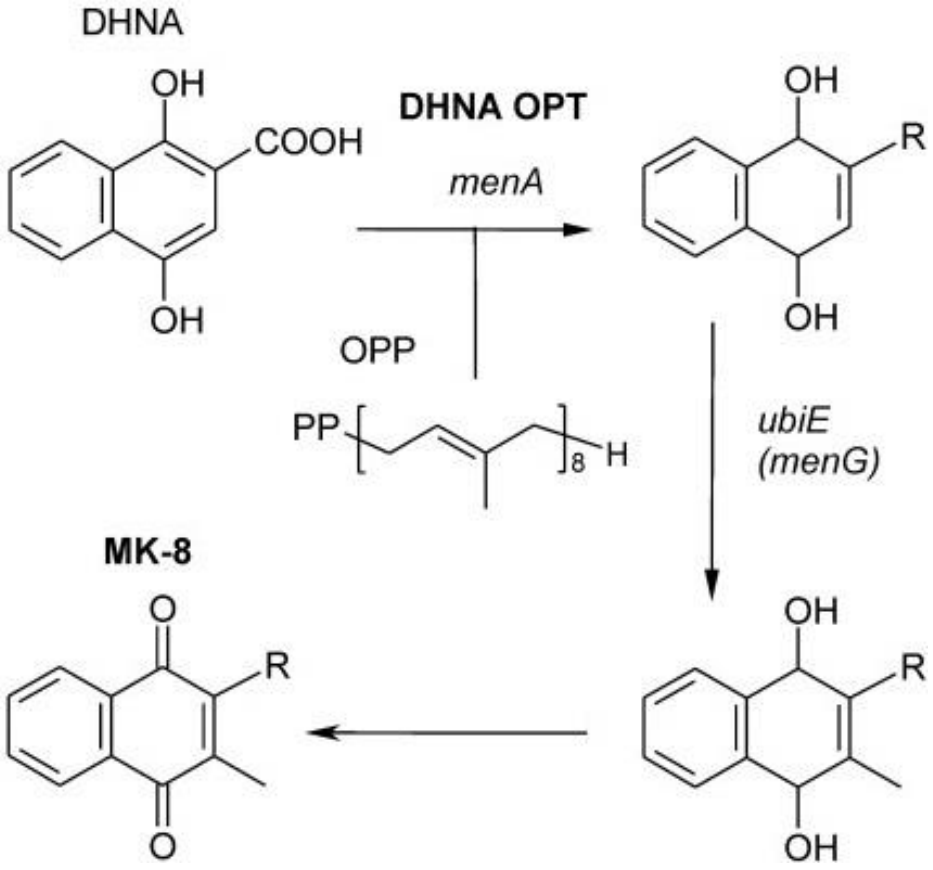

Figure 1.7 – Biosynthesis of Menaquinone. 1,4-dihydroxy-2-naphthoate (DHNA) is derived from chorismate and functions as the head group precursor for menaquinone. DHNA octaprenyltransferase (DHNA OPT) is encoded by the gene menA, and catalyzes the condensation reaction between DHNA and the isoprenoid side chain (R). The naphthoate group is methylated to yield menaquinol, which is further oxidized to menaquinone. From Nowicka and Kruk (2010).

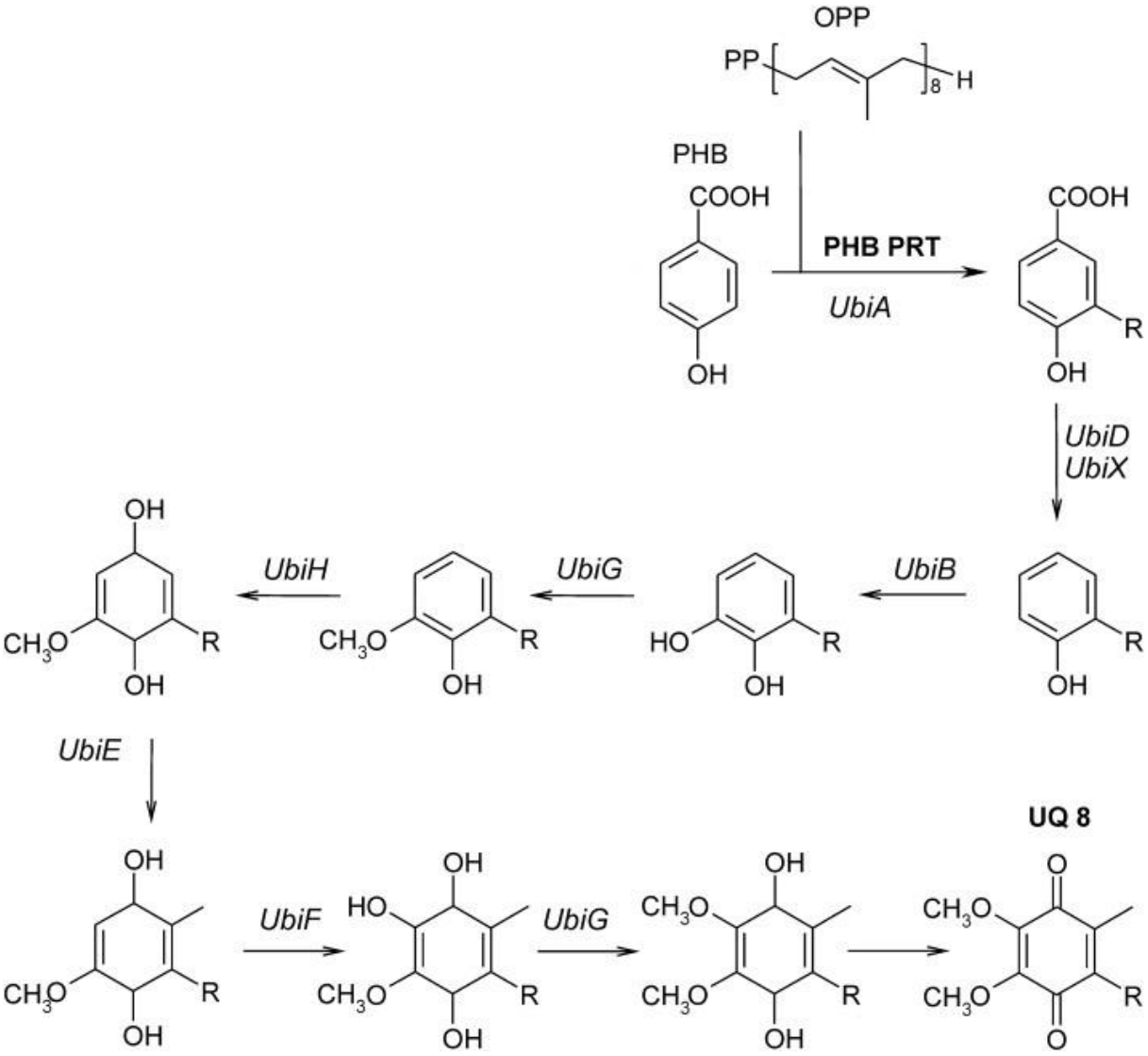

Figure 1.8 – Ubiquinone Biosynthesis. 4-hydroxybenzoate (PHB) is the head group precursor for ubiquinone synthesis and PHB prenyltransferase (PRT) catalyzes condensation of PHB with the isoprenoid side chain. The benzoate head group undergoes a decarboxylation reaction, three hydroxylation steps, two O-methylations and a C-methylation to produce ubiquinol, which is further oxidized to ubiquinone. From Nowicka and Kruk (2010).

3.2. Biosynthesis of Quinones in Plants and Algae

Ubiquinones function in the respiratory electron chain located in the inner mitochondrial membrane of plants and algae. The general pathway for biosynthesis of this quinone is common for all three domains of life, although some differences exist. For example, the head group precursor, PHB, can be synthesized from tyrosine and the order of the aromatic ring modifications differs from bacteria (Kawamukai, 2009). The biosynthetic pathway of phylloquinone (PhQ) is analogous to the synthesis of menaquinone in bacteria and archaea (Fig. 1.7), except that the prenyltransferase catalyzing the condensation step utilize phytyl diphosphate as a substrate instead of prenyl diphosphate (Lichtenthaler, 1999).

In the plastoquinone (PQ) biosynthesis pathway in plants and algae, homogentisate (HGA) derived from tyrosine is used as the head group precursor and the isoprenoid side chain is formed in the DXP pathway (Bouvier *et al.*, 2005). The condensation reaction is carried out by homogenisate solanesyl transferase, and further methylation is required to produce plastoquinone (Fig. 1.9).

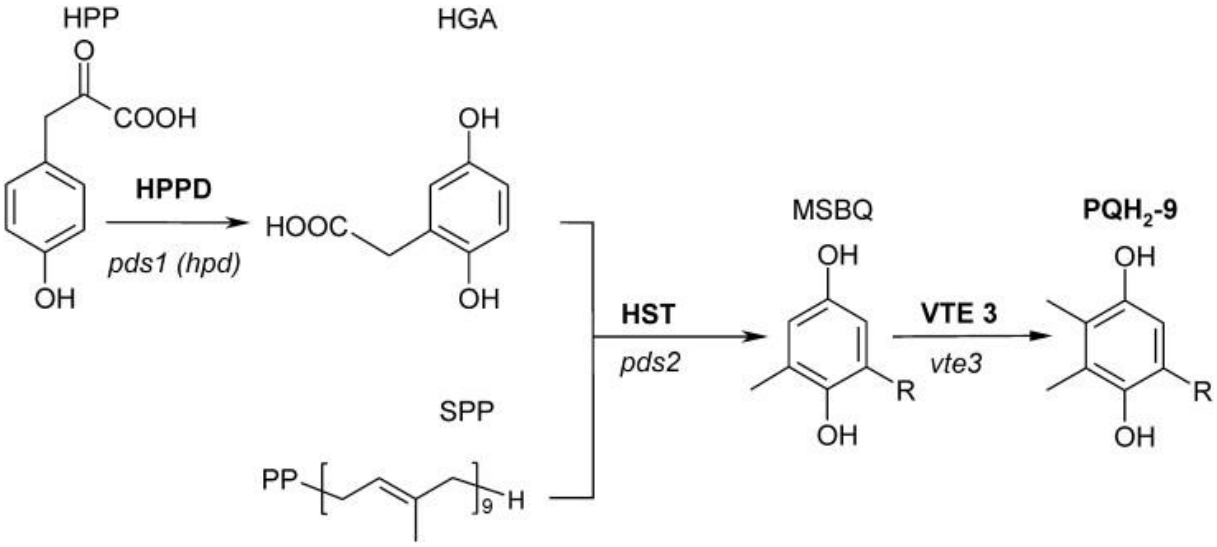

Figure 1.9 – Biosynthesis of Plastoquinone in Plants and Algae. The head group precursor for biosynthesis of plastoquinone in plants and algae is homogenisate (HGA), derived from p-hydroxyphenylpyruvate (HPP) using HPP dioxygenase (HPPD). Homogenisate solanesyl transferase (HST) catalyzes the condensation with the isoprenoid side chain. A MPBQ/MSBQ methyltransferase (VTE3) adds a methyl group to the quinone ring, producing plastoquinol. From Nowicka and Kruk (2010).

There are indications that the biosynthetic pathway of plastoquinone in cyanobacteria differs from that of plants and algae. The enzyme 4-hydroxyphenylpyruvate dioxygenase (HPPD) catalyzes an important step in the PQ biosynthesis pathway in plants and algae, the formation of the head group precursor HGA. Disruption of the *hpd* gene encoding HPPD in *Arabidopsis thaliana* results in a mutant that is deficient in plastoquinones (Norris *et al.*, 1995). Conversely, disruption of an open reading frame in the cyanobacterium *Synechocystis sp.* PCC 6803 with homology to the *hpd* gene in plants, did not affect levels of plastoquinone nor cell growth and photosynthesis (Dähnhardt *et al.*, 2002). These results indicate that HGA is not required for plastoquinone synthesis in cyanobacteria. Recent studies have identified 4-hydroxybenzoate (PHB) as the head group precursor and 4-hydroxybenzoate solanesyltransferase as the enzyme that catalyzes the condensation of head group and isoprenoid chain in plastoquinone synthesis in *Synechocystis sp.* PCC 6803 (Sadre *et al.*, 2012). As mentioned earlier, PHB is the head group precursor for UQ biosynthesis. Open reading frames that are homologous to genes involved in ubiquinone biosynthesis in other species exist in all known cyanobacterial genomes and it is speculated that UQ and PQ synthesis may share a common core of enzymes (Hohmann-Marriott and Blankenship, 2011).

3.3. Changes in Quinone Composition under Variable Environmental Conditions

Bacteria are exposed to highly variable environmental conditions and have evolved mechanisms to enhance their ability to survive when ecological conditions become less favorable. In some species, quinones play an important role in maintaining metabolic flexibility when the cell has to adopt to conditions with changing redox characteristics, such as oxygen availability. *Escherichia coli* is endowed with a highly versatile respiratory chain comprising different quinones under variable growth conditions (Bekker *et al.*, 2007). Ubiquinone is the main quinone involved in aerobic and nitrate respiration whereas either demethyl-menaquinone (DMK) or menaquinone serves as the main electron-transferring quinone in anaerobic respiration using other electron acceptors (Soballe and Poole, 1999; Unden, 1988; Wissenbach *et al.*, 1992). Recently, an oxygen-dependent utilization of menaquinone and ubiquinone has also been reported in Purple bacteria (Schoepp-Cothenet *et al.*, 2009).

Synechocystis sp. PCC 6803 is capable of growing both photoautotrophically on CO_2 and heterotrophically in the dark on D-glucose (Smith, 1983). When oxygen becomes depleted, the cyanobacterium can shift from aerobic respiration to anaerobic respiration. This shift is associated with the anaerobic production of H_2 by a bidirectional hydrogenase and makes *Synechocystis* sp. PCC 6803 a favored organism for studies on biotechnological applications linked to hydrogen production. Currently, there is no evidence of a shift in the quinone composition during aerobic-anaerobic transitions in cyanobacteria, and all photosynthetic and respiratory electron transport is thought to proceed via PQ. Open reading frames homologous to genes involved in naphthoquinone biosynthesis are present in all known cyanobacterial genomes and may contribute to a shift in the type of quinone utilized for electron transport under anaerobic conditions, similar to the behavior observed in *E. coli* and Purple bacteria.

4. *Synechocystis* sp. PCC 6803 as a Model System

Synechocystis sp. PCC 6803 (hereafter *Synechocystis* 6803) is a unicellular, halotolerant cyanobacterium capable of both photoautotrophic and heterotrophic growth, and can therefore be classified as a facultative photoheterotroph (Rippka *et al.*, 1979). This strain is commonly found in freshwater ecosystems and contributes to the productivity of these areas. *Synechocystis* 6803 has been one of the most popular organisms for genetic and physiological studies of photosynthesis for two reasons: the strain is naturally transformable and can grow photo-heterotrophically on glucose. Type IV pili mediate the uptake of DNA, followed by incorporation into the genome by homologous double recombination (Williams, 1988; Yoshihara *et al.*, 2001). The widespread use of *Synechocystis* 6803 as a model system resulted in complete sequencing of its genome in 1996, as the first photosynthetic organism to have its genome sequenced (Kaneko *et al.*, 1996). Sequencing results, including information on gene structure and function, can be found in the established genome database for cyanobacteria – Cyanobase. A tremendous amount of information on photosynthesis has been generated through functional genomics, proteome and transcriptome studies in *Synechocystis* 6803 since sequencing results became available (Ikeuchi and Tabata, 2001).

4.1. Intertwined Electron Transport Chains

A main reason for the evolutionary success of cyanobacteria is their successful combination of effective metabolic pathways (Vermaas, 2001). Both photosynthetic and respiratory electron transports take place within the thylakoid membrane, an organization that is quite unique. This enables cyanobacteria to coordinate oxygenic photosynthesis and respiration simultaneously in the same compartment. The electron transport chains of *Synechocystis* 6803 have evolved to share common components in the membrane (Fig 1.10). The pool of plastoquinones, the cytochrome b_6f complex and the soluble carriers in the lumen (plastocyanin, or sometimes cytochrome c_6) are utilized as redox-active components for both photosynthesis and respiration (Schmetterer, 2004). Either Cyt c_6 (previously known as Cyt c_{553}) or copper-containing PC are required for efficient photosynthesis and respiration in *Synechocystis* 6803 and their expression is regulated by the copper concentration of the growth medium (Duran *et al.*, 2004; Zhang, L. *et al.*, 1992). Much research has been focused on how environmental factors affect utilization of different components in the bio-energetic processes, but the function of the branched ETCs of cyanobacteria is still not completely understood.

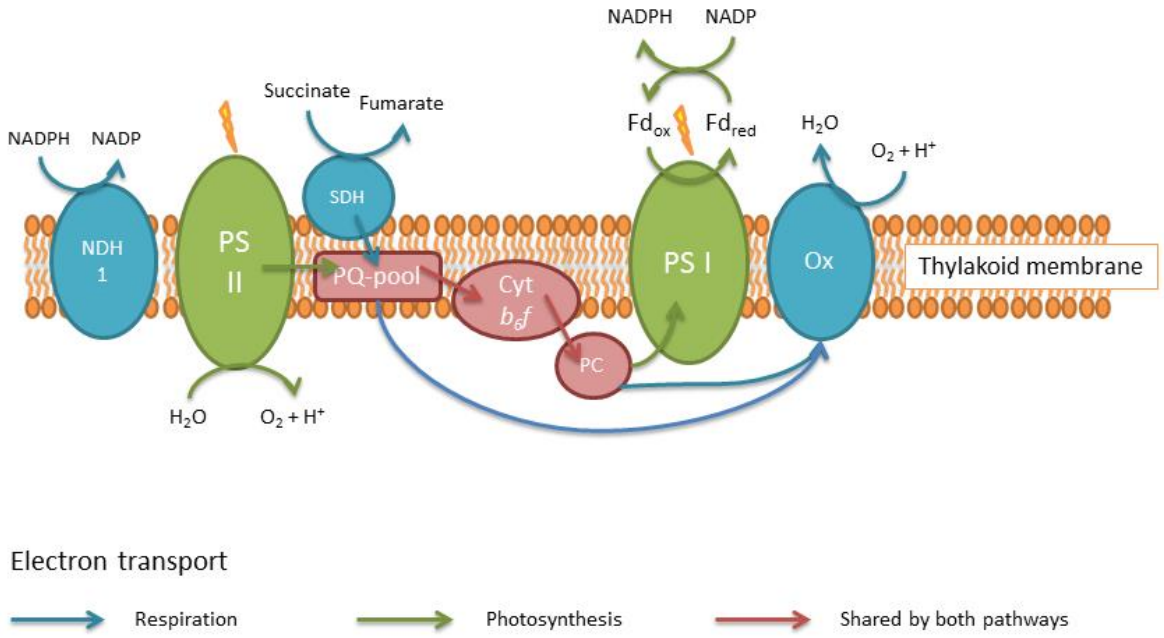

Figure 1.10 – Intertwined Electron Transport Chains in Cyanobacteria. Complexes and electron transport in the thylakoid membrane of *Synechocystis* 6803, utilized for respiration (blue) and photosynthesis (green). Some components are utilized by both electron transport chains (red). Abbreviations: NDH 1, type 1 NADPH dehydrogenase; PS II, photosystem II; SDH, succinate dehydrogenase; PQ, plastoquinone; Cyt b_6f, the cytochrome b_6f complex; PC, plastocyanin; PS I, photosystem I; Ox, terminal oxidase (could be a cytochrome c oxidase, a quinol oxidase or an alternative respiratory terminal oxidase).

5. Techniques Utilized for Phenotypic Characterization of *Synechocystis* 6803

To gain further insights into the synthesis and utilization of quinones in *Synechocystis* 6803, open reading frames assumed to be involved in quinone synthesis can be genetically deleted. Such inactivation of a given gene can reveal the function of the gene product of interest. The following sections describe techniques utilized in this study to generate gene-deletion constructs, assess the functionality of the photosynthetic machinery and analyze the composition of photosynthetic lipids in *Synechocystis 6803*.

5.1. SLIC Cloning

Sequence and ligation independent cloning (SLIC) allows the assembly of multiple DNA fragments in a single reaction using *in vitro* homologous recombination and single-strand annealing (Li, M. Z. and Elledge, 2007). Single-stranded overhangs in the insert and vector fragments are generated by an exonuclease and vector assembly is achieved by combining these fragments. Transformation of this *in vitro* generated vector construct into a bacterial host allows the endogenous repair machinery to ligate these fragments into a vector that can replicate in the host. A schematic representation of SLIC cloning is provided in Figure 1.11.

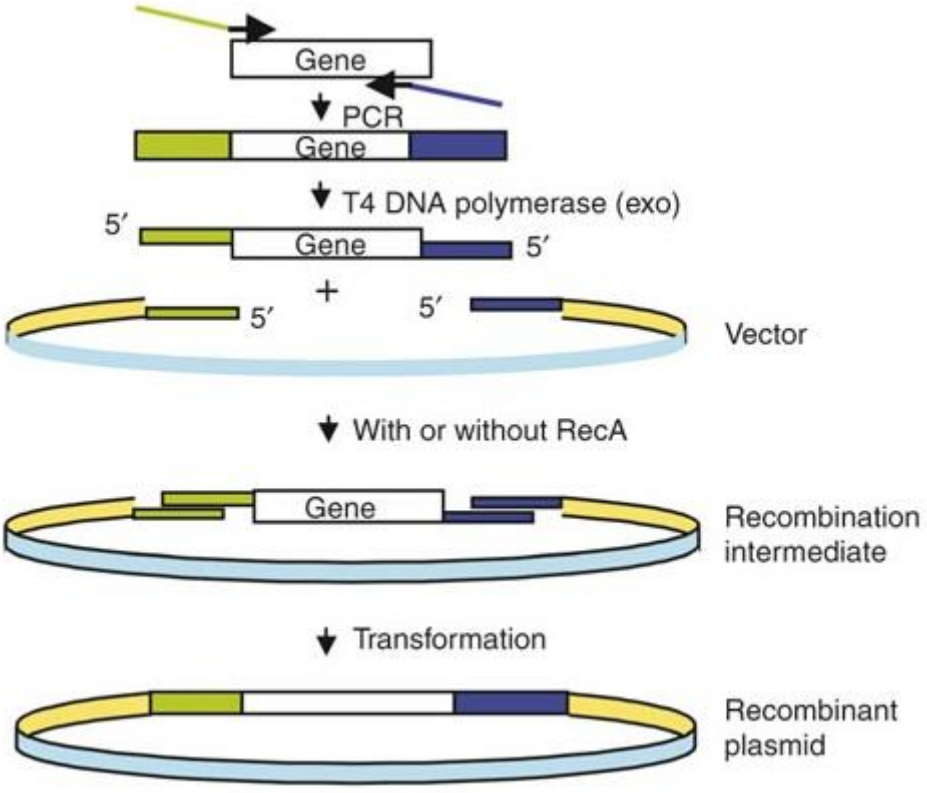

Figure 1.11 – SLIC Cloning. A schematic representation of the production of recombinant DNA using sequence and ligation independent cloning (SLIC). Single-stranded overhangs in both insert and vector are generated by an exonuclease and assembly is achieved by homologous recombination. Transformation generates a recombinant plasmid. From Li, M. Z. and Elledge (2007).

5.1.1. BioBricks™ as a Cloning Tool

BioBricks™ are standard biological parts of DNA designed to introduce abstraction and standardization into biological engineering, first described by (Knight, 2003). The idea is to make interchangeable parts that simplify the construction of new biological systems. A BioBrick part is held in a circular DNA vector and is flanked by universal and precisely defined prefix and suffix sequences (Fig. 1.12). The prefix sequence is located upstream of the BioBrick part and contains restriction sites for EcoRI and XbaI, whereas the suffix sequence is located downstream and contains restriction sites for SpeI and PstI. A NotI restriction site is included in both flanking sequences, separating the two other restriction sites. This setup enables the creation of larger BioBrick parts by assembling smaller ones in a desired order. In the ligation process, a mixed SpeI/XbaI site is formed between inserts and can no longer function as a restriction site. The only restriction sites left are present in the prefix and suffix sequences flanking the new and improved BioBrick part. An important aspect in the use of BioBricks™ is to avoid flanking region restriction sites in both the BioBrick part and in the vector molecule.

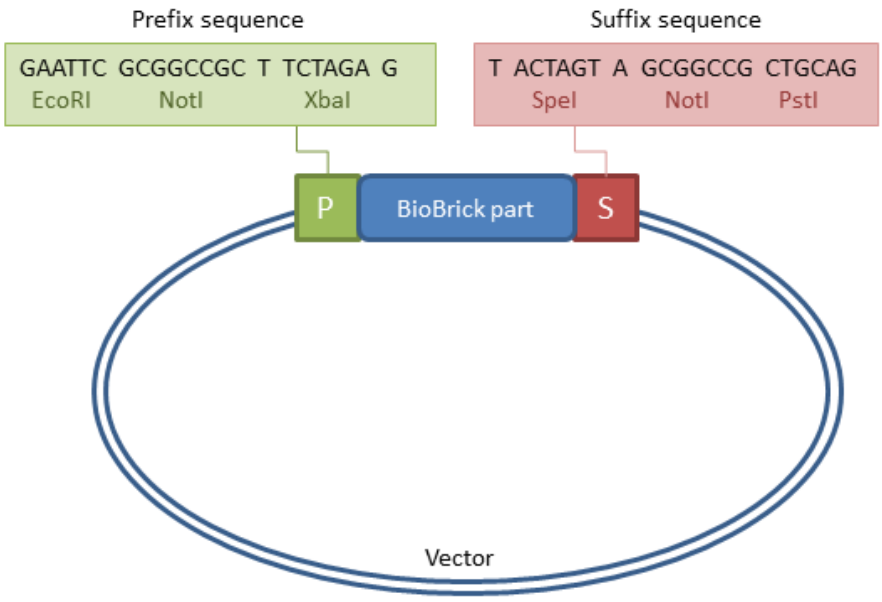

Figure 1.12 – BioBricks ™. A BioBrick part flanked by defined prefix and suffix sequences, held in a circular DNA vector. Restriction sites in the prefix and suffix sequences are indicated.

5.2. Spectroscopic Techniques

The large amount of pigments synthesized by *Synechocystis* 6803 provide basis for analysis of the identity and quantity of these pigments. Due to the association of these pigments with PS I and PS II, an assessment of the overall state of the photosynthetic machinery can be provided using various spectroscopic techniques.

5.2.1. *In Vivo* Absorption

In vivo absorption spectra allow determination of relative ratios of specific pigments in relation to one another, providing information about phenotypical properties of different strains. Chlorophyll *a* (Chl *a*) is the only chlorophyll synthesized in cyanobacteria and produces two major absorption bands at 435 and 680nm. β-carotene and zeaxanthin are among the carotenoids found in *Synechocystis* 6803 and give a single three-fingered peak in the 430-500nm region. The major light-harvesting systems of cyanobacteria and red algae are phycobiliproteins (PBPs), consisting of tetrapyrrolic chromophores (bilins) covalently bound to proteins. Phycobiliproteins found in *Synechocystis* 6803 are phycocyanin (PHC) and allophycocyanin (APC), absorbing at 620 and 650nm, respectively. Figure 1.13 shows an *in vivo* absorption spectrum of *Synechocystis* 6803 and the absorption spectra of individual pigments found in this species.

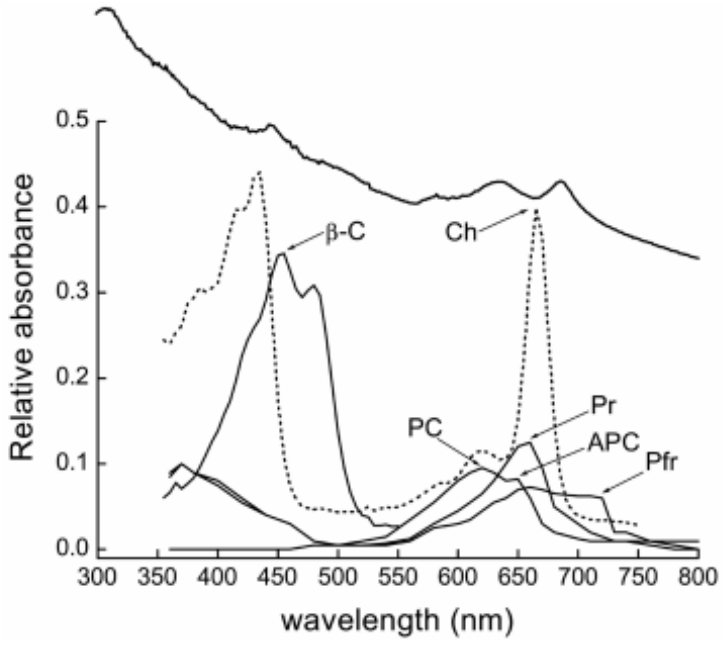

Figure 1.13 – Absorption Spectra of Cyanobacterial Pigments and Whole Cells. Upper solid line indicates the in vivo absorption spectrum of *Synechocystis* 6803 and the remaining lines indicate the characteristic absorption peak of each pigment: β-C, β-carotene; PC, phycocyanin; Ch, chlorophyll a; Pr, red-absorbing phytochromes; Pfr, far-red absorbing phytochromes; APC, allophycocyanin. From Chung *et al.* (2004).

5.2.2. 77K Fluorescence

Fluorescence analysis depends on the phenomenon that when a pigment absorbs the energy of a photon and enters an excited state, it can return to its ground state by emission of a fluorescence photon, of a wavelength longer than that of the photon initially absorbed. At room temperature, chlorophyll *a* fluorescence is emitted predominantly (~90 %) from PS II (Govindjee, 1995). At 77 K, the electron transport characteristics of photosynthetic reaction centers change. Due to this change, PS I, which is a very efficient excitation quencher at room temperature (therefore exhibiting low fluorescence), exhibits a higher fluorescence yield at 77 K. Furthermore, absorption and fluorescence spectra become sharper due to the decrease of vibrations in the photosynthetic machinery. Emission spectra with a scanning emission wavelength and a fixed excitation wavelength of either 440 nm (chlorophyll *a* excitation) or 580 nm (PBPs excitation) are routinely performed to analyze the excitation transfer from antenna systems to the special reaction center chlorophylls of PS I and PS II (Fig. 1.14). These spectra are then often normalized to either PS I (emission peak at 720 nm) or PS II (emission peak at 685 and 695 nm) in order to determine changes in the ratio between the two photosystems or variations in the excitation transfer between phycobiliproteins and the photosystem.

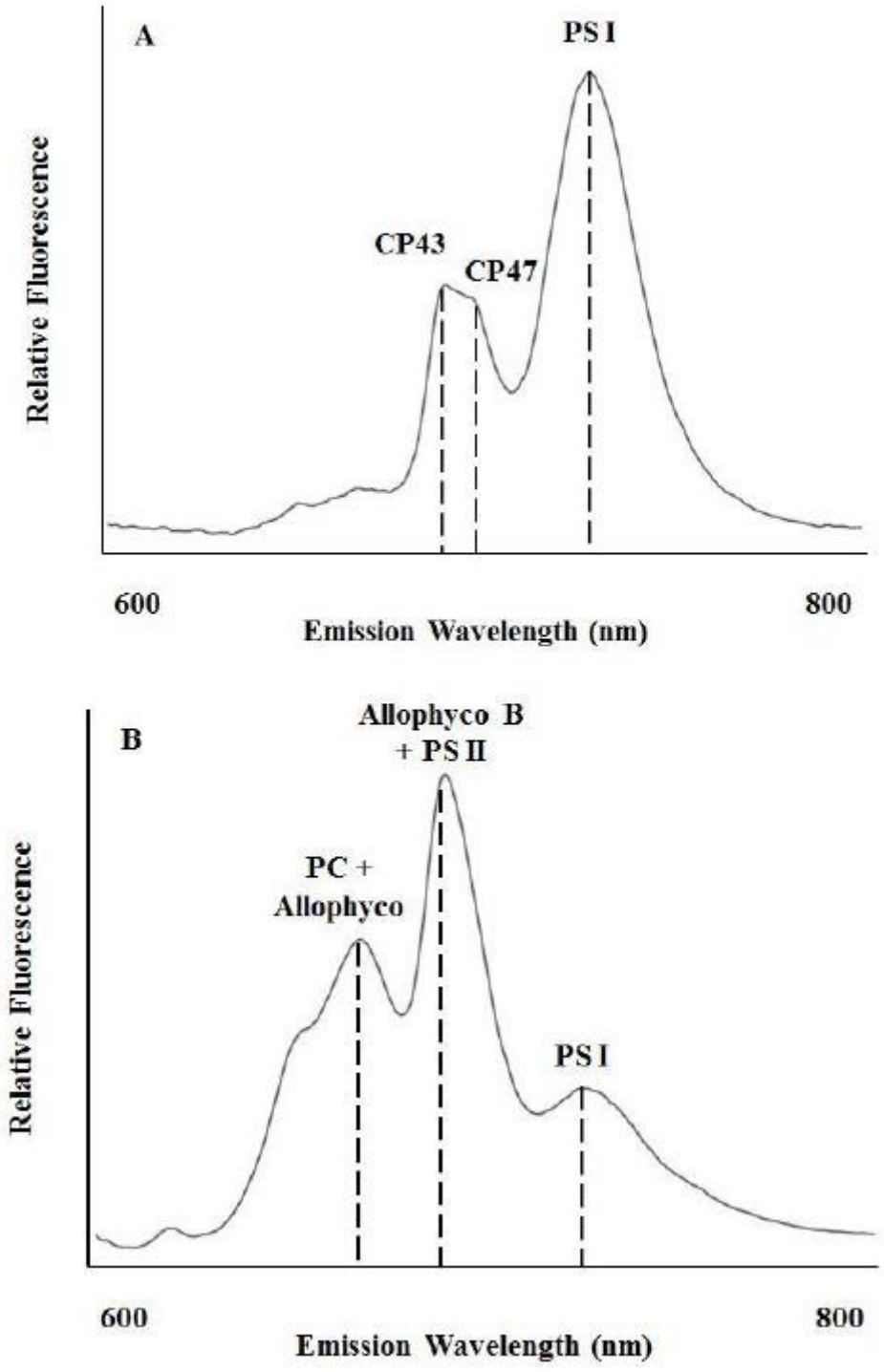

Figure 1.14 – 77K Fluorescence Emission Spectra. Schematic representation of fluorescence emission traces of Synechocystis 6803 using 440 nm (A) and 580 nm (B) excitation wavelengths. Abbreviations: CP43 and CP47, antenna chlorophyll-binding proteins of PS II; PS I, photosystem I; Allophyco, allophycocyanin; Allophyco B, allophycocyanin B; PS II; photosystem II. From Lamb (2012).

5.2.3. Pulse Amplitude Modulation Fluorescence

The pulse amplitude modulation (PAM) fluorescence technique allows both qualitative and quantitative information on the organization and functioning of the photosynthetic apparatus by analysis of fast and slow chlorophyll *a* fluorescence induction kinetics (Rohàcek and Bartàk, 1999). The method has become a routine tool for non-invasive assessment of photosynthetic electron transport in higher plants, algae, and cyanobacteria. Light energy absorbed by the reaction center chlorophyll of PS II (P680) can be utilized to drive photochemistry in which an electron is transferred from P680 to the primary quinone acceptor of PS II (Q_A). Alternatively, absorbed light energy can be lost from PS II as fluorescence or heat (Baker, 2008). These three processes (charge separation, fluorescence and heat generation) are in direct competition for excitation energy, meaning that if the rate of one process increases, the rates of the other two will decrease (Butler, 1978).

In PAM fluorometry, fluorescence is induced by a constant, weak light source of a given wavelength, and is measured as F_0 in dark-adapted cells. Under these conditions, all PS II reaction centers are believed to be in the open (oxidized) state. A saturating light pulse is applied, which closes (reduces) all PS II reaction centers, resulting in maximal fluorescence (F_M). The main modulator of Chl fluorescence is the oxidation state of Q_A (Duysens and Sweers, 1963), although additional mechanisms have been identified as fluorescence modulators in plants and algae; such as the reduction state of P680, the electrochemical potential across the thylakoid membrane and the association of light-harvesting complexes with either PS I or PS II (Butler, 1972; Genty *et al.*, 1989; Wollman and Delepelaire, 1984). Inhibitors of electron transport can be added to modulate the redox state of the photosynthetic ETC. The inhibitor 3-(3,4-dichlorophenyl)-1,1-dimethylurea (DCMU) blocks the electron transfer from PS II to the PQ pool and 2,5-dibromo-3-methyl-6-isopropyl-*p*-benzoquinone (DBMIB) prevents the oxidation of PQ by the cytochrome b_6f complex (Trebst, 1980). In light conditions, DCMU will oxidize the PQ pool whereas DBMIB will reduce the PQ pool. Figure 1.15 shows modulation of fluorescence upon oxygen depletion in the green algae *Chlamydomonas reinhardtii*.

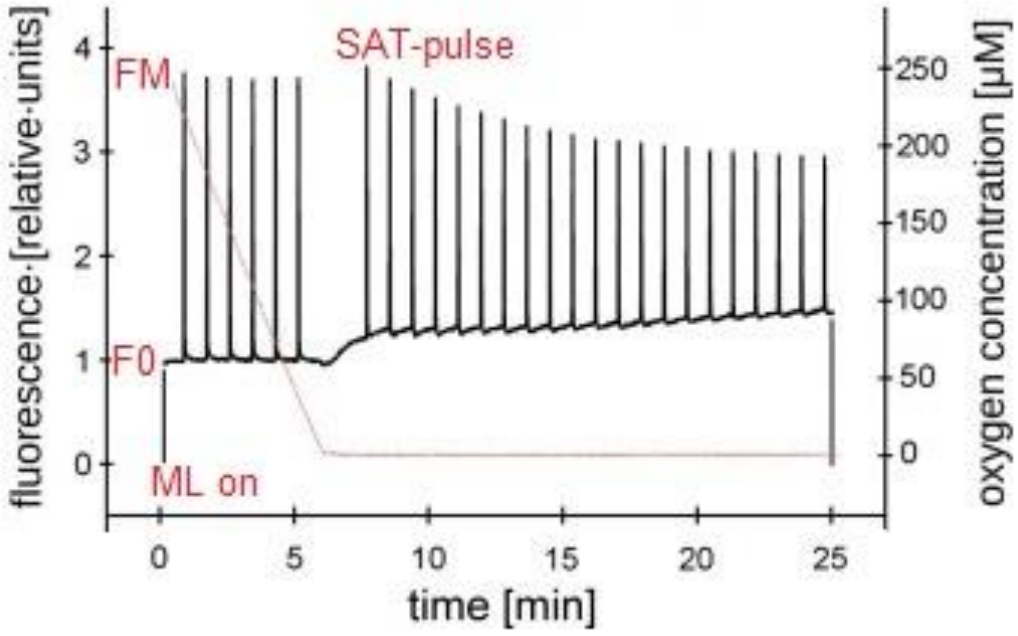

Figure 1.15 – PAM Fluorescence Traces upon Depletion of Oxygen. Pulse amplitude modulation (PAM) fluorescence traces (black) in Chlamydomonas reinhardtii when a continuous measuring light (ML) and saturating (SAT) light pulses are applied to dark-adapted cells. Background fluorescence (F0) and maximal fluorescence (FM) are indicated. Anaerobic conditions were achieved (red line) and the increase in F_0 and decrease in F_M are indications of fluorescence modulation due to depletion of oxygen. From Hohmann-Marriott *et al.* (2010).

5.3. Analysis of Photosynthetic Lipids

Analysis of the lipid content of a cell is divided into an extraction procedure and a detection system. Such analyses can be very laborious considering the large amount of different classes of lipids present in the cell. Additionally, homogeneity between classes and minimal differences in polarity creates challenges associated with extraction, separation, identification and quantification. Lipid contents of photosynthetic organisms are larger than that of heterotrophic organisms, and confer an even higher degree of complexity to the analysis. Thus far, no single analytical system exists for the analysis of all photosynthetic lipids (chlorophylls, carotenoids and quinones) without combining various, complementary technologies.

5.3.1. Thin-Layer Chromatography

Thin-layer chromatography (TLC) is a simple chromatography technique used to separate compounds in a mixture. TLC is performed on a sheet of glass, metal or plastic coated with a thin layer of solid absorbent, usually silica, alumina or cellulose (stationary phase). The TLC plates are placed in a developing chamber, and compounds in the sample mixture are separated by a solvent or solvent system (mobile phase) which is drawn up the plate via capillary action. Compounds will vary in solubility in the mobile phase and in adsorption to the stationary phase, resulting in different mobility rates allowing separation. Photosynthetic lipids are well suited for separation by thin-layer chromatography due to the coloration of the pigments, eliminating the visualization step in this process. TLC can be used in combination with mass analysis but this is a laborious method, compared to automated procedures such as high performance liquid chromatography (HPLC).

5.3.2. Liquid Chromatography – Mass Spectrometry

Liquid chromatography-mass spectrometry (LC-MS) is a technique within analytical chemistry that combines the separation capabilities of liquid chromatography (LC) with analyses of masses by mass spectrometry (MS). Present day LC-MS methods utilize HPLC instrumentation in which the sample is forced by a liquid at high pressure (mobile phase) through a column filled with small particles (stationary phase) packed to accomplish the desired separation. An improvement of this instrumentation is the ultra-performance liquid chromatography (UPLC), which runs separations in a column packed with even smaller particles and higher flow rates, for increased resolution and sensitivity.

Reverse-phase chromatography employs a hydrophobic stationary phase and a polar mobile phase. Consequently, hydrophobic molecules adsorb to the stationary phase and can be eluted by decreasing the polarity of the mobile phase. Photosynthetic lipids, such as chlorophyll, carotenoids and isoprenoid quinones, are relatively hydrophobic compounds and may be good candidates for separation by reverse-phase chromatography.

A mass spectrometer consists of an ion source, a mass analyzer and a detector. To overcome fragmentation upon ionization of biological macromolecules, electrospray ionization (ESI) or atmospheric-pressure chemical ionization (APCI) can be employed. Ionization can either be

carried out in positive or negative mode, in which ions are produced by either the transfer or the abstraction of a hydrogen atom, respectively. Mass analyzers separate the produced ions according to mass-to-charge (*m/z*) rations. A quadrupole (Q) mass analyzer consists of four parallel rods and provides a radio frequency voltage between them, allowing ions only in a certain range of *m/z*-ratios to reach the detector at any time. Another common mass analyzer is the time-of-flight (TOF) which uses an electric field to accelerate ions through the system. Molecules with identical charges will have the same kinetic energy and the time it takes for them to reach the detector will be dependent only on the masses. The detector records the beam of ions that passes through the system either by the charge induced or by the current that arises. The absorption properties of photosynthetic lipids can advantageously be recorded using a diode array detector (DAD) as an addition to the instrumentation.

6. Aims of Research

The main objective of this thesis is to study the photosynthetic lipids, with a particular focus on isoprenoid quinones in *Synechocystis* 6803. Secondary objectives are to develop methods for analysis of photosynthetic lipids, to evaluate the biosynthetic pathway of plastoquinone in cyanobacteria and to assess whether a shift in quinone composition can be initiated under limiting oxygen conditions.

Candidate genes that may be involved in the biosynthesis of plastoquinone in cyanobacteria will be identified using bioinformatics approaches in conjunction with the current understanding of isoprenoid quinone synthesis pathways in plants and other bacteria. Gene deletion strains will be constructed and characterized to assess the involvement of candidate genes in the synthesis of quinones in *Synechocystis* 6803. Phenotypic differences will be determined utilizing spectroscopic techniques and analysis of photosynthetic lipids by mass spectrometry.

A physiological focus of this thesis is based on the hypothesis that cyanobacteria can modulate the composition of quinones upon depletion of oxygen. For this, the physiological characterization will explore the operating efficiency of the photosynthetic machinery and the

composition of different quinones under limiting oxygen conditions for both wild-type and mutant strains.

The analytical focus of this thesis is the optimization of conditions for extraction, separation and characterization of photosynthetic lipids. This work provides the basis for detection of differences in lipid composition between wild-type and gene deletion strains.

The results obtained by this work will provide a greater understanding of the biosynthesis and utilization of isoprenoid quinones in cyanobacteria.

Chapter 2: Materials and Methods

1. Bacterial Strains and Growth conditions

1.1. General Techniques

Standard microbial sterile techniques were applied throughout this research. All work with microorganisms was performed in a laminar flow hood. Solutions were prepared with deionized water (ddH_2O) and sterilized by autoclaving at 121°C for 20 min or by filter-sterilization (VWR, USA). DNA samples, enzymes and their buffers were stored at -20°C. All percentages and ratios represent volume to volume (v/v) ratios, unless otherwise specified.

1.2. *Synechocystis* sp. PCC 6803 Strains

The *Synechocystis* 6803 strain was received from the laboratory of Julian Eaton-Rye (University of Otago, New Zealand). This strain is glucose-tolerant (GT), indicated as GT-O1, and is derived from the original GT strain isolated by Williams (1988). The genomic sequence of this strain was recently published (Morris *et al.*, 2014).

1.2.1. Growth and Maintenance

Synechocystis 6803 cells were maintained on BG11 (Rippka *et al.*, 1979) agar plates at 22°C. Cells were grown photoautotrophically in BG11 medium at constant temperature (30°C) and illumination. Liquid cultures were grown at 166 µE $m^{-2}s^{-1}$ and agar plates were incubated with a light intensity of 200 µE $m^{-2}s^{-1}$. *Synechocystis* sp. mutant strains were propagated onto BG11 agar plates containing glucose (5mM) and appropriate antibiotics (Eaton-Rye, 2011). Liquid cultures were established in 500mL Erlenmeyer flasks that have been specifically modified (see Fig. 2.1) to provide filtered aeration via small aquarium pumps. To prevent dehydration of cell cultures, the air was initially bubbled through sterilized water before entering the Erlenmeyer culture flasks.

Figure 2.1 – Culture Flask. 500 mL Erlenmeyer flask specifically modified for growth of *Synechocystis* 6803.

The stock solutions required to make BG11 medium are given in Table 2.1. To obtain 1 L of BG11, 10 mL of 100x BG11 stock and 1 mL each of 1000x ammonium iron (III) citrate, 1000x Na_2CO_3 and 1000x K_2HPO_4 stock solutions was combined with water to a final volume of 1 L (Eaton-Rye, 2011). BG11 agar plates were prepared by supplementing the above BG11 media with 10 mM TES-NaOH buffer (pH 8.2), 0.3 % (w/v) sodium thiosulphate and 1.5 % (w/v) bacteriological agar (Sigma-Aldrich, USA). Any glucose, herbicides and antibiotics (Table 2.2) were added after autoclaving the media.

Table 2.1 – BG11 Medium Stock Solutions. Composition of stock solutions for liquid BG11 medium used for growth of *Synechocystis* 6803.

Stock	Ingredients	Amount
100x BG11 stock	$NaNO_3$	149.60 g/L
	$MgSO_4 \cdot 7H_2O$	7.49 g/L
	$CaCl_2 \cdot 2H_2O$	3.60 g/L
	Citric acid	0.60 g/L
	0.25M Na-EDTA, pH 8.0	1.12 mL/L
	Trace minerals	100 mL/L
	Deionized water	Up to 1 L
Trace minerals stock	H_3BO_3	2.860 g/L
	$MnCl_2 \cdot 4H_2O$	1.810 g/L
	$ZnSO_4 \cdot 7H_2O$	0.222 g/L
	$Na_2MoO_4 \cdot 2H_2O$	0.390 g/L
	$CuSO_4 \cdot 5H_2O$	0.079 g/L
	$Co(NO_3)_2 \cdot 6H_2O$	0.0494 g/L
	Deionized water	Up to 1 L
1000x ferric ammonium citrate stock	Ammonium iron (III) citrate, brown	0.60 g/100 mL
1000x Na_2CO_3 stock	Na_2CO_3	2.00 g/100 mL
1000x K_2HPO_4 stock	K_2HPO_4	3.05 g/100 mL

Table 2.2 – Additions for BG11 Medium. Concentrations of stock solutions, final concentration in media and preparation of additions to BG11 media.

Solution	Stock	Final concentration	Preparation
Glucose	1 M	5 mM	Autoclave, store at 4°C
DCMU	20 mM	20 µM	Make in methanol, store at -20°C
DBMIB	20 mM	20 µM	Make in ethanol, store at -20°C
Kanamycin	50 mg/mL	25 µg/mL	Filter-sterilize, store at -20 or 4°C

2. Optimization of Lipid Extraction, Separation and Characterization

In order to extract photosynthetic lipids (chlorophylls, carotenoids and quinones) from *Synechocystis* 6803 in one procedure, different extraction solvents were evaluated for their extraction yield. The separation of the photosynthetic lipids by TLC was optimized using different development solvent systems. In addition, a method for the simultaneous characterization and identification by LC-MS of chlorophylls, carotenoids and isoprenoid quinones was developed.

2.1. Lipid Extraction

Four extraction solvent systems ranging in polarity were evaluated for their ability to extract photosynthetic lipids from *Synechocystis* 6803. A mixture of methanol and chloroform (MeOH:$CHCl_3$, 2:1) and a less polar mixture of the same solvents, chloroform/methanol ($CHCl_3$:MeOH, 2:1) was prepared using analytical grade solvents (Normapur, VWR). Isopropanol (IPA, GPR rectapur, VWR) and tetrahydrofuran (THF, Seccosolv, Merck) were also evaluated for their extraction yield of photosynthetic lipids.

For pigment extraction, cells were grown photoautotrophically in liquid BG11 medium as described above, until an OD_{750} of 0.5 was reached. Cells were harvested by centrifugation and 60 mg of cells were resuspended in 400 µL of extraction solvent (4°C). The suspension was centrifuged at 13,000 rpm for 2 min and the supernatant was stored in Eppendorf tubes. A total of three extractions were carried out in sequence from the same cell pellet. Extracts were evaluated by absorption spectroscopy using a NanoDrop 2000 (Thermo Scientific, USA) scanning from 220-750nm.

2.2. Separation by TLC

Silica gel TLC plates (Sigma-Aldrich) containing a fluorescent indicator (254 nm) were utilized for the visual separation of pigments and lipids extracted from Synechocystis 6803. Lipid extracts (2x 10 µL) were applied in the standard manner. The development systems 30 % acetone (LiChrosolv, Merck) in hexane (LiChrosolv, Merck) as described by Quach *et al.* (2004), 40 % and 25 % chloroform in hexane adapted from Wood and Crane (1969) and pure hexane were evaluated for their ability to separate chlorophylls, carotenoids and quinones by TLC. Plates were placed in a closed chamber with the different development systems mentioned above as the mobile phase. Bands were visualized under UV light using a GelDoc (BioRad, USA). Retention ratios (R_f values) were calculated using equation 2.1.

$$R_f = \frac{distance\ moved\ by\ solute}{distance\ moved\ by\ solvent} \qquad \text{[Equation 2.1]}$$

Bands were scraped off the TLC plate and dissolved in methanol, prior to centrifugation (13 000, 1 min) for the removal of silica residues. Absorption spectra were measured for each band using a NanoDrop 2000 (Thermo Scientific, USA) to identify the components separated by TLC.

2.3. Characterization of Lipids by LC-MS

Different gradients were evaluated for the ability to separate chlorophyll, carotenoids and quinones using UPLC. First, a gradient of methanol (A) and 2-propanol (B) was tested by dissolving extracted lipids in a mixture of methanol and 2-propanol. Second, a gradient using methanol/water (80:20) as mobile phase A and dichloromethane as B was tested. Third, methanol was used as mobile phase A and dichloromethane as mobile phase. For the latter two gradients, lipids were dissolved in chloroform. The ionization of all compounds in a lipid extract using MS is difficult to achieve with a single ionization mode. The recordings of both ESI and APCI in the same run, but in two separate channels, were therefore evaluated. Standards of chlorophyll *a* (provided by Professor Kalbe Razi Naqvi, Norwegian University of Science and Technology), β-carotene (Sigma-Aldrich, USA), α-tocopherol (provided by

Professor Kalbe Razi Naqvi, NTNU) and ubiquinone-10 (provided by Professor Julian Eaton-Rye, University of Otago) were used to assess the separation and characterization of compounds from the chemical classes of chlorophylls, carotenoids and isoprenoid quinones.

Samples were analyzed in a system consisting of a Waters Acquity UPLC™ (Milford, USA) coupled to a Waters Synapt G2 MS QTOF equipped with both an APCI and an ESI source in and a diode array detector. Separation was performed in an Acquity BEH C18 column (50 x 2.1 mm, 1.7 µm) using the different mobile phases mentioned above. The flow rate was 0.400 mL/min and the injection volume was 1.0 µL. Temperature of the column and the autosampler chamber was set to 40 and 15°C, respectively. Data was acquired with a scan time of 0.1 seconds over a mass range of 50-2000 in the ESCI+ polarity mode. The corona current was set to 3.4 µA and cone voltage to 40 V, with a desolvation gas flow of 1000 L/hour and a cone gas flow of 10 L/hour. The probe temperature was 500°C and the source temperature was 150°C. Accurate mass measurements were ensured by the LockSpray™ probe at a flow rate of 15 µL/min. The quadrupole LM resolution was 4.7 and the HM resolution was 15.0. The data acquired was processed using MassLynx version 4.1 and the TransOmics Platform (Waters, USA).

3. BioBrick Cloning and *Synechocystis* 6803 Mutagenesis

The principle of BioBrick cloning was demonstrated by assembling an antibiotic resistance cassette with a Biobrick containing the gene for red fluorescent protein (*mCherry*) in a standard Biobrick plasmid, pSB1A3. A gene disruption cassette was designed and constructed to produce a *Synechocystis* 6803 single gene deletion mutant. The gene disruption cassette was cloned into a Litmus28i plasmid and consisted of gene flanking regions (amplified from *Synechocystis* 6803 genomic DNA) separated by a kanamycin-resistance cassette. *Synechocystis* 6803 incorporates plasmid DNA that is contained in its growth medium into its genome via homologous recombination.

3.1. Polymerase Chain Reaction

Polymerase chain reactions (PCR) were utilized to amplify fragments for the generation of gene deletion plasmids and to analyze strain segregation after transformation. *Synechocystis* 6803 cells were used as template for colony PCR amplification of gene flanking regions and verification of complete mutant segregation. Plasmid DNA was used as PCR template for amplifying the plasmid backbone and the resistance cassettes.

3.1.1. Touchdown PCR

Touchdown PCR minimizes amplification of non-specific sequences. This method employs an initial annealing temperature above the projected melting temperature (T_m) of the primers and then progressively transitions to lower temperatures per completed cycle (Korbie and Mattick, 2008). Phusion High-Fidelity DNA polymerase (Thermo Scientific, USA) was employed to amplify DNA sequences. PCR-reactions (50 µL total volume) were set up on ice according to Table 2.3 and were run in a Mastercycler gradient (Eppendorf, USA) at conditions listed in Table 2.4. PCR products were cleaned using a QIAquick PCR purification kit (Qiagen, Düsseldorf Germany).

Table 2.3 – 50 µL Reaction for PCR using Phusion HF DNA Polymerase.

Reaction components	Volume (µL)	Final concentration
Water, autoclaved	31.0	-
5X Phusion HF buffer	10.0	1X
Forward primer (10 µM)	2.5	0.5 µM
Reverse primer (10 µM)	2.5	0.5 µM
dNTPs (10mM)	2.5	500 µM
Template DNA	1.0	Variable
Phusion DNA polymerase	0.5	0.02 U/µL

Table 2.4 – Thermocycler Conditions for Touchdown PCR using Phusion Polymerase.

Step	Temperature (°C)	Time (h:mm:ss)	Number of cycles
Initial denaturation	98	0:10:00	1
Amplification	98 69 (-1°C for each cycle) 72	0:00:10 0:00:30 0:01:30	13
Amplification	98 58 72	0:00:10 0:00:30 0:01:30	22
Final extension	72	0:05:00	1
Hold	4		

3.1.2. Primer Sequences

Oligonucleotide primers were designed and analyzed using the online application PrimerQuest and OligoAnalyzer 3.1 from Integrated DNA technologies (IDT). Primer sequences for amplifying kanamycin and chloramphenicol resistance cassettes were obtained from Poteete *et al.* (2006). Primers for PCR were ordered from Sigma-Aldrich (St. Louis, MO, USA).

Resistance cassettes carrying BB prefix and suffix

Kanamycin forward
5'- GAATTCGCGGCCGCTTCTAGAGCACGTTGTGTCTCAAAATCTC
Kanamycin reverse
5'- CTGCAGCGGCCGCTACTAGTATACAACCAATTAACCAATTCTG
Chloramphenicol forward
5'- GAATTCGCGGCCGCTTCTAGAGATGAGACGTTGATCGGCACG
Chloramphenicol reverse
5'- CTGCAGCGGCCGCTACTAGTAATTCAGGCGTAGCACCAGGC

sll1653 –deletion construct

M13 forward (PstI)
5'- ACGCTGCAGCATGGTCATAGCTGTTTCC
M13 reverse (XbaI)
5'- CGTTCTAGAGTCGTGACTGGGAAAACC
*1653*_LF forward
5'- GGTTTTCCCAGTCACGACTCTAGAACGGGGTTTGAGTGGGATGAAG
*1653*_LF reverse
5'- CTAGAAGCGGCCGCGAATTCCCTGAGTCGGTTGGGTTAATAG
BB_prefix forward
5'- GAATTCGCGGCCGCTTCTAG
BB_suffix reverse
5'- TACTAGTAGCGGCCGCTGCAG
*1653*_RF forward
5'- TACTAGTAGCGGCCGCTGCAGCATCGCCGCTGGTTTAATG
*1653*_RF reverse
5'-
GGAAACAGCTATGACCATGCTGCAGCGTACGTCACAGATGGTGAAAGAA

3.2. Restriction Cutting

An antibiotic resistance cassette for chloramphenicol resistance were made into a BioBrick compatible construct by PCR amplification using primers containing the BioBrick prefix and suffix sequences (Section 3.2.1). A restriction enzyme digest of the PCR product was set up with EcoRI-HF and SpeI. The plasmid pSB1A3 containing *mCherry* was digested with EcoRI-HF and XbaI to generate a gap in front of the BioBrick for assembly with the antibiotic resistance cassettes into a new BioBrick. One µL of CutSmart buffer (NEB, USA) and 0.25 µL of each enzyme were added to 8.5 µL of each DNA sample. The restriction mixture was incubated at 37°C for 1 hour and inactivated at 80°C for 20 min.

3.3. Separation of DNA Fragments by Gel Electrophoresis

PCR products and DNA fragments generated by restriction cutting were separated by gel electrophoresis to verify the correct length of the products. DNA fragments were separated using 0.8 % (w/v) agarose gels to which 10000x GelGreen™ (Biotium, USA) was added in 1x TAE buffer (40 mM Tris, 20 mM acetic acid and 1 mM EDTA). Running conditions were 85V for 1 hour at room temperature. Prior to loading, samples were mixed with 10x loading dye (0.25% bromophenol blue, 0.25% xylene cyanol FF and 30% glycerol). A 1 kb GeneRuler™ DNA ladder (Thermo Scientific) was utilized for fragment length analysis. DNA was visualized by exposure to UV light and gel images were captured using a GelDoc (BioRad, USA).

3.4. DNA Ligation

Production of recombinant plasmids incorporated two methods; traditional ligation, consisting of specific restriction digests followed by a ligase facilitated ligation, and the SLIC method, using a Gibson Assembly kit.

3.4.1. Restriction Based Cloning

Restriction digests were purified using a QIAquick® PCR purification kit (Qiagen, Germany). A ligation reaction was carried out at an insert to vector molar ratio of 6:1, using 10ng of vector. A 10 µL ligation mixture was set up using 1 µL of 10x T4 DNA ligase buffer, 0.5 µL T4 DNA ligase (NEB, USA) and 8.5 µL of DNA, and was incubated at 4°C overnight. The ligase was inactivated at 65°C for 20 min.

3.4.2. Gibson Cloning

Fragments amplified using specifically designed primers were assembled in a Gibson Assembly Master mix (NEB, USA). One hundred nanograms of plasmid backbone and a threefold excess of inserts were utilized, with a total of 0.2-1.0 pmoles DNA in the reaction. A 20 µL assembly reaction was set up by adding 10µL Gibson Assembly Master mix to the fragments. Samples were incubated in a thermocycler at 50°C for 15 min. Half the assembly mix (10 µL) was used for heat-shock transformation 100 µL of *E. coli* (DH5α).

3.5. Making Competent *E. coli* cells

20 mL of SOC medium was inoculated with a single colony of *E. coli* DH5α and grown in a shaking incubator overnight at 37°C. The overnight culture was diluted by transfer into 300 mL pre-heated ΨB media and allowed to grow to an OD_{600} of 0.3-0.4. Cells were then incubated on ice for 5min, transferred to pre-chilled 50 mL Falcon tubes and centrifuged for 10 min at 4000 rpm at 4°C. Cells were resuspended in 15 mL chilled TfBI solution (pH 5.8) and centrifuged immediately at 4000 rpm for 10 min (4°C). Cell pellets were gently resuspended in 1 mL of chilled TfBII solution (pH 7.0). Competent cells were snap-frozen using dry ice immersed in ethanol, and stored in aliquots of 100 µL at -80°C. Reagents for making competent *E. coli* cells are listed in Table 2.5

Table 2.5 – Reagents for Making Competent *E. coli* DH5α Cells.

ΨB media (500 mL)	2.5 g yeast extract 10 g bactotryptone 0.38 g KCl pH 7.6 with KOH (Autoclave and add 17 mL sterile 1 M $MgSO_4$)
TfBI solution (500 mL)	1.47 g potassium acetate 4.95 g $MnCl_2$ 6.05 g RbCl 0.74 g $CaCl_2$ 75 mL glycerol pH 5.8 with 0.2 M acetic acid (Filter-sterilize and store at 4°C)
TfBII solution (100 mL)	10 mL 100 mM MOPS (pH 7.0) 1.10 g $CaCl_2$ 0.12 g RbCl 15 mL glycerol pH 7.0 with KOH (Autoclave and store at 4°C in the dark)
SOC solution (1 L)	20 g bactotryptone 5 g yeast extract 0.584 g NaCl 0.186 g KCl (Autoclave and add 10 mL of sterile 1 M $MgSO_4$ and 20 mL of sterile 1 M glucose)

3.6. Heat-Shock Transformation of Competent *E. coli* cells

Competent cells were thawed on ice for 5-10min. Ligation mixture DNA (10 µL) was added and cells were incubated on ice for a further 30 min. Cells were then subjected to 42°C for 45 seconds followed by a further 2 min on ice. Five hundred µL of LB medium (Table 2.6) was added and cells were incubated at 37°C with 225 rpm shaking for 1 hour. Cell culture (50 µL) was spread directly onto an LA (Table 2.6) plate with appropriate antibiotics. The remaining 450 µL was centrifuged for 1 min at 8000 rpm, resuspended in 50 µL LB media, and spread on a second LA plate. Plates were incubated overnight at 37°C.

Table 2.6 – Medium and Antibiotic Additions for *E. coli* Growth.

LB medium (1L)	10 g tryptone 10 g NaCl 5 g yeast extract	
LA medium (1L)	15 g agar Added to LB medium	
Antibiotic additions	**Stock concentration**	**Final concentration**
Kanamycin	50 mg/mL	50 µg/mL
Chloramphenicol	30 mg/mL	30 µg/mL

3.7. Small-Scale Plasmid Isolation

Plasmid DNA was isolated from liquid, overnight cultures of *E. coli* using a Wizard® Plus SV miniprep kit (Promega, Madison USA).

3.8. Transformation of *Synechocystis* 6803

Liquid cultures were grown in the presence of glucose to an OD_{750} of 0.4-0.5. Cells were centrifuged at 2500 g for 10 min and suspended in 0.5 mL BG11 medium to a final OD_{750} of 2.5. Approximately 5 µg of plasmid DNA was added the concentrated cells and incubated at 30°C for 6 hours with 30 µE $m^{-2}s^{-1}$ irradiation and gentle shaking at the 3 h mark. Negative controls with no DNA were also included. Samples were spread over sterile nucleopore Track-Etch membranes (Whatman, UK) on BG11 plates supplemented with glucose and incubated for 12 h. The filters, with cells attached, were then transferred to plates containing glucose and the appropriate antibiotic. After two weeks, single colonies were picked and streaked-out weekly for three weeks to ensure complete segregation. Colony PCR was used to verify complete segregation.

4. Phenotypic Characterizations

The single gene deletion strain, *Synechocystis* 6803 Δ*sll1653*, was generated by molecular biology techniques described above and the resulting phenotype was characterized. Measurements of growth, oxygen consumption and generation were carried out, in addition to the analysis of photosynthetic pigments by spectroscopic techniques. Lipids were extracted to detect differences in the lipid composition between species according to the methods developed for lipid extraction, separation and characterization.

4.1. Growth Curve

BG11 solid medium was prepared as described above. In addition, BG11 medium containing a high concentration of salt (400 mM) was prepared. Agar plates without additions and with addition of glucose and glucose/DCMU were poured for both low salt and high salt media. Wild-type and Δ*sll1653* strains were spotted onto plates (5 µL cells) at an OD of 1.0, 0.1 and 0.01, with three replicates for each strain and OD (Figure 2.2). Plates were incubated at 30°C in normal light (200 µE/m^2s) and high light (500-700 µE/m^2s). Images were taken at start of the growth experiments, then twice a day for four days, and once a day the remaining three days.

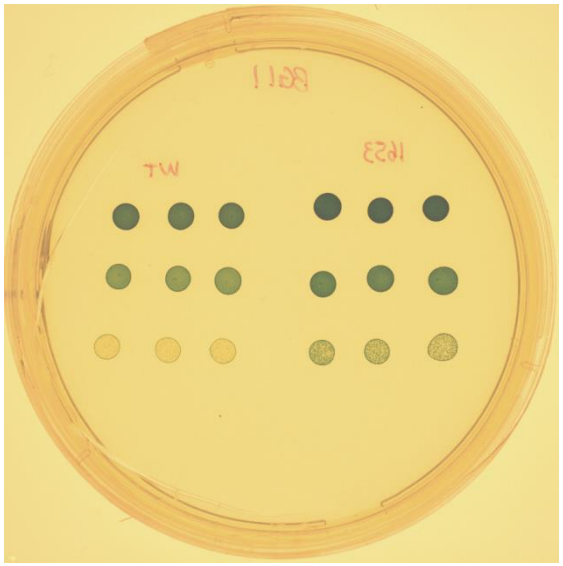

Figure 2.2 – Agar Plate for Generation of Growth Curve. Wild-type (left) and Δsll1653 mutant strain (right) spotted onto BG11 agar plate at an OD of 1.0 (top), 0.1 (middle) and 0.01 (bottom)

4.1.1. Plate-Imager

The sample, grown on a agar containing specific media, was placed on the custom-built imaging stage (Fig. 2.3) and subjected to a broad spectrum, diffuse, LED light (IKEA, Sweden) source from beneath. A digital camera (EOS M, Canon), housed opposite to the sample, imaged the resulting light pattern formed. The Canon EOS M was used to capture RAW images, which reflect the uncorrected signal detected by each photodiode.

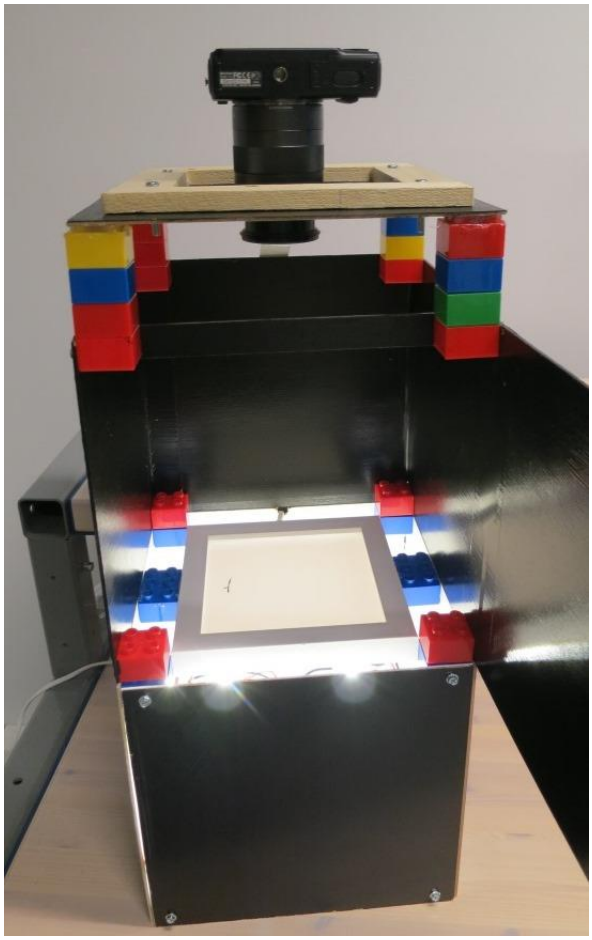

Figure 2.3 – Plate-Imager. Custom-designed imaging system for generation of solid-media growth curves.

4.1.2. Calculation of Cell Density Values

RAW image files were used in a series of Python scripts to calculate cell densities and generate growth curves. First, RAW images of a single plate imaged at different time points were assembled into RGB image stacks (MRC format) and the time points of image

acquisition were determined and stored. Images within the image stacks were aligned by hand using the program midas included in the IMOD package (http://bio3d.colorado.edu/imod/). Secondly, grey-scale images consisting of the combined RGB were computed. The imod packages were used to mark the position of colonies within each stack. Third, custom made Python scripts calculated the cell density values for individual colonies in each stack. This density data was saved in a separate file together with the image acquisition time points. Growth curves were constructed from this data by correcting for the agar background.

The doubling time (DT) of *Synechocystis* 6803 and Δ*sll1653* strains on different media were calculated using equation 2.2;

$$DT = (\Delta t \times \ln 2) / \ln \frac{D2}{D1} \qquad \text{[Equation 2.2]}$$

where D_2 and D_1 are the cell density values at the end and the beginning of the time interval (t) that spans the exponential growth phase, respectively. The doubling time describes the time required for the cell to divide or for the population to double, and is given in hours/doubling.

4.2. Oxygen Evolution

Evolution of oxygen was measured in *Synechocystis* wild-type and Δ*sll1653* mutant strain upon exposure to increasing light intensities. *Synechocystis* cells were centrifuged and resuspended in BG11 medium to a final chlorophyll concentration of 10 µg/mL. $NaCO_3$ (4 %) was added to avoid depletion of CO_2 during measurements. Oxygen evolution was recorded using an Oxygraph electrode (Hansatech Instruments, UK), calibrated with air-saturated water and 100 mM sodium dithionate (zero oxygen). Illumination was provided by a multi-color PAM (Heinz Walz GmbH, Germany) by setting up a light curve according to Table 2.7 using the PamWin-3 software.

Table 2.7 – Light Curve Conditions for Measuring Oxygen Evolution. The photosynthetically active radiation (PAR) is given in units of µmol photons $m^{-2}s^{-1}$ and intensity as relative units.

Step	1	2	3	4	5	6	7	8	9	10	11	12	13	14	15	16	17	18	19	20
PAR	55	87	55	173	55	316	55	568	55	1016	55	1554	55	2174	55	2950	55	3967	55	5355
Intensity	0	2	0	4	0	6	0	8	0	10	0	12	0	14	0	16	0	18	0	20
Time	30	180	30	180	30	180	30	180	30	180	30	180	30	180	30	180	30	180	30	180

4.3. Respiration Rate

The respiration rate of *Synechocystis* wild-type and Δ*sll1653* mutant strain was determined in the absence and presence of glucose using an Oxygraph electrode (Hansatech Instruments). Cells were suspended in BG11 to an OD_{750} of 2.0 and placed in an airtight chamber in the dark with stirring (100 rpm). Oxygen concentration was recorded for 7 min, with the addition of glucose after 3 min.

4.4. Absorption and Fluorescence Spectroscopy

Differences in the synthesis of photosynthetic pigments and the overall state of the photosynthetic machinery were evaluated in both the wild-type and the gene deletion strain using spectroscopic techniques.

4.4.1. Chlorophyll Concentration

Chlorophyll concentration was determined for the cell cultures by suspending 100 µL of concentrated cells in 1 mL methanol, centrifuge at 13 000 rpm (5 min) and measure the OD_{663} of the supernatant using glass cuvettes. Chlorophyll concentration was calculated according to equation 2.4:

$$Chl\ conc. = \frac{OD_{663} * dilution\ factor}{82} \qquad \text{[Equation 2.4]}$$

The concentration is given in mg/mL Chl *a*.

4.4.2. *In Vivo* Absorption

Cell absorption spectra were determined using a Hitachi U-3010 spectrophotometer with an integrating sphere (150 mm). *Synechocystis* wild-type and Δ*sll1653* mutant strain were grown in BG11 liquid and were harvested and resuspended in BG11 to an OD_{750} of 0.3. Absorption spectra were run at a sampling interval of 1.00 nm and a scan speed of 300 nm/min to achieve a high resolution spectrum in the 400-800 nm region. The spectra were normalized by subtracting the average of the tail (750-800 nm).

4.4.3. 77 K Fluorescence

Fluorescence emission spectra were measured at 77K with a Triax-320 imaging spectrograph (Horiba). Cells were suspended in BG11 to a final OD_{750} of 1.0 and transferred into glass tubes prior to freezing in liquid nitrogen. Chlorophyll *a* and phycobiliproteins were excited at 440 and 580 nm, respectively, and fluorescence emission was detected in a scan from 650 to 800 nm. Traces were normalized to the PS I peak at 724 nm (chlorophyll *a*) and 722 nm (phycobilisomes).

To assess whether a change in the ratio of chlorophylls or phycobilisomes associated with the two different photosystems could be observed upon a transition from aerobic to anaerobic conditions, wild-type and Δ*sll1653* strain were grown anaerobically by bubbling with argon

gas. Samples were taken at start and after 10, 20, 40 and 80 min, followed by freezing in liquid nitrogen and measurement of fluorescence emission.

4.4.4. PAM Fluorescence

Simultaneous oxygen and chlorophyll fluorescence measurements were recorded using a setup that combined an Oxygraph electrode (Hansatech Instruments) and a multi-color PAM fluorometer (Heinz Walz GmbH). *Synechocystis* wild-type and mutant (Δ*sll1653*) strain were diluted in BG11 to an OD_{750} of 2.0 and transferred into an air-tight compartment in the dark. Pulse modulated fluorescence was induced by a low intensity (setting: 10, 1016 µmol photons $m^{-2}s^{-1}$) measuring light (625 nm) and maximum fluorescence yield (F_M) was obtained by applying a white saturating light pulse of full intensity (setting: 20, 5355 µmol photons $m^{-2}s^{-1}$) every 60 seconds. Cells were subjected to depletion of oxygen by addition of glucose and glucose oxidase (4.5 U/mL). DBMIB was added to block electron transfer at the b_6f complex. Fluorescence data was recorded for 80 min with a modulation frequency of 100 Hz. A Python script was applied to reduce the data volume by 1:10 in the F_0 regions, while keeping all measurements in the F_M regions.

4.5. Lipid Analysis

Lipids were extracted from *Synechocystis* 6803 and Δ*sll1653* strain and the extracts were analyzed by LC-MS. Cells were grown photoautotrophically and samples were taken at the start of the experiment, after 16, 18, 20, 21, 22, 23 and 24 hours to make conditions anaerobic.

Sixty milliliters were harvested and resuspended in a cryotube with 1 mL BG11. Cells were centrifuged at 13,000 rpm for 2 min and the tubes were covered with aluminum foil, followed by incubation at 30°C to allow cells to consume oxygen present causing the transition into anaerobic conditions inevitable. The sample taken after 24 hours was not subjected to anaerobic conditions and functioned as an aerobic control. Lipid extraction was initiated immediately after the last sample had been taken.

Thirty micrograms of cells was suspended in 200 µL chloroform/methanol (2:1) and centrifuged at 13 000 rpm for 2 min. Two sequential extractions were performed and then

extracts were combined. The organic phase extracts were dried under a stream of nitrogen at 30°C. Residues were suspended in 200 µL of chloroform and subjected to separation and characterization by LC-MS.

Samples were analyzed in a system consisting of a Waters Acquity UPLC™ (Milford, USA) coupled to a Waters Synapt G2 MS QTOF equipped with an ESCI source. Separation was performed in an Acquity BEH C18 column (50 x 2.1 mm, 1.7 µm) using methanol + 0.05 % formic acid as mobile phase A and dichloromethane as mobile phase B under the following conditions: 1 % B for 5 min, 50 % B for 2 min and 99 % B for 4 min. Other parameters were set as described in section 2.3. The data acquired was processed using MassLynx version 4.1 and the TransOmics Platform (Waters, USA) and standardized relative abundance of lipids were calculated according to equation 2.5 and 2.6:

$$Standardized\ abundance = \frac{detection\ signal\ lipid}{detection\ signal\ chlorophyll\ a + \text{pheophytin}} \quad \text{[Equation 2.5]}$$

$$Relative\ abundance\ to\ Chl\ a\ = \frac{standardized\ abundance\ for\ lipid}{standardized\ abundance\ for\ Chl\ a} * 100 \quad \text{[Equation 2.6]}$$

Chapter 3: Results

1. Introduction

The primary aim of this research was to investigate photosynthetic lipids produced by the cyanobacterium *Synechocystis* 6803, with a particular focus on isoprenoid quinones. Secondary objectives were the development of methods for analysis of photosynthetic lipids, evaluation of the biosynthetic pathway of plastoquinone in cyanobacteria and the assessment of a potential shift in quinone composition under limiting oxygen conditions. In order to detect differences in lipid composition as a consequence of environmental or genetic manipulation, methods for extraction, separation and characterization of chlorophylls, carotenoids and isoprenoid quinones were optimized. Candidate genes that might be involved in the biosynthetic pathway of plastoquinone in cyanobacteria were identified through *in silico* analyses. The candidate gene *sll1653* was genetically deleted in *Synechocystis* 6803 followed by the characterization of the resulting phenotype using techniques within spectroscopy and mass spectrometry. The operating efficiency of the photosynthetic machinery and the composition of quinones upon depletion of oxygen were also evaluated in both wild-type and mutant strain.

2. Optimization of Lipid Extraction, Separation and Characterization

Conditions for extraction, separation and characterization of lipids from *Synechocystis* 6803 were optimized to detect chlorophylls, carotenoids and isoprenoid quinones simultaneously. An overview of the photosynthetic lipids that are expected to be synthesized in *Synechocystis* 6803 is provided in Appendix I, with their chemical structure, molecular mass and light absorption maximum. Data that forms the basis for the presented results are given in Appendix III.

2.1. Extraction of Photosynthetic Lipids

Lipids, in particular chlorophylls and carotenoids, have historically been extracted using a mixture of methanol and chloroform (Bligh and Dyer, 1959; Folch *et al.*, 1957). These protocols include multiple steps to isolate and purify total lipids from cell material. Methods for isolation of photosynthetic lipids have commonly been developed for plant tissues. However, the simultaneous isolation of chlorophylls, carotenoids and quinones has thus far not been extensively studied in cyanobacteria. Based on previous studies (Martinis *et al.*, 2011; Bligh and Dyer, 1959), different extraction solvents were evaluated for their extraction yields of photosynthetic lipids in a simple one-step procedure.

The solvent systems MeOH:$CHCl_3$ (2:1), $CHCl_3$:MeOH (2:1), IPA and THF were evaluated for their extraction yield of photosynthetic lipids from *Synechocystis* 6803. A total of three extractions were carried out and extracts were evaluated by absorption spectroscopy. Figure 3.1 shows the visual differences between extracts and Figure 3.2 provides a comparison between the three sequential extractions for each solvent systems.

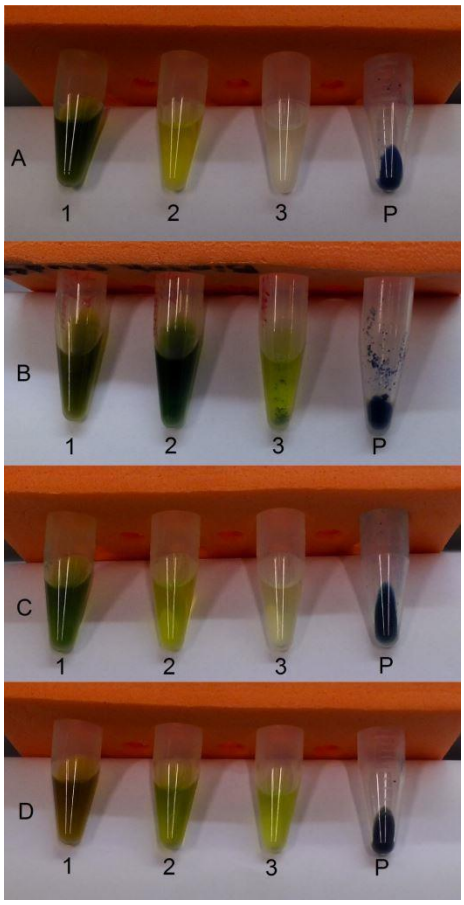

Figure 3.1 – Lipid Extracts and Pellets. Different solvent systems were evaluated for the extraction yield of photosynthetic lipids from *Synechocystis* 6803. A: MeOH/$CHCl_3$ (2:1), B: $CHCl_3$/MeOH (2:1), C: IPA and D: THF. Numbers represent the sequential extracts and P is the pellet left after three extractions.

Color of an extract provides a good indication of whether photosynthetic lipids have been extracted from the cells. The extracts (Fig. 3.1) had similar colors, except for the first extraction with THF which was browner than the others. The green color was predominant due to chlorophyll *a*, easily identified in the absorption spectra (peaks at 435 and 665 nm). Carotenoids provide the shoulder of the peak in the 400-500 nm region and the yellow color of the extracts. Isoprenoid quinones absorb in the UV region and are not visible by naked eye. In the absorption spectra, however, peaks were observed in the 250-320 nm region. A blue color of the pellet is to be expected if the PBPs remain in the cell and are not extracted in the organic solvent phase, which was also observed.

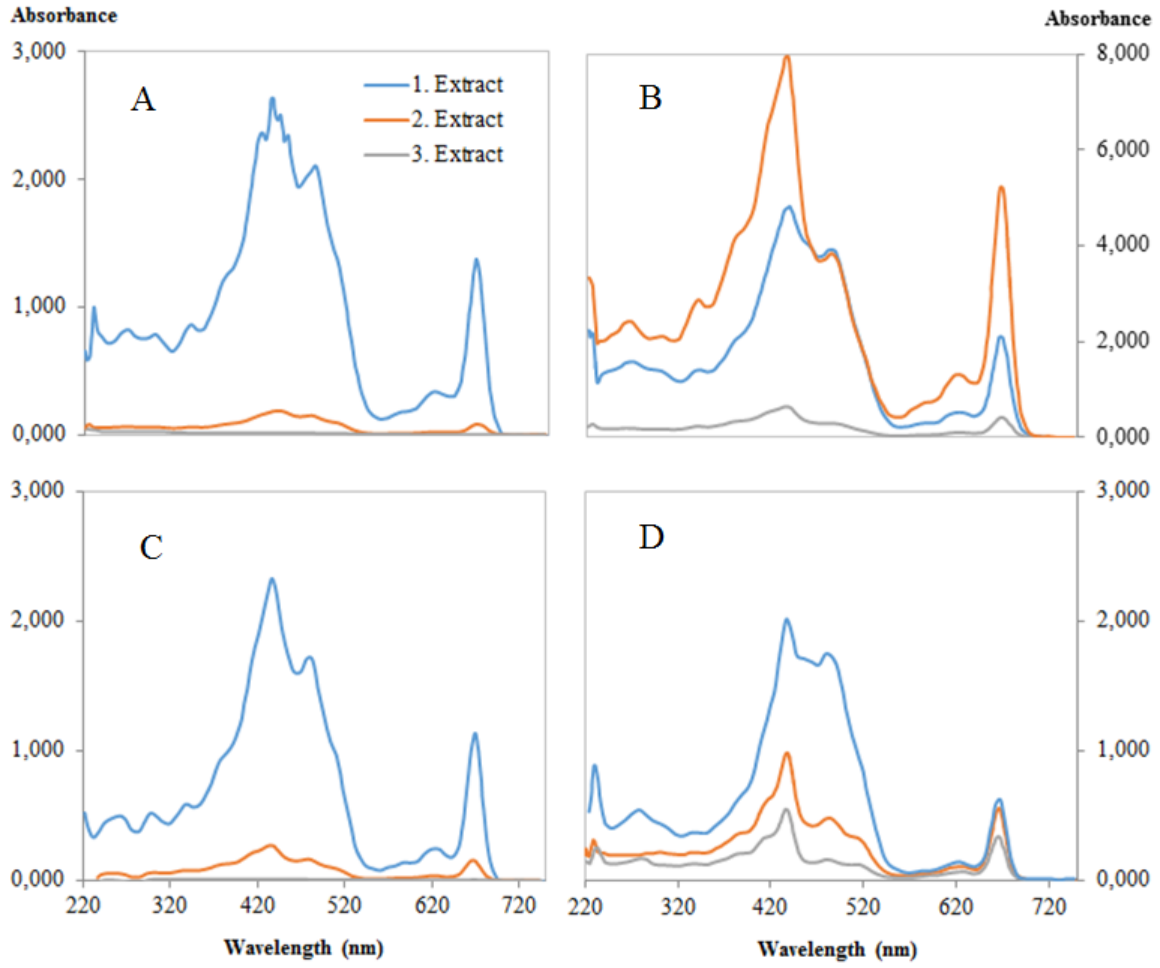

Figure 3.2 – Absorption Spectra of Lipid Extracts. First (blue), second (orange) and third (grey) lipid extract from *Synechocystis* 6803 using A; MeOH:$CHCl_3$ (2:1), B; $CHCl_3$:MeOH (2:1), C; IPA and D; THF as extraction systems. Spectrum B has a different absorbance scale due to the high absorbance measured for this extract.

The highest absorbance and therefore extraction of pigments was measured for the first extraction for all solvent systems except for $CHCl_3$:MeOH (Fig. 3.2A), in which the second extraction provided the highest peak. For both IPA and MeOH:$CHCl_3$, it was mainly the first extract that were rich in pigments whereas pigments can be found in all three extracts with THF and $CHCl_3$:MeOH. This can also be seen by the color of the extracts.

Figure 3.3 compares the absorption spectra of the first extract for all solvent systems. Conditions for extraction were identical, only varying in the extraction solvent system utilized. Hence, the absorption measured can be compared between solvent systems to assess which system is best suited for extraction of photosynthetic lipids. The measured absorbance

was highest for the extraction with $CHCl_3$:MeOH, more than a three-fold higher compared to that measured for extraction with THF (chlorophyll peak at 665 nm). Extraction using $CHCl_3$:MeOH and THF seems to be efficient in extracting isoprenoid quinones which absorb in the 250-330 nm region. Chlorophyll and carotenoids are readily detected in all extracts, although the highest yield was observed for extraction with $CHCl_3$:MeOH.

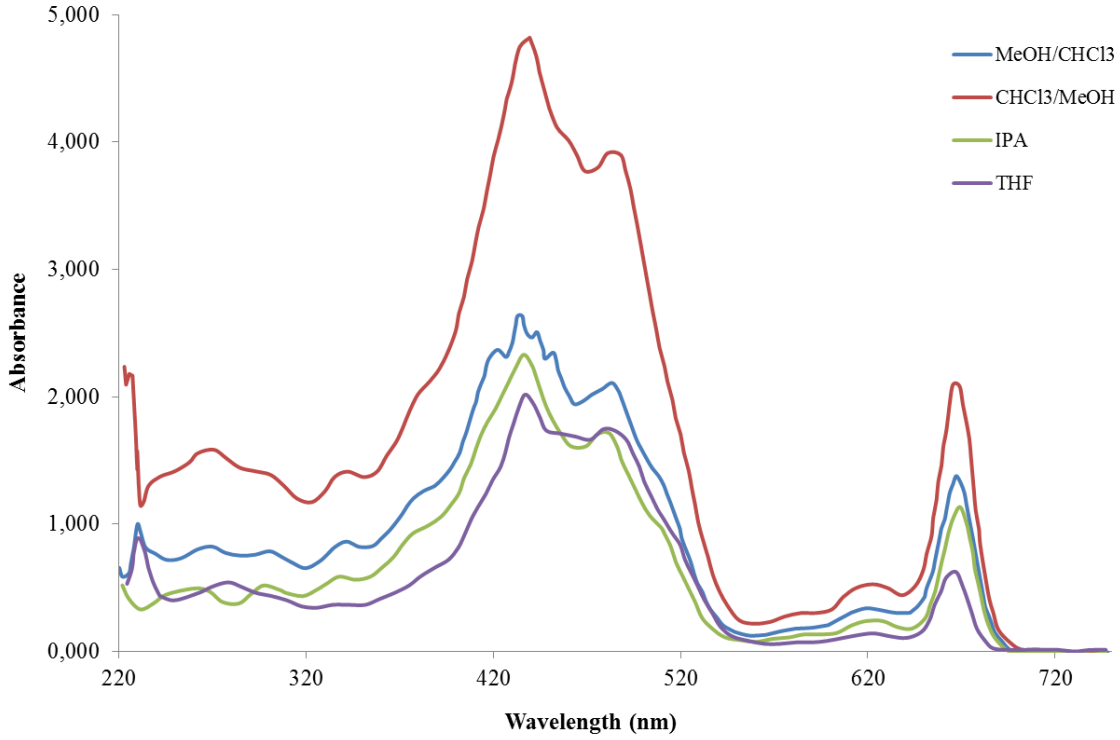

Figure 3.3 – Comparison between Extraction Solvent Systems. Photosynthetic lipids were extracted from *Synechocystis* 6803 using MeOH:$CHCl_3$ (2:1) (blue), $CHCl_3$:MeOH (2:1) (red), isopropanol (green) and tetrahydrofuran (purple). Traces represent the first extraction made.

2.2. Separation by TLC

Photosynthetic lipids extracted from *Synechocystis* 6803 were separated by TLC using the development systems hexane-acetone (70:30), hexane-chloroform (60:40), hexane-chloroform (75:25) and pure hexane. These solvent systems were evaluated for the ability to separate chlorophylls, carotenoids and isoprenoid quinones.

Hexane-acetone proved to be a well-suited development system for the separation of carotenoids and chlorophylls. All bands were visible by eye (Fig 3.4) and no further bands were observed under UV-light. The evaporation of IPA from the plate did not take place as fast as for the other solvent systems, causing an incomplete separation of components.

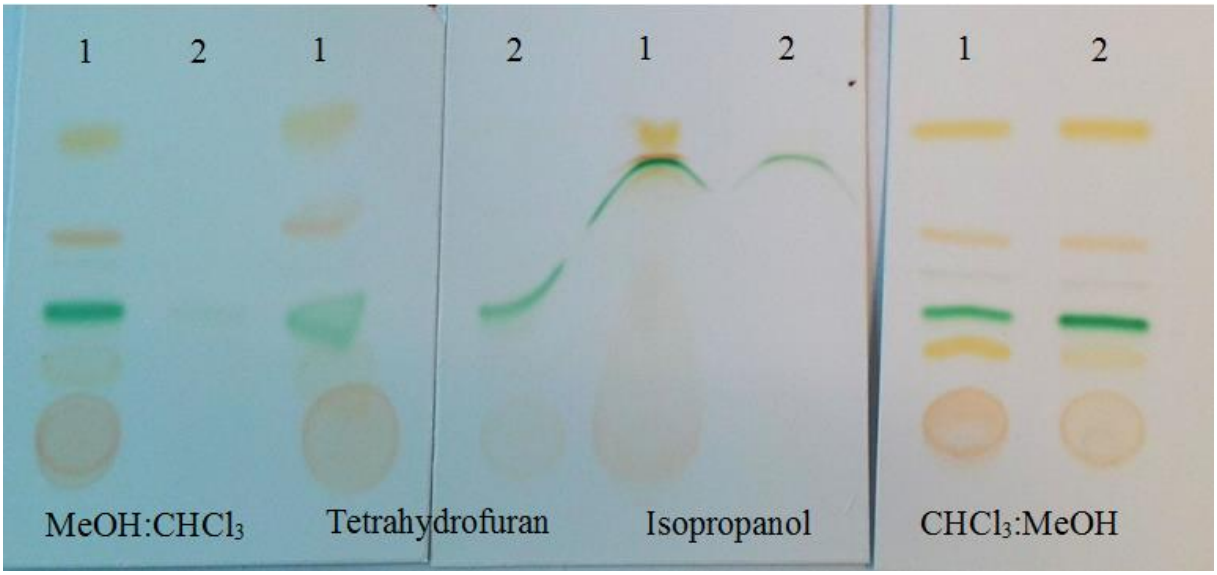

Figure 3.4 – TLC Separation of Extracts by Hexane-Acetone. Lipid extracted from *Synechocystis* 6803 using MeOH:$CHCl_3$, tetrahydrofuran, isopropanol and $CHCl_3$:MeOH as extraction solvents, separated on TLC plates using hexane-acetone (70:30) as development system. Numbers represent the first and second extract made.

Again, the extraction solvent chloroform-methanol (2:1) stands out as the best choice for extracting chlorophyll and carotenoids. Bands are stronger and sharper than for the other extraction systems when separated by TLC. The bands were scraped off the plate and dissolved in methanol, and the isolated compounds were identified by absorption spectroscopy. Table 3.1 provides an overview of the components in the $CHCl_3$:MeOH extract

separated by TLC using hexane-acetone as development system, with their respective absorption peaks and R_f-value.

Table 3.1 – Pigments Separated by TLC using Hexane-Acetone as Development System. Lipids were separated on TLC plates with hexane-acetone (70:30) after extraction with $CHCl_3$:MeOH from *Synechocystis* 6803. Absorption by pigments dissolved in methanol was determined by spectroscopy and absorption maxima are indicated in bold. Retention ratios (R_f) were calculated according to equation 2.1.

Band no. (from bottom up)	**Color**	**Absorption peaks** (nm)	**Retention ratio** (R_f)	**Identified as**
1	Yellow-orange	-	0.19	Xanthophyll
2	Green	**435**, 620, 665	0.26	Chlorophyll *a*
3	Grey	**420**, 665	0.34	Pheophytin *a*
4	Orange	**460**	0.43	Echinenone
5	Yellow	430, **450**, 475	0.65	β-carotene

Plastoquinone could be separated from the rest of the lipids in the extract using hexane-chloroform (75:25) as a development solvent. The band was visualized under UV-light (Fig 3.5) and an R_f-value of 0.54 was calculated for plastoquinone. Two additional bands with a yellow/orange color were observed under normal light. Absorption spectroscopy of the UV-detectable compound isolated from the TLC plate revealed an absorption peak at 255 nm, indicating the presence of oxidized plastoquinone in the extract. Hexane did not ensure separation of any of the extract components and was hence unsuited as a development solvent for TLC separation of photosynthetic lipids. A band could be detected under UV-light when TLC plates were developed with hexane-chloroform (60:40), but this band was weaker than for development with hexane-chloroform (75:25). Phylloquinone could not be detected by TLC separation with any of the development systems tested.

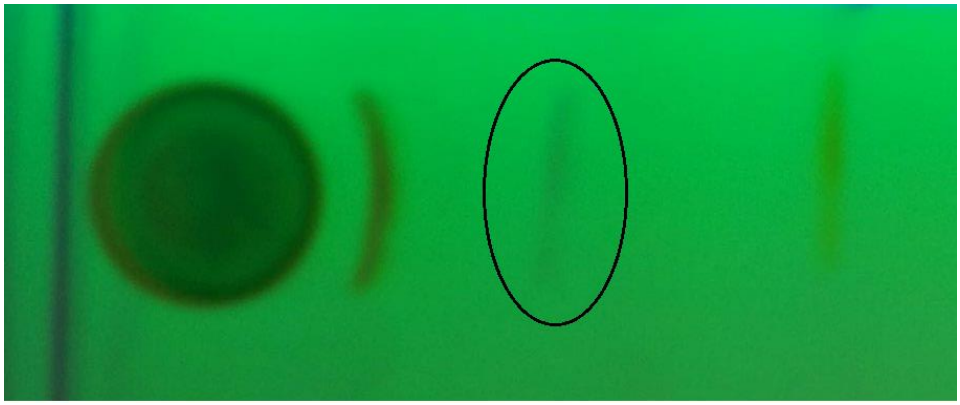

Figure 3.5 – Thin-layer Chromatogram for Plastoquinone. Photosynthetic lipids extracted with $CHCl_3$:MeOH from *Synechocystis* 6803 were separated by TLC using a mixture of hexane and chloroform (75:25) as development system. The circled band (plastoquinone) was detected under UV light whereas the other bands could be seen by naked eye.

2.3. Characterization by LC-MS

Current protocols for the separation of all photosynthetic lipids using liquid chromatography are challenging and laborious due to the wide span of compound polarities. A gradient that starts with a relatively polar mobile phase and that ends up using a non-polar mobile phase should be applied on a reverse-phase column to elute all compounds of interest. Samples are ideally dissolved in a solvent with a similar polarity to the starting mobile phase, and all components must be soluble in this solvent. Conditions for separating chlorophylls, carotenoids and isoprenoid quinones by UPLC and the consecutive ionization and determination of their masses by qTOF-MS were evaluated. Standards of chlorophyll *a*, β-carotene and the quinones α-tocopherol and ubiquinone were utilized to optimize parameters for reverse-phase chromatography using C18 columns. Three different gradients were tested; MeOH (A) – IPA (B), MeOH/H_2O (A, 80:20) – dichloromethane (B, DCM) and MeOH (A) – DCM (B) for separation of the standards. Electrospray (ESI) and atmospheric pressure (APCI) were compared in positive ionization mode using the same standards.

Separation of the standards proved to be difficult using MeOH– IPA as a gradient due to the marginal eluting power for the most non-polar compounds such as β-carotene and ubiquinone. The second gradient evaluated, MeOH/H_2O – dichloromethane gave poor separation, as could be seen by split peaks and compounds eluting over the entire chromatogram. The best

gradient proved to be the MeOH-DCM, for which all standards could be separated under the same conditions. Chromatograms of all standards are given in Appendix III.

Electrospray ionization in the positive mode provided the best mass spectra and molecular ion radicals $[M]^+$ could be detected for all standards. The resolution of the chlorophyll *a* standard was low and the compound could only be detected from ESI in positive mode. The base peak of chlorophyll *a* was 907.52 although the expected mass (893.49) could be observed at the same retention time in addition to a mass of 871.57. Ionization of β-carotene could be carried out by both APCI and ESI, although APCI produced a molecular ion of higher mass than expected (567.46). Ubiquinone and α-tocopherol could be detected from both APCI and ESI. The retention times and the mass-to-charge ratio in positive APCI and ESI modes for all standards are given in Table 3.2 and mass spectra are provided in Appendix III. Data recorded for the diode array was not included due to an offset in the 350-500 nm region caused by a calibration error on the instrument that occurred after a manufacturer certified maintenance.

Table 3.2 – Retention Times and Masses of Standards Detected by UPLC-APCI/ESI-qTOF-MS. Mass-to-charge (*m/z*) ratios were detected from APCI and ESI in positive ionization mode, 'nd' is given if the compound was not detected in the resulting mass spectrum.

Standard	**Retention time**	**APCI (+)**		**ESI (+)**	
	min	ion	*m/z*	ion	*m/z*
chlorophyll *a*	1.98	nd	nd	$[M+H]^+$	893.54
β-carotene	3.36	$[M+H]^+$	567.46	$[M+H]^+$	536.43
ubiquinone	4.01	$[M+Na]^+$	885.68	$[M+Na]^+$	885.68
α-tocopherol	1.61	$[M]^+$	429.38	$[M]^+$	429.38

3. *In Silico* Analysis of Cyanobacterial Plastoquinone Synthesis

The biosynthetic pathway of plastoquinone in cyanobacteria remains unresolved. However, the identification of 4-hydroxybenzoate (PHB) as the head group precursor for plastoquinone biosynthesis in cyanobacteria gave rise to the hypothesis that ubiquinone and plastoquinone synthesis are evolutionary related (Sadre *et al.*, 2012; Hohmann-Marriott and Blankenship, 2011). If these pathways share a common core of enzymes, homologous genes will be found in both cyanobacteria and species that synthesize ubiquinone, such as *E. coli*. Candidate genes and enzymes were identified using online resources.

KEGG (Kyoto Encyclopedia of Genes and Genomes) is a comprehensive genome database providing information about gene annotations and functional assignment of these genes into metabolic pathways. This database is a good resource for understanding biological systems from the molecular level (Kanehisa, 2000). Cyanobase contains sequencing data from cyanobacterial species, and also provides information about the location of genes and the function of the gene products (Nakamura *et al.*, 1998). Both KEGG and Cyanobase can easily be connected to BLAST (Basic Local Alignment Search Tool), a program utilized to compare a query nucleotide or protein sequences to reference sequences in a database (Altschul *et al.*, 1990). The output from BLAST is the expectation value "E", which expresses the statistical significance of the matches. This parameter describes the number of hits that are expected to be received by chance, when searching a database of a certain size. If the E-Value is closer to "0" the "significance" of the match is higher. Matches with an E-value lower than 10e-6 were regarded as related, having a similar function as the query gives rise to.

3.1. Identification of Candidate Genes in *Synechocystis* 6803

Based on knowledge about the synthesis of ubiquinone in *E. coli* (Fig. 1.8), a likely synthesis pathway from PHB to plastoquinol was constructed and is presented in Figure 3.6. In this scheme, prenylation of 4-hydroxybenzoate is followed by a decarboxylation catalyzed by an enzyme homologous to the 3-octaprenyl-4-hydroxybenzoate decarboxylase in *E. coli*. A hydroxyl group is then introduced by a monooxygenase followed by one or multiple C-

methyltransferase(s) that catalyze the attachment of two methyl group onto the quinone ring structure.

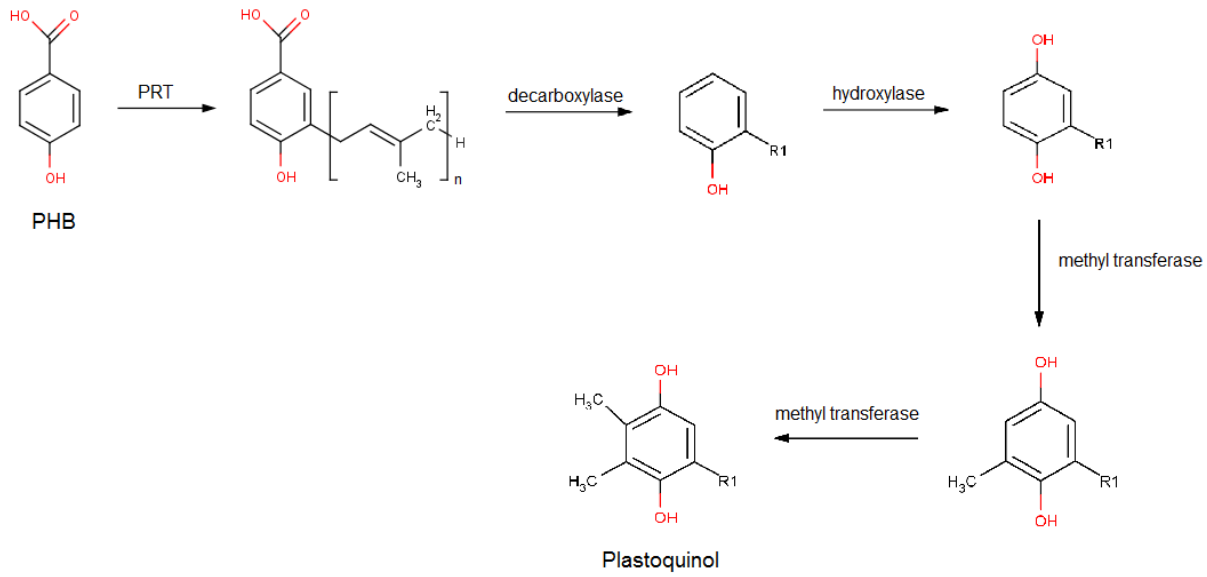

Figure 3.6 – Hypothesized Pathway for Plastoquinone Synthesis in Cyanobacteria. The biosynthesis of plastoquinol from the aromatic precursor 4-hydroxybenzoate (PHB), catalyzed by a prenyltransferase (PRT), a decarboxylase, a hydroxylase and two methyltransferases.

Sadre *et al.* (2012) previously identified 4-hydroxybenzoate solanesyltransferase, encoded by *slr0926*, as the prenyltransferase (PRT) involved in plastoquinone synthesis in *Synechocystis* 6803. Candidate enzymes involved in the decarboxylation, hydroxylation and methylation reactions of the quinone ring were identified through BLASTP searches. BLASTP allows a protein query (sequences for proteins involved ubiquinone synthesis in *E. coli* K-12 MG1655) to be compared to protein sequences in a database, in this case the genome database for *Synechocystis* 6803 (taxid: 1148).

The genes *ubiD* and *ubiX* encode isofunctional enzymes with 3-octaprenyl-4-hydroxybenzoate lyase (decarboxylation) activity in the biosynthesis pathway of ubiquinone in *E. coli* (Zhang, H. and Javor, 2003). BLAST identified the gene product of *sll0936* in *Synechocystis* 6803 as a homolog to UbiD with an E-value of 9e-152 and an identity of 45 %. This gene is listed in CyanoBase to be 1506 nucleotides is length and is translated into a 501 amino acids long peptide. BLAST describes Sll0936 as a hypothetical protein whereas

Cyanobase annotates the gene product as a putative oxidoreductase. The UbiX homolog in *Synechocystis* 6803 was identified as the gene product of *slr1099*, an aromatic acid decarboxylase, with an E-value of 2e-43 an identity of 42 %. The gene is 621 nucleotides long and encodes a 206 amino acids long product.

Three FAD-dependent hydroxylases (monooxygenases) function in ubiquinone synthesis in *E. coli*; UbiB, UbiH and UbiF (Meganathan, 2001). They catalyze the hydroxylation reactions at position 6, 4 and 5 of the quinone ring, respectively. Whereas UbiB and UbiF add hydroxyl groups that are further subjected to O-methylation reactions, UbiH incorporates the oxygen involved in the redox reactions of the quinone ring. BLAST identified an ABC1-like hypothetical protein (Sll0095) as a homolog to UbiB in *Synechocystis* 6803, with an E-value of 6e-58 and an identity of 32 %. ABC1-like proteins are essential for electron transfer in the *bc1* complex in yeast in addition to its involvement in ubiquinone production in *E. coli*. The protein sequences of both UbiH and UbiF produced a hit to the protein encoded by *slr1300* in *Synechocystis* 6803 (E-values of 3e-58 and 4e-59 and identities of 32 and 34 %, respectively). This protein is annotated as a FAD-binding monooxygenase with a conserved site for hydroxylation of ubiquinone.

In *E. coli*, the genes *ubiG* and *ubiE* encode methyltransferases for the O- and C-methylation steps in ubiquinone synthesis, respectively. UbiE has also been shown to be involved in the synthesis of menaquinone in this organism (Lee *et al.*, 1997)No significant matches to *ubiG* were found in *Synechocystis* 6803, although several proteins were found to possess the S-adenosylmethionine methyltransferase superfamily domain. The protein sequence for UbiE produced a hit in *Synechocystis* 6803 to a methyltransferase encoded by the gene *sll1653*, with an identity of 31 % and an E-value of 2e-34. Other matches of relevance included the genes *slr0407*, *sll0829* and *slr1618*, which encode hypothetical proteins in *Synechocystis* 6803 but are annotated as ubiquinone/menaquinone methyltransferases in other cyanobacterial species (Appendix II).

3.2. Identification of Homologs in Other Cyanobacterial Species

To assess whether the candidate genes are involved in plastoquinone synthesis in *Synechocystis* 6803, they can be genetically deleted, followed by an analysis of the phenotype

in the strain carrying the deletion. As plastoquinone is an essential component of the photosynthetic ETC, identifying the presence of putative orthologs in other cyanobacterial species is a straight forward way of verifying an essential function of the candidate genes. Such genes were identified through blast2 reciprocal best hit pairs between the identified gene in *Synechocystis* 6803 and genome databases for cyanobacteria (taxid: 1117), using Cyanobase as a resource. The identified orthologs in 14 cyanobacterial species are listed in Appendix II.

A high sequence similarity (>86 %) was found between the putative decarboxylase Sll0936 and orthologous genes in other cyanobacterial species, such as *Anabaena* sp. PCC 7120, *Nostoc punctiforme* ATCC 29133 and *Microcystis aeruginosa* NIES-843. For the putative decarboxylase Slr1099 sequence similarities were lower compared to Sll0936, in which 76.0 %, 77.5 % and 77.6 % was identical to the query *slr1099* in the same species, respectively. A hit in *Cyanothece* sp. PCC 8801, described as a 3-octaprenyl-4-hydroxybenzoate carboxylase, was 80.9 % identical to the *sll1099* gene.

Orthologs of the putative hydroxylase Sll0095 were described as hypothetical proteins in most cyanobacterial species, although some were described as ABC-1 domain proteins. The ortholog in the purple bacterium *Rhodopseudomonas palustris* CGA009 was described as the ubiquinone biosynthesis protein AarF (renamed UbiB), but only shared 27.8 % sequence identity with the *sll0095* gene. The putative hydroxylase Slr1300 produced hits to hydroxylases described to be involved in ubiquinone synthesis in many cyanobacterial species, although sequence similarities were quite low (~50 % or lower).

The putative methyltransferase Sll1653 in *Synechocystis* 6803 is orthologous to enzymes described as menaquinone biosynthesis methyltransferases in most cyanobacterial species. Sequence identities range from 27.8 % in *Rhodopseudomonas palustris* CGA009 to 64.2 % in *Synechococcus* sp. PCC 7002. Hits to the *slr0407* gene are described as probable methyltransferases or ubiquinone/menaquinone methyltransferases with sequence similarities around 30 %. The same description is given for orthologs of Sll0829 but with overall higher sequence similarities (up to 60 %) compared to Slr0407. The *slr1618* gene was found to have orthologs in many cyanobacterial species described as putative methyltransferases of type 11 and 12, with sequence identities around 30 %.

4. Production of a Novel BioBrick

Originally, it was planned to use resistance cassettes in BioBrick format to construct deletion mutants. However, this strategy was later revoked and Gibson cloning was used to generate the deletion construct (section 5). This section demonstrates the principle of BioBrick cloning by producing a novel BioBrick consisting of the genes encoding red fluorescent protein (*mCherry*) and antibiotic resistance against chloramphenicol (*cat*), held in a standard BioBrick cloning plasmid. The constructed BioBrick can be utilized to replace genes targeted for genetic inactivation. Presence of BioBrick prefix and suffix sequences will provide an easy way of assembling gene deletion constructs. Insertion of this BioBrick will ensure a straight-forward selection of colonies due to the red color conferred by the *mCherry* gene and the growth on chloramphenicol conferred by the *cat* gene.

The antibiotic resistance cassette for chloramphenicol was converted into a BioBrick compatible construct by PCR amplification using specifically designed primers with the BioBrick prefix and suffix sequences (Fig. 1.12). The cassette was digested with the restriction enzymes EcoRI and SpeI and the plasmid pSB1A3 (Fig. 3.7A), containing the *mCherry* BioBrick, was digested with EcoRI and XbaI. Fragments were assembled by traditional ligation, resulting in the formation of a new BioBrick consisting of both the *cat* and *mCherry* genes (Fig. 3.7B). The plasmid was amplified by transformation into *E. coli* DH5α and colonies were selected for growth on chloramphenicol and expression of the *mCherry* gene, resulting in red-colored colonies (Fig. 3.8). Restriction digest analysis using EcoRI and SpeI, producing two fragments of 2.1 kb and 1.6 kb, validated construction of the correct plasmid (Fig. 3.9).

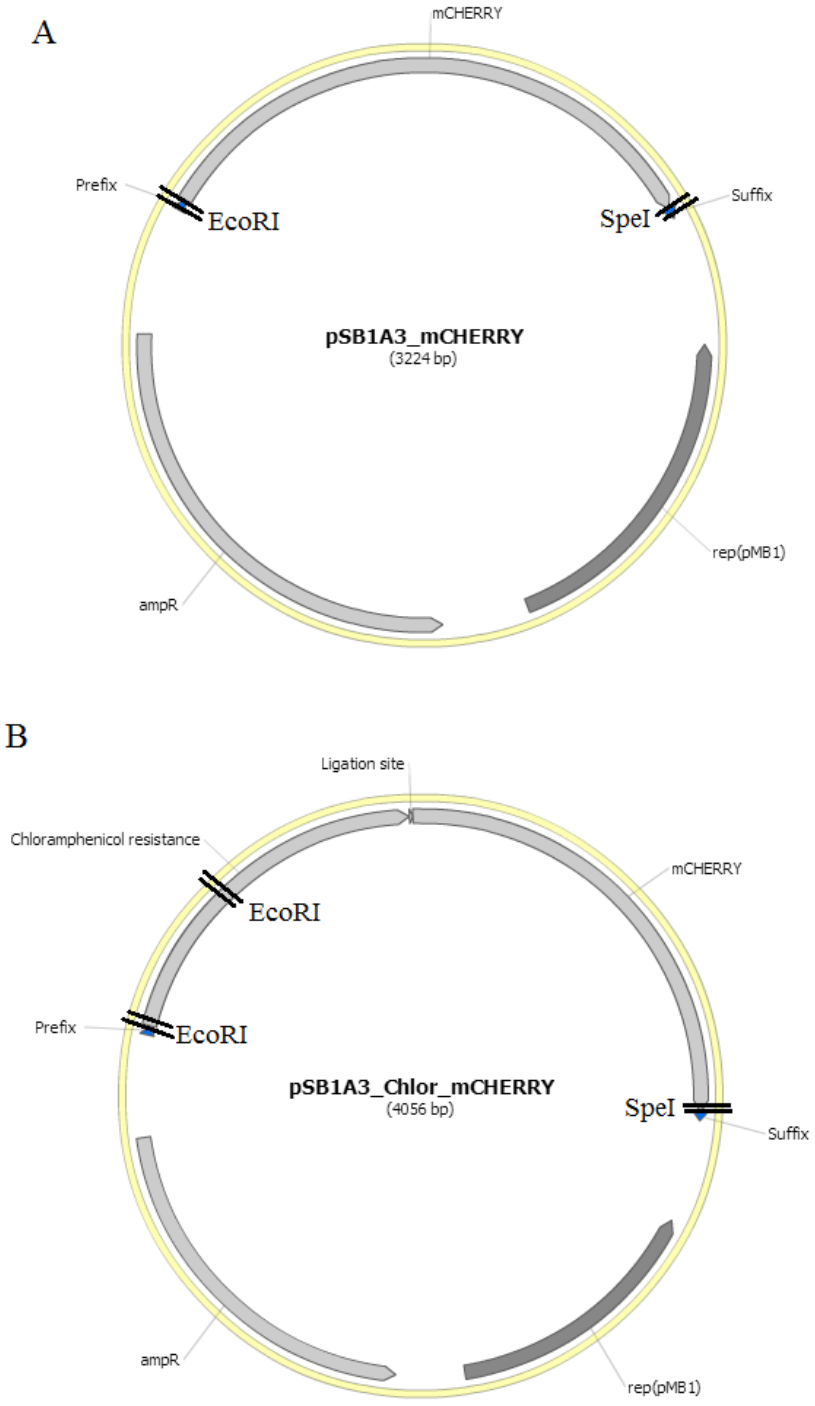

Figure 3.7 – BioBrick Plasmids. A BioBrick compatible chloramphenicol resistance cassette was assembled with the BioBrick for the red fluorescent protein (mCherry), held in the BioBrick standard assembly plasmid (pSB1A3). Cut sites for EcoRI and SpeI are found in the prefix and suffix sequences, respectively.

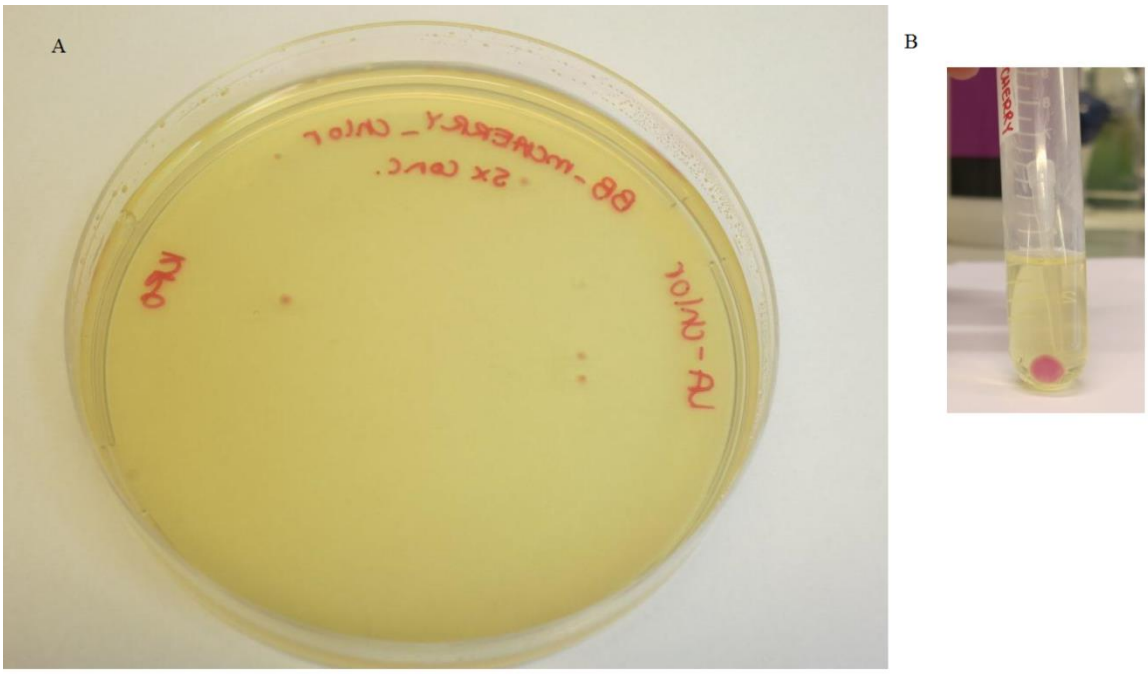

Figure 3.8 – *E. coli* Transformed with the Constructed BioBrick Plasmid. Colonies with a red color, growing on chloramphenicol were selected (A) and grown in liquid cultures (B) for the amplification of the constructed plasmid.

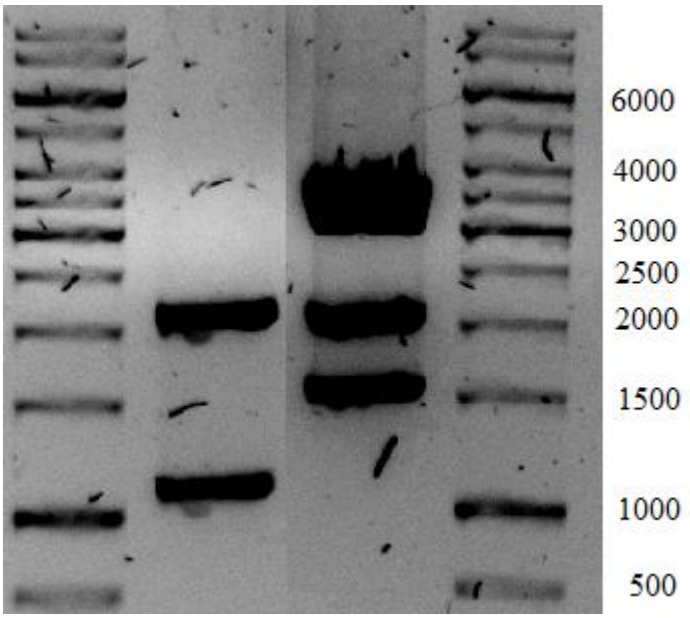

Figure 3.9 – BioBrick Digest. The original pSB1A3 plasmid (left) and the constructed BioBrick plasmid (right) were analyzed by restriction digestion using EcoRI and SpeI. Two fragments originated from the pSB1A3 plasmid (1.1 kb and 2.1 kb) and three fragments originated from the constructed plasmid (1.5 kb, 2.1 kb and 3.5 kb). Bands below 0.5 kb are not a part of this picture.

5. Generation of the *Synechocystis* Δ*sll1653* Strain

The gene *sll1653*, encoding a methyltransferase involved in the biosynthetic pathway of phylloquinone in *Synechocystis* 6803 (Sakuragi *et al.*, 2002), was genetically deleted. A phylloquinone precursor, lacking a methyl group should therefore be generated in the mutant strain. The same methyltransferase may also be involved in the methylation step of plastoquinone synthesis, as indicated above. The objective of deleting *sll1653* was to gain further insights into the biosynthetic pathway of plastoquinones and the potential utilization of different quinones under aerobic and anaerobic conditions.

Four DNA fragments were amplified by PCR using specifically designed primers (Section 4.1.2 in Chapter 2) for Gibson assembly (Gibson *et al.*, 2009). Flanking regions on the left (0.6 kb) and right (0.5 kb) side of the *sll1653* gene were amplified by from *Synechocystis* 6803 and the pLitmus28i backbone (2.6 kb) and kanamycin resistance cassette (1.0 kb) were amplified from plasmid DNA (Fig. 3.10).

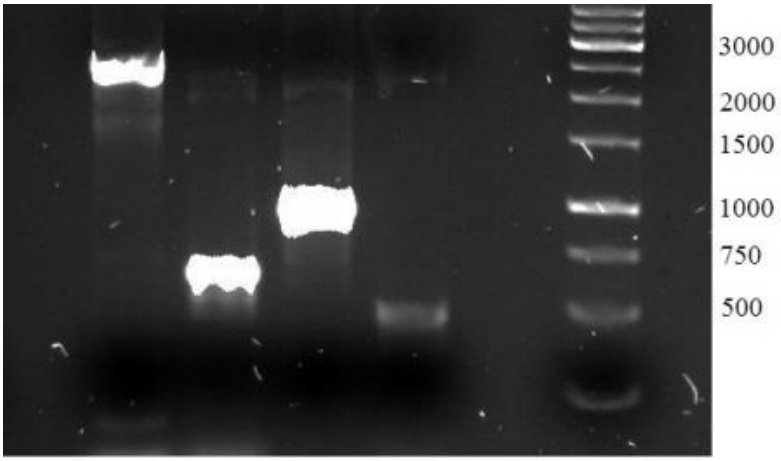

Figure 3.10 – PCR Amplification of Fragments for Construction of *sll1653*-Deletion Construct. From left to right: pLitmus backbone, left flanking region, kanamycin resistance cassette, right flanking region and GeneRuler™ 1 kb DNA Ladder.

Gibson cloning takes advantage of double stranded DNA fragments with complementary ends which can be assembled simultaneously in the presence of three enzymes and a single buffer system. An exonuclease generates 3' single-stranded overhangs, followed by the activity of a polymerase and a DNA ligase that fill in and seals the gaps between the assembled DNA, respectively (Gibson *et al.*, 2009). The PCR-amplified fragments were assembled using a

Gibson Assembly Master mix, followed by transformation of the resulting plasmid into *E. coli* DH5α. The isolated plasmid was verified as the correct Δ*sll1653* plasmid (Fig. 3.11) by DNA sequencing (data not shown).

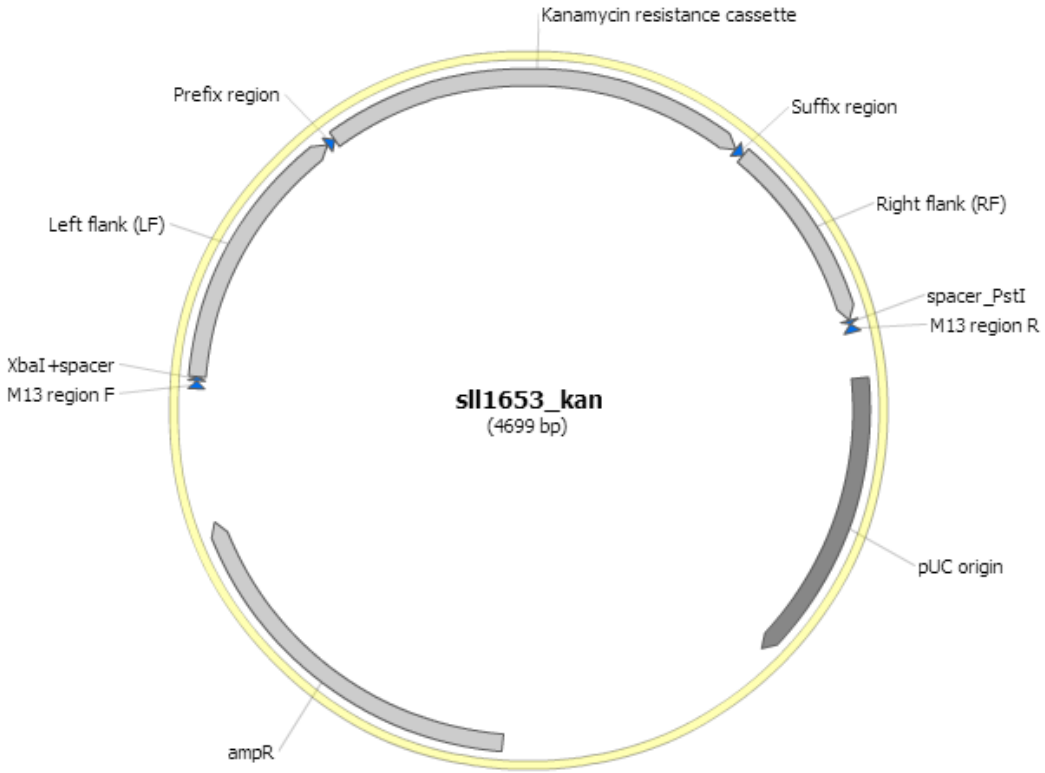

Figure 3.11 – *sll1653*-Deletion Plasmid. Plasmid construct for homologous integration of a kanamycin resistance gene in the place of the gene *sll1653* of *Synechocystis* 6803. The pLitmus28i backbone contains an ampicillin resistance cassette (ampR). The plasmid contains the BioBrick prefix and suffix sequences.

The Δ*sll1653* plasmid was introduced to the wild-type strain of *Synechocystis* to allow integration of the deletion construct into the host genome. Cells were grown on BG11 medium supplemented with glucose. Resulting colonies were picked and streaked-out on fresh BG11 medium with glucose and kanamycin and grown for three weeks, allowing the isolation of the desired Δ*sll1653* strain. Complete segregation was verified by colony PCR using the *1653*_LF forward and *1653*_RF reverse primers. A DNA fragment of 1.7 kb was

amplified from the wild-type and a 2.2 kb fragment was amplified from the Δ*sll1653* strain upon genotyping (Fig. 3.11C). The increase in fragment size of the mutant compared to the wild-type represents the incorporation of the kanamycin resistance cassette, as illustrated in Figure 3.11. Characterization of the Δ*sll1653* strain was performed in order to determine whether this gene is involved in plastoquinone synthesis and if phylloquinone can replace plastoquinone under anaerobic conditions in *Synechocystis* 6803 (see section 6 and 7).

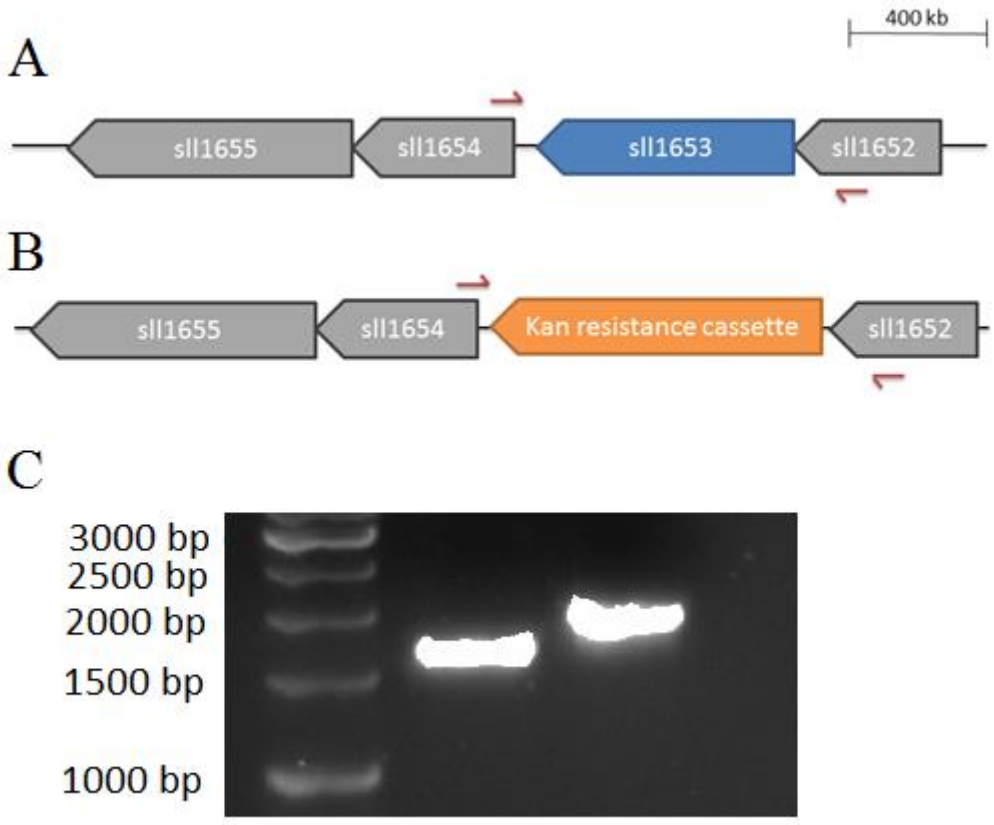

Figure 3.12 – Construction of Δ*sll1653* Strain. (A) Chromosomal DNA from wild-type *Synechocystis* indicating the position of *sll1653 relative* to flanking genes. (B) Chromosomal DNA for Δ*sll1653* strain after homologous recombination that replaces *sll1653* with the antibiotic resistance cassette for kanamycin. (C) Colony PCR products of wild-type (1.7 kb) and Δ*sll1653* strain (2.2 kb) using the primers indicated (red arrows).

6. Phenotypic Characterization of the Δ*sll1653* Mutant

The Δ*sll1653* deletion strain of *Synechocystis* 6803 was characterized and compared to the wild-type. The Δ*sll1653* strain is deficient in a methyltransferase shown to be involved in phylloquinone biosynthesis (Sakuragi *et al.*, 2002), but this enzyme may also be involved in the methylation step of plastoquinone synthesis. The presence of demethylated phylloquinone or plastoquinone is expected to have an impact on growth, electron transport and synthesis of photosynthetic lipids. Assessments of the growth characteristics, the operating efficiency of the photosystems and the electron transport chain, as well as the composition of photosynthetic lipids in both wild-type and mutant strain were thus carried out.

6.1. Growth Curves

Both wild-type and mutant strain were subjected to different conditions in order to determine growth characteristics. The Δ*sll1653* strain is expected to have a deficiency in electron transport since the secondary electron acceptor of PS I, phylloquinone, lacks a methyl group. Conditions that rely on a functional PS I (PS I-stress) can be induced in several ways. In the presence of glucose, electrons do not need to be generated by PS II, because the degradation of glucose already provides electrons. In glucose-grown *Synechocystis* 6803, cyclic electron transport via PS I is therefore dominant.

Electron generation via PS II can be further restricted by the herbicide DCMU. This herbicide occupies the binding site for Q_B in PS II, hence the cell is dependent on electron generated from glucose and ATP generated via cyclic electron flow around PS I or respiration. High concentrations of salt (NaCl) forces *Synechocystis* 6803 to implement cyclic electron transport for the production of ATP, utilized for export of ions. High light and the increase in photosynthetic electron transport rate may also reveal deficiencies in the photosynthetic electron transport components, specifically PS I in the *sll1653* deletion strain.

Wild-type and the Δ*sll1653* strain were grown on BG11 agar medium in the presence of high and low concentrations of salt under normal (NL) and high light (HL). In addition, growth in

the presence of glucose and glucose plus DCMU was evaluated. Images of the agar plates were taken for a total of eight days at different time points using a custom-built Plate-Imager (Chapter 2, section 5.5.1). Cell density data was calculated from the RAW image files and growth curves were constructed from this data by correcting for the agar background (Fig. 3.13).

Growth of the mutant strain Δ*sll1653* was similar to and even exceeded the growth of the wild-type strain for most conditions evaluated under normal light. The only difference observed was on solid BG11 medium supplemented with salt, glucose and DCMU, in which no growth occurred (Fig 3.12F). Under high light conditions, however, the Δ*sll1653* strain failed to grow on BG11 medium supplemented with glucose (Fig. 3.12C). Still, growth was observed on the plates with glucose and DCMU (Fig. 3.12E). In addition, no growth was observed on the high salt concentration plates when the mutant was grown in the presence of glucose or glucose plus DCMU under high light. All additions to the medium clearly caused a reduction in growth for both strains. A high concentration of salt seems to be tolerable if the medium is not additionally supplemented with glucose or glucose plus DCMU. Figures 3.13D and F indicate this, and the experiment did not proceed long enough to reach stationary growth under these conditions.

The doubling time describes the time required for the population to double its size. This parameter was determined for *Synechocystis* 6803 and the mutant Δ*sll1653* strain when subjected to growth on different media and are given in Table 3.3. The doubling times presented are the average of three experiments and were calculated from the exponential phase of the growth curves.

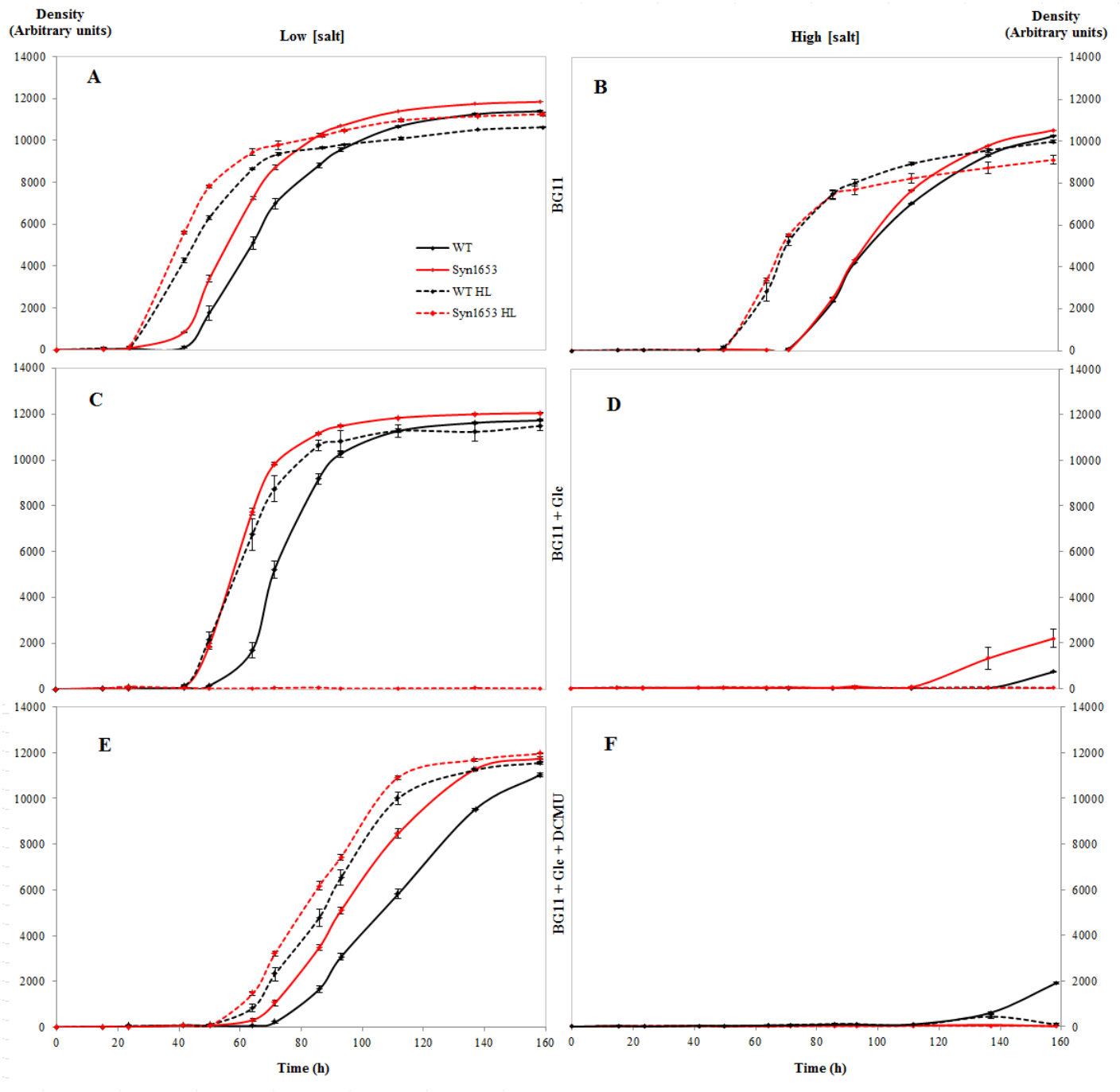

Figure 3.13 – Growth Curves. *Synechocystis* wild-type (black) and mutant strain Δ*sll1653* (red) were grown on various solid BG11 media: (A) Normal BG11 medium, (B) BG11 with high salt concentration (400 mM NaCl), (C) BG11 supplemented with glucose, (D) BG11 + glucose at high salt concentration, (E) BG11 medium supplemented with glucose and DCMU, (F) BG11 + glucose + DCMU at high salt concentration. Cells were grown under normal light (solid trace) and high light conditions (dashed trace). Densities represent the average of three colonies (*n*=3) and are given in arbitrary units with indicated standard errors.

Table 3.3 – Doubling times for Wild-type and Δ*sll1653*. Strains were grown on solid BG11 with various supplements under normal (NL) and high light (HL) conditions. Doubling times were calculated according to equation 2.2, taking the average for three replicates (*n* =3). Standard deviations were calculated and are given for each growth rate. Hyphen indicates that no growth was observed.

Medium	**Doubling time (h)**			
	Wild-type		Δ*sll1653*	
	NL	HL	NL	HL
BG11	7.8 ± 1.04	6.4 ± 1.41	6.9 ± 0.05	6.1 ± 1.43
+ high [salt]	8.6 ± 3.65	7.7 ± 0.95	7.9 ± 0.53	5.4 ± 0.32
BG11 Glc	7.0 ± 0.14	6.5 ± 1.72	6.4 ± 0.65	-
BG11 Glc DCMU	15.1 ± 1.74	9.4 ± 0.61	14.0 ± 1.72	7.6 ± 1.18

The Δ*sll1653* strain has shorter doubling times than the wild-type on all media evaluated under normal light. The addition of 400 mM salt to the BG11 medium increases the doubling time by over an hour for both wild-type and mutant strain under normal light. Under high light, the addition of salt decreases the doubling time of the mutant whereas the wild-type still grows slower compared to the growth on BG11 medium. The supplementation with glucose is critical for the Δ*sll1653* strain under high light, an observation that was also confirmed by preliminary experiments.

6.2. Oxygen Evolution

Oxygen evolution by dark-adapted wild-type and Δ*sll1653* strain was measured upon exposure to increasing light intensities. Figure 3.14 displays the production of oxygen for both strains at constantly changing light intensities.

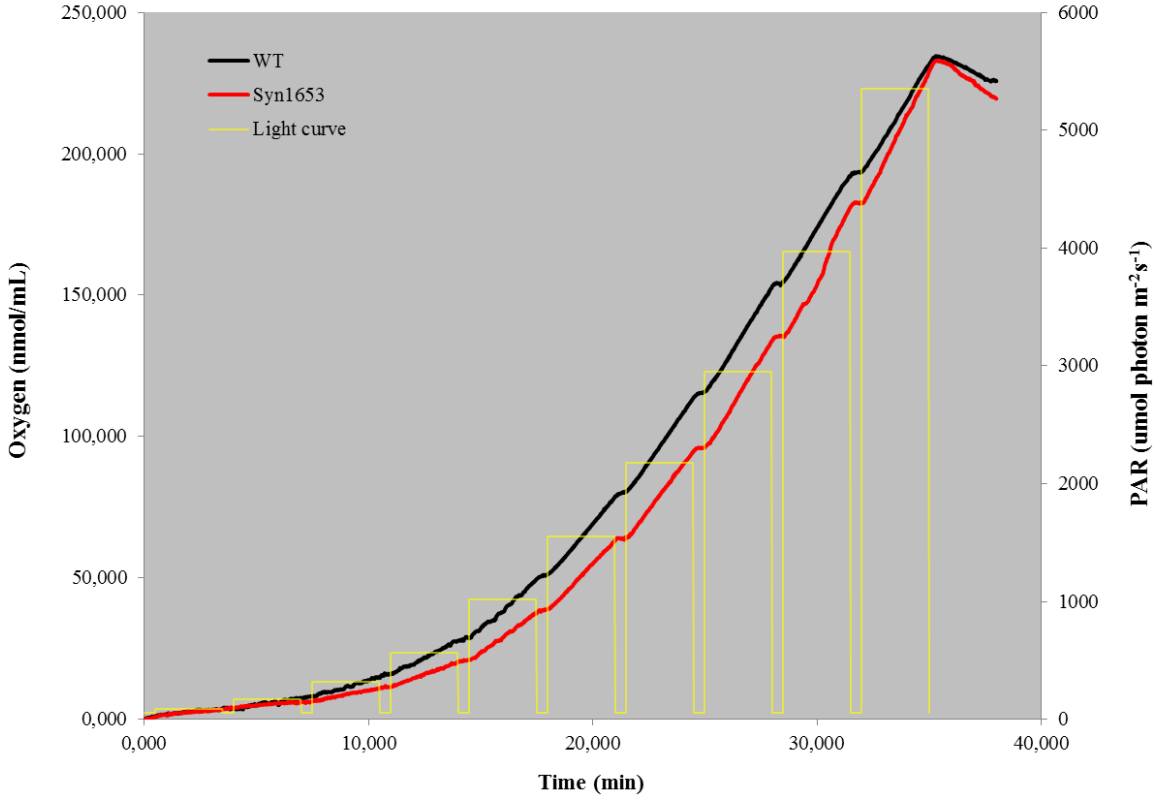

Figure 3.14 – Oxygen Evolution. *Synechocystis* 6803 (WT, black trace) and the mutant strain Δ*sll1653* (Syn1653, red) were subjected to increasing light intensities (yellow) while measuring the production of oxygen. The data represents the average of three measurements (*n*=3) at a chlorophyll concentration of 10 µg/mL.

Wild-type cells are able to produce more oxygen than the mutant strain Δ*sll1653* for all light intensities above 173 µmol photons/m^2s^1. However, the Δ*sll1653* strain has a steeper oxygen curve and at the highest light intensity (5355 µmol photons/m^2s^1) the final concentration of oxygen is similar to that of the wild-type. The efficiency of photosynthesis was evaluated by plotting the production of oxygen per minute and per photon irradiated against light intensities (Fig. 3.15). The rate of oxygen evolution in the wild-type levels out at a light intensity of 3000 µmol photons/m^2s^1 whereas the mutant does not reach this plateau until the photon flux exceeds 4000 µmol photons/m^2s^1. The efficiency of photosynthesis per photon irradiated is highest at the lowest light intensity evaluated (87 µmol photons/m^2s). Reaction centers in the wild-type become saturated between 300 and 1000 µmol photons $m^{-2}s^{-1}$ whereas this saturation occurs at a higher light intensity (550-1550 µmol photons $m^{-2}s^{-1}$) for the mutant. The wild-type strain also appears to be more susceptible to photoinhibition at higher light intensities compared to the Δ*sll1653* strain.

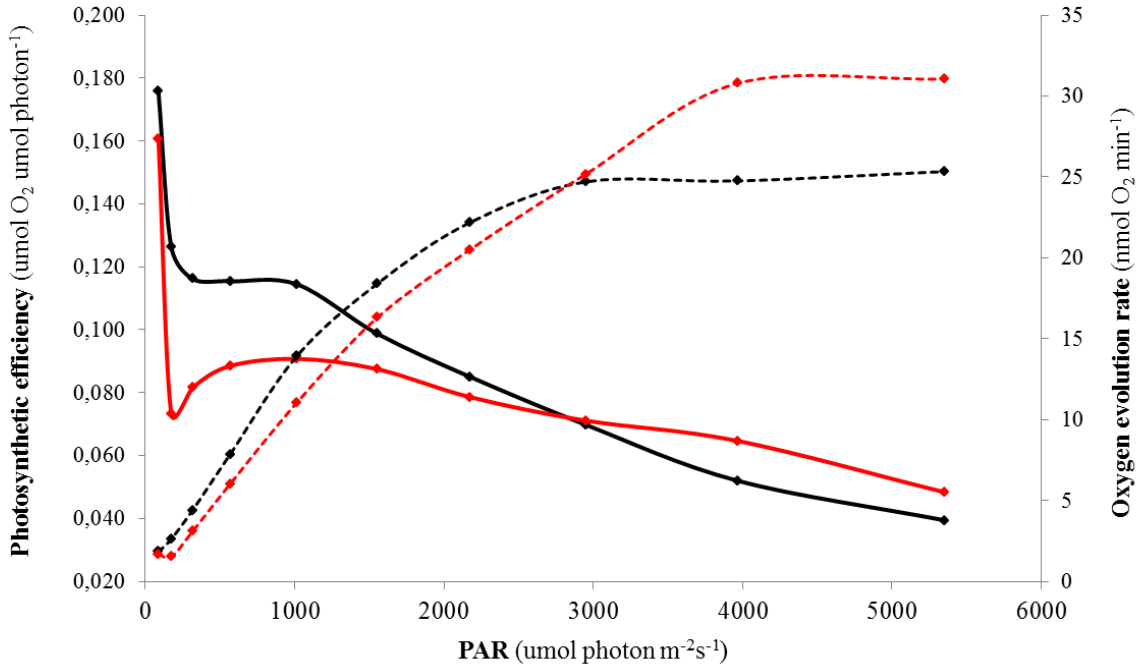

Figure 3.15 – Photosynthetic Efficiency and Oxygen Evolution Rates at Different Light Intensities. Production of oxygen per minute (dashed) and per photon irradiated (solid) for wild-type (black) and mutant cells (red) at different light intensities. Traces represent the average of three independent measurements performed at identical chlorophyll concentrations (10 µg/mL).

6.3. Respiration Rates

The consumption of oxygen by wild-type and mutant strains in the absence and presence of glucose was measured and respiration rates were determined for both strains. The consumption of oxygen prior to and after addition of glucose is graphically displayed in Figure 3.16. Rates of respiration are given in Table 3.4.

Table 3.4 – Respiration Rates. Oxygen concentration was measured for dark-adapted cultures of wild-type and mutant strain and the rate of oxygen consumption in the presence and absence of glucose was calculated. The respiration rates are given as average values for *n* number of measurements with associated standard deviations.

Strain	***n***	**Respiration rate (nmol O_2 min^{-1} OD^{-1})**	
		÷ glucose	+ glucose
Wild-type	3	0.61 ± 0.24	2.22 ± 0.65
Δ*sll1653*	2	0.17 ± 0.06	0.37 ± 0.04

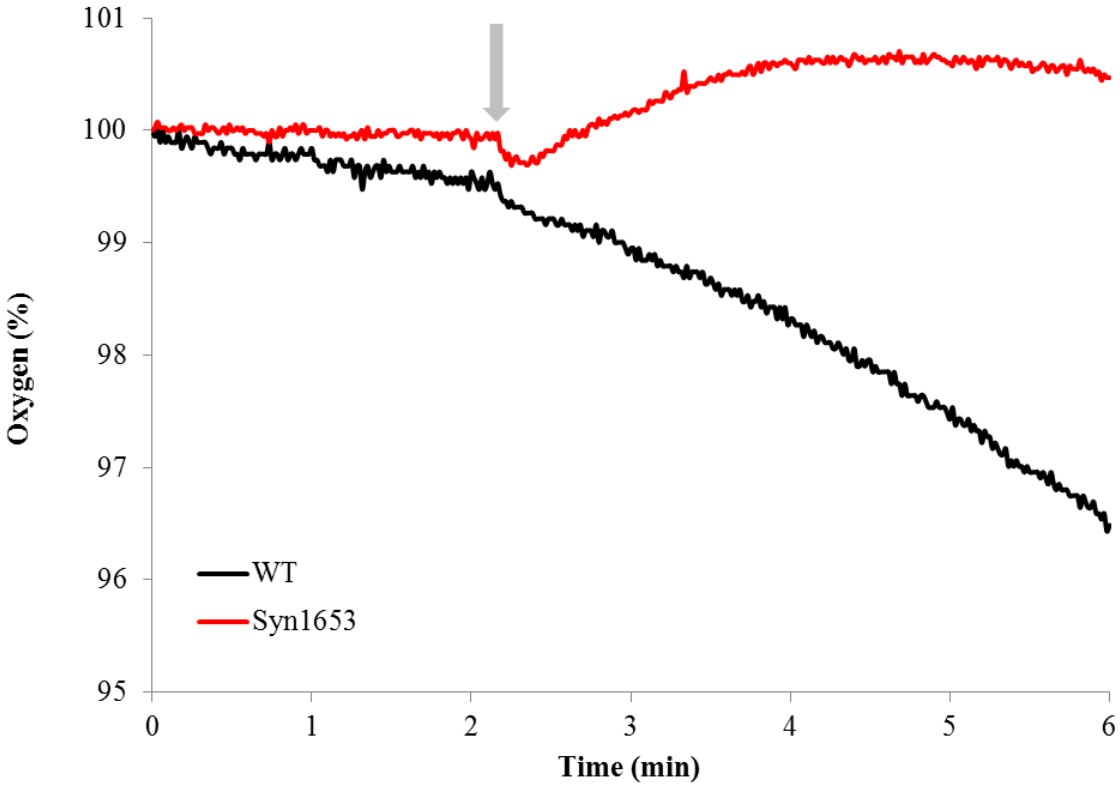

Figure 3.16 – Oxygen Consumption. *Synechocystis* 6803 WT (black trace) and *Synechocystis* Δ*sll1653* (red) were placed in an airtight chamber in the dark and oxygen concentration was recorded. Glucose was added to the cells, indicated by the arrow.

The deletion of the *sll1653* gene influences respiration both in the presence and absence of glucose. An increase in oxygen concentration was observed after addition of oxygenated glucose solution and the mutant was unable to remove this introduced oxygen efficiently from the medium even 4 minutes after glucose was added. Also, the respiration rate is considerably lower for the mutant compared to the wild-type.

6.4. Pigment Composition

The composition of pigments in *Synechocystis* 6803 was determined by *in* vivo absorption spectroscopy. Cell absorption spectra were measured for wild-type and the Δ*sll1653* strain using a spectrophotometer with an integrating sphere, scanning from 400 to 800 nm (Fig.

3.17). This setup makes light scattering by the cells negligible. Cell absorption was normalized by OD_{750} measured by a normal spectrophotometer.

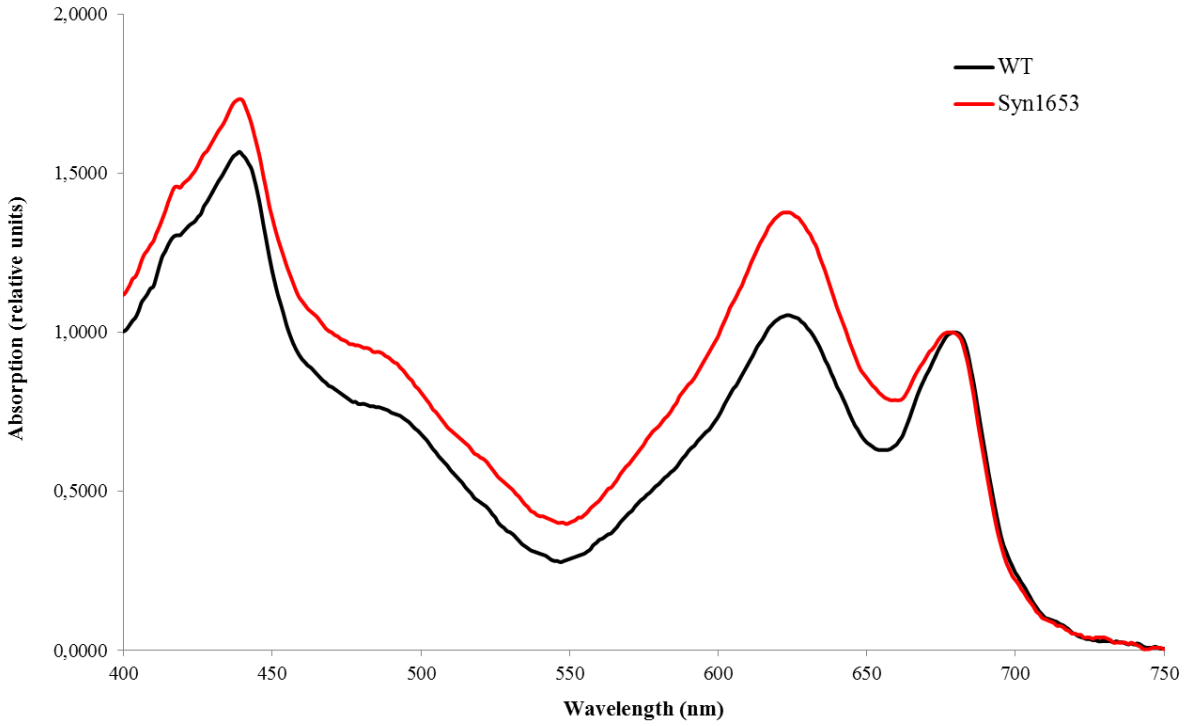

Figure 3.17 – *In Vivo* Absorption Spectra. Cell absorption was recorded for wild-type (black) and the Δ*sll1653* mutant (red) in a scan from 400 nm to 800 nm, at an OD_{750} of 0.3.

The mutant strain accumulates more photosynthetic pigments than the wild-type; especially phycobilins as indicated by the peak at 624 nm. The ratio of phycobilins and carotenoids to chlorophyll *a* was calculated by dividing the maximum absorbance at 624 and 487 nm by the maximum absorbance at 680 nm, respectively (Table 3.6). A chlorophyll concentration of 10 µg/mL corresponded to an OD_{750} of 2.0 for both wild-type and mutant strains.

Table 3.5 – Relative Ratios of Carotenoids and Phycobiliproteins to Chlorophyll *a* Determined by *In Vivo* Absorption Spectroscopy. The absorption for carotenoids (Car, 487 nm) and phycobiliproteins (Phyco, 624 nm) was divided by the absorption for chlorophyll *a* (Chl *a*, 680 nm).

Strain	Relative Car : Chl *a*	Relative Phyco : Chl *a*
Wild-type	0.76	1.05
Δ*sll1653*	0.93	1.38

6.5. Photosystems and Light-Harvesting Antennas

Fluorescence emission spectra were measured at 77 K by the excitation of chlorophyll *a* and phycobiliproteins at 440 and 580 nm, respectively. The resulting fluorescence traces were normalized to the PS I peak at 724 nm for the excitation of chlorophyll *a* or at 722 nm for the excitation of phycobiliproteins. Fluorescence emission spectra are displayed in Figure 3.18.

The PS I fluorescence peak (724 nm) and the two peaks at 685 and 695 nm (linked to the antenna pigments of PS II) provide characteristic features to determine changes in PS I relative to PS II when excited at 440 nm. The ratio between the two photosystems was identical in the wild-type and mutant, as can be seen in Figure 3.18A where the traces completely overlap. When excited at 580 nm, the peaks at 722 and 685 nm originate from the antenna pigments associated with PS I and PS II, respectively. The mutant strain showed an increase in the fluorescence yield of the 685 nm peak compared to the wild-type. The ratio of phycobiliproteins associated with PS II to those associated with PS I was 2.73 for the wild-type and 3.53 for the mutant.

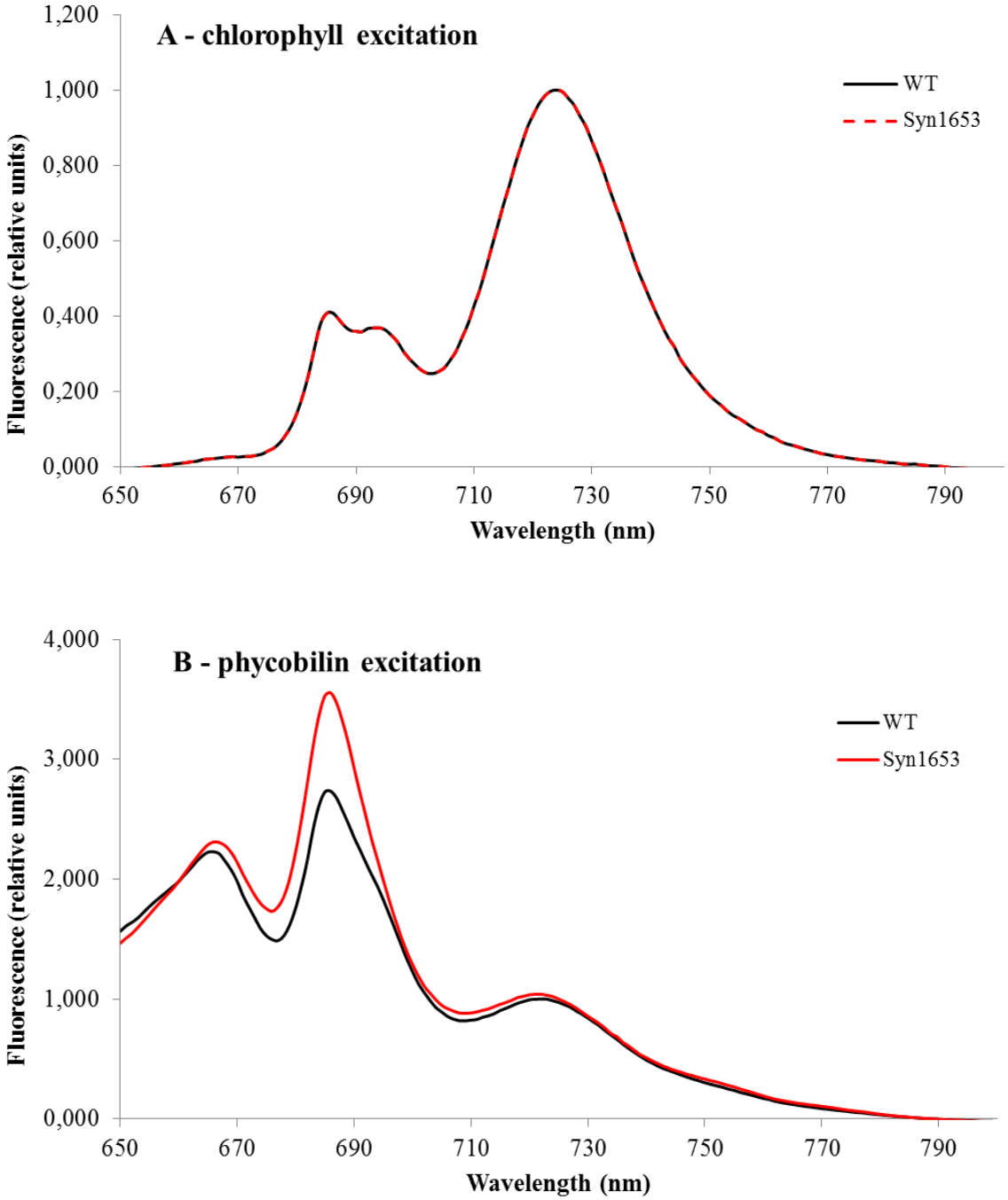

Figure 3.18 – 77 K Fluorescence Emission Spectra of Wild-Type and Δ*sll1653* Mutant Strain. Cells were excited at 440 (A) and 580 nm (B) and traces were normalized to the PS I peak at 724 and 722 nm for chlorophyll *a* and phycobiliprotein excitation, respectively. Traces for chlorophyll *a* excitation (440 nm) in wild-type and mutant completely overlaps (A).

6.6. Photosynthetic Lipid Composition

Lipids were extracted from wild-type and Δ*sll1653* cells grown photoautotrophically and the extracts were analyzed by UPLC-qTOF-MS. The MassLynx software from Waters was utilized to search the chromatograms for photosynthetic lipids that could be synthesized in *Synechocystis* 6803 (see Appendix I). The base peak intensity (BPI) chromatograms for the total lipid extract and mass spectra of individual lipids from wild-type and mutant are shown in Appendix III. A summary of photosynthetic lipids identified in the extracts are listed in Table 3.6 with their respective retention times, masses and relative abundance based on detection signal information. The chlorophyll *a* detection signal was used to standardize the samples as spectrophotometric data indicated that the same amount of chlorophyll is present in wild-type and Δ*sll1653* strain (Fig. 3.17).

Table 3.6 – Photosynthetic Lipids Detected by UPLC-qTOF-MS. Compounds identified in lipid extracts from *Synechocystis* 6803 and the mutant strain Δ*sll1653* using ESI in positive mode. Chl *a* standardized relative abundance was calculated according to equations 2.5-2.6.

Lipid	**Retention time**	***m/z***	**Chl *a* standardized relative abundance**	
	min		WT	Mut
Chlorophyll *a*	1.98	893.54	100.0	100.0
Chlorophyll *a* oxidized	1.98	907.52	288.3	517.7
Pheophytin *a*	1.98	871.58	348.6	289.6
Chlorophyllide *a*	1.98	614.24	41.3	30.9
β-carotene	3.35	536.43	136.4	165.2
Echinenone	2.16	550.42	120.2	119.5
Hydroxy-echinenone	1.02	566.41	33.1	31.5
Lutein/zeaxanthin	0.85	568.43	73.3	102.4
Myxoxanthophyll	0.62	730.52	321.5	265.9
Myxoxanthophyll-fucoside	0.77	758.51	25.8	48.5
Plastoquinone-9				
- oxidized	1.43	749.53	139.7	140.2
- reduced	1.62	751.53	477.7	574.4
Phylloquinone	2.28	451.36	5.1	0.0
α-tocopherol	1.62	430.38	2.9	8.3

6.6.1. Chlorophylls

For chlorophylls, the base peak had *m/z* ratio of 907.52. The peak at 893.53 was much smaller, but could still be detected in both the wild-type (Fig 3.19) and the mutant. The masses of pheophytin *a* (871.58) and chlorophyllide *a* (614.24) were also observed, indicating the lack of the magnesium ion and the hydrophobic tail from the chlorophyll *a* molecule, respectively. Phaeophorbide *a*, a degradation product of Chl *a*, could not be detected in the mass spectrum. The relative abundance of the oxidized Chl *a* was higher in the mutant whereas more pheophytin *a*, a potential degradation product of Chl *a* and electron carrier within PS II, was found in the wild-type.

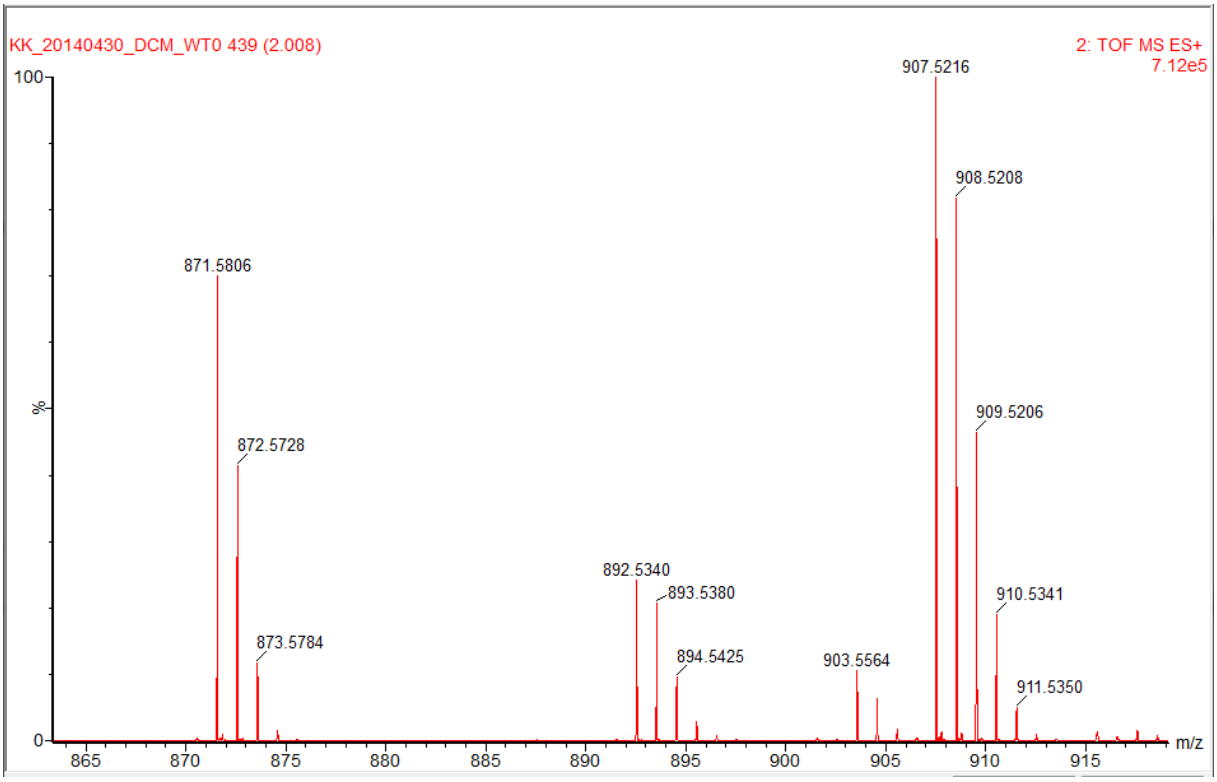

Figure 3.19 – Chlorophylls in the Wild-Type. Chlorophylls were eluted after 2.00 min and the masses were recorded in positive ESI mode for the wild-type (A) and mutant (B). The peak at 871.58 represents pheophytin *a* and the peak at 893.54 represents chlorophyll *a*. An additional peak was observed at 907.52, which may be an oxidized product of chlorophyll *a*.

6.6.2. Carotenoids

Relative to Chl *a*, the carotenoid with the highest abundance was myxoxanthophyll and the MS signal indicated that the wild-type extract contained more of this lipid. Zeaxanthin and lutein are isomers only varying in the location of the double bond in one of the ring structures. Hence, these compounds will have the same polarity and molecular mass and can only be distinguished from one another by absorption spectroscopy, in which a shift towards the red can be observed for lutein. Unfortunately, the diode array had a large offset in this region and was thus not utilized. The mutant appears to accumulate more of β-carotene, myxoxanthophyll-fucoside and zeaxanthin or lutein compared to the wild-type. Indicated levels of echinenone and the more polar hydroxyl-echinenone were similar in both strains.

6.6.3. Isoprenoid quinones

Oxidized plastoquinone was eluted after 1.43 min whereas reduced plastoquinone (plastoquinol) was eluted after 1.62 min. Figure 3.20 shows the chromatogram for separation of plastoquinone from the extract. Plastoquinone was found in both the wild-type and the mutant strain. The relative abundance of plastoquinone to Chl *a* seems to be slightly higher in the mutant, in which the increase was solely due to reduced PQ.

The deletion of the *sll1653* gene should generate a mutant deficient in phylloquinone, which was confirmed by mass spectrometry. Figure 3.21 displays the chromatogram when a search for the mass of phylloquinone was performed and Figure 3.22 shows the relative abundance of phylloquinone in the mutant and wild-type strains using the TransOmics platform.

Another isoprenoid quinone synthesized by *Synechocystis* 6803 is α-tocopherol. The compound eluted at the same time as the α-tocopherol standard (Table 3.2) and reduced plastoquinone. The mutant extract contained more of α-tocopherol relative to Chl *a* compared to the wild-type.

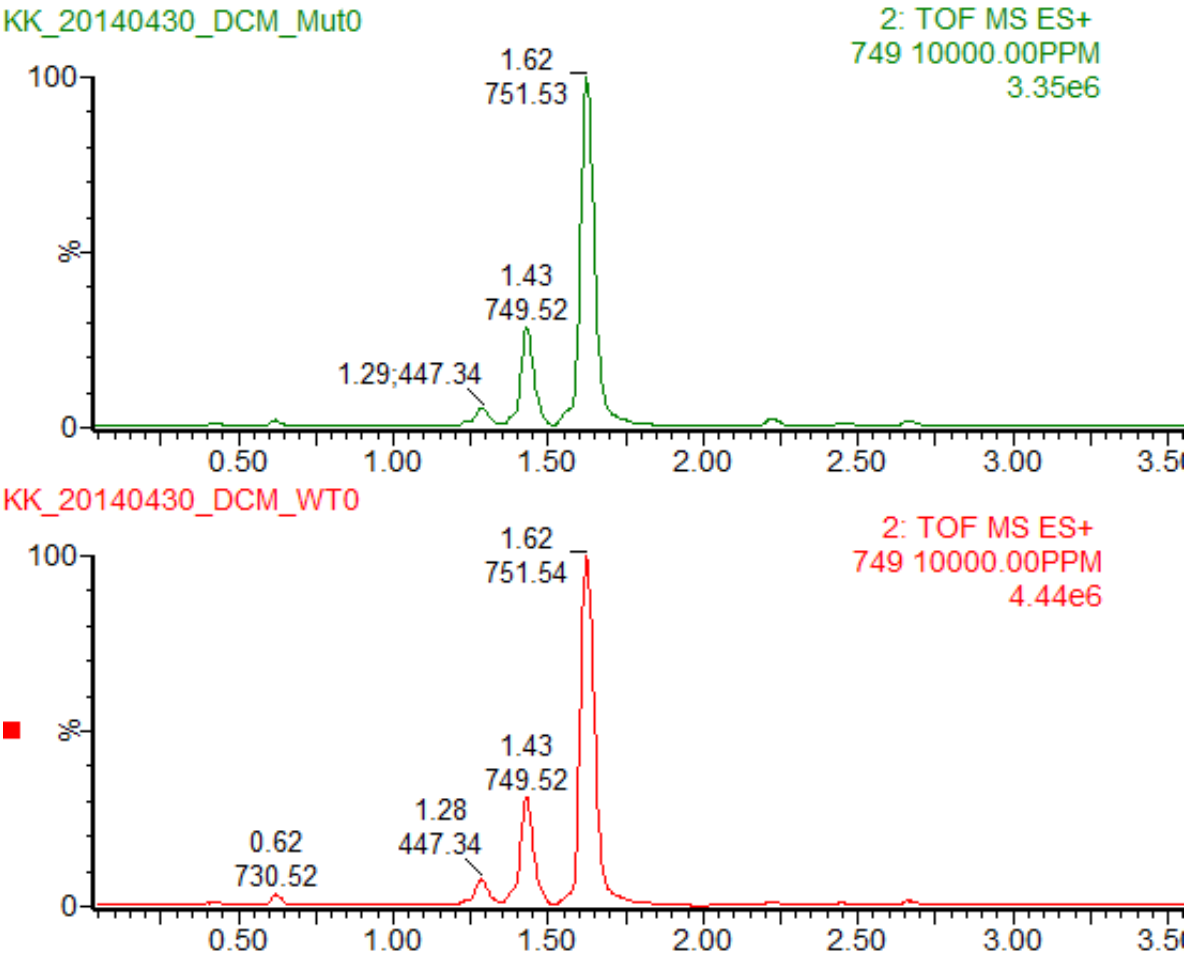

Figure 3.20 – Chromatogram for Oxidized and Reduced Plastoquinone. Plastoquinones found in the extract from wild-type cells (bottom) and mutant cells (top). Reduced plastoquinone (751.53) is eluted after 1.62 min and oxidized plastoquinone (749.52) after 1.43 min.

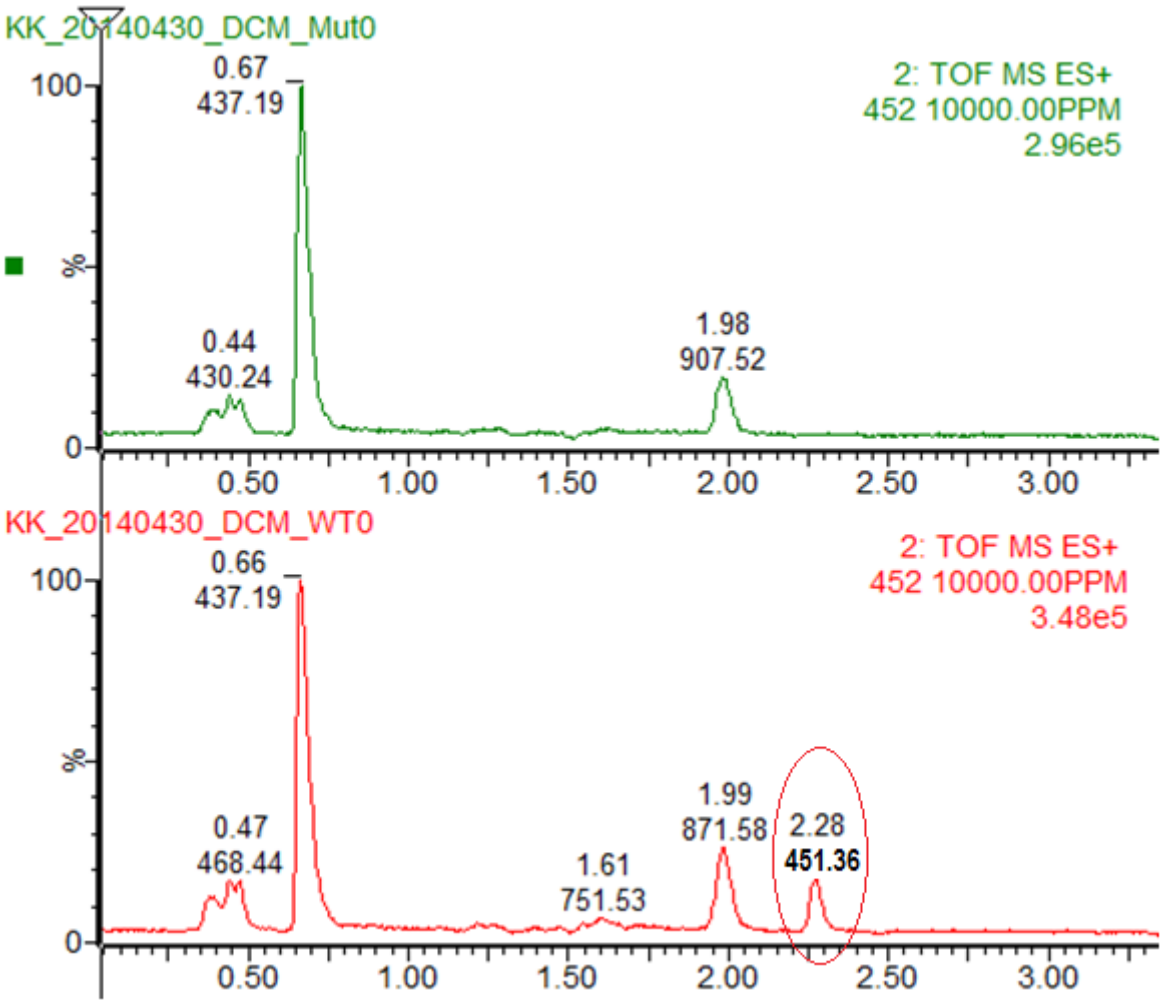

Figure 3.21 – Chromatogram for Identification of Phylloquinone. The peak at 2.28 min (circled) is observed for the wild-type (bottom) but not for the mutant (top) when searching for the expected mass of phylloquinone (451.70 g/mol).

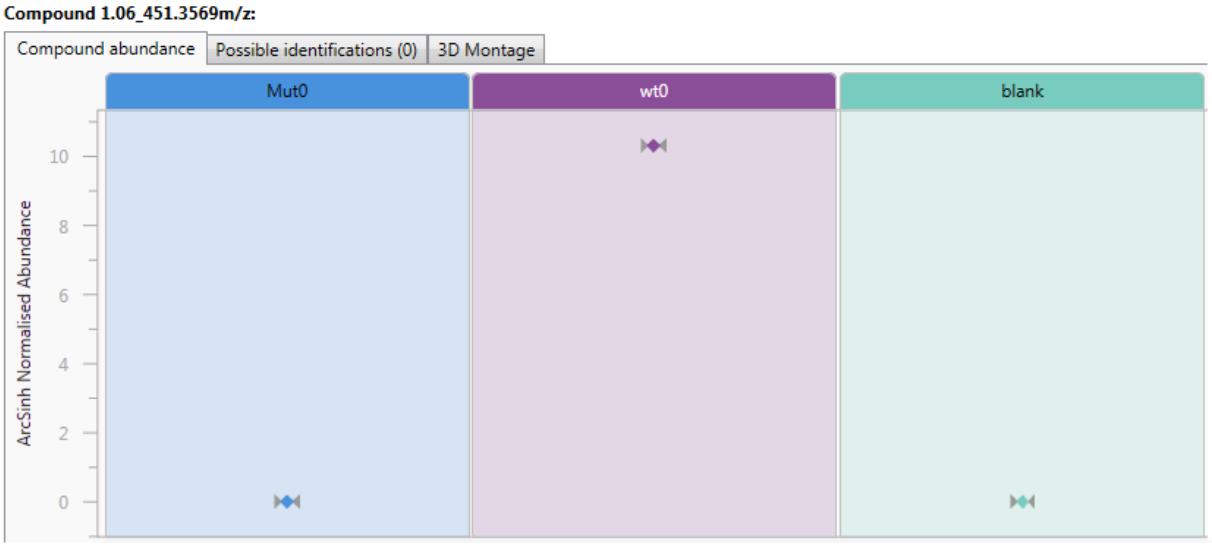

Figure 3.22 – Relative Abundance of Phylloquinone in the Mutant and Wild-Type. ArcSinh normalized abundance of phylloquinone (mass 451.36) was calculated using the TransOmics software from Waters. Mut0 is the extract from Δ*sll1653* and wt0 is the extract from wild-type cells, a blank sample was also included.

7. Transition from Aerobic to Anaerobic Conditions

Synechocystis 6803 is capable of shifting from aerobic to anaerobic respiration upon the depletion of oxygen. In some other facultative anaerobes, oxygen-dependent utilization of either menaquinone (anaerobic conditions) or ubiquinone (aerobic conditions) has been reported (Bekker *et al.*, 2007; Schoepp-Cothenet *et al.*, 2009). Cyanobacteria do not possess these quinones but synthesize derivatives thereof, known as plastoquinone and phylloquinone. To assess whether a shift in the composition of quinones occurred, *Synechocystis* 6803 and the mutant Δ*sll1653* strain were subject to anaerobic conditions.

7.1. State 1 – State 2 Transition

The distribution of excitation energy between PS II and PS I may be altered upon changes in the redox state of the plastoquinone pool. This alteration of energy distribution is known as a state transition, in which the light harvesting antenna can be associated with PS II (state 1) or PS I (state 2). The modulation of excitation energy distribution was investigated by 77 K fluorescence emission spectroscopy. Dark-adapted, oxygenated wild-type and mutant cultures were subject to bubbling with argon gas, to drive the depletion of oxygen. Samples were taken at the start of the experiment and after 10, 20, 40 and 80 min of anaerobic growth. Fluorescence emission was induced by exciting phycobilins at 580 nm and the traces were normalized to the PS I peak at 725 nm (Fig. 3.23).

The fluorescence yield from the mutant cells was overall higher compared to the wild-type, but a state transition could still be observed for both strains. The measurement at 80 min for the mutant was excluded, as this fluorescence trace contained a high level of noise, likely due to boiling of nitrogen. The peak at 685 nm slowly decreases as a function of anaerobic incubation time indicating the transfer of light-harvesting phycobilisomes from PS II to PS I.

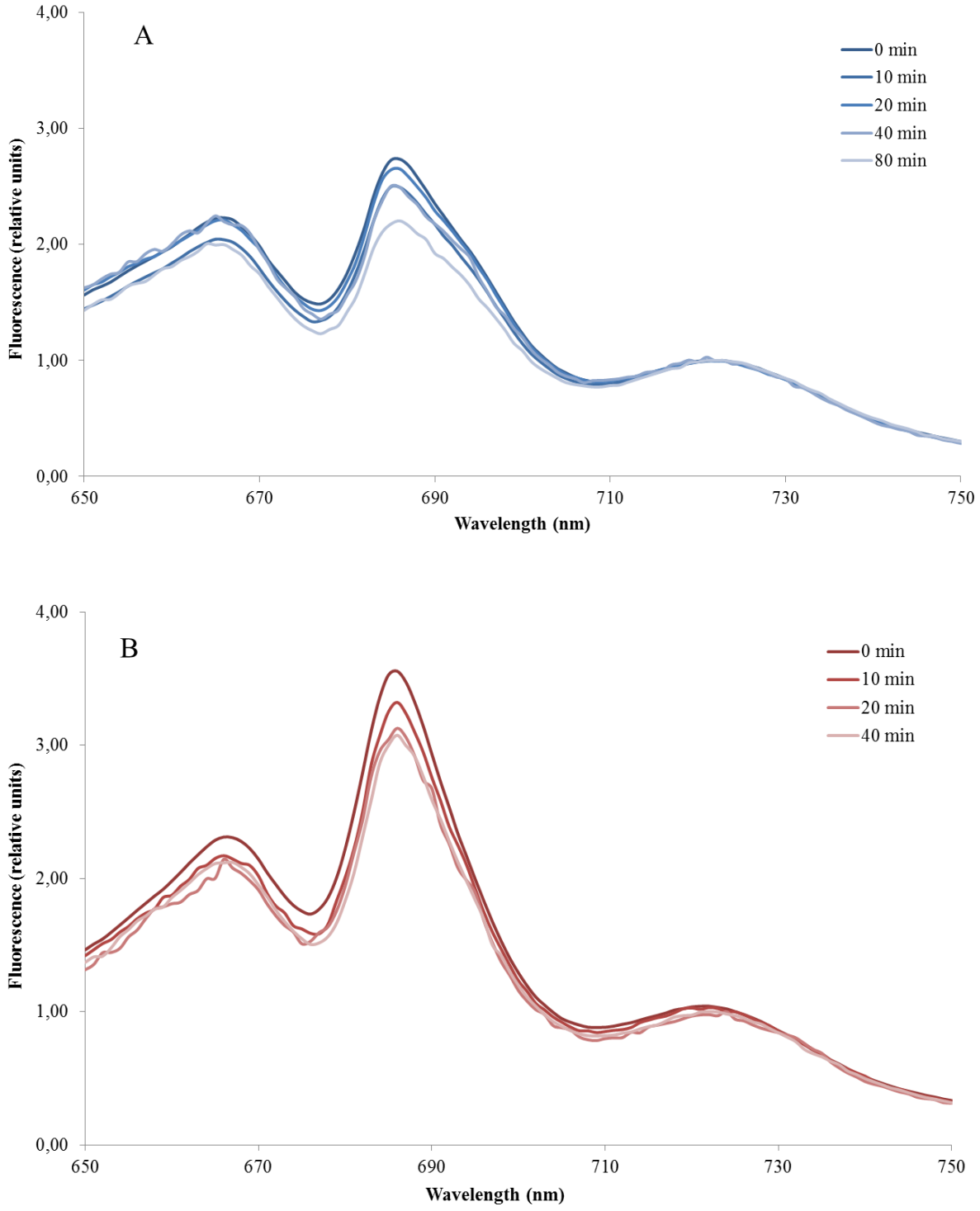

Figure 3.23 – State Transition Induced by Depletion of Oxygen. Fluorescence emission was measured at 77 K after excitation at 580 nm for wild-type (A) and mutant cells (B) grown anaerobically for 0, 10, 20, 40 and 80 min. A reduction in the 685 nm peak was observed.

7.2. Functioning of the Electron Transport Chain

Pulse-modulated fluorescence traces were recorded for dark-adapted wild-type and mutant strains upon depletion of oxygen to assess the overall state of the electron transport chain. Oxygen was depleted by the addition of glucose and glucose oxidase. The baseline, known as F_0, represents oxidized reaction centers in PS II and the maximal fluorescence (F_M) is the state where all reaction centers are reduced.

An increase in F_0 was observed for both mutant and wild-type upon a transition from aerobic to anaerobic respiration (Fig. 3.24). The PAM fluorescence traces were similar in both strains, although the fluorescence yield seems to 'reset' to a larger extent in the mutant upon prolonged adaptation to anaerobic conditions. Three individual peaks (marked as A-C in Figure 3.24) were extracted from wild-type fluorescence data to assess the redox state of Q_A at different stages of anaerobic adaption. In the early stages after anaerobic adaption (Fig. 3.25A) the fluorescence level, after a saturating light pulse, slowly decreases to the pre-pulse level. After further adaptation (Fig. 3.25B), the minimum fluorescence level slowly increases after a light pulse. After prolonged adaptation (Fig. 3.25C), a light pulse induces a fluorescence level below the pre-pulse fluorescence level, which then slowly increases. The increase in minimum fluorescence yield under anaerobic conditions is thought to be due to the reduction of the PQ-pool and a slow accumulation of Q_A^- in some of the reaction centers. During light pulses some oxidized PQ is produced as PS I disposes of electrons and this electron 'hole' oxidizes Q_A^- via oxidizing the PQ-pool.

DBMIB was introduced to make results independent of differences in PS I, caused by genetic deletion of the *sll1653* gene. DBMIB blocks the binding site of PQ in the b_6f complex. Addition of DBMIB should therefore separate PS II and PS I function, with PS II being the only photosystem that interacts with the PQ-pool. The presence of alternative quinones whose synthesis may be induced by anaerobic conditions could be expected to affect the behavior of chlorophyll *a* fluorescence under limiting oxygen concentrations. For example, fluorescence was utilized to assess whether another quinone could interact with the PQ-pool. The same increase in F_0 was observed for both strains in the presence of DBMIB (Fig. 3.26). This rise in F_0 occurred faster (11 min) and at a greater rate for the mutant compared to the wild-type (20 min). The reset in fluorescence yield could still be observed in the presence of DBMIB for

both strains, still to a greater extent in the mutant, but this was an unexpected observation. The blockage of the cytochrome b_6f complex by DBMIB should cause a constantly high fluorescence yield because the PQ-pool will no longer be able rescue the Q_A^-, which is slowly accumulating under anaerobic conditions.

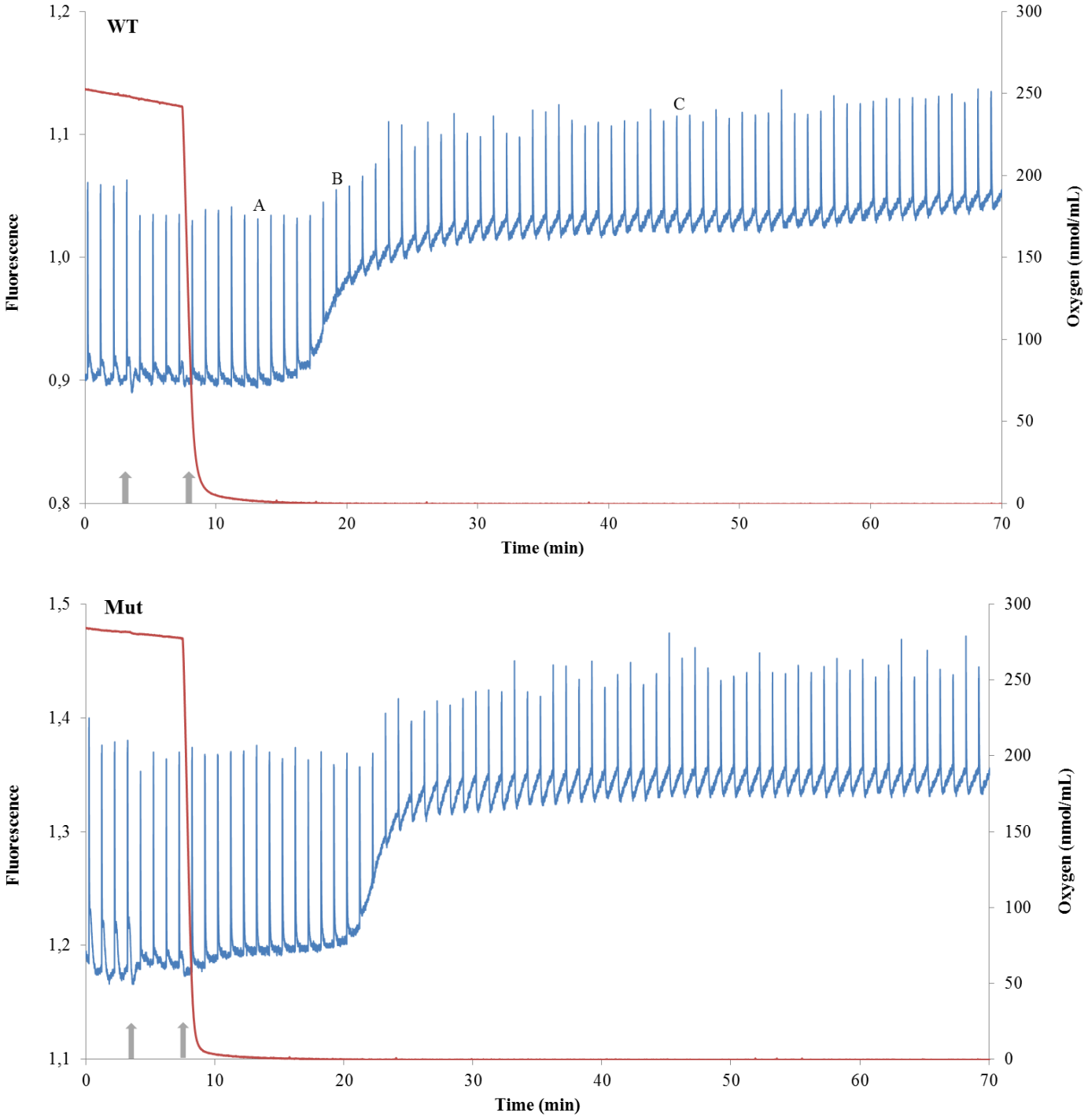

Figure 3.24 – PAM Fluorescence Traces upon Oxygen Depletion. Pulse modulated fluorescence (blue trace) was induced by a low intensity measuring light (625 nm) and maximum fluorescence yield was obtained by applying a white saturating light pulse every 60 sec. Wild-type (WT) and Δ*sll1653* mutant (Mut) cells were depleted of oxygen (red trace) by addition glucose (first arrow from the left) and glucose oxidase (second arrow). Letters A-C represent individual peaks shown in Figure 3.25.

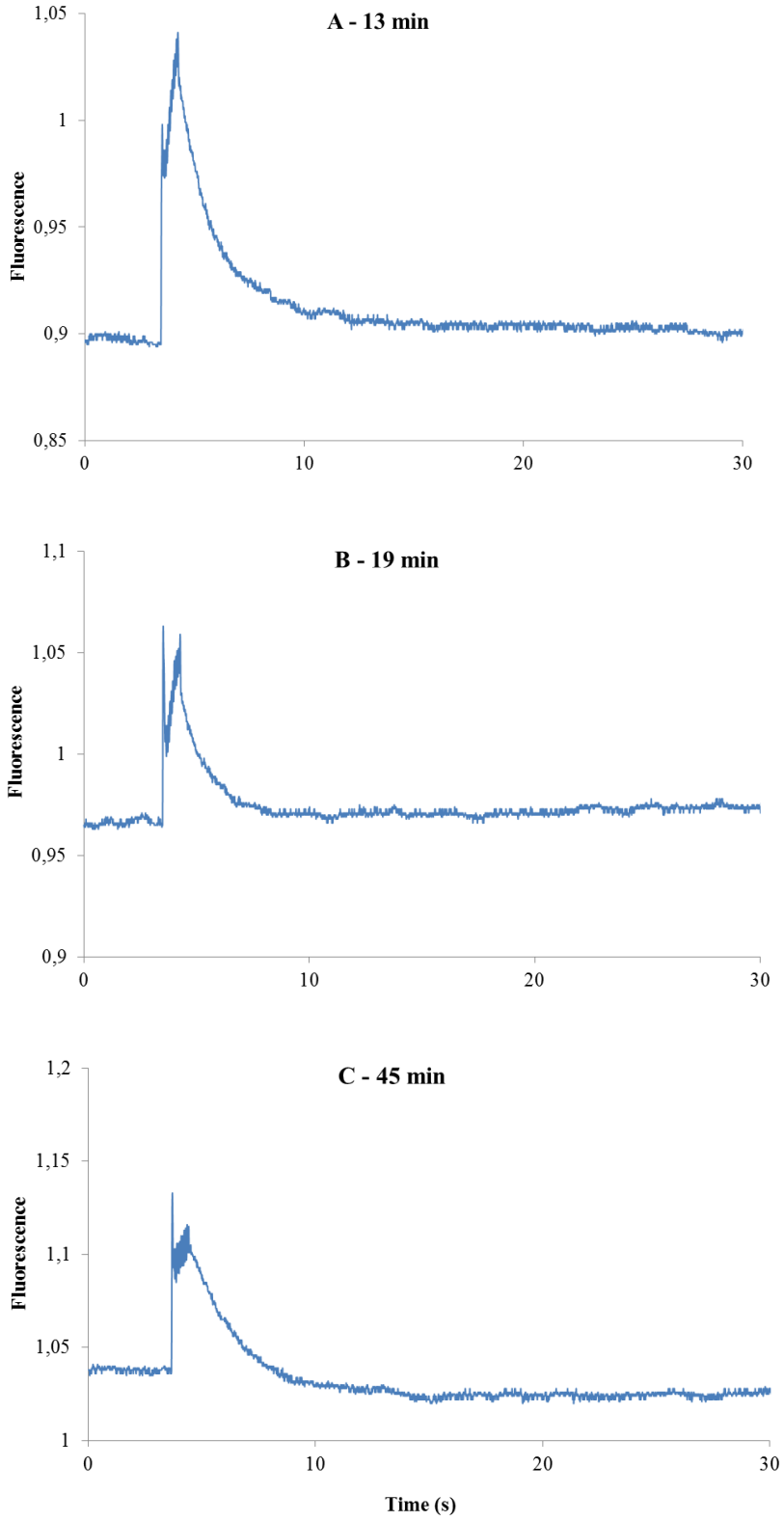

Figure 3.25 – Single Peak PAM Fluorescence Traces. Single fluorescence peaks at three different time points were extracted from wild-type (WT) data in Figure 3.24. Peaks represent fluorescence yield right after the depletion of oxygen (A), upon the initial (B) and slow (C) rise in F_0. Cells were treated with glucose and glucose oxidase.

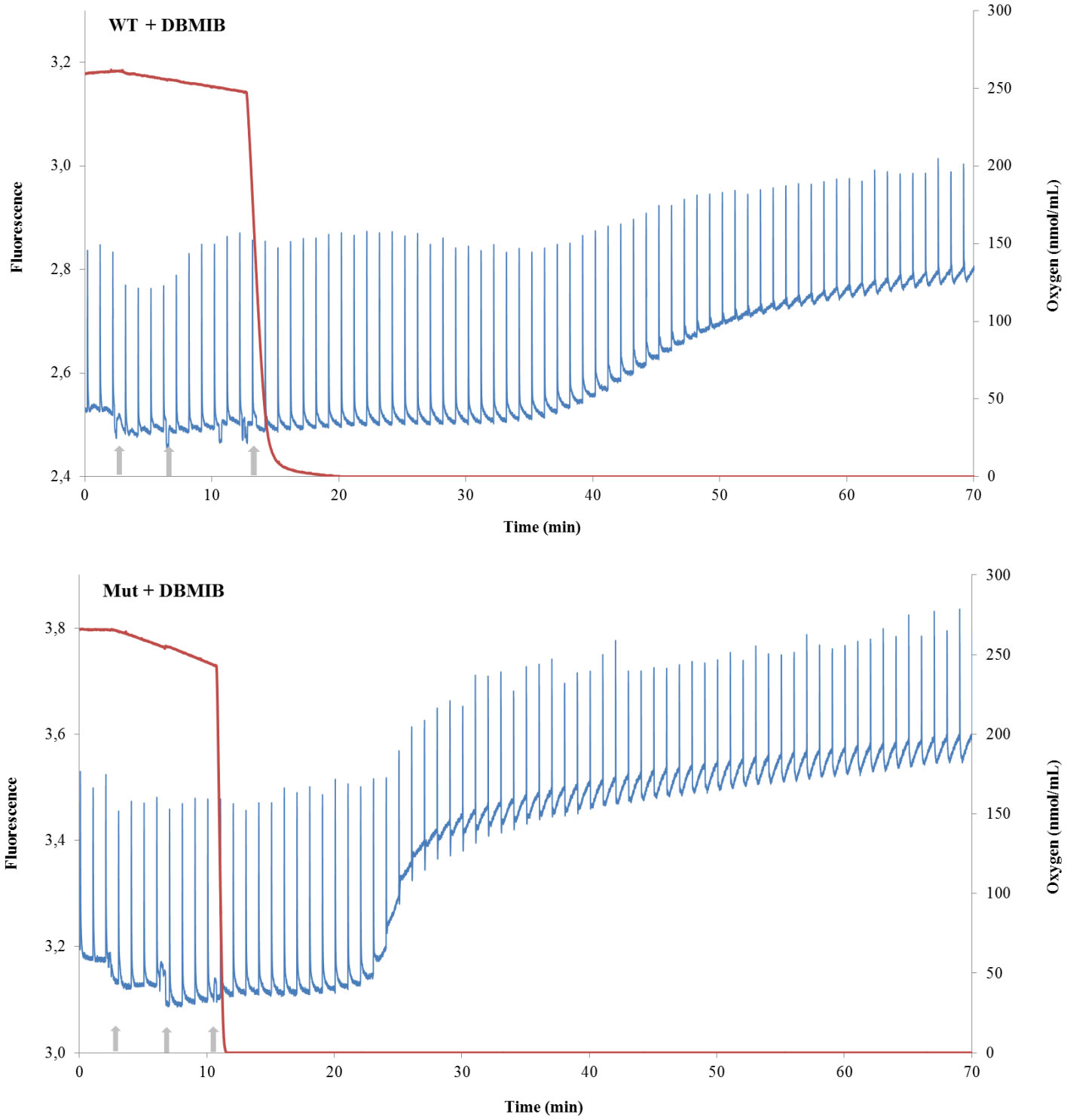

Figure 3.26 – PAM Fluorescence Traces upon Depletion of Oxygen and Treatment with DBMIB. Pulse modulated fluorescence (blue trace) was induced by a low intensity measuring light (625 nm) and maximum fluorescence yield was obtained by applying a white saturating light pulse every 60 sec. Wild-type (WT) and Δ*sll1653* mutant (Mut) cells were depleted of oxygen (red trace) by addition glucose (first arrow from the left) and glucose oxidase (third arrow). DBMIB was added (second arrow) to assess if variations exist that are independent on differences within PS I.

7.3. Quinone Composition

Lipids were extracted from wild-type and Δ*sll1653* cells grown aerobically and anaerobically for 24 hours. Extracts were analyzed by UPLC-qTOF-MS to assess whether a shift in the composition of quinones occurs during a transition from aerobic to anaerobic conditions. The TransOmics software from Waters was utilized to find the relative abundance of plastoquinone and phylloquinone in the extracts from wild-type and mutant cells. As can be seen from Figure 3.27, the mutant was deficient in phylloquinone under both aerobic and anaerobic conditions as is to be expected due to the deletion of the *sll1653* gene. The level of phylloquinone does not seem to change upon a transition from aerobic to anaerobic respiration in the wild-type. The mutant has lower levels of both oxidized and reduced plastoquinone under aerobic conditions compared to the wild-type, but accumulates plastoquinone as it encounters anaerobic conditions to a level that is equal to the wild-type.

Figure 3.27 – Relative Abundance of Quinones under Aerobic and Anaerobic conditions. The TransOmics software was utilized to graphically present the ArcSinh normalized abundance of phylloquinone (A), oxidized plastoquinone (B) and reduced plastoquinone (C) in the extracts derived from wild-type and mutant cells grown under aerobic and anaerobic conditions.

Chapter 4: Discussion

1. Introduction

The objective of this research was to investigate the photosynthetic lipids (chlorophylls, carotenoids and quinones) produced by *Synechocystis* 6803, with a particular focus on isoprenoid quinones. Secondary objectives were the development of methods for analysis of photosynthetic lipids, evaluation of the biosynthetic pathway of plastoquinone in cyanobacteria and the assessment of a potential shift in quinone composition under limiting oxygen conditions. Methods for extraction, separation and characterization of photosynthetic lipids were developed and implemented in order to examine the lipid contents of *Synechocystis* 6803. Candidate genes hypothesized to be involved in the plastoquinone biosynthetic pathway of cyanobacteria were identified through *in silico* analyses and the candidate gene *sll1653* was genetically deleted in *Synechocystis* 6803. The resulting phenotype was characterized using spectrophotometrical techniques and mass spectrometry. In order to determine whether cyanobacteria can modulate the composition of quinones upon depletion of oxygen, the operating efficiency of the photosynthetic machinery and the composition of quinones in wild-type and Δ*sll1653* strain were evaluated under limiting oxygen conditions.

2. Analysis of Photosynthetic Lipids in *Synechocystis* 6803

Investigation of the photosynthetic lipid contents in *Synechocystis* 6803 was the main focus of this research. In order to evaluate the lipids produced by this cyanobacterium, methods for the simultaneous extraction, separation and characterization of chlorophylls, carotenoids and isoprenoid quinones had to be developed. Methods were then implemented to analyze the lipids extracted from *Synechocystis* 6803.

2.1. Development of Methods for Photosynthetic Lipid Analysis

Extraction of photosynthetic lipids from *Synechocystis* 6803 using organic solvent systems and the consecutive separation of extracts by TLC were optimized. For identification of individual lipids in the extracts, a UPLC-qTOF-MS protocol was developed to simultaneously detect chlorophylls, carotenoids and isoprenoid quinones.

2.1.1. Extraction of Photosynthetic Lipids

The solvent system consisting of chloroform and methanol (2:1) stands out as the best solution for extracting photosynthetic lipids from *Synechocystis* 6803 (Chapter 3, section 2.1). This system was capable of extracting both polar and non-polar lipids and may also have caused a better penetration of the cell membrane, which is consistent with the findings of Sheng *et al.* (2011), although their research was focused on extraction of non-polar fatty acids for bio-based fuel production. Relatively polar lipids such as zeaxanthin and myoxanthophyll will dissolve in the upper methanol phase whereas non-polar lipids like β-carotene will be situated in the lower chloroform phase. Out of three sequential extractions with $CHCl_3$:MeOH (2:1) , the first extract had a lower yield of photosynthetic lipids compared to the second extract, and the third extract was almost free of lipids. In further work lipids should therefore be extracted with $CHCl_3$:MeOH in two sequential extractions that can be combined afterwards.

Absorption in the UV region could be observed when lipids were extracted with $CHCl_3$:MeOH and THF (Fig. 3.3) with maxima at 268 nm and 278 nm, respectively. Due to the degradation of THF over time, small amounts of stabilizing chemicals, such as butylated hydroxytoluene (BHT), are added to counteract the degradation. BHT absorbs in the UV region with a maximum at 275 nm (Akkbik *et al.*, 2011) and therefore dominated the absorption in this part of the spectrum, impedes the interpretation of results. Chloroform is stabilized with ethanol and the absorption peak should therefore originate from the quinone content of the extract.

2.1.2. Separation by TLC

Separation of lipids extracted from *Synechocystis* 6803 by thin-layer chromatography (Fig. 3.4 and 3.5, Chapter 3 section 2.2) was implemented for the generation of photosynthetic lipid standards. These standards were supposed to provide the basis for optimization of LC-MS analysis but the concentrations of the isolated lipids were too low at the volumes required. An increase in both the amount of cells utilized in the extraction protocol and the volume of extract applied to the TLC plates could improve the yield of individual lipids. However, such alterations might result in an overload of the plate. The preferred way of increasing lipid yield would therefore be to run several TLC separations in parallel and combining the lipid isolated from each band afterwards and then concentrate extracts by evaporation.

Thin-layer chromatography still provided a good indication of the lipids that had been extracted from *Synechocystis* 6803. This method was utilized, together with absorption spectroscopy data, to determine that $CHCl_3$:MeOH was the most efficient solvent system for extraction of photosynthetic lipids. The identification of individual lipids separated by TLC was conducted by comparing the resulting absorption spectra to literature values for absorption (Appendix I). The only lipid that could not be identified in this way was the one isolated from the band of shortest retention ratio. The separation pattern was compared to that described for spinach extracts (Quach *et al.*, 2004), and may represent a xanthophyll molecule. Suitable candidates may be myxoanthophyll, myxoxanthophyll-fucoside, lutein or zeaxanthin. Based on analyses of carotenoid contents of *Synechocystis* 6803 by Takaichi *et al.* (2001), two xanthophyll bands were expected to be found: a myxoxanthophyll and zeaxanthin. The solvent system (30 % acetone in hexane) may not have been polar enough to

separate both of the xanthophylls from the extract components, as might be indicated by the orange color of the applied spots (Fig. 3.4).

The band identified as plastoquinone (under UV-light) could be detected between bands for β-carotene and echinenone when TLC plates were developed with a mixture of hexane and chloroform (Fig 3.5). The plastoquinone band should therefore have been observed upon the development with hexane-acetone as well, but could not be detected. An explanation for this might be that the band was present, only too weak to be detected under the conditions used. The reduction in polarity in the solvent system hexane-chloroform compared to hexane-acetone may also provide better solubility of plastoquinone in the mobile phase.

2.1.3. Characterization by LC-MS

Based on standards of chlorophyll *a*, β-carotene, ubiquinone and α-tocopherol, conditions for separation of photosynthetic lipids by UPLC and the consecutive ionization and determination of masses by qTOF-MS were optimized (Chapter 3, section 2.3). Based on results presented in Table 3.2, the most suitable mode of ionization of photosynthetic lipids (represented by these standards) was ESI.

The observed mass of 907.52 for chlorophyll *a* is exactly the same as the mass of chlorophyll *b*, but may represent an oxidation product of chlorophyll *a* since this standard is not assumed to contain chlorophyll *b*. Detection of a compound with a mass of 871.57 in the same standard suggests that the magnesium ion have been removed from the porphyrin ring structure of chlorophyll *a*, resulting in pheophytin *a*. Oxidation products could not be detected after ESI for the other standards, which indicates that the chlorophyll *a* standard was oxidized. Ideally, another standard should have been applied to optimize the protocol. The expected mass of ubiquinone-10 is 863.34 g/mol whereas the observed base peak for UQ was 885.68. This increase in mass could be explained from the adduction of a sodium ion during the ionization stage and this mass was also detected by Teran (2001).

The range of photosynthetic lipids synthesized by *Synechocystis* 6803 exceeds that of the standards utilized for optimizing the LC-MS protocol. Still, these standards represent compounds of different polarities and should therefore provide a good basis for optimization of photosynthetic lipid separation by UPLC. The most polar standard compound was α-

tocopherol and, ideally, a standard of higher polarity should have been applied to evaluate separation of xanthophylls. However, when using the polar solvent methanol as mobile phase A, it is assumed that the most polar lipids will be eluated as well. The disadvantage of using these standards is the optimization of ionization conditions because compounds may respond differently to various ionization techniques. Thus, running ESI and APCI modes simultaneously (using an ESCI source) allows high-throughput analysis and may help identify compounds that otherwise can only be detected in one ionization mode (Gallagher *et al.*, 2003).

2.2. Analysis of Lipids Extracted from *Synechocystis* 6803

Lipids were extracted from wild-type and Δ*sll1653* cells using a mixture of chloroform and methanol (2:1) and the contents were analyzed by UPLC-ESCI-qTOF-MS (Table 3.6, Chapter 3 section 6.6). The solvent system implemented does not specifically extract photosynthetic lipids such as chlorophylls, carotenoids and quinones. Hence, a large amount of membrane and other lipids will also be present in the extract. For the interpretation of data, calculated masses of lipids assumed to be synthesized in *Synechocystis* 6803 (Appendix I) were utilized to search the spectrograms. This works for the purpose of mapping the major photosynthetic lipids in *Synechocystis* 6803, but the method needs to be adapted prior to detection of unknown lipids. Modifications to the extraction protocol may target specific lipids better, thus making the data interpretation less time consuming. In addition, more effort should be directed towards the production of standards to confirm the retention times and observed masses of the lipids listed in Table 3.6.

A base peak of 893 (*m/z*) was expected for chlorophyll *a* in the extracts from *Synechocystis* 6803. The base peak of 907.52 in the chlorophyll *a* standard was interpreted to be due to the oxidation of the standard. Upon detection of the same base peak in the extract it can only be assumed that chlorophyll *a* becomes oxidized during the sample preparation or LC-MS analysis. Most likely, oxidation occurs when the organic phase extracts are dried under a steam of nitrogen at 30°C. Base peaks for other photosynthetic lipids detected using ESI+ do not reveal major oxidation products. Still, the oxidation of chlorophyll *a* is problematic and a reduction in temperature during solvent evaporation might eliminate this problem. The

relatively high abundance of pheophytin *a* could be explained from the fact that UPLC separation is performed with a mobile phase containing 0.05 % formic acid. Treatment with acids is known to remove the magnesium ion from chlorophyll *a*, creating pheophytin *a*. In future work with LC-MS analysis of photosynthetic lipids the addition of formic acid to mobile phase A should be avoided, although this can reduce the resolution of separation.

LC-MS can be considered a semi-quantitative method if sample preparation conditions are identical. Extracts were prepared from equal amounts of cells under similar conditions and the detection signal information was utilized to calculate the relative abundance of lipids compared to chlorophyll *a*. Detection signals were standardized to the detection signal sum of Chl *a*, oxidized Chl *a* and pheophytin *a*. This was done to correct for the oxidation and removal of the magnesium ion from Chl *a* under sample preparation and the sum should therefore represent the total chlorophyll concentration. Based on the observation that the chlorophyll *a* concentration is similar in both strains (Fig. 3.17 and 3.18A, Chapter 3 section 6.4-6.5), the standardized relative abundance of each lipid was thereafter divided by the standardized relative abundance of Chl *a*. These calculated relative abundances can only be used to give an indication of the relative ratio between different lipids and may be associated with large deviations. This can be seen for the lipid extracts of wild-type and mutant cells (Table 3.6), in which large difference exist for oxidized chlorophyll *a*. Since samples are prepared the same way, this number was expected to be similar in wild-type and mutant. Preferably, samples should have been analyzed multiple times to give an indication of the associated errors, but the time scope of this project and repeated break-down repair and maintenance of the instrument did not allow for this.

Analysis of the lipid extract from *Synechocystis* 6803 revealed the presence of most photosynthetic lipids assumed to be synthesized in this organism (listed in Appendix I). However, it was difficult to distinguish zeaxanthin and lutein from each other. Most likely, the *m/z* peak of 568.43 represents zeaxanthin which has previously been identified in *Synechocystis* 6803 and other cyanobacteria (Takaichi *et al.*, 2001; Armstrong, 1997).

3. BioBrick Cloning

A novel BioBrick consisting of the genes encoding red fluorescent protein (*mCherry*) and antibiotic resistance against chloramphenicol (*cat*), held in a standard BioBrick cloning plasmid, was produced (Chapter 3, section 4). Transformation of *E. coli* was considered to be successful due to the observation of red-colored colonies on medium supplemented with chloramphenicol (Fig. 3.8). According to the plasmid map in Figure 3.7, a digest of the correctly constructed plasmid should produce fragments of 0.35, 1.6 and 2.1 kb. The 350 bp band could not be observed; instead a band was observed around 3.5 kb, but this was clearly overloaded. This could indicate a partial digest with SpeI, resulting in fragments of 3.7 and 0.35 kb. The small size of the 350 bp fragment and the overlay of loading dye in this area could be the reason this fragment was not observed. Still, the 1.6 kb fragment indicates that a chloramphenicol cassette has been included in the BioBrick which previously had a length of 1.1 kb. Also, the growth on chloramphenicol and the red pellet color are solid indications that the correct BioBrick had been constructed.

The BioBrick was constructed for the application in genetic inactivation of targeted genes. As mentioned in the Chapter 1, special considerations must be taken to avoid the presence of prefix and suffix restriction sites in both the BioBrick part and the vector molecule. The presence of the EcoRI restriction site in the chloramphenicol cassette was not known as this project was initiated. This does not mean that the BioBrick cannot be used, but special care must be taken. When applying this BioBrick in molecular genetic work, the utilization of EcoRI can be avoided by using XbaI for restriction cutting instead. Also, this BioBrick should not be used for genetic deletion of genes if analysis of mutant phenotype is dependent on spectroscopic analysis. The expression of the mCherry protein confers a red color of the cells which may be detected in an *in vivo* absorption spectrum. Transformation of *Synechocystis* 6803 with a construct that contains this BioBrick should therefore be avoided.

4. Biosynthetic Pathway of Plastoquinone in Cyanobacteria

A particular focus of this thesis has been directed towards the function and synthesis of isoprenoid quinones. There are indications that the biosynthetic pathway of plastoquinone in cyanobacteria differs from that of plants and algae. Candidate genes hypothesized to be involved in the unresolved biosynthetic pathway of plastoquinone in cyanobacteria were identified through *in silico* analyses. The candidate gene *sll1653* was then genetically deleted from *Synechocystis* 6803 to evaluate its role in plastoquinone synthesis in this cyanobacterium.

4.1. Candidate Genes

The unresolved biosynthetic pathway of plastoquinone in cyanobacteria was investigated based on the hypothesis that plastoquinone and ubiquinone synthesis are evolutionary related (Chapter 3, section 3). Candidate genes were identified through BLASTP, in which protein sequences for enzymes involved in ubiquinone synthesis in *E. coli* were compared to protein sequences in the genome database for *Synechocystis* 6803. Putative orthologs to the candidate genes were then identified in other cyanobacterial species using Cyanobase.

4.1.1. Decarboxylases

Homologs to the decarboxylases UbiD and UbiX in *E. coli* were identified as the gene products of *sll0936* and *slr1099* in *Synechocystis* 6803. Orthologs with high sequence similarities were found in 14 other cyanobacterial species. In *E. coli*, the expression of *ubiD* and *ubiX* are dependent on the carbon source under aerobic conditions and *ubiX* has been shown to be the only one of these decarboxylase genes that are expressed under anaerobic conditions (Zhang, H. and Javor, 2003). Since *Synechocystis* 6803 is a facultative anaerobe organism, the genes *sll0936* and *slr1099* might be regulated in the same way upon changes in the availability of oxygen. Sequence identities above 80 % in other cyanobacterial species strongly support the hypothesis that these genes are involved in the synthesis of plastoquinone in *Synechocystis* 6803 and other cyanobacteria. In fact, the work of Pfaff *et al.* (2014) recently

confirmed the involvement of *sll0936* and *slr1099* in the decarboxylation step of plastoquinone synthesis in *Synechocystis* 6803.

4.1.2. Hydroxylases

The gene *sll0095* was identified in *Synechocystis* 6803 as a homolog to *ubiB*, a FAD-dependent hydroxylase involved in ubiquinone synthesis in *E. coli*. In addition, the *slr1300* gene was found to match the sequences of both *ubiH* and *ubiF* from *E. coli*. The descriptions given for the identified orthologs strongly suggest the involvement of the *slr1300* gene in the hydroxylation step of plastoquinone synthesis in cyanobacteria. The genetic inactivation of this gene was attempted by Sakuragi (2004) but failed due to incomplete segregation of the genome, which might indicate the importance of the *slr1300* gene in *Synechocystis* 6803. Generation of a Δ*slr1300* strain might be accomplished if transformed cells are grown in the presence of 2-nonaprenyl-6-methoxy-1,4-benzoquinone, the hypothesized product of the reaction catalyzed by the UbiH homolog. Due to the absence of methoxy substituents in plastoquinone, an UbiB homolog is actually not required for the introduction of hydroxyl groups that can be further methylated. Still, *sll0095* can be involved in the synthesis pathway if the utilization of hydroxylases changes under various environmental conditions. Alexander and Young (1978) demonstrated the utilization of alternative hydroxylases in the aerobic and anaerobic synthesis pathway of ubiquinone in *E. coli*. As a consequence of the metabolic features of *Synechocystis* 6803, both *sll0095* and *slr1300* should be evaluated for their involvement in the biosynthetic pathway of plastoquinone.

4.1.3. Methyltransferases

Several homologs of the UbiE methyltransferase were found in *Synechocystis* 6803. The most obvious candidate to this methylation step, identified through the *in silico* analyses, was the enzyme encoded by *sll1653*. Conserved orthologs of this enzyme were found in all 14 cyanobacterial species evaluated. The methyltransferase encoded by *sll1653* has already been proved to be involved in the biosynthetic pathway leading to phylloquinone (Sakuragi *et al.*, 2002) and its potential involvement in PQ synthesis can be hypothesized from the fact that UbiE confers bi-functional methyltransferase activity in both ubiquinone and menaquinone syntheses in *E. coli* (Lee et al., 1997). In previous studies where *sll1653* have been genetically

deleted (Sakuragi *et al.*, 2002), PS I particles were investigated to assess the effect of impaired phylloquinone synthesis, in particular the lack of a methyl group. The impact on the photosynthetic machinery as a whole and electron transport in particular should be evaluated to assess the role of s*ll1653* in plastoquinone synthesis. Other methyltransferase candidates found in *Synechocystis* 6803 were the proteins Slr0407, Sll0829 and Slr1618. Since the synthesis of PQ requires the delivery of two methyl groups, more than one methyltransferase may be involved in this pathway and several candidates could therefore be considered for genetic inactivation. If methyltransferase isoenzymes regulated in response to environmental changes exist in *Synechocystis* 6803, as discussed by Sadre *et al.* (2012), the identification of the enzyme catalyzing the PQ methylation step will become more complex. For example, a decrease in the PQ level will not be as evident upon genetic deletion of candidate genes if isoenzymes are found in this biosynthesis pathway.

4.2. The Δ*sll1653* Deletion Strain

The gene deletion strain Δ*sll1653* of *Synechocystis* 6803 was constructed by homologous integration of a kanamycin resistance cassette in the place of the gene *sll1653*, which is hypothesized to be involved in the methylation reactions of plastoquinone (Chapter 3, section 5). The involvement of the same methyltransferase in phylloquinone synthesis will also confer a deficiency in PS I (Sakuragi *et al.*, 2002). The Δ*sll1653* strain was characterized to assess the involvement of this gene in quinone biosynthesis (Chapter 3, section 6).

4.2.1. The Strain Does Not Grow on Glucose under High Light Conditions

The Δ*sll1653* strain was able to grow both photoautotrophically and photoheterotrophically on glucose under normal light conditions (200 µE $m^{-2}s^{-1}$) with doubling times slightly lower than that of the wild-type (Table 3.3, Chapter 3 section 6.1). The mutant was unable to grow on glucose under high light conditions (500-700 µE $m^{-2}s^{-1}$) unless the medium was supplemented with DCMU (Fig. 3.13). Competitive binding of DCMU to the Q_B site of PS II blocks electron transfer to plastoquinone and prevents the formation of damaging reductants by PS II. It can be argued that, in the absence of DCMU, utilization of glucose as a carbon source in combination with high light conditions lead to an over-reduction of the PQ-pool and

the subsequent production of reactive oxygen species (ROS), causing damage to essential cell constituents and failure to grow. A lack of respiratory capacity may be the source of the postulated increased reduction of the PQ-pool in the mutant and is further discussed in Section 4.4.2. The same phenomenon was observed when the *menA* and *menB* genes (also involved in phylloquinone synthesis) were genetically deleted in *Synechocystis* 6803 and cells were grown on glucose and atrazine, an herbicide which also targets the Q_B site (Johnson *et al.*, 2000)Growth of the mutant strain was not expected to exceed the growth of the wild-type in any of the conditions tested. However, under some conditions (growth on BG11 and with addition of glucose or glucose plus DCMU) the mutant showed increased growth rates compared to the wild-type. This might indicate that the potential lack of methyl groups in PQ does not affect electron transport to a large degree or that the only deficiency is located to the A_1 site of PS I. It is concluded that the deletion of the *sll1653* gene does not have a major impact on survival of *Synechocystis* 6803.

4.2.2. Decreased Respiratory Capacity

The Δ*sll1653* strain showed decreased respiratory capacity, especially in the presence of glucose (Table 3.4, Chapter 3 section 6.2). The observed reduction in respiratory capacity could be caused by the accumulation of demethylated plastoquinone in the PQ-pool. However, there are no indications of a PQ lacking the methyl group from mass spectrometry measurements and this emerges as a field of future research, as additional analysis is not possible at present. Changes in the PQ molecule may prevent the interaction with components downstream in the ETC, such as the cyt b_6f complex, plastoquinol oxidase, cytochrome *c* oxidase or the alternate respiratory terminal oxidase (Berry *et al.*, 2002; Pils and Schmetterer, 2001). The direct interaction between the reduced plastoquinone and the respiratory terminal oxidases, however, might become altered as the *sll1653* gene is deleted. This could indicate that the methyltransferase encoded by *sll1653* catalyzes the methylation of another quinone, which might function as a mobile link between the PQ-pool and the terminal oxidases.

In addition, the respiratory capacity could be affected by the input of electrons into the respiratory ETC. Due to the hypothesized defect in PS I (caused by an alteration in phylloquinone), cyclic electron transport might be impaired. Cyclic electron transport in *Synechocystis* 6803 can follow several pathways, one of them where electrons are donated

from NADPH to PQ via the NDH-1 (Ogawa, 1991). The activity or the amount of electron donors present, such as type I or II NAD(P)H dehydrogenases and succinate dehydrogenase, may be altered as a consequence of reduced cyclic electron transport in the mutant strain. Even though growth analyses suggest that the Δ*sll1653* mutant is not noteworthy impaired in photosynthetic electron transport under normal light conditions (Fig. 3.13B), a down-regulation of the dehydrogenases may result in a reduced respiratory capacity. Such down-regulation can prevent the over-reduction of the PQ-pool and hence the production of ROS in the mutant cell.

4.2.3. The Strain is More Protected against Photoinhibition

Measurements of oxygen evolution (Fig. 3.14 and 3.15, Chapter 3 section 6.2) indicate a smaller antenna size of the mutant compared to the wild-type. A larger antenna enhances the rate of light absorption and the production of oxygen. However, the immediate electron acceptor of PS II, Q_A, becomes highly reduced at increasing light intensities and is dependent on forward electron transport to prevent radical formation. The rapid photoinhibition or photodamage for wild-type cells can thus be explained from the larger antenna size. The higher respiratory capacity of the wild-type (Fig. 3.16) does not seem to protect the cells from photodamage through the activity of the water-water cycle (Asada, 1999). A smaller antenna size of the Δ*sll1653* strain can explain the lower rate of photoinhibition. Additionally, the Δ*sll1653* strain appears to possess more carotenoids that may also help in protecting the photosynthetic machinery under high light.

In vivo absorption spectroscopy revealed elevated levels of carotenoids in the Δ*sll1653* strain (Fig. 3.17, Chapter 3 section 6.4), and LC-MS analysis further supports an increase in the carotenoids β-carotene, myxoxanthophyll-fucoside and zeaxanthin in the mutant strain (Table 3.6, Chapter 3 section 6.6). These carotenoids have been demonstrated to protect cells from high light-mediated photodamage caused by ROS formation in *Synechocystis* 6803 (Schäfer *et al.*, 2005). Schäfer *et al.* (2005) also showed that echinenone only participates in photoprotection to a small extent and may explain the similar levels of echinenone and hydroxyl-echinenone in wild-type and mutant cells. The isoprenoid quinone α-tocopherol has been shown to possess photoprotective properties and overlapping functions with carotenoids in *C. reinhardtii* (Li, Z. *et al.*, 2012). Elevated levels of both carotenoids and α-tocopherol

suggest that the Δ*sll1653* strain is adapted against photooxidative stress. If this increase in photoprotective carotenoids is caused by the modified phylloquinone in PS I or to alterations in other quinone molecules, especially plastoquinone, remains to be determined.

4.2.4. Methylation of PQ is Not Solely Dependent on the *sll1653* Gene

Involvement of the *sll1653* gene in phylloquinone synthesis was confirmed by LC-MS analysis in which the peak for phylloquinone was missing for the mutant (Fig. 3.21, Chapter 3 section 6.6). Still, a peak for demethylated phylloquinone could not be detected at the same retention time as for phylloquinone and this should be investigated further in the future (as access to analyzing software has expired). The detection of plastoquinone in lipid extracts from both wild-type and mutant cells (Fig 3.20) indicate that the methyltransferase encoded by *sll1653* is either not involved in the biosynthetic pathway of plastoquinone in *Synechocystis* 6803 or that several methyltransferases function in close conjugation to methylate the plastoquinone molecule. Lack of one or both methyl groups should change the redox potential and the binding characteristics of the plastoquinone and hence have an impact on electron transport and growth of the organism. As previously described, growth of the mutant strain was not significantly different from the wild-type except for growth under high light conditions on media supplemented with glucose. Also, neither a single nor a double demethylated plastoquinone could be detected in the mass spectrum for the mutant; further supporting the conclusion that *sll1653* is not involved in plastoquinone synthesis.

5. Effects of Oxygen Depletion in *Synechocystis* 6803

Wild-type and mutant cells were subject to anaerobic conditions to assess whether a shift in the utilization of quinones could be observed (Chapter 3, section 7). Transition from aerobic to anaerobic conditions was achieved in several ways; by bubbling with argon gas, addition of glucose oxidase and by cellular respiration of O_2 in the dark. The effect of oxygen depletion was studied using spectroscopic and mass spectrometric techniques.

5.1. Glucose Oxidase Affects State Transition from PS II to PS I

A state transition, in which the phycobilisomes translocate from PS II to PS I, was observed for both wild-type and Δ*sll1653* cells upon depletion of oxygen in the dark (Fig. 3.23, Chapter 3 section 7.1). The reduction of the PQ pool or a closely associated electron carrier is believed to control this state 1 to state 2 transition (Mullineaux and Allen, 1990). Normally, this state transition can also be observed in PAM fluorescence spectra as a decrease in F_M when cells adapt to anaerobic conditions (see Fig. 1.15). However, this could not be observed in the PAM fluorescence traces recorded for wild-type nor mutant. A separate experiment using glucose oxidase to induce anaerobic conditions followed by measurements of 77 K fluorescence emission at 580 nm (data not shown) did not indicate a state transition from PS II to PS I, as was observed when anaerobic conditions were initiated by bubbling with argon gas (Fig. 3.23). Based on these results, it is hypothesized that the use of glucose oxidase inhibits the state transition. This enzyme uses O_2 as an electron acceptor in the oxidation of β-D-glucose to gluconic acid, leading to the production of hydrogen peroxide as a byproduct (Bankar *et al.*, 2009). *Synechocystis* 6803 possesses A-type flavoproteins that reduces O_2 into water using electrons from PS I, without the production of hydrogen peroxide that is observed in the Mehler reaction of chloroplasts (Helman *et al.*, 2003; Mehler, 1951). It might be reasoned that glucose oxidase outcompetes the A-type flavoproteins for oxygen produced by PS II, thus electron generated from PS I are no longer needed for reduction of O_2 and light-harvesting antennas will continue to be associated with PS II. Still, such PS I-dependent O_2 consumption will not take place in the dark and cannot explain why this state transition could not be observed in the 77 K fluorescence emission spectrum when oxygen was depleted by the action of glucose oxidase. Future research will be required to assess why glucose oxidase does not induce state transitions although it clearly induces anaerobic conditions.

5.2. Depletion of Oxygen Causes an Increase in F_0

The reliability of the PAM data may be questioned due to the effect of glucose oxidase, but the lack of oxygen in the medium should still confer the same alterations to electron transport regardless of how oxygen was depleted. The rise in F_0 induced by oxygen depletion (Fig. 3.24, Chapter 3 section 7.2) can be interpreted as accumulation of electrons in the ETC

causing a reduction of the PQ-pool and subsequent reduction of Q_A. This was also observed in studies of oxygen depletion in *C. reinhardtii* by Hohmann-Marriott *et al.* (2010). Differences between mutant and wild-type were negligible, indicating that the deletion of *sll1653* does not impact the functionality of the ETC to a large extent. If phylloquinone were to substitute plastoquinone under anaerobic conditions, electron transport should have been impaired or altered in the mutant.

Immediately after depletion of oxygen (Fig. 3.25A), a SAT-pulse completely reduces Q_A (yielding a high fluorescence) which then recovers to the oxidized state by the transfer of electrons to plastoquinone. Saturating light-pulses oxidize the PQ-pool by the action of PS I allowing the transfer of newly generated electrons forward through the ETC. As electrons accumulate in the PQ-pool, an initial rise in F_0 was observed. Fluorescence was reset by the saturating light-pulses but to a higher level than that reflecting a fully reduced PQ-pool (Fig. 3.25B). Hence, Q_A^- could not be completely rescued and quenching of fluorescence by Q_A^0 is reduced resulting in F_0 increase. Prolonged exposure to anaerobic conditions induced a slow increase in F_0, at least for the wild-type (Fig. 3.24) and a single SAT-pulse in this region revealed that fluorescence resets to a level below F_0 measured prior to application of the SAT-pulse (Fig. 3.25C). This indicates that the redox state of Q_A changes from slightly reduced (~ 30 % Q_A^-) via completely reduced (100 % Q_A^-) upon exposure to a saturating light pulse and completely oxidized (0 % Q_A^-) before it recovers to the starting point (~ 30 % Q_A^-). This can be interpreted as the oxidation of PQ by the action of PS I, via the cytochrome *b_6f* complex.

5.2.1. Q_A^- Can Still Be Rescued in the Presence of DBMIB

When cells were treated with DBMIB, the same rise in F_0 and the reset of fluorescence yield were observed for both wild-type and mutant strains (Fig. 3.26, Chapter 3 section 7.2) and the results were similar to those in the absence of DBMIB. This observation deviated from the expected increase in fluorescence signal due to the inhibition of plastoquinol oxidation by the cytochrome *b_6f* complex. Especially, the reset in fluorescence yield upon prolonged exposure to limiting oxygen availability is an interesting observation because the application of SAT-pulses should not generate oxidized species that can rescue the Q_A^-. Somehow electrons must be transferred from the reduced PQ-pool to the excited reaction center of PS I, avoiding the route via the *b_6f* complex. Quinones represent possible candidates for this type of electron

transport due to their mobility in the thylakoid membrane. The deletion of the *sll1653* gene seems to induce a larger reset in fluorescence under these conditions (Fig. 3.26), which might indicate that there is a stronger connection between the PQ-pool and PS I in this strain. Schuurmans *et al.* (2014) recently showed that the DBMIB did not reduce the PQ-pool under very low oxygen conditions and suggest that regulatory processes are controlled via sensing of other components – not by the redox state of the PQ-pool. Further research should therefore be focused on identification of possible components involved in the transition from aerobic to anaerobic conditions.

5.3. PQ is Not Replaced by PhQ under Anaerobic Conditions

The determination of relative abundances of plastoquinone and phylloquinone by MS under aerobic and anaerobic growth conditions revealed that the level of these quinones did not change as a consequence of oxygen limitation in the wild-type (Fig. 3.27, Chapter 3 section 7.3). Due to storing of the samples prior to analysis by LC-MS, reduced plastoquinone in the extract from anaerobic cultivated cells was probably oxidized, causing an increase in the abundance of oxidized plastoquinone. The relative abundance of plastoquinone in the Δ*sll1653* strain seemed to be slightly elevated under anaerobic conditions. As previously discussed, isoenzymes exist in other facultative anaerobic species that function in quinone biosynthesis under variable environmental conditions (Alexander and Young, 1978). If the methyltransferase encoded by *sll1653* has a role in plastoquinone synthesis, it is not under anaerobic conditions. Increased amounts of phylloquinone would have been observed if this quinone replaced plastoquinone upon depletion of oxygen, thus without this increase it is concluded that such shift does not occur in *Synechocystis* 6803.

Chapter 5: Conclusions

The primary objective of this project was to investigate photosynthetic lipids, in particular the function of isoprenoid quinones in *Synechocystis* 6803. Secondary objectives were the development of methods for analysis of photosynthetic lipids, evaluation of the biosynthetic pathway of plastoquinone in cyanobacteria and the assessment of a potential shift in quinone composition under limiting oxygen conditions.

Methods for extraction, separation and characterization of photosynthetic lipids were optimized. A mixture of chloroform and methanol (2:1) was determined to be the most efficient solvent system for extraction of chlorophylls, carotenoids and isoprenoid quinones from *Synechocystis* 6803. Separation of extracted components by TLC was optimized, although this method was primarily used as an indicator of extraction yield from different extraction systems. A method for analyzing the photosynthetic lipid content of *Synechocystis* 6803 by UPLC-qTOF-MS was developed and implemented. This method revealed the presence of most photosynthetic lipids assumed to be synthesized in *Synechocystis* 6803, listed in Table 3.6.

The biosynthesis of plastoquinone in cyanobacteria was evaluated and candidate genes assumed to be involved in this pathway were identified using bioinformatics approaches in conjunction with the current understanding of isoprenoid quinone synthesis pathways in plants and other bacteria. The candidate gene *sll1653* was genetically deleted in *Synechocystis* 6803 and the resulting phenotype was characterized. The Δ*sll1653* strain exhibit similar growth characteristics as the wild-type but shows deficiencies when grown in the presence of glucose under high light. Lipid analyses revealed elevated levels of phycobilins and photoprotective antioxidants such as carotenoids and α-tocopherol. The mutant strain was, as expected, impaired in the last step of phylloquinone synthesis (Sakuragi *et al.*, 2002) but did not possess reduced levels of plastoquinone or major deficiencies in electron transport compared to the wild-type. Thus, it is concluded that *sll1653* does not encode the methyltransferase that is solely responsible for methylation of plastoquinone in *Synechocystis* 6803.

A physiological focus of this thesis was based on the hypothesis that cyanobacteria can modulate the composition of quinones upon depletion of oxygen. Wild-type and Δ*sll1653* strains exhibited similar responses to anaerobic conditions, such as a state transition (in which light-harvesting antennas relocate from PS II to PS I) and a reduction of the PQ-pool (observed as an increase in F_0), when assessed by spectroscopic techniques. Mass spectrometry analyses of photosynthetic lipids extracted from cells grown aerobically and anaerobically did not reveal significant changes in the composition of plastoquinone and phylloquinone as a consequence of this transition. The conclusion is that plastoquinone is not replaced by phylloquinone under limiting oxygen concentration. However, unexpected results were obtained when cells were treated with DBMIB, indicating the existence of a link between PS I and the PQ pool that is independent of the cytochrome b_6f complex under anaerobic conditions. Further research should therefore be focused on identification of possible components involved in the transition from aerobic to anaerobic conditions.

Future Research

The biosynthetic pathway of plastoquinones in cyanobacteria still remains unresolved. Development of methods that specifically extracts isoprenoid quinones will reduce the work load associated with data acquisition in LC-MS analysis of total lipid extracts and is a necessity if this biosynthetic pathway is to be completely described. The method developed in this project, however, will also prove useful for other students and candidates working on photosynthetic lipid production. Some modifications to the method are still required, for example in preparation of samples and avoidance of formic acid in mobile phase A to reduce the oxidation of lipids prior to analysis. Further work with TLC separation of photosynthetic lipids would provide standards for optimizing LC-MS for different classes of lipids, minimizing the after work with identification of individual lipids.

Results obtained indicate that *sll1653* does not encode the main methyltransferase involved in plastoquinone synthesis, and thus other candidate genes should be evaluated for their involvement in this step. Due to the requirement of two methyl groups in the plastoquinone molecule, double or several-fold mutants should be generated and characterized to evaluate the overall effect on plastoquinone synthesis. Also, genes hypothesized to be involved in other parts of this pathway should be genetically deleted. If genes identified through the *in silico* analysis prove not to be a part of the plastoquinone pathway, more advanced bioinformatics approaches should be considered to identify new candidates.

Depletion of oxygen and the subsequent adaption to anaerobic respiration in *Synechocystis* 6803 is an interesting field of research, especially because this shift is associated with the production of H_2 by a bidirectional hydrogenase and may be utilized for biotechnological applications. Identification of components that may serve a function in the donation of electrons, electron transport and as terminal electron acceptors in anaerobic respiration will provide greater understanding of the complex electron transport processes in the thylakoid membranes of cyanobacteria. PAM fluorometry serves as a suitable method for the overall assessment of electron transport in photosynthetic organisms and more work should thus be focused on the interpretation of fluorescence quenching under anaerobic conditions.

Unexpected results regarding the maintenance of electron transport in the presence of DBMIB and absence of oxygen still requires an explanation. The existence of another isoprenoid quinone or a mobile phylloquinone may provide an explanation for the observed link between the PQ-pool and PS I under anaerobic conditions in *Synechocystis* 6803.

References

Akkbik, M. , Assim, Z. B. & Ahmad, F. B. (2011) Optimization and Validation of Rp-Hplc-Uv/Vis Method for Determination Phenolic Compounds in Several Personal Care Products. *International Journal of Analytical Chemistry,* **2011,** 1-9.

Alexander, K. & Young, I. G. (1978) Alternative Hydroxylases for the Aerobic and Anaerobic Biosynthesis of Ubiquinone in Escherichia Coli. *Biochemistry,* **17,** 4750-4755.

Altschul, S. F. , Gish, W. , Miller, W. , Myers, E. W. & Lipman, D. J. (1990) Basic Local Alignment Search Tool. *J Mol Biol,* **215,** 403-10.

Armstrong, G. A. (1997) Genetics of Eubacterial Carotenoid Biosynthesis: A Colorful Tale. *Annual Review of Microbiology,* **51,** 629-659.

Asada, K. (1999) The Water-Water Cycle in Chloroplasts: Scavenging of Active Oxygens and Dissipation of Excess Photons. *Annual Review of Plant Biology,* **50,** 601-639.

Baker, N. R. (2008) Chlorophyll Fluorescence: A Probe of Photosynthesis in Vivo. *Annu Rev Plant Biol,* **59,** 89-113.

Bankar, S. B. , Bule, M. V. , Singhal, R. S. & Ananthanarayan, L. (2009) Glucose Oxidase — an Overview. *Biotechnology Advances,* **27,** 489-501.

Bekker, M. , Kramer, G. , Hartog, A. F. , Wagner, M. J. , De Koster, C. G. , Hellingwerf, K. J. & De Mattos, M. J. (2007) Changes in the Redox State and Composition of the Quinone Pool of Escherichia Coli During Aerobic Batch-Culture Growth. *Microbiology,* **153,** 1974-80.

Bentley, R. & Meganathan, R. (1982) Biosynthesis of Vitamin K (Menaquinone) in Bacteria. *Microbiol Rev,* **46,** 241-80.

Berry, S. , Schneider, D. , Vermaas, W. F. & Rogner, M. (2002) Electron Transport Routes in Whole Cells of Synechocystis Sp. Strain Pcc 6803: The Role of the Cytochrome Bd-Type Oxidase. *Biochemistry,* **41,** 3422-9.

Blankenship, R. E. (2002) *Molecular Mechanisms of Photosynthesis*. Oxford: Blackwell Science Ltd.

Bligh, E. G. & Dyer, W. J. (1959) A Rapid Method of Total Lipid Extraction and Purification. *Canadian Journal of Biochemistry and Physiology,* **37,** 911-917.

Bouvier, F. , Rahier, A. & Camara, B. (2005) Biogenesis, Molecular Regulation and Function of Plant Isoprenoids. *Prog Lipid Res,* **44,** 357-429.

Butler, W. L. (1972) On the Primary Nature of Fluorescence Yield Changes Associated with Photosynthesis. *Proc Natl Acad Sci U S A,* **69,** 345-378.

Butler, W. L. (1978) Energy Distribution in the Photochemical Apparatus of Photosynthesis. *Annu Rev Plant Physiol,* **29**.

Calvin, M. & Benson, A. A. (1948) The Path of Carbon in Photosynthesis. *Science,* **107,** 476-480.

Chung, Y.-H. , Park, Y. M. , Moon, Y.-J. , Lee, E.-M. & Choi, J.-S. (2004) Photokinesis of Cyanobacterium Synechocystis Sp. Pcc 6803. *Journal of Photoscience,* **11,** 89-94.

Clarke, C. (2000) New Advances in Coenzyme Q Biosynthesis. *Protoplasma,* **213,** 134-147.

Duran, R. V. , Hervas, M. , De La Rosa, M. A. & Navarro, J. A. (2004) The Efficient Functioning of Photosynthesis and Respiration in Synechocystis Sp. Pcc 6803 Strictly Requires the Presence of Either Cytochrome C6 or Plastocyanin. *J Biol Chem,* **279,** 7229-33.

Duysens, L. N. M. & Sweers, H. E. (1963) Mechanisms of Two Photochemical Reactions in Algae as Studied by Means of Fluorescence *in:* Physiologists, J. S. O. P. (ed.) *Studies on Microalgae and Photosynthetic Bacteria.* Tokyo: Univeristy of Tokyo Press.

Dähnhardt, D. , Falk, J. , Appel, J. , Van Der Kooij, T. , Schultz-Friedrich, R. & Krupinska, K. (2002) The Hydroxyphenylpyruvate Dioxygenase from Synechocystis Sp. Pcc 6803 Is Not Required for Plastoquinone Biosynthesis. *FEBS Letters,* **523,** 177-181.

Döring, G. , Bailey, J. L. , Kreutz, W. , Weikard, J. & Witt, H. T. (1968) Some New Results in Photosynthesis - the Action of Two Chlorophyll-a 1-Molecules in Light Reaction I of Photosynthesis. *Die Naturwissenschaften,* **55,** 219-224.

Döring, G. , Renger, G. , Vater, J. & Witt, H. T. (1969) Properties of the Photoactive Chlorophyll-Aii in Photosynthesis. *Zeitschrift fur Naturforschung. Teil B: Chemie, Biochemie, Biophysik, Biologie,* **24,** 1139-1143.

Döring, G. , Stiehl, H. H. & Witt, H. T. (1967) A Second Chlorophyll Reaction in the Electron Chain of Photosynthesis--Registration by the Repetitive Excitation Technique. *Zeitschrift fur Naturforschung. Teil B: Chemie, Biochemie, Biophysik, Biologie,* **22,** 639-644.

Eaton-Rye, J. J. (2011) Construction of Gene Interruptions and Gene Deletions in the Cyanobacterium Synechocystis Sp. Strain Pcc 6803. *Methods Mol Biol,* **684,** 295-312.

Folch, J. , Lees, M. & Stanley, G. H. S. (1957) A Simple Method for the Isolation and Purification of Total Lipides from Animal Tissues. *Journal of Biological Chemistry,* **226,** 497-509.

Förster, T. (1965) Delocalized Excitation and Excitation Transfer *in:* Sinanoglu, O. (ed.) *Modern Quantum Chemistry Istanbul Lectures.* New York: Academic Press.

Gallagher, R. T. , Balogh, M. P. , Davey, P. , Jackson, M. R. , Sinclair, I. & Southern, L. J. (2003) Combined Electrospray Ionization-Atmospheric Pressure Chemical Ionization Source for Use in High-Throughput Lc-Ms Applications. *Anal Chem,* **75,** 973-7.

Genty, B. , Briantais, J.-M. & Baker, N. R. (1989) The Relationship between the Quantum Yield of Photosynthetic Electron Transport and Quenching of Chlorophyll Fluorescence. *Biochimica et Biophysica Acta,* **990,** 87-92.

Gibson, D. G. , Young, L. , Chuang, R.-L. , Venter, C. J. , Hutchison, C. A. & Smith, H. O. (2009) Enzymatic Assembly of DNA Molecules up to Several Hundred Kilobases. *Nat Methods,* **6,** 343-345.

Govindjee (1995) Sixty-Three Years since Kautsky: Chlorophyll a Fluorescence. *Aust. J. Plant Physiol.,* **22,** 131-160.

Govindjee & Veit, W. (2010) *Z-Scheme of Electron Transport in Photosynthesis* [Online]. http://www.life.illinois.edu/govindjee/Z-Scheme.html: Life sciences Univeristy of Illinois at Urbana-Champaign. [Accessed 03.09.2013].

Helman, Y. , Tchernov, D. , Reinhold, L. , Shibata, M. , Ogawa, T. , Schwarz, R. , Ohad, I. & Kaplan, A. (2003) Genes Encoding a-Type Flavoproteins Are Essential for Photoreduction of O2 in Cyanobacteria. *Current Biology,* **13,** 230-235.

Hill, R. & Bendall, F. (1960) Function of the Two Cytochrome Components in Chloroplasts: A Working Hypothesis. *Nature,* **186,** 136-137.

Hohmann-Marriott, M. F. & Blankenship, R. E. (2011) Evolution of Photosynthesis. *Annual Review of Plant Biology,* **62,** 515-548.

Hohmann-Marriott, M. F. , Takizawa, K. , Eaton-Rye, J. J. , Mets, L. & Minagawa, J. (2010) The Redox State of the Plastoquinone Pool Directly Modulates Minimum Chlorophyll Fluorescence Yield in Chlamydomonas Reinhardtii. *FEBS Lett,* **584,** 1021-6.

Ian Ragan, C. & Cottingham, I. R. (1985) The Kinetics of Quinone Pools in Electron Transport. *BBA Reviews On Bioenergetics,* **811,** 13-31.

Ikeuchi, M. & Tabata, S. (2001) Synechocystis Sp. Pcc 6803 — a Useful Tool in the Study of the Genetics of Cyanobacteria. *Photosynthesis Research* **70,** 73-83.

Johnson, T. W. , Shen, G. , Zybailov, B. , Kolling, D. , Reategui, R. , Beauparlant, S. , Vassiliev, I. R. , Bryant, D. A. , Jones, A. D. , Golbeck, J. H. & Chitnis, P. R. (2000) Recruitment of a Foreign Quinone into the A1 Site of Photosystem I. I. Genetic and Physiological Characterization of Phylloquinone Biosynthetic Pathway Mutants in Synechocystis Sp. Pcc 6803. *Journal of Biological Chemistry,* **275,** 8523-8530.

Kanehisa, M. (2000) *Post-Genome Informatics*. New York: Oxford Univeristy Press.

Kaneko, T. , Sato, S. , Kotani, H. , Tanaka, A. , Asamizu, E. , Nakamura, Y. , Miyajima, N. , Hirosawa, M. , Sugiura, M. , Sasamoto, S. , Kimura, T. , Hosouchi, T. , Matsuno, A. , Muraki, A. , Nakazaki, N. , Naruo, K. , Okumura, S. , Shimpo, S. , Takeuchi, C. , Wada, T. , Watanabe, A. , Yamada, M. , Yasuda, M. & Tabata, S. (1996) Sequence Analysis of the Genome of the Unicellular Cyanobacterium Synechocystis Sp. Strain Pcc6803. Ii. Sequence Determination of the Entire Genome and Assignment of Potential Protein-Coding Regions. *DNA Res,* **3,** 109-36.

Kawamukai, M. (2009) Biosynthesis and Bioproduction of Coenzyme Q10 by Yeasts and Other Organisms. *Biotechnol Appl Biochem,* **53,** 217-26.

Knight, T. 2003. Idempotent Vector Design for Standard Assembly of Biobricks. Available: http://hdl.handle.net/1721.1/21168 [Accessed 20.02.2014].

Korbie, D. J. & Mattick, J. S. (2008) Touchdown Pcr for Increased Specificity and Sensitivity in Pcr Amplification. *Nature Protocols,* **3,** 1452-1456.

Lamb, J. J. 2012. *The Role of Type Iv Pili of Synechocystis Sp. Pcc 6803 in Extracellular Electron Transfer*. Master of Science, University of Otago.

Lange, B. M. , Rujan, T. , Martin, W. & Croteau, R. (2000) Isoprenoid Biosynthesis: The Evolution of Two Ancient and Distinct Pathways across Genomes. *Proc Natl Acad Sci U S A,* **97,** 13172-7.

Lee, P. T. , Hsu, A. Y. , Ha, H. T. & Clarke, C. F. (1997) A C-Methyltransferase Involved in Both Ubiquinone and Menaquinone Biosynthesis: Isolation and Identification of the Escherichia Coli Ubie Gene. *J Bacteriol,* **179,** 1748-54.

Li, M. Z. & Elledge, S. J. (2007) Harnessing Homologous Recombination in Vitro to Generate Recombinant DNA Via Slic. *Nat Methods,* **4,** 251-6.

Li, Z. , Keasling, J. D. & Niyogi, K. K. (2012) Overlapping Photoprotective Function of Vitamin E and Carotenoids in Chlamydomonas. *Plant Physiol,* **158,** 313-23.

Lichtenthaler, H. K. (1999) The 1-Deoxy-D-Xylulose-5-Phosphate Pathway of Isoprenoid Biosynthesis in Plants. *Annu Rev Plant Physiol Plant Mol Biol,* **50,** 47-65.

Lohr, M. (2011) Carotenoid Metabolism in Phytoplankton *in:* Roy, S., Llewellyn, C. A., Egeland, E. S. & Johnsen, G. (eds.) *Phytoplankton Pigments.* New York: Cambridge University Press.

Martinis, J. , Kessler, F. & Glauser, G. (2011) A Novel Method for Prenylquinone Profiling in Plant Tissues by Ultra-High Pressure Liquid Chromatography-Mass Spectrometry. *Plant Methods,* **7,** 23-35.

Meganathan, R. (2001) Ubiquinone Biosynthesis in Microorganisms. *FEMS Microbiol Lett,* **203,** 131-9.

Mehler, A. H. (1951) Studies on Reactions of Illuminated Chloroplasts: I. Mechanism of the Reduction of Oxygen and Other Hill Reagents. *Archives of Biochemistry and Biophysics,* **33,** 65-77.

Morris, J. N. , Crawford, T. S. , Jeffs, A. , Stockwell, P. A. , Eaton-Rye, J. J. & Summerfield, T. C. (2014) Whole-Genome Re-Sequencing of Two "Wild-Type" Strains of the Model Cyanobacterium Synechocystis Sp. Pcc 6803. *New Zealand Journal of Botany,* **52,** 36-47.

Mullineaux, C. W. & Allen, J. F. (1990) State 1-State 2 Transitions in the Cyanobacterium Synechococcus 6301 Are Controlled by the Redox State of Electron Carriers between Photosystems I and Ii. *Photosynth Res,* **23,** 297-311.

Nakamura, Y. , Kaneko, T. , Hirosawa, M. , Miyajima, N. & Tabata, S. (1998) Cyanobase, a Www Database Containing the Complete Nucleotide Sequence of the Genome of Synechocystis Sp. Strain Pcc6803. *Nucleic Acids Research,* **26,** 63-67.

Nelson, D. L. & Cox, M. M. (2008) *Lehninger Principles of Biochemistry*. 5 ed. New York: W.H. Freeman and Company.

Nohl, H. (1986) Quinones in Biology: Functions in Electron Transfer and Oxygen Activation. *Advances in Free Radical Biology & Medicine,* **2,** 211–279.

Norris, S. R. , Barrette, T. R. & Dellapenna, D. (1995) Genetic Dissection of Carotenoid Synthesis in Arabidopsis Defines Plastoquinone as an Essential Component of Phytoene Desaturation. *Plant Cell,* **7,** 2139-49.

Nowicka, B. & Kruk, J. (2010) Occurrence, Biosynthesis and Function of Isoprenoid Quinones. *Biochim Biophys Acta,* **1797,** 1587-605.

Ogawa, T. (1991) A Gene Homologous to the Subunit-2 Gene of Nadh Dehydrogenase Is Essential to Inorganic Carbon Transport of Synechocystis Pcc6803. *Proc Natl Acad Sci U S A,* **88,** 4275-9.

Osborne, B. A. & Geider, R. J. (1987) The Minimum Photon Requirement for Photosynthesis. *New Phytologist,* **106,** 631-644.

Pfaff, C. , Glindemann, N. , Gruber, J. , Frentzen, M. & Sadre, R. (2014) Chorismate Pyruvate-Lyase and 4-Hydroxy-3-Solanesylbenzoate Decarboxylase Are Required for Plastoquinone Biosynthesis in the Cyanobacterium Synechocystis Sp. Pcc6803. *J Biol Chem,* **289,** 2675-86.

Pils, D. & Schmetterer, G. (2001) Characterization of Three Bioenergetically Active Respiratory Terminal Oxidases in the Cyanobacterium Synechocystis Sp. Strain Pcc 6803. *FEMS Microbiol Lett,* **203,** 217-22.

Poteete, A. R. , Rosadini, C. & St Pierre, C. (2006) Gentamicin and Other Cassettes for Chromosomal Gene Replacement in Escherichia Coli. *Biotechniques,* **41,** 261-2, 264.

Quach, H. T. , Steeper, R. L. & Griffin, G. W. (2004) An Improved Method for the Extraction and Thin-Layer Chromatography of Chlorophyll a and B from Spinach. *Journal of Chemical Education,* **81,** 385-387.

Rippka, R. , Deruelles, J. , Waterbury, J. B. , Herdman, M. & Stanier, R. Y. (1979) Generic Assignments, Strain Histories and Properties of Pure Cultures of Cyanobacteria. *Journal of General Microbiology,* **111,** 1-61.

Rohàcek, K. & Bartàk, M. (1999) Technique of the Modulated Chlorophyll Fluorescence: Basic Concepts, Useful Parameters and Some Applications. *Photosynthetica,* **37,** 339-363.

Sadre, R. , Pfaff, C. & Buchkremer, S. (2012) Plastoquinone-9 Biosynthesis in Cyanobacteria Differs from That in Plants and Involves a Novel 4-Hydroxybenzoate Solanesyltransferase. *Biochem. J.,* **442,** 621-629.

Sakuragi, Y. 2004. *Cyanobacterial Quinomics.* Doctor of Philosophy, Pennsylvania State University.

Sakuragi, Y. , Zybailov, B. , Shen, G. , Jones, A. D. , Chitnis, P. R. , Van Der Est, A. , Bittl, R. , Zech, S. , Stehlik, D. , Golbeck, J. H. & Bryant, D. A. (2002) Insertional Inactivation of the Meng Gene, Encoding 2-Phytyl-1,4-Naphthoquinone Methyltransferase of Synechocystis Sp. Pcc 6803, Results in the Incorporation of 2-

Phytyl-1,4-Naphthoquinone into the a(1) Site and Alteration of the Equilibrium Constant between a(1) and F(X) in Photosystem I. *Biochemistry,* **41,** 394-405.

Schmetterer, G. (2004) Cyanobacterial Respiration *in:* Bryant, D. (ed.) *The Molecular Biology of Cyanobacteria.* Netherlands: Springer

Schoepp-Cothenet, B. , Lieutaud, C. , Baymann, F. , Vermeglio, A. , Friedrich, T. , Kramer, D. M. & Nitschke, W. (2009) Menaquinone as a Pool Quinone in a Purple Bacterium. *Proc Natl Acad Sci USA,* **106,** 8549-8554.

Schuurmans, R. M. , Schuurmans, J. M. , Bekker, M. , Kromkamp, J. C. , Matthijs, H. C. & Hellingwerf, K. J. (2014) The Redox Potential of the Plastoquinone Pool of the Cyanobacterium Synechocystis Species Strain Pcc 6803 Is under Strict Homeostatic Control. *Plant Physiol,* **165,** 463-75.

Schäfer, L. , Vioque, A. & Sandmann, G. (2005) Functional in Situ Evaluation of Photosynthesis-Protecting Carotenoids in Mutants of the Cyanobacterium Synechocystis Pcc6803. *Journal of Photochemistry and Photobiology B: Biology,* **78,** 195-201.

Sheng, J. , Vannela, R. & Rittmann, B. E. (2011) Evaluation of Methods to Extract and Quantify Lipids from Synechocystis Pcc 6803. *Bioresour Technol,* **102,** 1697-703.

Smith, A. J. (1983) Modes of Cyanobacterial Carbon Metabolism. *Ann Microbiol (Paris),* **134B,** 93-113.

Soballe, B. & Poole, R. K. (1999) Microbial Ubiquinones: Multiple Roles in Respiration, Gene Regulation and Oxidative Stress Management. *Microbiology,* **145,** 1817-30.

Szkopińska, A. (2000) Ubiquinone. Biosynthesis of Quinone Ring and Its Isoprenoid Side Chain. Intracellular Localization. *Acta Biochimica Polonica,* **47,** 469-480.

Takaichi, S. , Maoka, T. & Masamoto, K. (2001) Myxoxanthophyll in Synechocystis Sp. Pcc 6803 Is Myxol 2'-Dimethyl-Fucoside, (3r,2's)-Myxol 2'-(2,4-Di-O-Methyl-Alpha-L-Fucoside), Not Rhamnoside. *Plant Cell Physiol,* **42,** 756-62.

Teran, E. E. T. 2001. *Ubiquinone Reacts with Nitric Oxide to Prevent the Activity of Purified Complex I.* Doctor of Philosophy Ph.D, University College London.

Trebst, A. (1980) Inhibitors in Electron flow: Tools for the Functional and Structural Localization of Carriers and Energy Conservation Sites. *Methods Enzymol.,* **69,** 675-715.

Unden, G. (1988) Differential Roles for Menaquinone and Demethylmenaquinone in Anaerobic Electron Transport of E. Coli and Their Fnr-Independent Expression. *Arch Microbiol,* **150,** 499-503.

Vermaas, W. F. J. (2001) Photosynthesis and Respiration in Cyanobacteria. *E. Life Sci.,* 1-8.

Weeden, N. F. (1981) Genetic and Biochemical Implications of the Endosymbiotic Origin of the Chloroplast. *Journal of Molecular Evolution,* **17,** 133-139.

Williams, J. G. K. (1988) Construction of Specific Mutations in Photosystem Ii Photosynthetic Reaction Center by Genetic Engineering Methods in Synechocystis 6803. *Methods Enzymol.,* **167,** 766-778.

Wissenbach, U. , Ternes, D. & Unden, G. (1992) An Escherichia Coli Mutant Containing Only Demethylmenaquinone, but No Menaquinone: Effects on Fumarate, Dimethylsulfoxide, Trimethylamine N-Oxide and Nitrate Respiration. *Arch Microbiol,* **158,** 68-73.

Witt, H. T. , Müller, A. & Rumberg, B. (1963) Electron-Transport System in Photosynthesis of Green Plants Analysed by Sensitive Flash Photometry. *Nature,* **197,** 987-991.

Wollman, F. A. & Delepelaire, P. (1984) Correlation between Changes in Light Energy Distribution and Changes in Thylakoid Membrane Polypeptide Phosphorylation in Chlamydomonas Reinhardtii. *J Cell Biol,* **98,** 1-7.

Wood, P. M. & Crane, F. L. (1969) Method for Determination of Plastoquinone a and Plastoquinol a Levels in Spinach Chloroplasts. *Analytical Biochemistry,* **36,** 127-135.

Yoshihara, S. , Geng, X. , Okamoto, S. , Yura, K. , Murata, T. , Go, M. , Ohmori, M. & Ikeuchi, M. (2001) Mutational Analysis of Genes Involved in Pilus Structure, Motility and Transformation Competency in the Unicellular Motile Cyanobacterium Synechocystis Sp. Pcc 6803. *Plant Cell Physiol,* **42,** 63-73.

Zhang, H. & Javor, G. T. (2003) Regulation of the Isofunctional Genes Ubid and Ubix of the Ubiquinone Biosynthetic Pathway of Escherichia Coli. *FEMS Microbiology Letters,* **223,** 67-72.

Zhang, L. , Mcspadden, B. , Pakrasi, H. B. & Whitmarsh, J. (1992) Copper-Mediated Regulation of Cytochrome C553 and Plastocyanin in the Cyanobacterium Synechocystis 6803. *J Biol Chem,* **267,** 19054-9.

Appendix

1. Photosynthetic Lipids in *Synechocystis* 6803
2. Identification of Genes Involved in Plastoquinone Synthesis in Cyanobacteria
3. Lipid Analysis

1. Photosynthetic Lipids in *Synechocystis* 6803

Photosynthetic organisms synthesize a range of lipids that function in light harvesting, photo-protection and electron transport. Chlorophylls constitute a major class of these lipids and are utilized in reaction centers and as light-gathering pigments. Carotenoids also function in light-harvesting, but have an additional role in photo-protection of the cell under high light conditions. One of the most important groups of compounds occurring in membranes of living organisms is the isoprenoid quinones, lipids involved in electron transport. *Synechocystis* 6803 is a cyanobacterium that synthesizes lipids in all these chemical classes and this appendix gives a brief overview of the photosynthetic lipids expected to be synthesized in this organism, their chemical structure and absorption spectra in methanol, unless otherwise specified.

Chlorophylls

Cyanobacteria only synthesize chlorophyll *a* (Chl *a*), the primary electron donor in the electron transport chain of oxygenic photosynthesis. This lipid is also found in plants and green algae, organisms known to synthesize chlorophyll *b* in addition to Chl *a*.

Chlorophyll *a*

Molecular formula: $C_{55}H_{72}MgN_4O_5$ Abs (nm): 432, 618, 652, 665 [1]

Molecular weight: 893.49

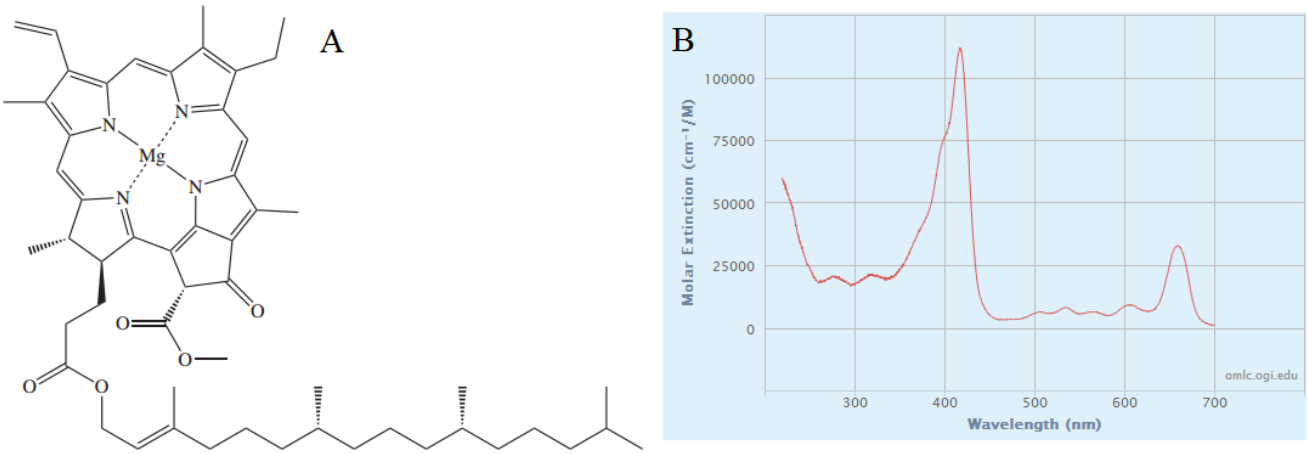

Figure A1.1 – Chemical structure (A) and absorption spectra (B) of chlorophyll *a*.

Carotenoids

Carotenoids comprise pure hydrocarbons (carotenes) and oxygenated structures (xanthophylls), with ring structures found at each end when synthesized by oxygenic phototrophs, such as *Synechocystis* 6803. Due to the extensive structural diversity of carotenoids synthesized by different organisms, they can be used for chemotaxonomic classification. Carotenoids such as β-carotene, zeaxanthin, echinenone, hydroxyechinenone, deoxymyxol 2'-dimethyl-fucoside and myxol 2'-dimethyl-fucoside have been identified in *Synechocystis* 6803 [2].

β-carotene

Molecular formula: $C_{40}H_{56}$ Abs (nm): (429), 449, 475 [1]

Molecular weight: 536.87

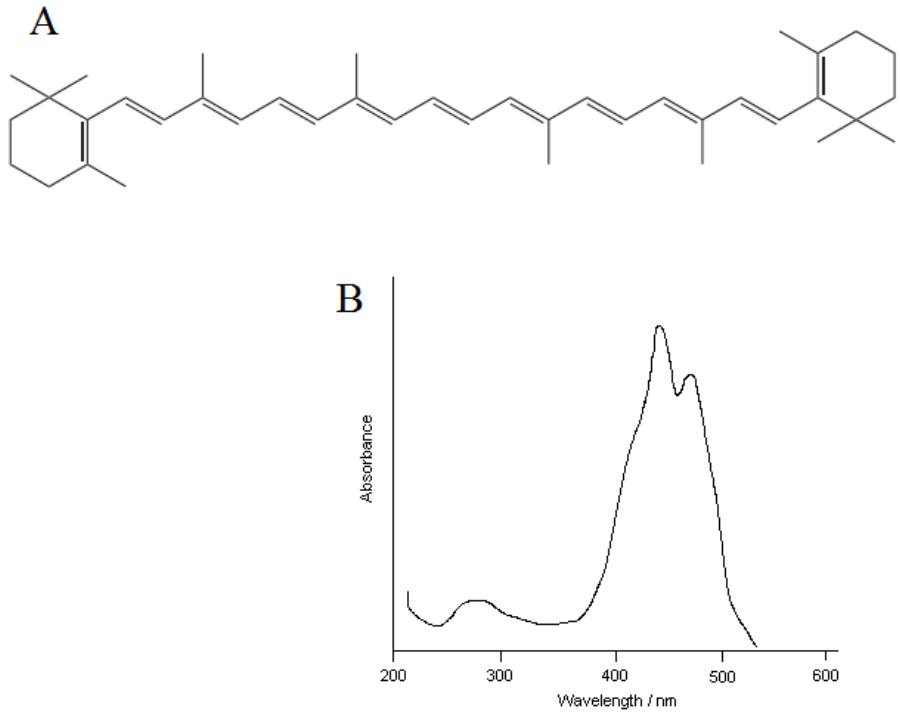

Figure A1.2 – Chemical structure (A) and absorption spectra (B) of β-carotene.

Echinenone

Molecular formula: $C_{40}H_{54}O$ Abs (nm): 460 [1]

Molecular weight: 550.86

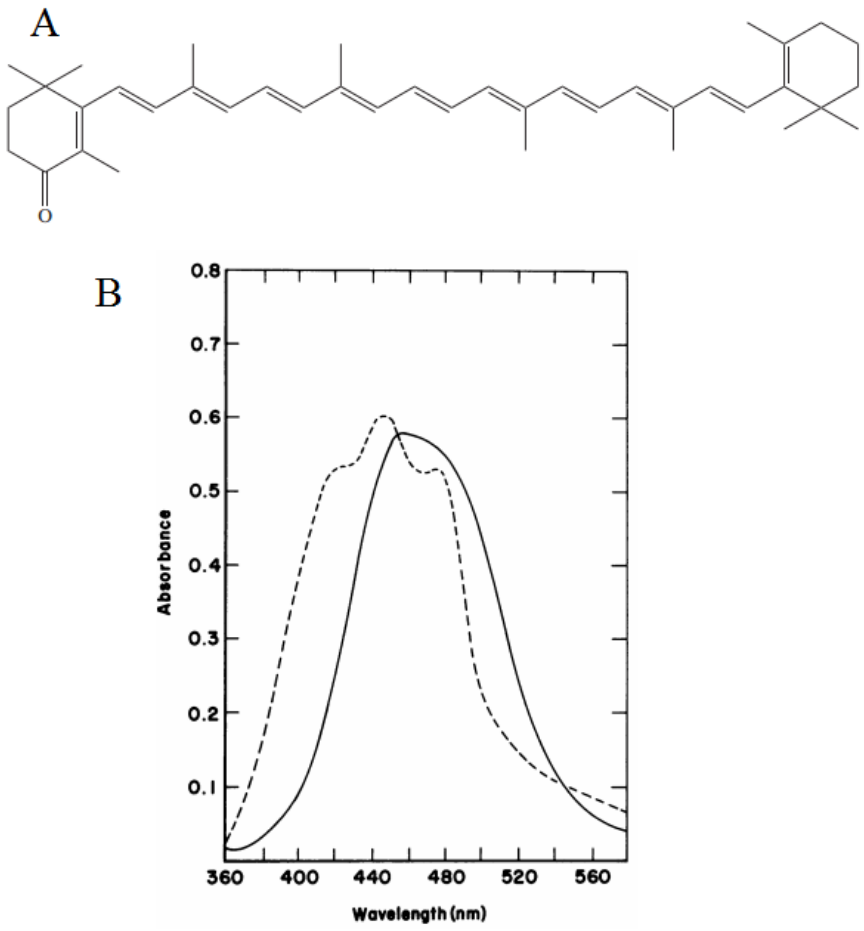

Figure A1.3 – Chemical structure (A) and absorption spectra (B) of oxidized (solid) and reduced (dashed) echinenone.

Hydroxy-echinenone

Molecular formula: $C_{40}H_{54}O_2$ Abs (nm): 460 [3]

Molecular weight: 566.86

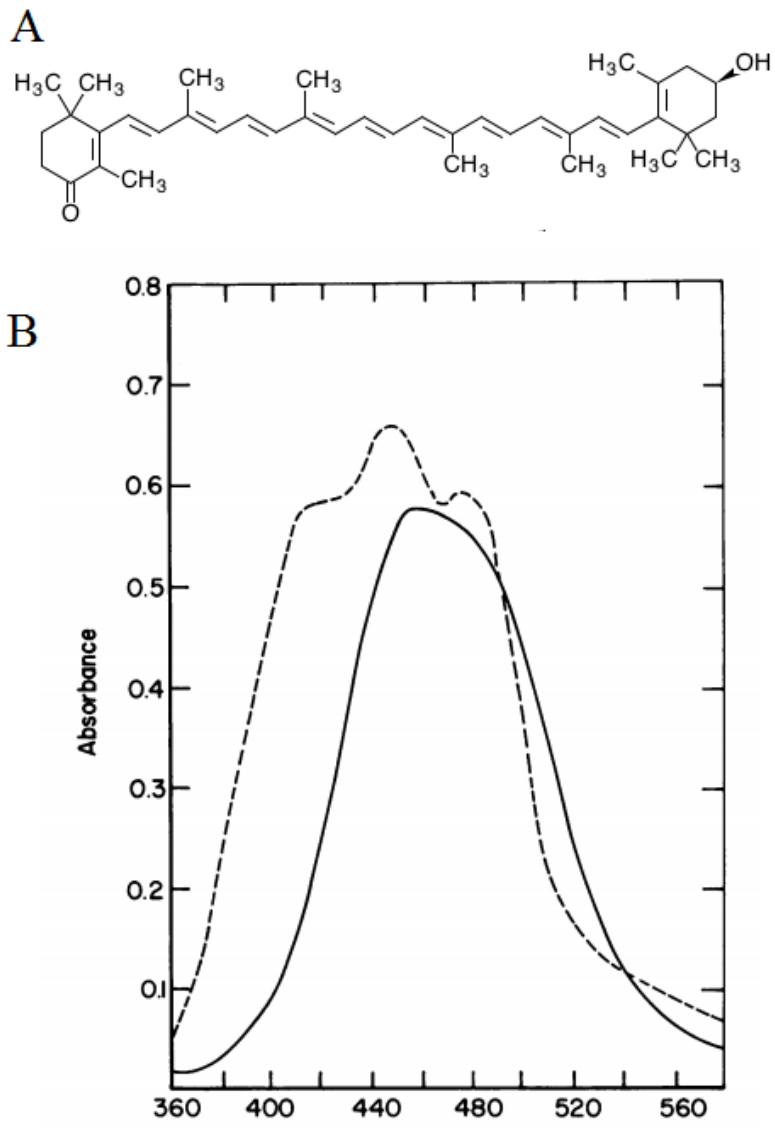

Figure A1.4 – Chemical structure (A) and absorption spectra (B) of reduced (dashed) and oxidized (solid) hydroxy-echinenone.

Lutein

Molecular formula: $C_{40}H_{56}O_2$ Abs (nm): (422), 443, 470 [1]

Molecular weight: 568.87

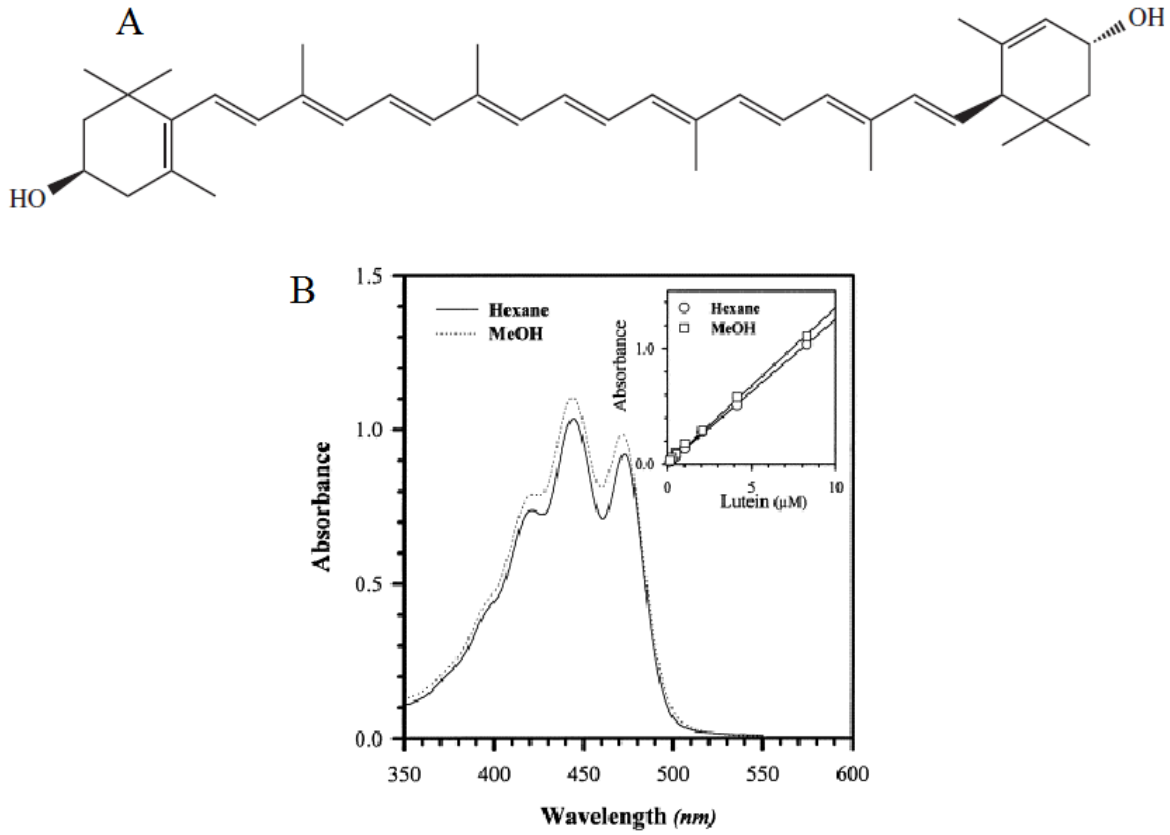

Figure A1.5 – Chemical structure (A) and absorption spectra (B) of lutein

Myxoxanthophyll

Molecular formula: $C_{46}H_{66}O_7$ Abs (nm): 446, 472, 502 [1]

Molecular weight: 731.02

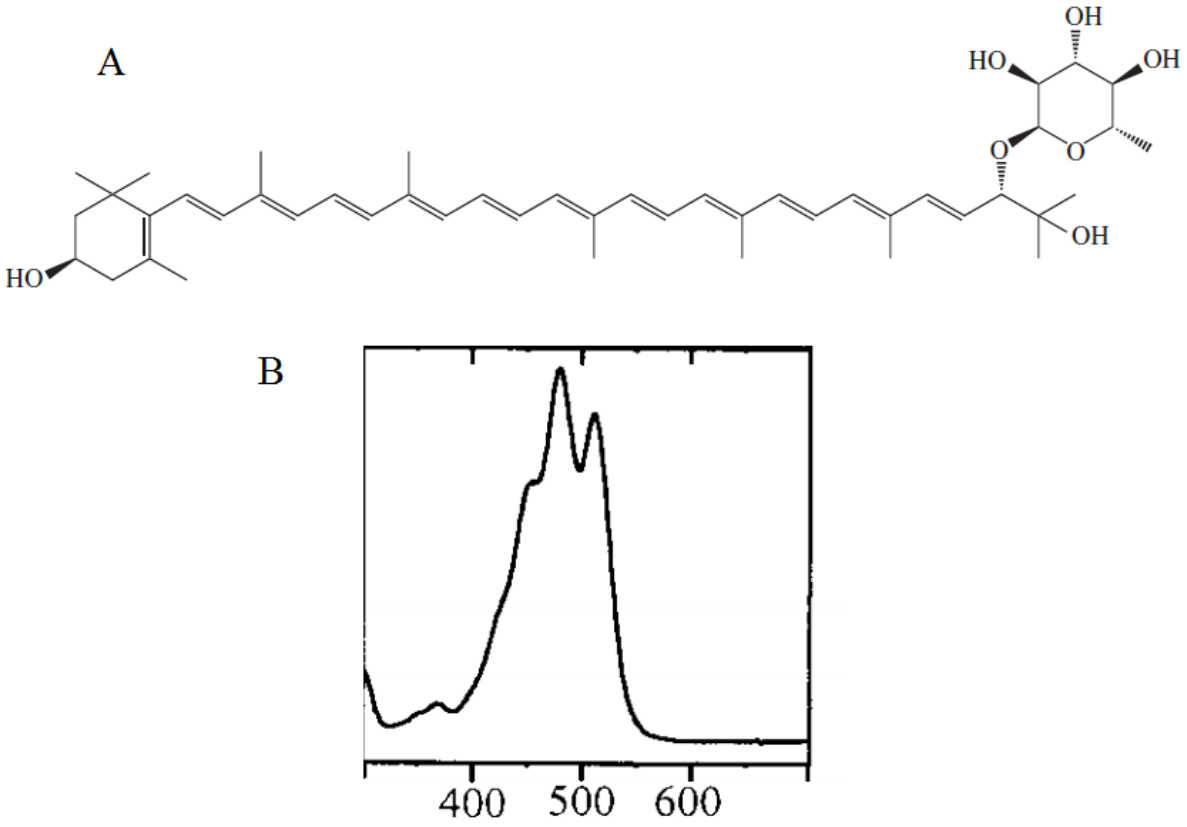

Figure A1.6 – Chemical structure (A) and absorption spectra (B) of myxoxanthophyll

Myxoxanthophyll-fucoside

Molecular formula: $C_{48}H_{70}O_7$ Abs (nm): 294, 365, 448, 473, 503 [2]

Molecular weight: 758.51

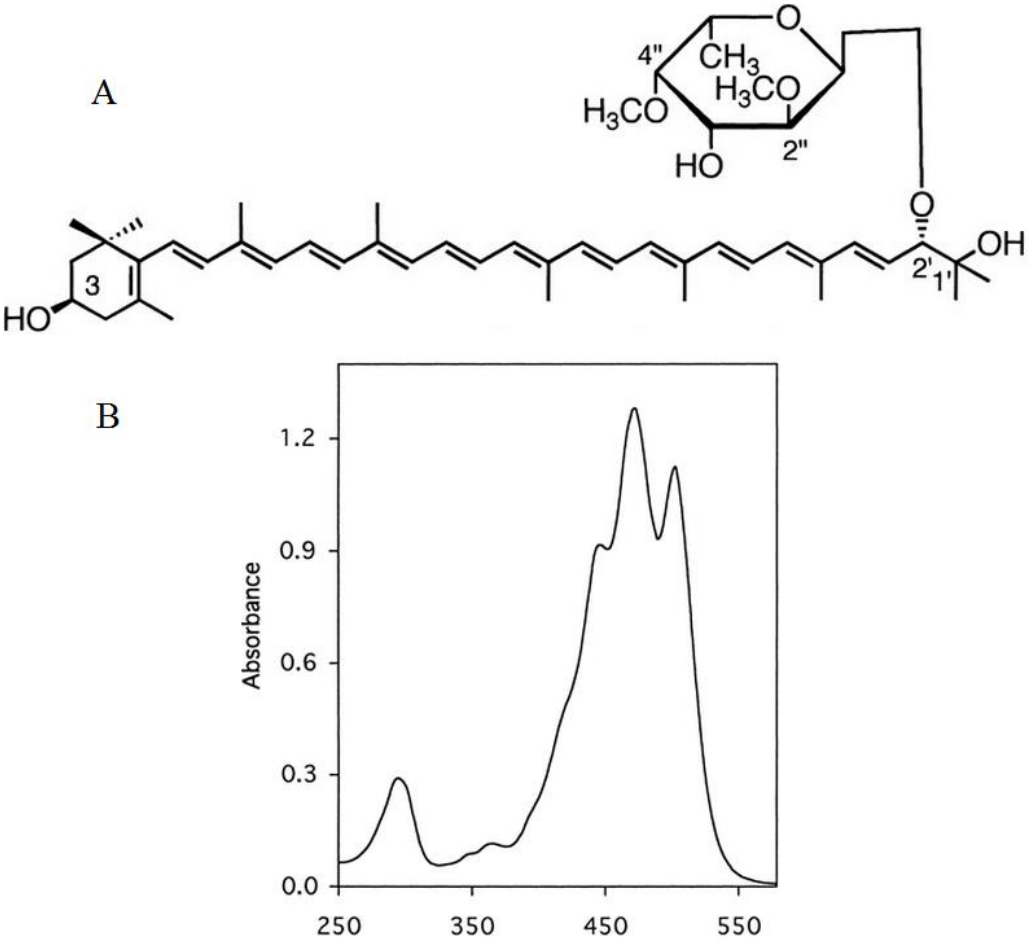

Figure A1.7 – Chemical structure (A) and absorption spectra (B) of myxoxanthophyll-fucoside

Zeaxanthin

Molecular formula: $C_{40}H_{56}O_2$ Abs (nm): (429), 449, 475 [1]

Molecular weight: 568.87

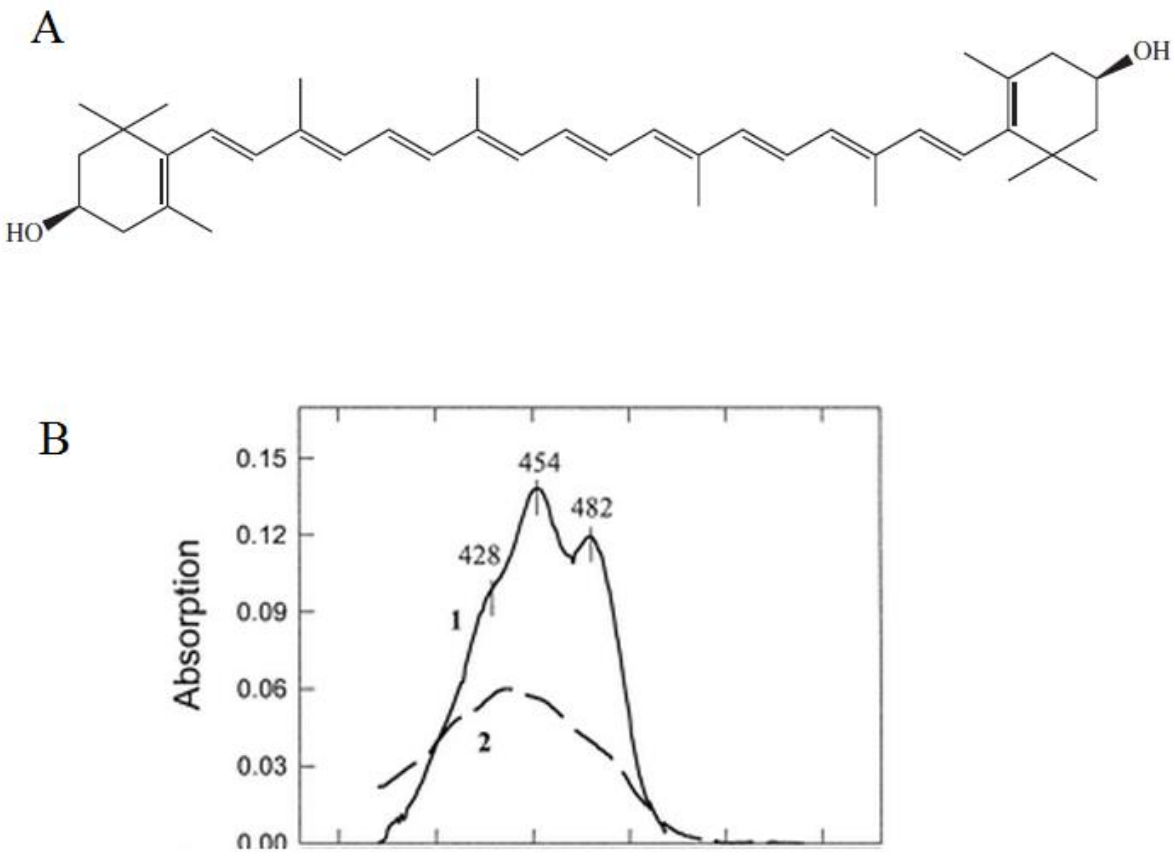

Figure A1.8 – Chemical structure (A) and absorption spectra (B) of zeaxanthin in ethanol.

Isoprenoid quinones

Quinones are aromatic compounds that can undergo a two-step reversible reduction, a feature that enables them to function as electron and proton carriers. These redox-active lipids are composed of a hydrophilic head group and an apolar isoprenoid side chain, which anchors them in the membrane lipid bilayers.

Plastoquinone-A (PQ-9)

Molecular formula: $C_{53}H_{80}O_2$ Abs (nm): 255 [4]

Molecular weight: 749.20

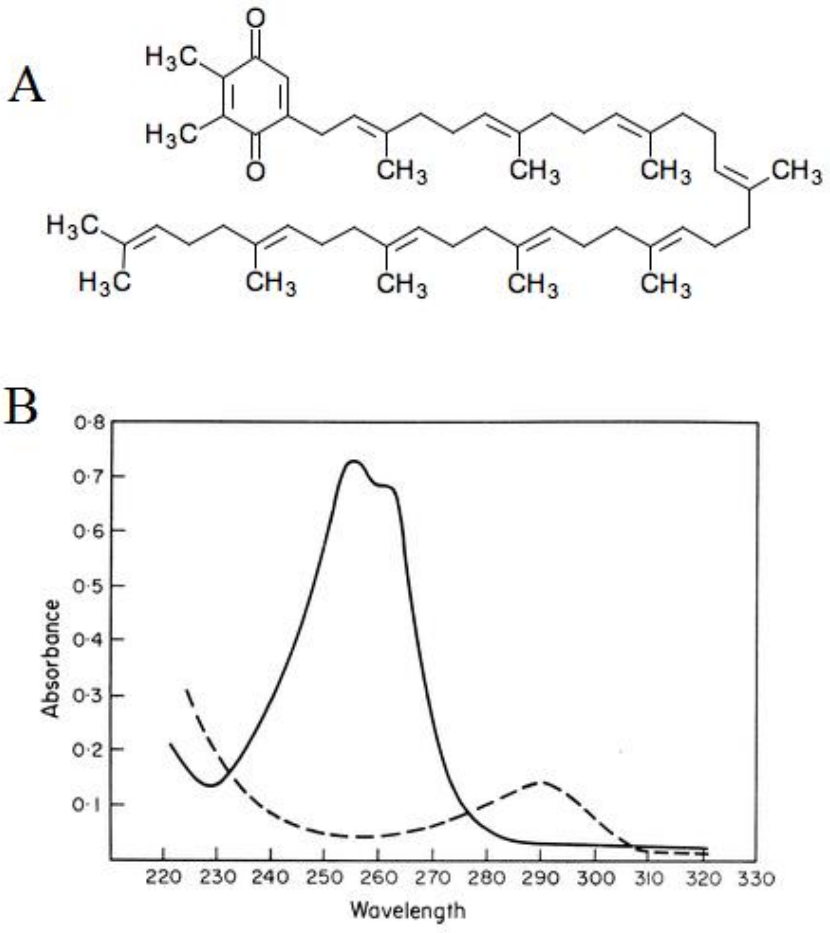

Figure A1.8 – Chemical structure (A) and absorption spectra (B) of oxidized (solid) and reduced (dashed) plastoquinone-9

Phylloquinone

Molecular formula: $C_{31}H_{46}O_2$ Abs (nm): 243, 248, 262, 270, 330 [5]

Molecular weight: 450.70

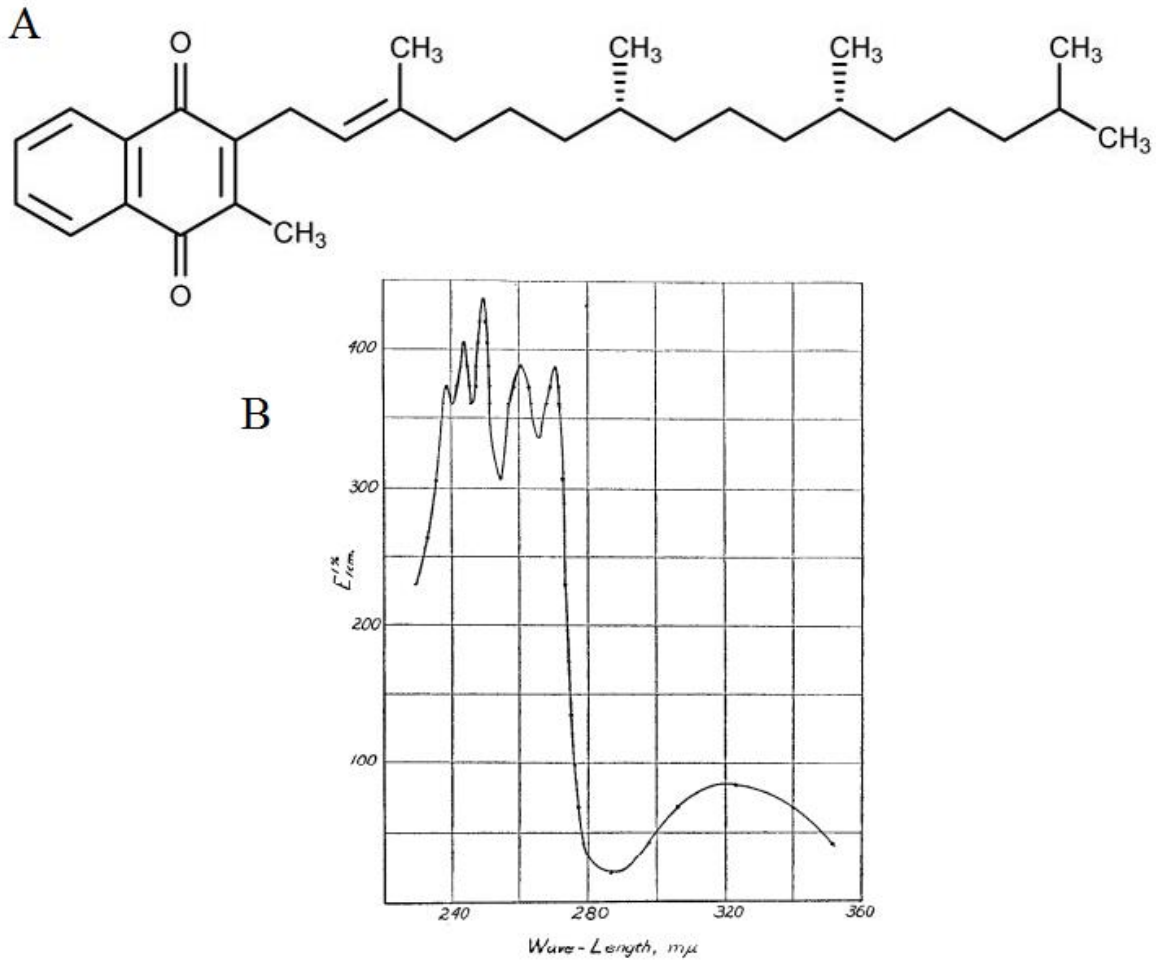

Figure A1.9 – Chemical structure (A) and absorption spectra (B) of phylloquinone in hexane.

α-tocopherol

Molecular formula: $C_{29}H_{50}O_2$ Abs (nm): 212, 292 [5]

Molecular weight: 430.71

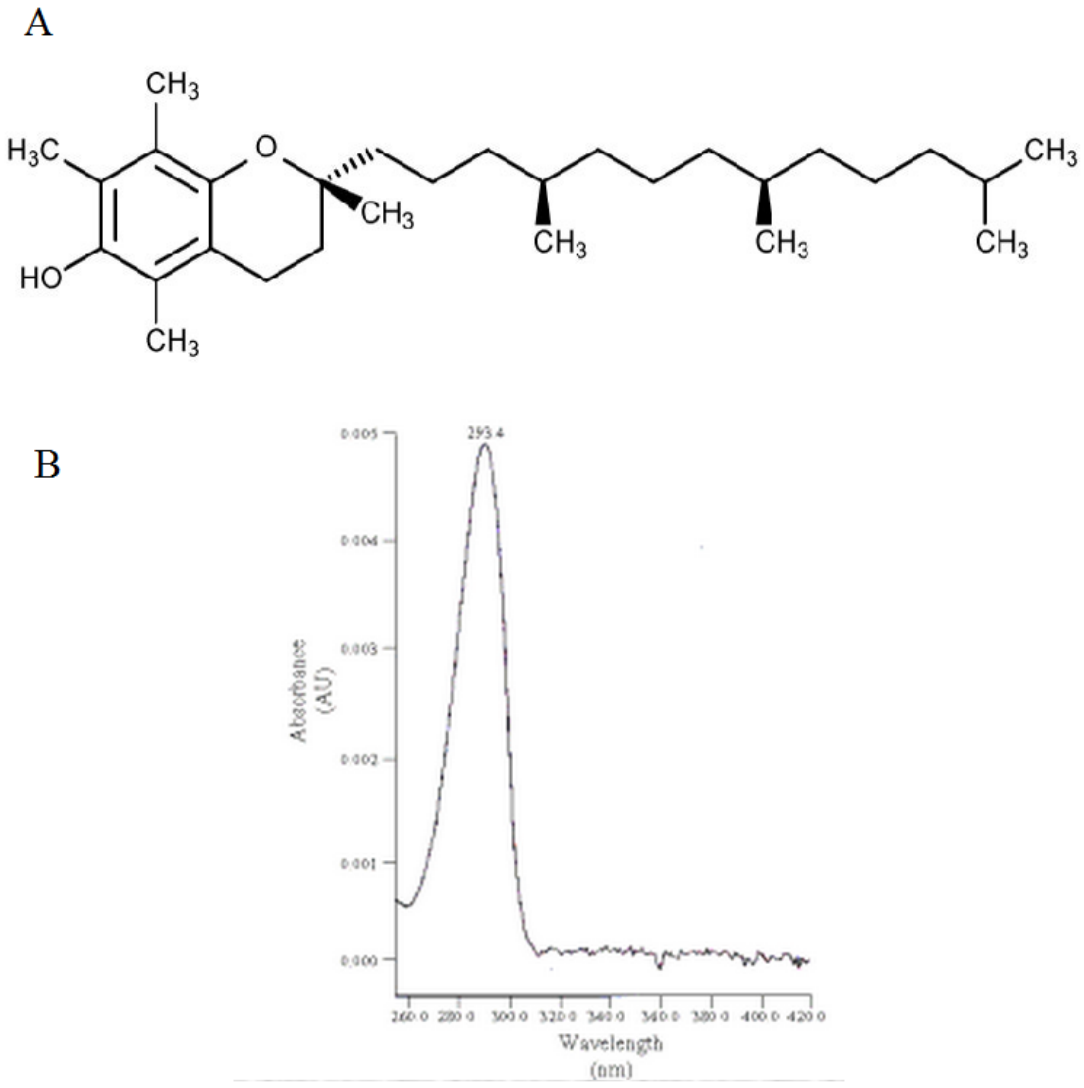

Figure A1.10 – Chemical structure (A) and absorption spectra (B) of α-tocopherol.

References

[1] Roy, S., Llewellyn, C.A, Egeland, E.S., Johnsen, G. Phytoplankton pigments - Characterization, Chemotaxonomy and Applications in Oceanography. Cambridge: Cambridge University Press; 2011

[2] Takaichi, S., Maoka, T., Masamoto, K. Myxoxanthophyll in Synechocystis sp. PCC 6803 is myxol 2'-dimethyl-fucoside, (3R,2'S)-myxol 2'-(2,4-di-O-methyl-alpha-L-fucoside), not rhamnoside. Plant Cell Physiol. 2001; 42 (7): 756-762

[3] Schwartzel, E.M., Cooney, J.J. Isolation of 4-hydroxyechinenone from Micrococcus roseus. J. Bacteriol. 1972; 112 (3): 1422-142

[4] Crane, F.L. Discovery of plastoquinones: a personal perspective. Photosynthesis research. 2010; 103 (3): 195-209

[5] Hatam, L.J., Kayden, H.J. A high-performance liquid chromatographic method for the determination of tocopherol in plasma and cellular elements of the blood. J. Lipid research. 1979; 20: 639-645

2. Identification of Genes Involved in Plastoquinone Synthesis in Cyanobacteria

Based on knowledge about the ubiquinone synthesis pathway in *Escherichia coli*, candidate genes encoding enzymes involved in the decarboxylation, hydroxylation and methylation steps of plastoquinone synthesis in the cyanobacterium *Synechocystis* sp. PCC 6803 were identified using BLASTP searches. If the selected genes are involved in cyanobacterial plastoquinone synthesis, orthologs should be identified in other cyanobacteria as well. Orthologs to the candidate genes identified in Chapter 3 (section 2.1) were found using CyanoBase and BLAST as resources. The identified genes encoding putative decarboxylases, hydroxylases and methyltransferases were:

Decarboxylases:	*sll0936* and *slr1099*
Hydroxylases:	*sll0095* and *slr1300*
Methyltransferases:	*sll1653, slr0407, sll0829* and *slr1618*

Table A3.1 lists the orthologs to the identified decarboxylases found in genome sequenced species of cyanobacteria. Orthologs to the identified hydroxylases and methyltransferases are listed in Table A3.2 and A3.3, respectively.

Table A3.1 – Orthologs to the putative decarboxylases encoded by *sll0936* and *slr1099*.

Genome	*sll0936*		*slr1099*	
	Identity (%)	Description	Identity (%)	Description
Synechocystis sp. PCC 6803	100.0	putative oxidoreductase	100.0	3-octaprenyl-4-hydroxybenzoate carboxy-lyase
Acaryochloris marina MBIC11017	83.3	3-octaprenyl-4-hydroxybenzoate carboxylyase	74.1	polyprenyl P-hydroxybenzoate and phenylacrylic acid decarboxylase
Anabaena sp. PCC 7120	88.8	hypothetical protein	76.0	3-octaprenyl-4-hydroxybenzoate carboxy-lyase
Arthrospira platensis NIES-39	87.2	3-octaprenyl-4-hydroxybenzoate carboxy-lyase	76.4	3-octaprenyl-4-hydroxybenzoate carboxy-lyase
Chlorobium tepidum TLS	21.8	alanyl-tRNA synthetase	30.8	trehalose synthase
Cyanothece sp. PCC 8801	88.6	UbiD family decarboxylase	80.9	3-octaprenyl-4-hydroxybenzoate carboxy-lyase
Gloeobacter violaceus PCC 7421	73.4	hypothetical protein	67.3	3-octaprenyl-4-hydroxybenzoate carboxy-lyase
Microcystis aeruginosa NIES-843	86.8	putative oxidoreductase	77.6	3-octaprenyl-4-hydroxybenzoate carboxy-lyase
Nostoc punctiforme ATCC 29133	89.0	UbiD family decarboxylase	77.5	3-octaprenyl-4-hydroxybenzoate carboxy-lyase
Prochlorococcus marinus str. MIT 9303	70.5	3-polyprenyl-4-hydroxybenzoate decarboxylase	50.3	aromatic acid decarboxylase
Rhodopseudomonas palustris CGA009	44.9	Carboxylyase-related protein	37.4	possible 3-octaprenyl-4-hydroxybenzoate carboxy-lyase
Synechococcus elongatus PCC 6301	82.4	3-octaprenyl-4-hydroxybenzoate carboxy-lyase UbiD	68.2	3-octaprenyl-4-hydroxybenzoate carboxy-lyase
Synechococcus sp. PCC 7002	86.0	3-octaprenyl-4-hydroxybenzoate carboxy-lyase	73.0	3-octaprenyl-4-hydroxybenzoate decarboxylase

Thermosynechococcus elongatus BP-1	81.8	putative oxidoreductase	70.5	3-octaprenyl-4-hydroxybenzoate carboxy-lyase
Trichodesmium erythraeum IMS101	35.3	microcompartments protein	54.4	3-octaprenyl-4-hydroxybenzoate carboxy-lyase

Table A3.2 - Orthologs to the putative hydroxylases encoded by *sll0095* and *slr1300*.

Genome	***sll0095***		***slr1300***	
	Identity (%)	Description	Identity (%)	Description
Synechocystis sp. PCC 6803	100.0	hypothetical protein	100.0	similar to 2-octaprenyl-6-methoxyphenol hydroxylase
Acaryochloris marina MBIC11017	40.3	ABC-1 domain protein	46.3	2-octaprenyl-6-methoxyphenyl hydroxylase
Anabaena sp. PCC 7120	42.3	hypothetical protein	51.5	probable 2-octaprenyl-6-methoxyphenol 4-monoxygenase; UbiH
Arthrospira platensis NIES-39	52.5	putative ATPase	48.1	probable 2-octaprenyl-6-methoxyphenol 4-monoxygenase; UbiH
Chlorobium tepidum TLS	36.4	hypothetical protein	30.1	geranylgeranyl hydrogenase
Cyanothece sp. PCC 8801	62.8	ABC-1 domain protein	56.9	Ubiquinone biosynthesis hydroxylase, UbiH/UbiF/VisC/COQ6 family
Gloeobacter violaceus PCC 7421	41.4	hypothetical protein	27.9	probable monooxygenase
Microcystis aeruginosa NIES-843	61.2	hypothetical protein	56.8	2-octaprenyl-6-methoxyphenol hydroxylase
Nostoc punctiforme ATCC 29133	42.0	hypothetical protein	50.9	UbiH/UbiF/VisC/COQ6 family ubiquinone biosynthesis hydroxylase
Prochlorococcus marinus str. MIT 9303	35.0	possible kinase	29.6	possible 2-octaprenyl-6-methoxyphenol 4-monoxygenase; UbiH

Rhodopseudomonas palustris CGA009	27.8	ubiquinone biosynthesis protein AarF, a gene required for the first monooxygenase step in CoQ biosynthesis, recently renamed ubiB	35.4	putative UbiH protein, 2-octaprenyl-6-methoxyphenol 4-monoxygenase
Synechococcus elongatus PCC 6301	40.2	hypothetical protein	45.4	2-octaprenyl-6-methoxyphenol hydroxylase
Synechococcus sp. PCC 7002	57.1	ABC1 family domain protein	51.3	Ubiquinone biosynthesis hydroxylase, UbiH/UbiF/VisC/COQ6 family
Thermosynechococcus elongatus BP-1	51.6	hypothetical protein	40.1	probable 2-octaprenyl-6-methoxyphenol 4-monoxygenase
Trichodesmium erythraeum IMS101	53.5	hypothetical protein	37.4	2-octaprenyl-6-methoxyphenyl hydroxylase

Table A3.3 - Orthologs to the putative methyltransferases encoded by *sll1653, slr0407, sll0829* and *slr1618*.

Genome	***sll1653***		***slr0407***		***sll0829***		***slr1618***	
	ID (%)	Description	ID (%)	Description	ID (%)	Description	ID (%)	Description
Synechocystis sp. PCC 6803	100.0	2-phytyl-1,4-benzoquinone methyltransferase	100.0	hypothetical protein	100.0	probable methyltransferase	100.0	unknown protein
Acaryochloris marina MBIC11017	58.7	ubiquinone/ menaquinone biosynthesis methyltransferase	25.8	methyltransferase, putative	32.3	ubiquinone/ menaquinone biosynthesis methyltransferase	29.5	methyltransferase, putative
Anabaena sp. PCC 7120	57.3	probable methyltransferase	33.1	probable methyltransferase	59.2	methyltransferase	33.3	methyltransferase

Arthrospira platensis NIES-39	56.1	ubiquinone/ menaquinone biosynthesis methyltransf erase	31.1	probable methyltransf erase	58.4	putative methyltransf erase	40.7	putative methyltransf erase
Chlorobium tepidum TLS	33.5	ubiquinone/ menaquinone biosynthesis methyltransf erase	33.3	methyltransf erase, putative	27.7	ubiquinone/ menaquinone biosynthesis methyltransf erase	30.8	ubiquinone/ menaquinone biosynthesis methyltransf erase
Cyanothece sp. PCC 8801	61.9	ubiquinone/ menaquinone biosynthesis methyltransf erase	26.8	ubiquinone/ menaquinone biosynthesis methyltransf erase	61.5	methyltransf erase type 11	28.4	methyltransf erase type 12
Gloeobacter violaceus PCC 7421	48.3	2-phytyl-1,4-benzoquinon e methyltransf erase	51.9	hypothetical protein	53.4	probable methyltransf erase	29.8	hypothetical protein
Microcystis aeruginosa NIES-843	53.8	menaquinone biosynthesis methyltransf erase UbiE	28.5	menaquinone biosynthesis methyltransf erase UbiE	61.0	methyltransf erase	31.1	probable 3-demethylubi quinone-9 3-O-methyltransf erase
Nostoc punctiforme ATCC 29133	57.3	ubiquinone/ menaquinone biosynthesis methyltransf erase	40.9	methyltransf erase type 11	60.2	methyltransf erase type 11	33.0	methyltransf erase type 12
Prochlorococcus marinus str. MIT 9303	47.6	ubiquinone/ menaquinone biosynthesis methyltransf erase	26.6	Putative methyltransf erase	38.5	possible methyltransf erase	37.1	possible methyltransf erase

Rhodopseudomonas palustris CGA009	27.8	ubiquinone/ menaquinone biosynthesis methlytransferase ubiE	31.7	UbiE/COQ5 methyltransferase	35.8	putative methyltransferase	28.2	putative 3-demethylubiquinone-9 3-methyltransferase
Synechococcus elongatus PCC 6301	54.0	ubiquinone/ menaquinone biosynthesis methyltransferase	34.4	ubiquinone/ menaquinone biosynthesis methyltransferase	50.0	probable methyltransferase	26.0	membrane-associated protein
Synechococcus sp. PCC 7002	64.2	menaquinone biosynthesis methyltransferase	23.8	methyltransferase	57.8	methyltransferase, UbiE/COQ5 family	32.7	menaquinone biosynthesis methyltransferase
Thermosynechococcus elongatus BP-1	50.7	similar to menaquinone biosynthesis methyltransferase	29.8	similar to menaquinone biosynthesis methyltransferase	55.8	probable methyltransferase	33.3	probable methyltransferase
Trichodesmium erythraeum IMS101	54.0	ubiquinone/ menaquinone biosynthesis methyltransferase	32.8	ubiquinone/ menaquinone biosynthesis methyltransferase	58.3	methyltransferase type 11	44.4	methyltransferase type 11

3. Lipid Analysis

Conditions for extraction, separation and characterization of lipids from *Synechocystis* 6803 were optimized to detect chlorophylls, carotenoids and isoprenoid quinones simultaneously. When a suitable method had been established, the lipid content of *Synechocystis* wild-type and Δ*sll1653* mutant strain were analyzed.

TLC separation

Lipids extracted with chloroform:methanol (2:1, v/v) were separated by thin-layer chromatography (TLC) using hexane:acetone (70:30) and hexane:chloroform (75:25 and 60:40). Resulting bands were scraped off and dissolved in methanol prior to the measurement of their absorption spectra (Fig. A3.1).

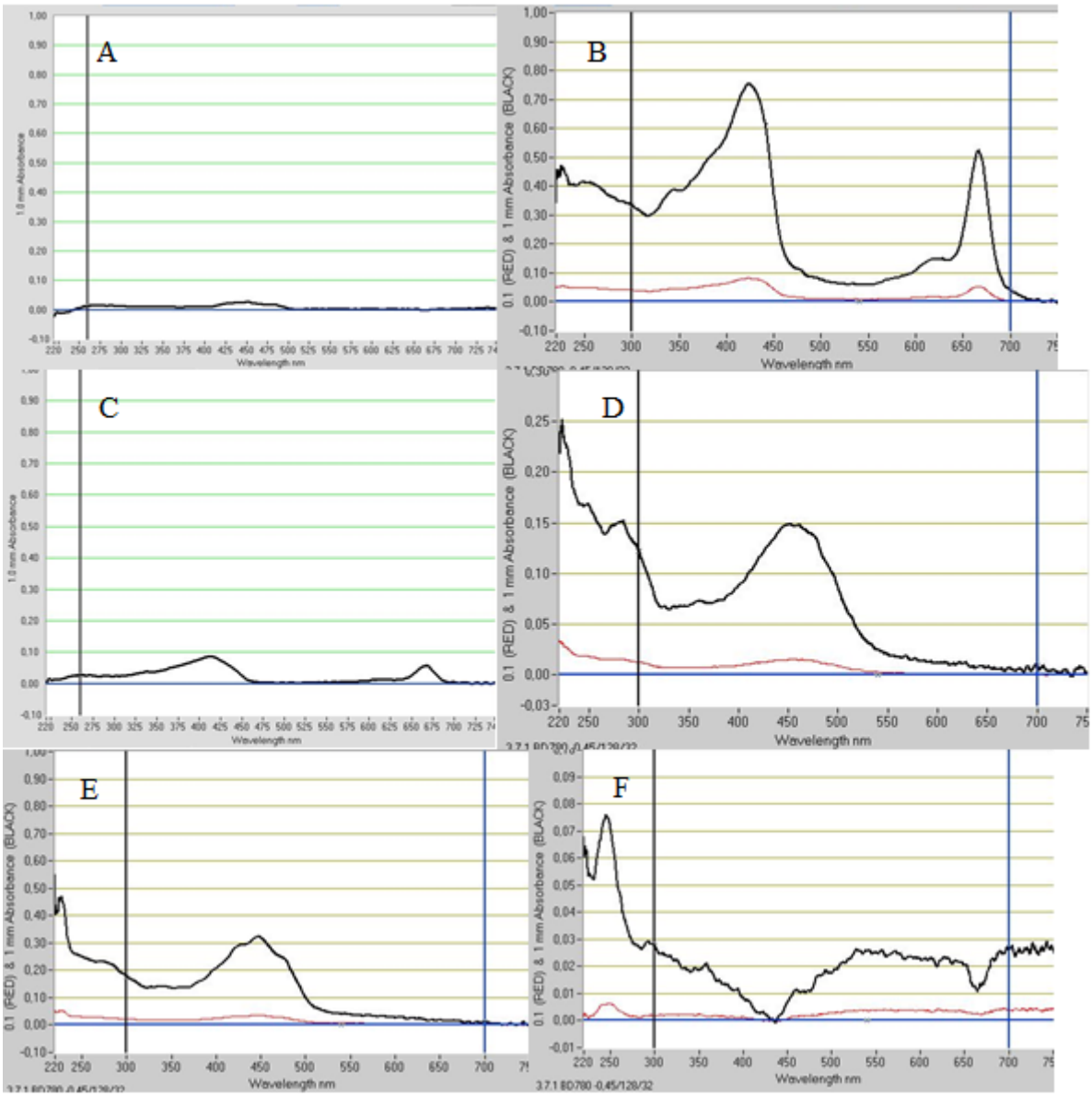

Figure A3.1 – Absorption spectra of pigments isolated from TLC plates. Photosynthetic lipids extracted from *Synechocystis* 6803 were separated by TLC and the resulting bands were scraped off and dissolved in methanol prior to analysis by absorption spectroscopy. A-E represent bands isolated from plates developed with 30 % acetone in hexane (Fig. 3.4), A being the band with the lowest retention ratio and E the band with the highest retention ratio. F is the absorption spectrum of the pigment detected under UV light (Fig. 3.5) when plates were developed with hexane-acetone (75:25, v/v).

Optimization of LC-MS

Conditions for characterization of photosynthetic lipids were optimized for LC-MS. Figure A3.2-A3.5 displays the chromatograms for the standards of chlorophyll *a*, β-carotene, ubiquinone and α-tocopherol separated by UPLC. The mass spectra of the respective standards are given in Figure A3.6-A3.9.

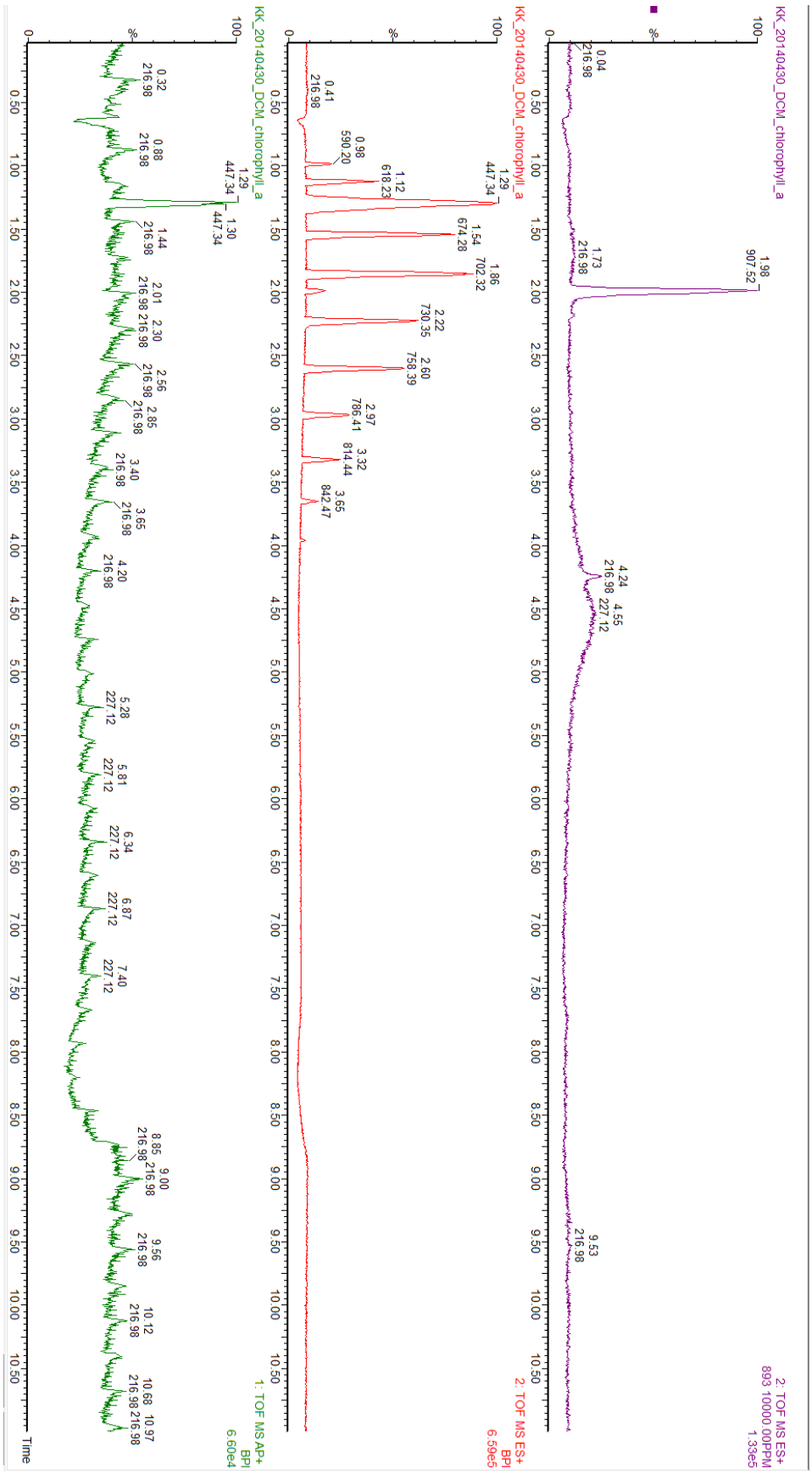

Figure A3.2 – Chromatogram of chlorophyll *a* standard.

A chlorophyll standard was separated by UPLC, ionized by APCI (green) and ESI (red) and detected in a qTOF-MS setup. Searching for the mass of chlorophyll *a* (893.49 g/mol) in Masslynx, indicates that the compound eluates after 1.98 min with a main m/z peak at 907.52.

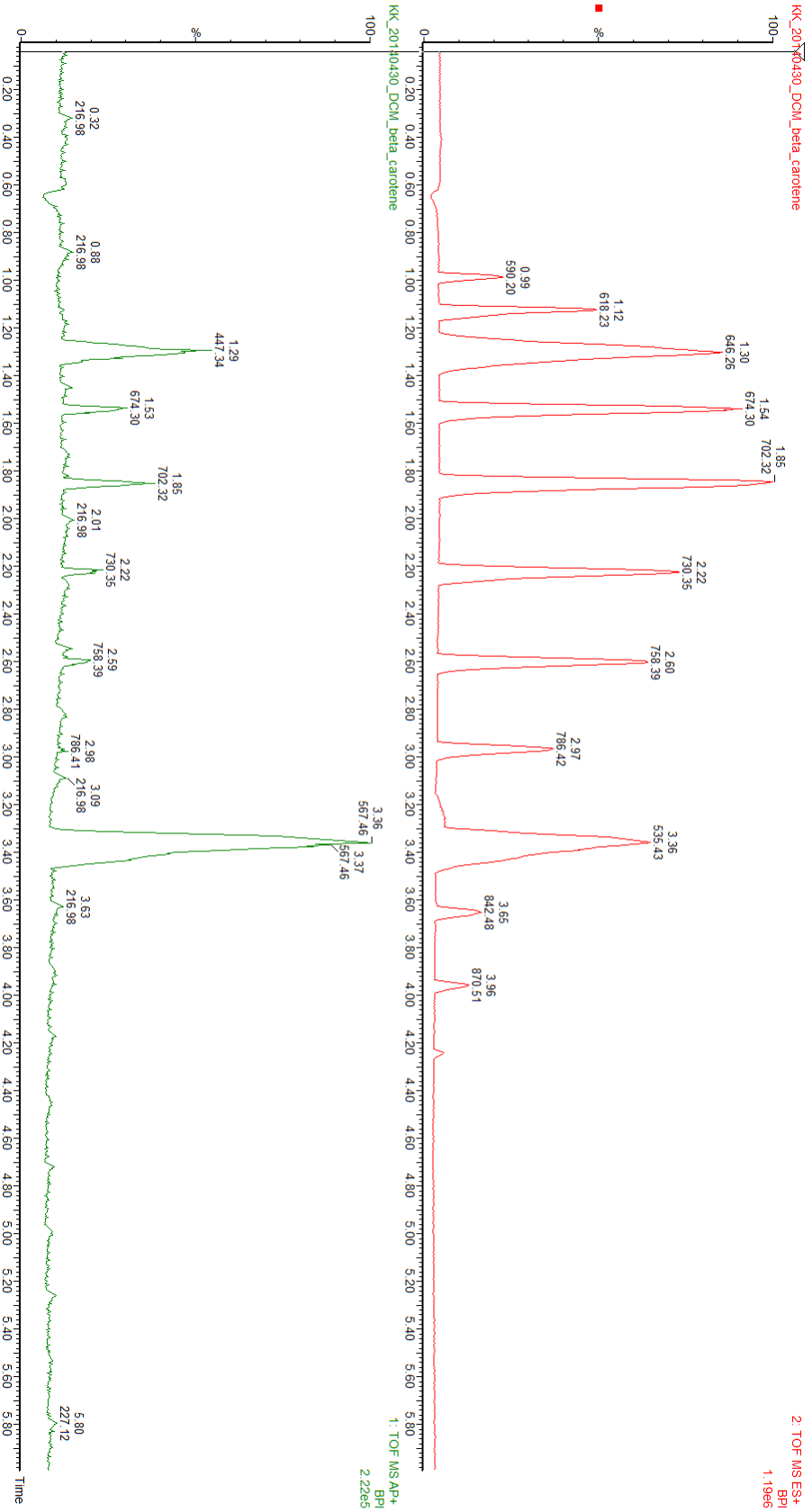

Figure A3.3 – Chromatogram of β-carotene standard.
A β-carotene standard was separated by UPLC, ionized by APCI (green) and ESI (red) and detected in a qTOF-MS setup. β-carotene eluates after 3.36 min with a main m/z peak at 535.43 when ionized by ESI and 567.46 when ionized by APCI.

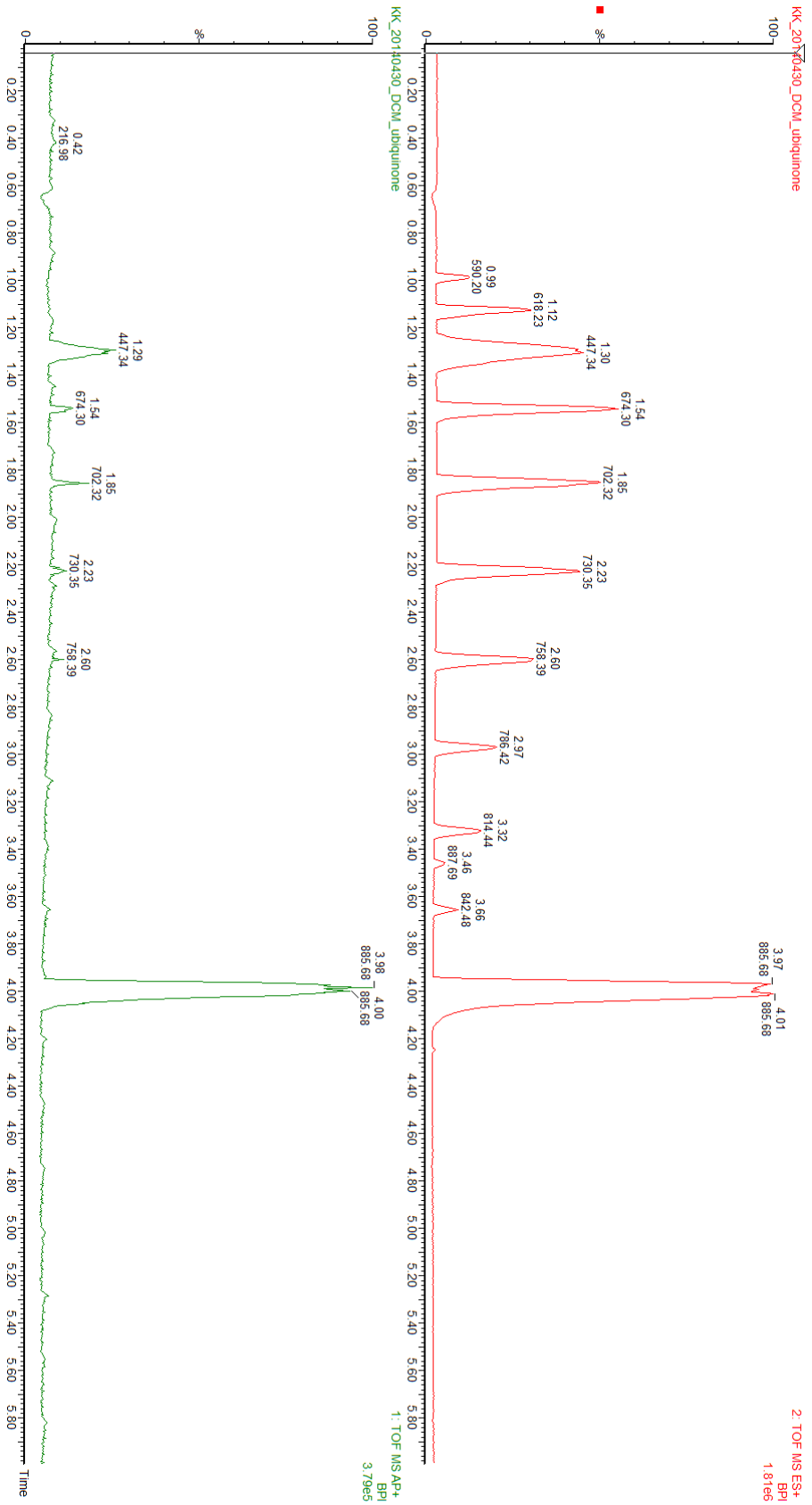

Figure A3.4 – Chromatogram of ubiquinone standard. A ubiquinone standard was separated by UPLC, ionized by APCI (green) and ESI (red) and detected in a qTOF-MS setup. Ubiquinone eluates after 4.00 min with a main m/z peak at 885.68.

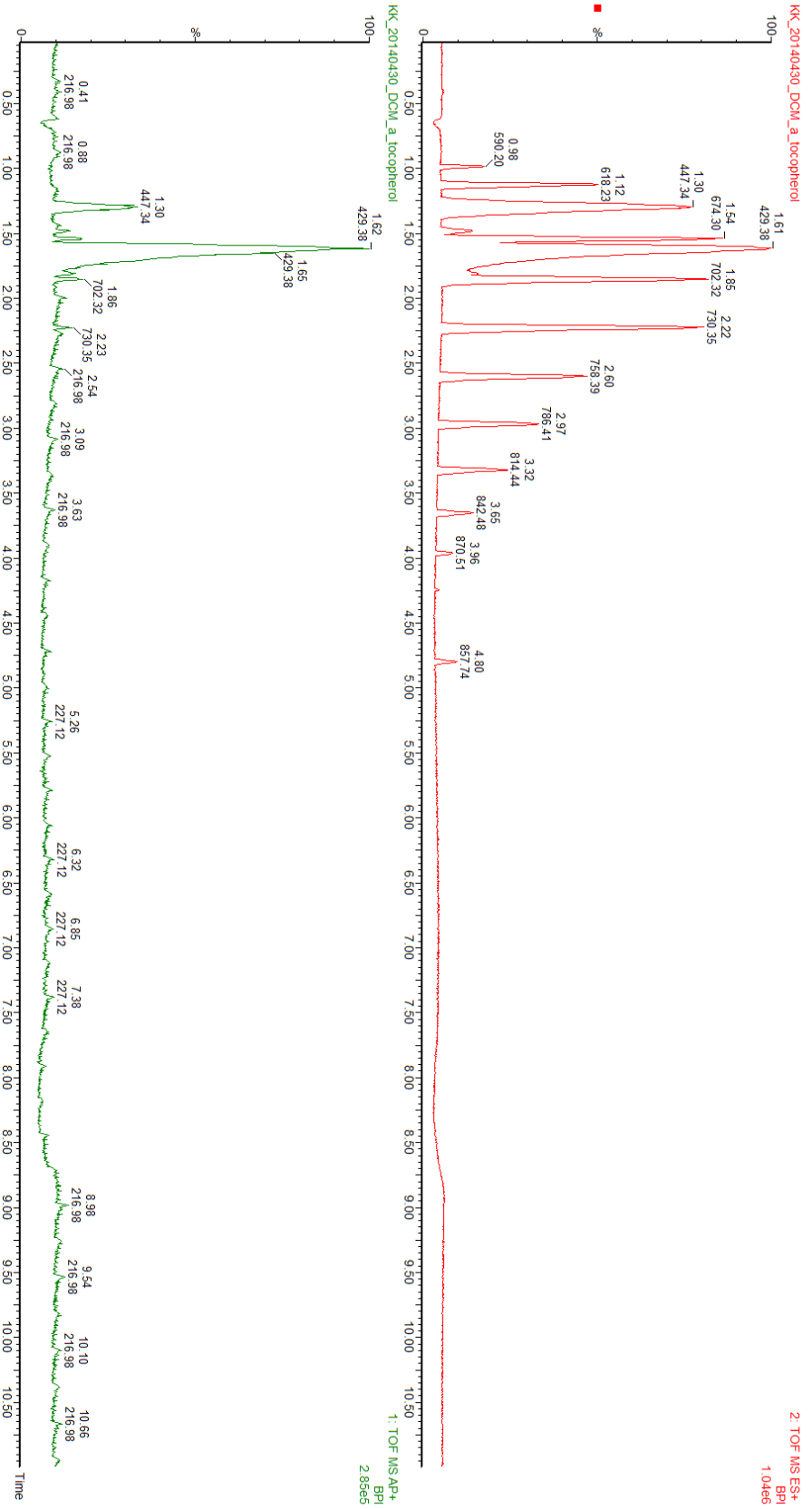

Figure A3.5 – Chromatogram of α-tocopherol standard. A ubiquinone standard was separated by UPLC, ionized by APCI (green) and ESI (red) and detected in a qTOF-MS setup. Ubiquinone eluates after 4.00 min with a main m/z peak at 885.68.

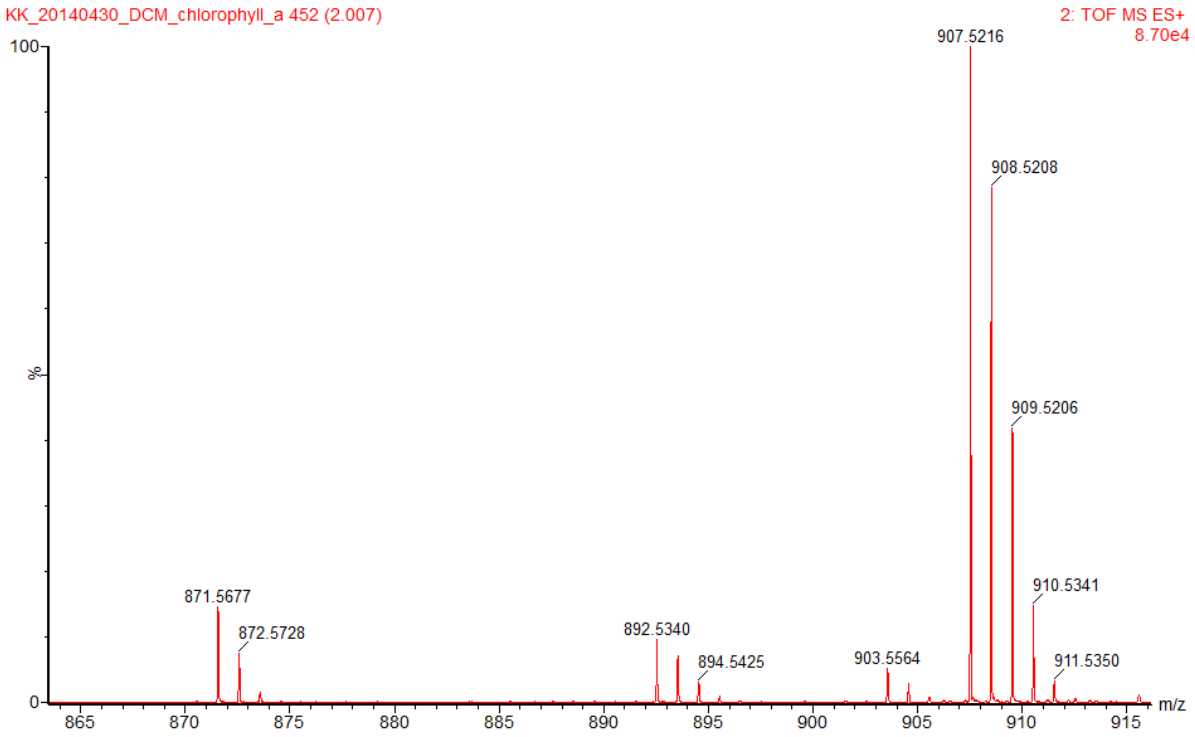

Figure A3.6 – Mass spectrum of the chlorophyll *a* standard. The mass detected for the chlorophyll *a* standard ionized by ESI, eluated after 2.00 min. Peaks at 871.58, 892.53 and 907.52 (m/z) were detected.

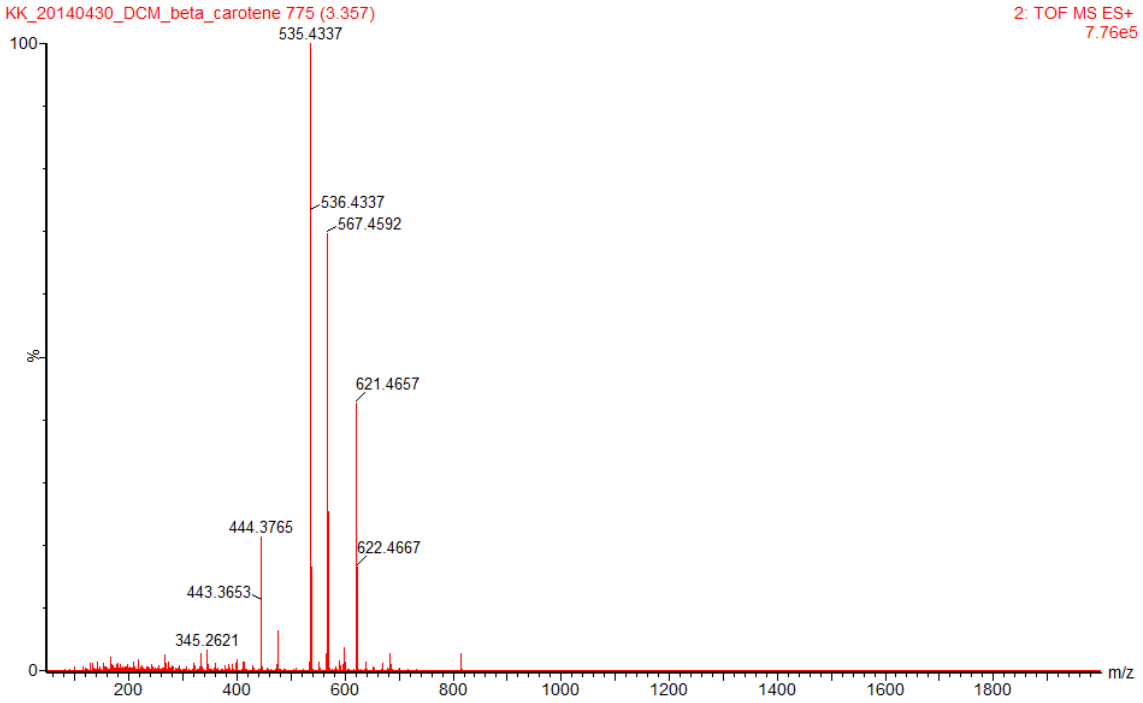

Figure A3.7 – Mass spectrum of the β-carotene standard. The mass detected for the β-carotene standard ionized by ESI and eluated after 3.36 min with a major m/z peak of 535.43.

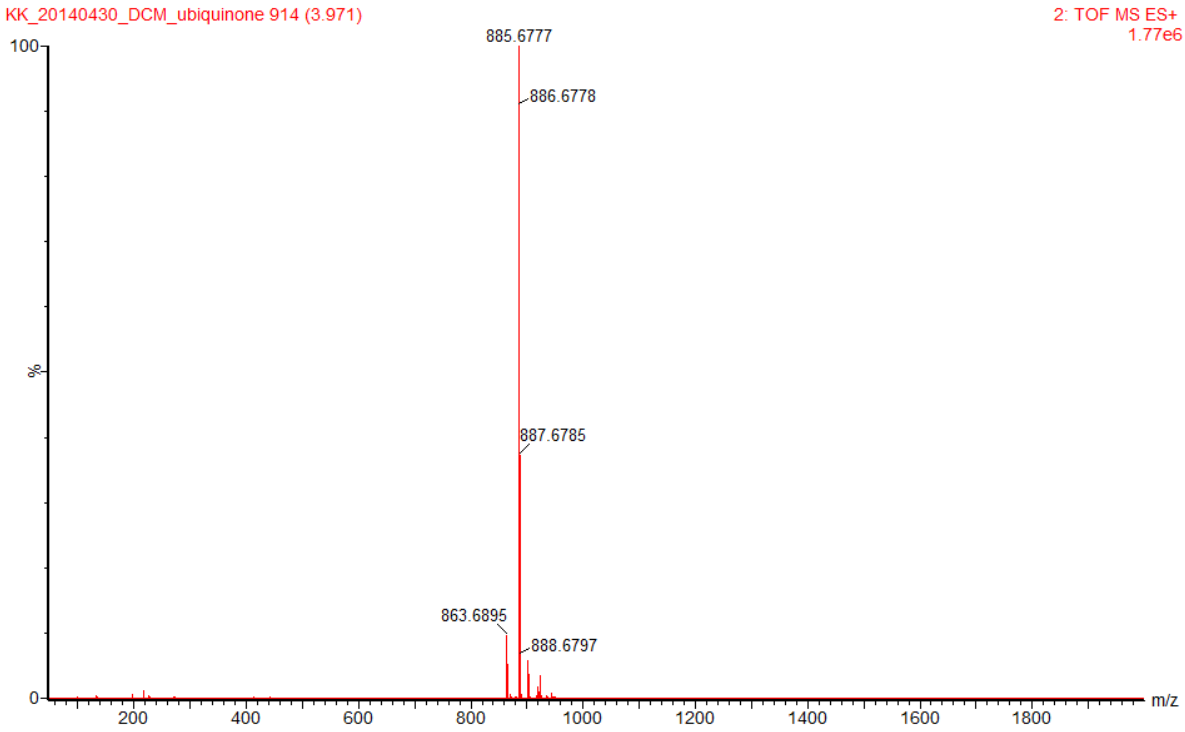

Figure A3.8 – Mass spectrum of the ubiquinone standard. The mass detected for the ubiquinone standard ionized by ESI and eluated after 3.97 min with a major m/z peak of 885.68.

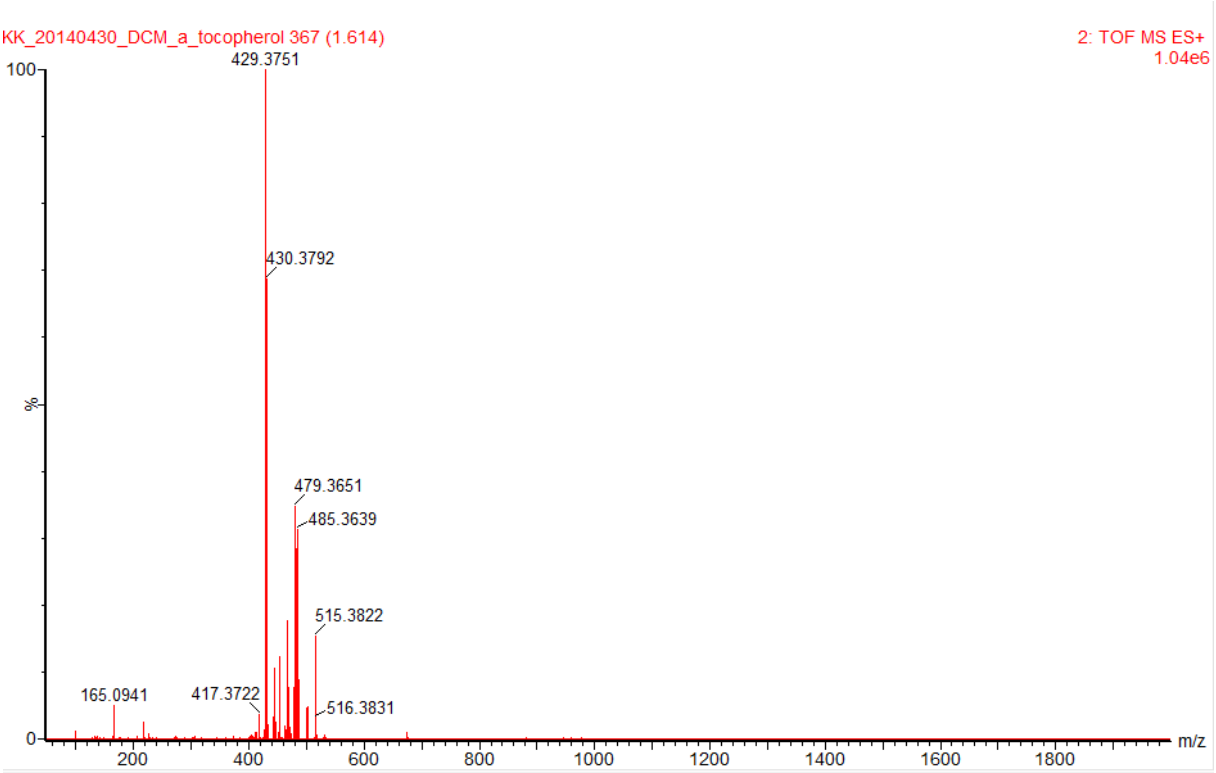

Figure A3.9 – Mass spectrum of the α-tocopherol standard. The mass detected for the α-tocopherol standard ionized by ESI and eluated after 1.62 min with a major m/z peak of 429.36.

Analysis of lipids extracted from *Synechocystis* 6803

The gene *sll1653,* encoding a methyltransferase involved in quinone biosynthesis, was genetically deleted from *Synechocystis* 6803. Analysis of the photosynthetic lipid content of wild-type and Δ*sll1653* mutant strain was performed using UPLC-ESI-qTOF-MS. Individual lipids were identified by searching the chromatograms for masses of photosynthetic lipids that could be synthesized in *Synechocystis* 6803 (listed in Appendix I). Figure A3.10 shows the entire chromatogram for lipids extracted from the wild-type and mutant strain. Figures A3.11 – A3.21 display mass spectra for identification of photosynthetic lipids in both strains and Table A3.1 provides a summary of the masses and detection signals for all lipids identified.

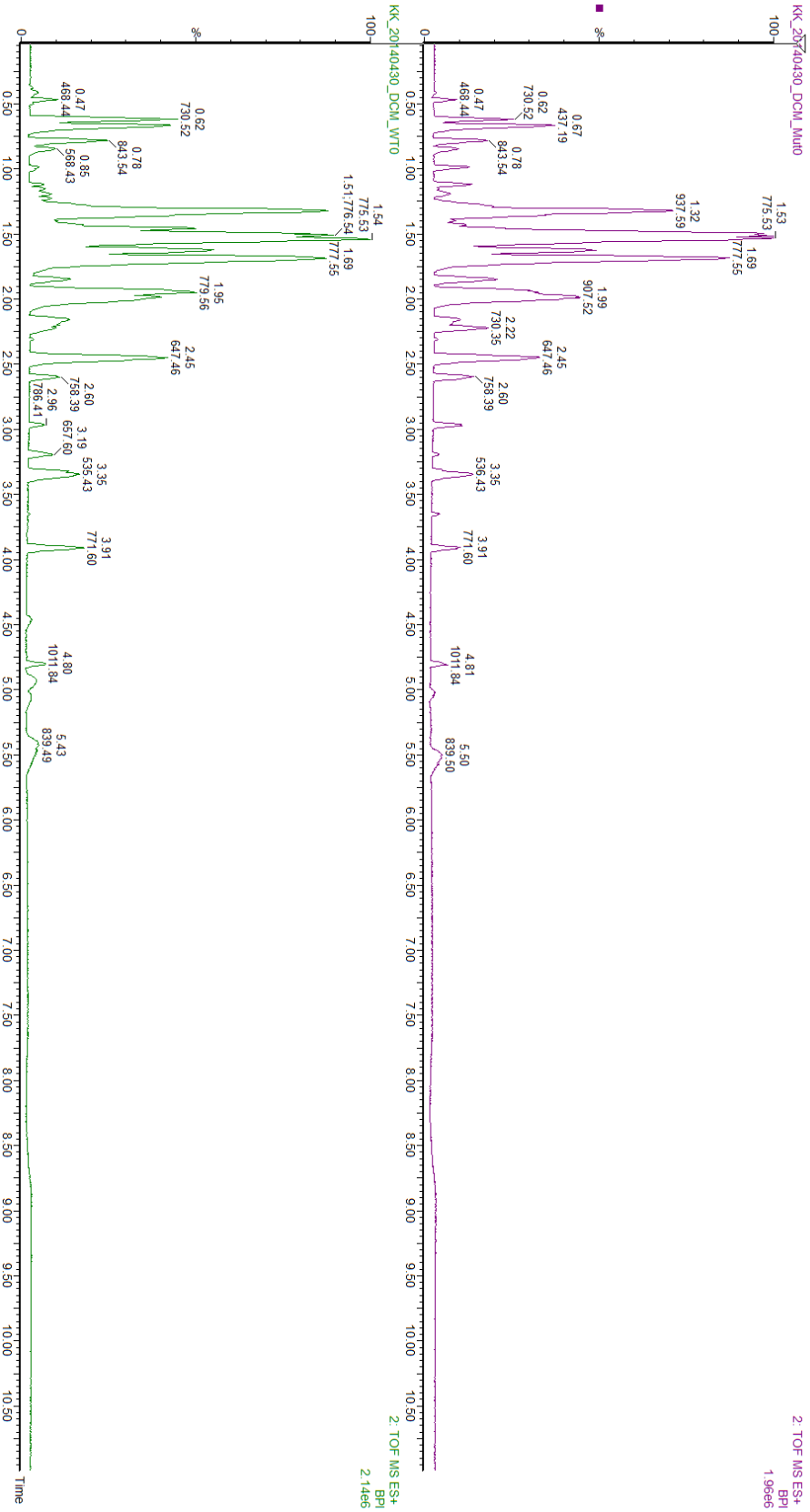

Figure A3.10 – Chromatogram of lipid extracts from wild-type and Δ*sll1653* strain. Components in the total lipid extract from wild-type (green) and mutant strain (purple) was separated by UPLC, ionized by ESI and detected in a qTOF-MS setup.

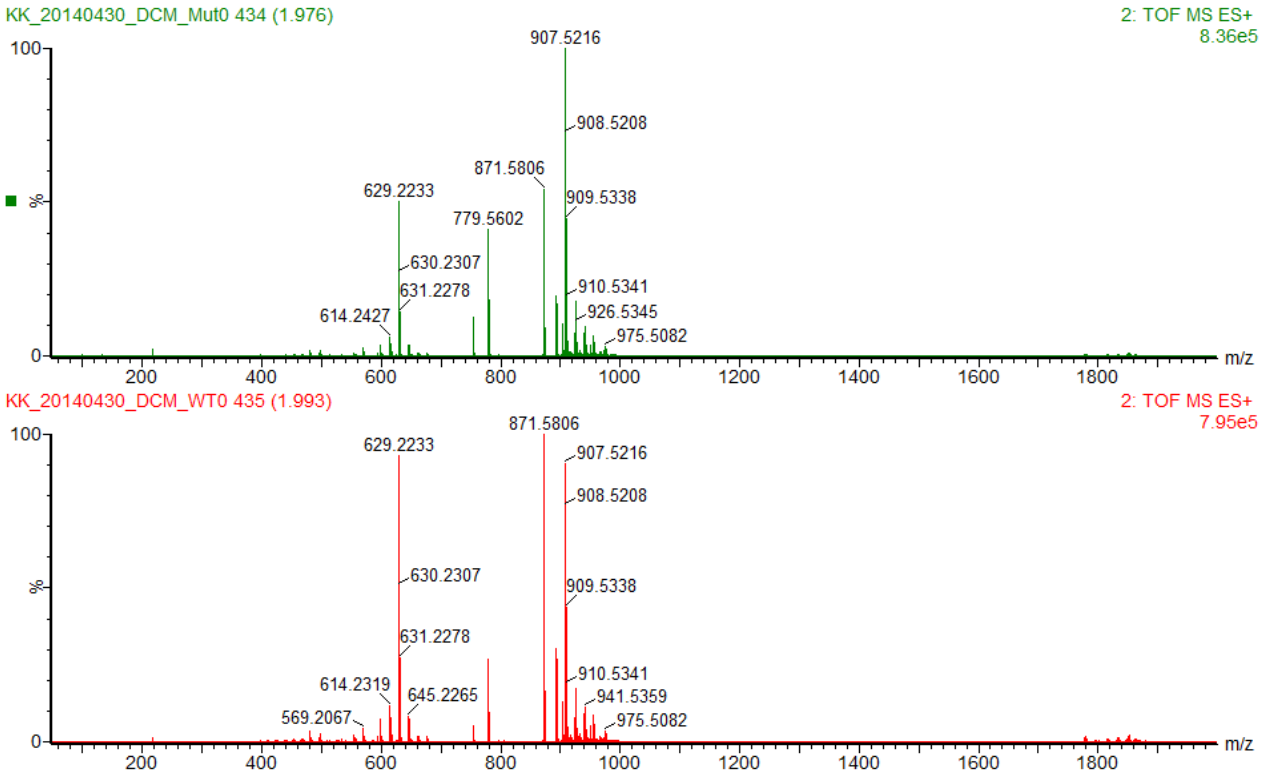

Figure A3.11 – Mass spectrum of chlorophyll *a*. Masses detected for chlorophylls (retention time 1.98) in wild-type (red) and the Δ*sll1653* strain (green). Mass of 614.24 represent chlorophyllide *a*, 871.58 represent pheophytin *a* and 907.52 is assumed to be an oxidation product of chlorophyll *a*. See Figure 3.19 for detailed identification of chlorophyll *a* and Table A3.1 for detection signal information.

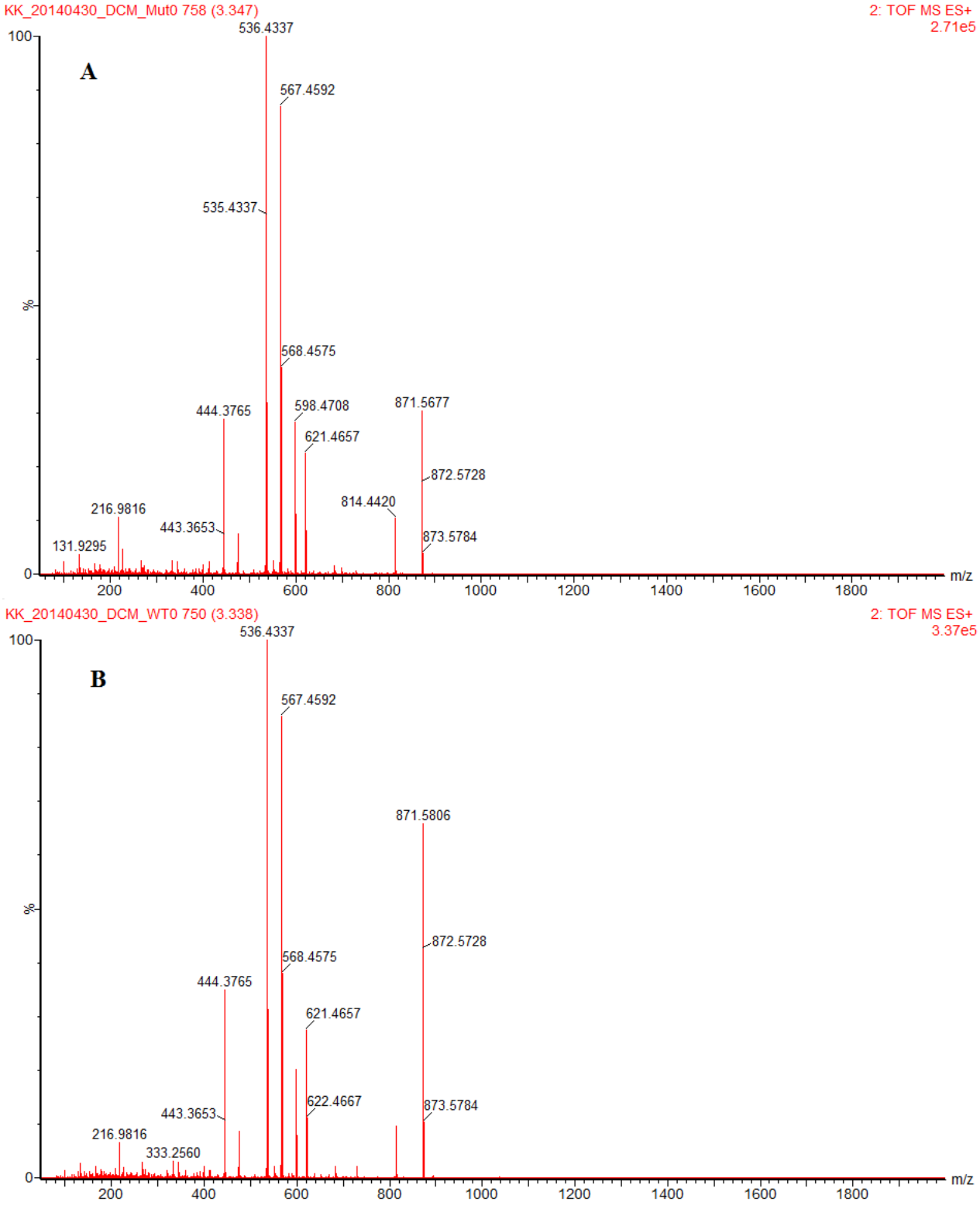

Figure A3.12 – Mass spectrum of β-carotene. A mass of 536.43 was detected for β-carotene in wild-type (B) and Δ*sll1653* strain (A), which was eluted after 3.35 min.

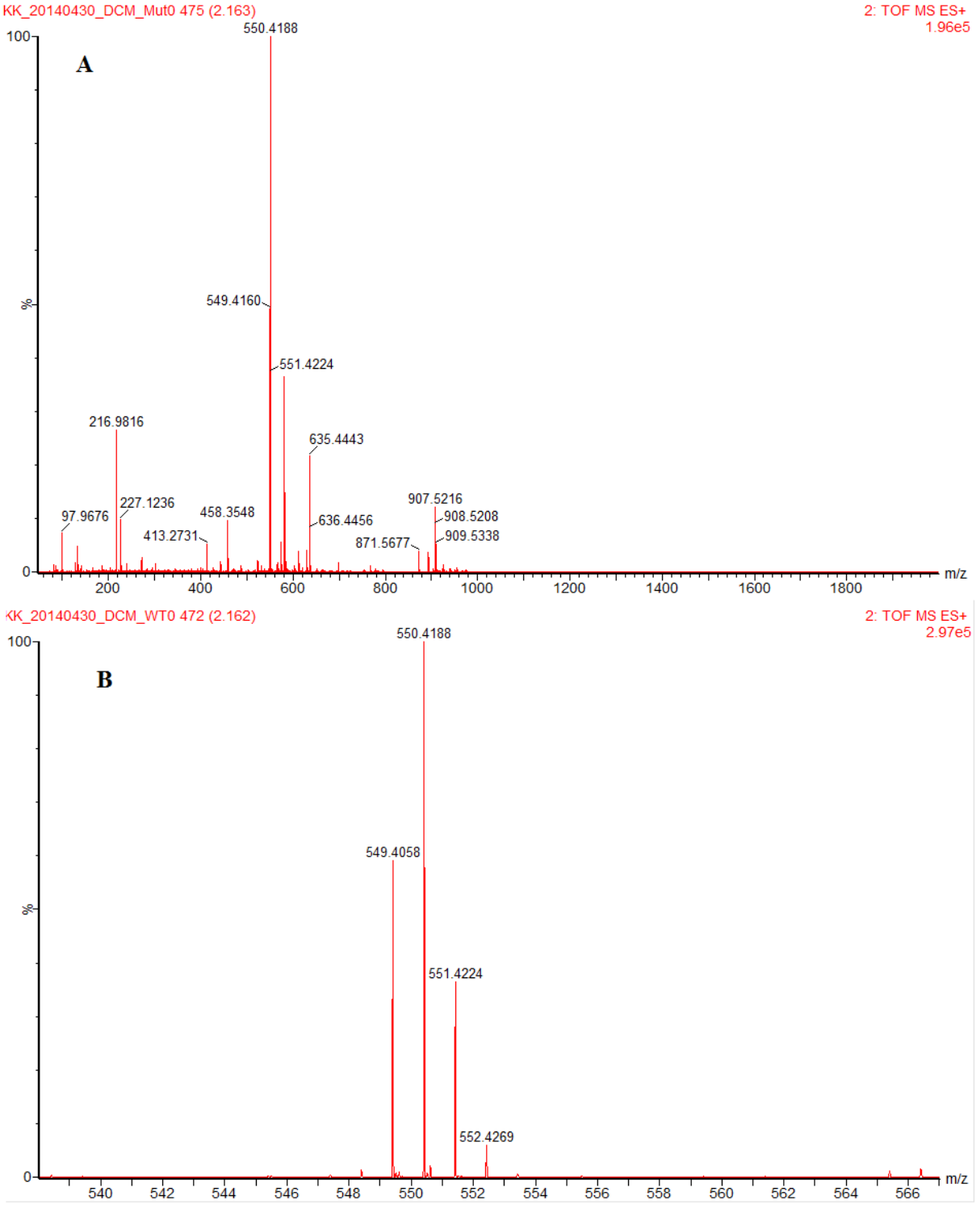

Figure A3.13 – Mass spectrum of echinenone. A mass of 550.42 was detected for echinenone in wild-type (B) and Δ*sll1653* strain (A), which was eluted after 2.16 min.

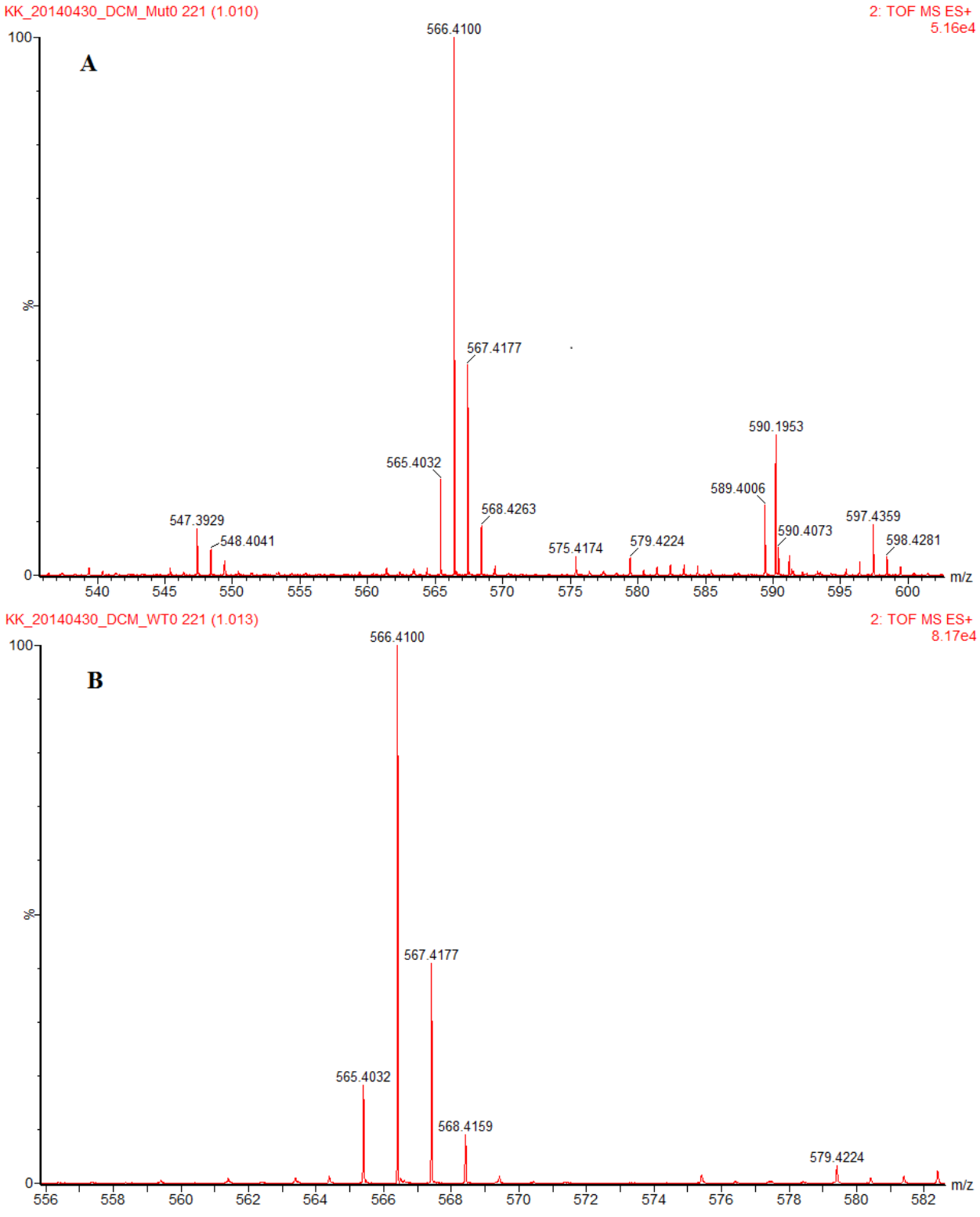

Figure A3.14 – Mass spectrum of hydroxy-echinenone. A mass of 566.41 was detected for hydroxy-echinenone in wild-type (B) and Δ*sll1653* strain (A), which was eluted after 1.02 min.

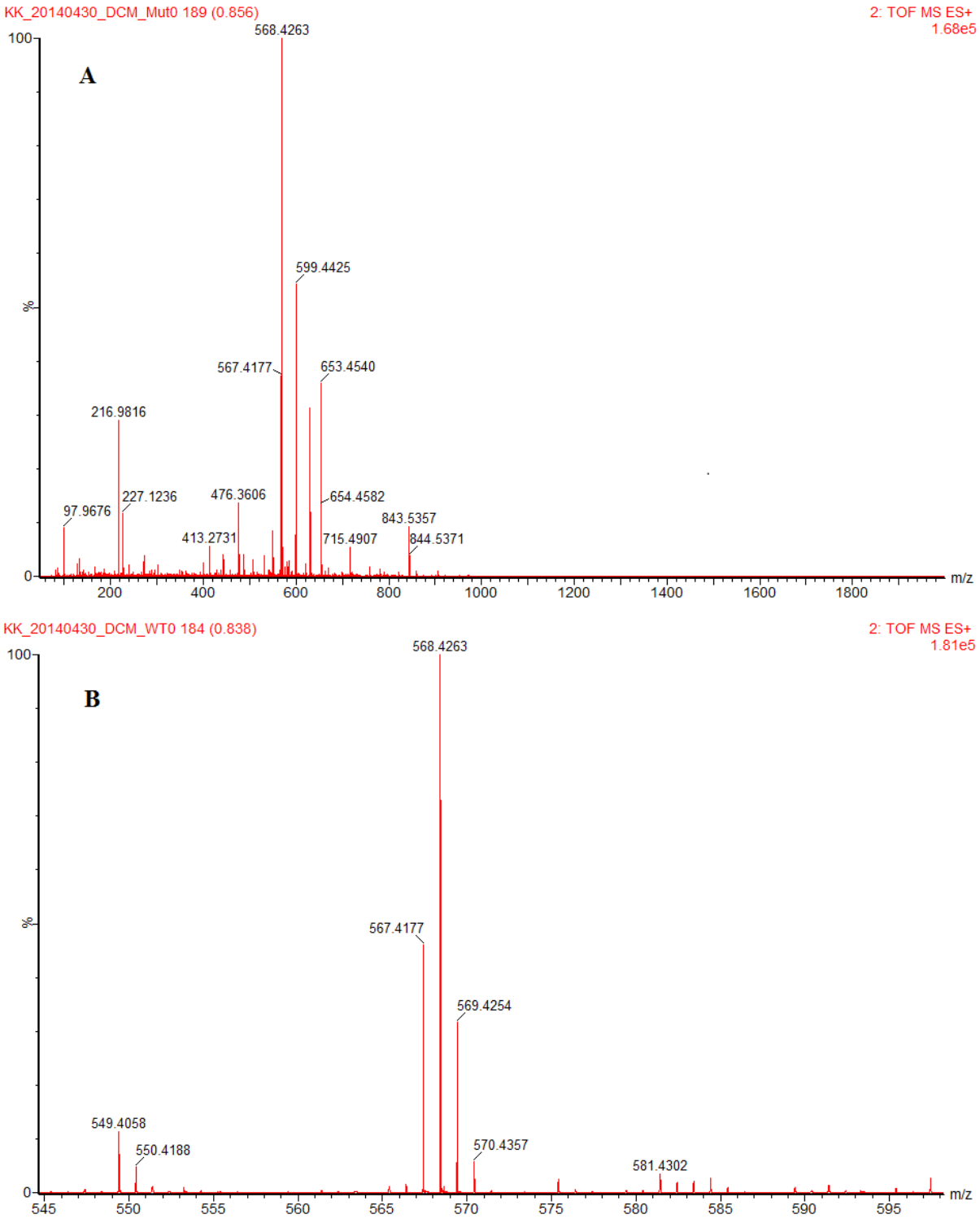

Figure A3.15 – Mass spectrum of zeaxanthin/lutein. A mass of 568.43 was detected for the compound identified as either zeaxanthin or lutein in wild-type (B) and Δ*sll1653* strain (A). The compound was eluted after 0.85 min.

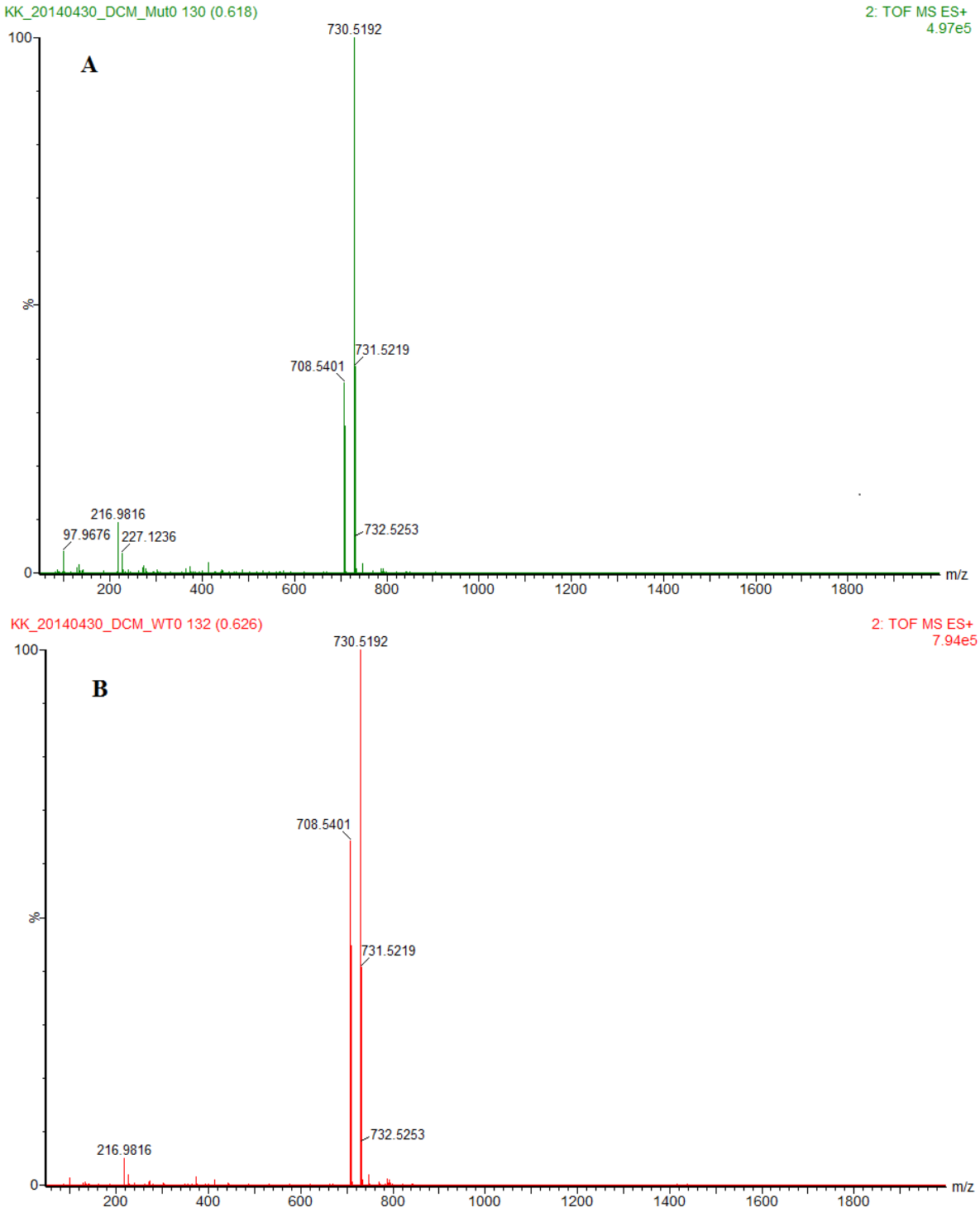

Figure A3.16 – Mass spectrum of myxoxanthophyll. A mass of 730.52 was detected for the compound identified as myxoxanthophyll in wild-type (B) and Δ*sll1653* strain (A). The compound was eluted after 0.62 min.

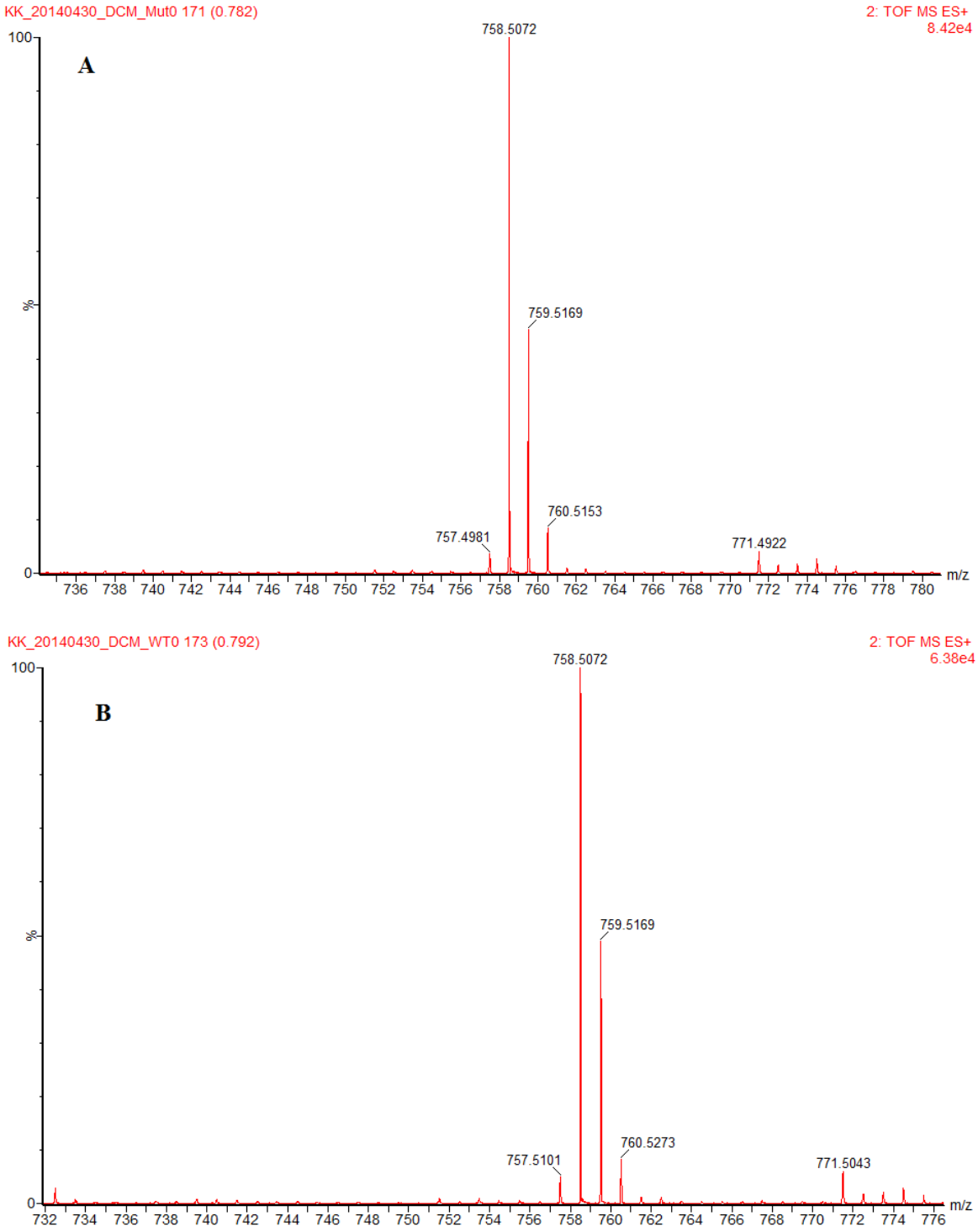

Figure A3.17 – Mass spectrum of myxoxanthophyll-fucoside. A mass of 758.51 was detected for the compound identified as myxoxanthophyll-fucoside in wild-type (B) and Δ*sll1653* strain (A). The compound was eluted after 0.77 min.

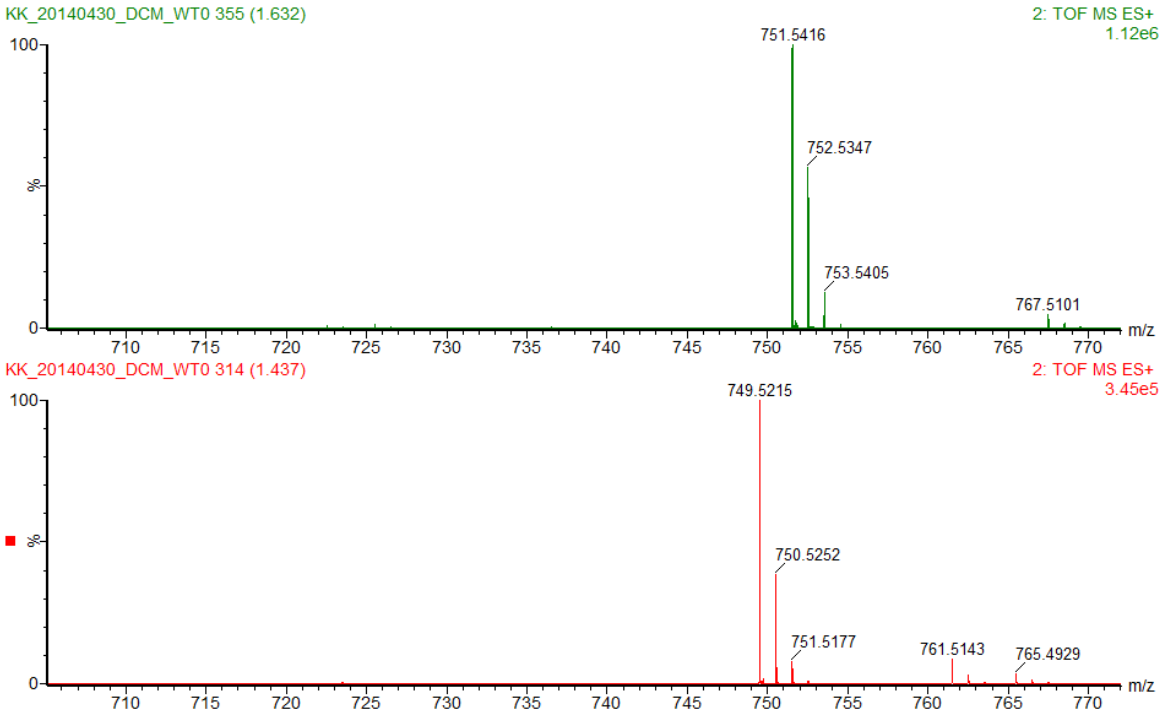

Figure A3.18 – Mass spectrum of plastoquinone extracted from wild-type. Masses of 751.54 and 749.52 were detected for reduced (green) and oxidized (red) plastoquinone, respectively. Reduced plastoquinone was eluted after 1.62 min whereas oxidized plastoquinone was eluted after 1.43 min.

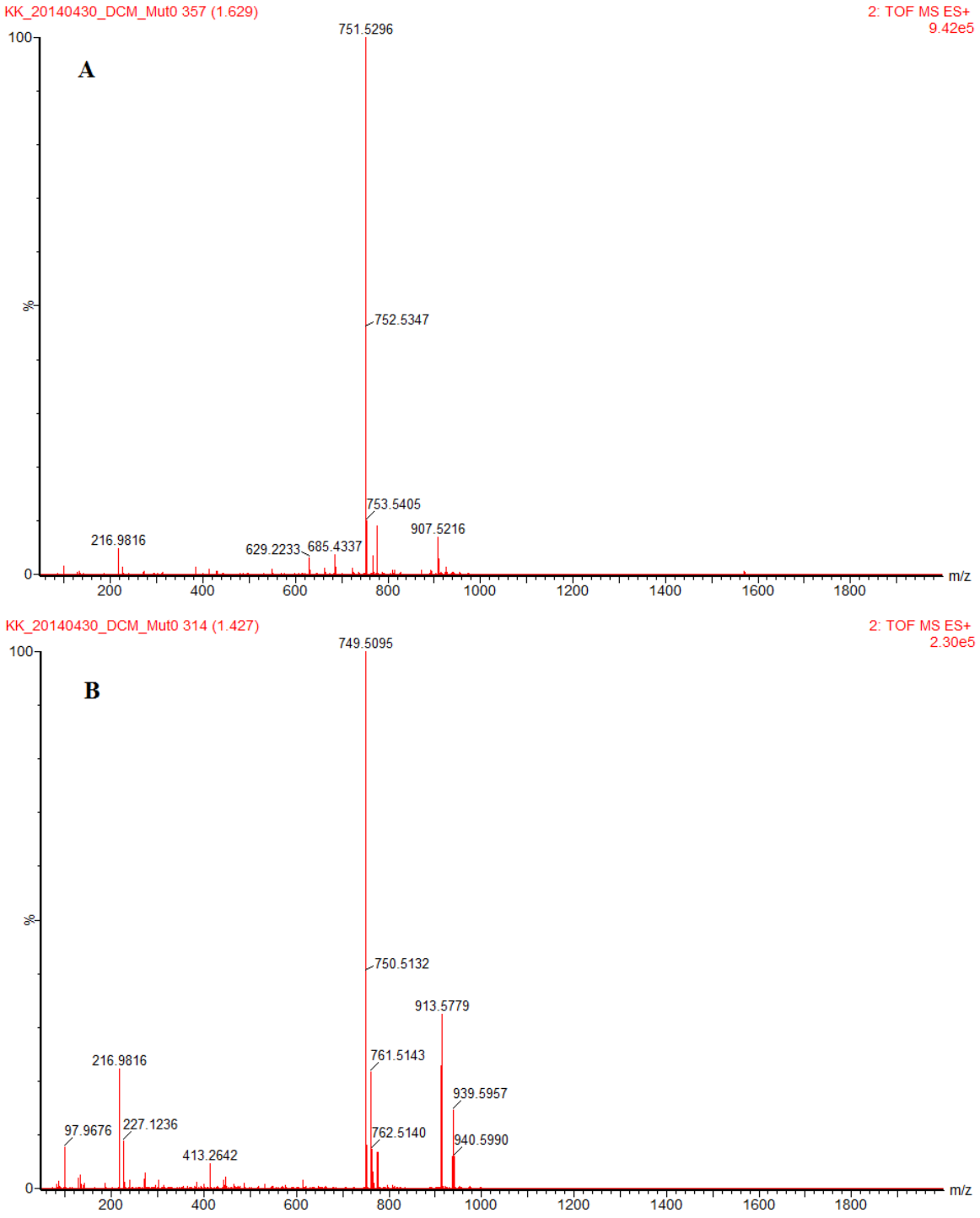

Figure A3.19 – Mass spectrum of plastoquinone extracted from Δ*sll1653* strain. Masses of 751.53 and 749.51 were detected for reduced (green) and oxidized (red) plastoquinone, respectively. Reduced plastoquinone was eluted after 1.62 min whereas oxidized plastoquinone was eluted after 1.43 min.

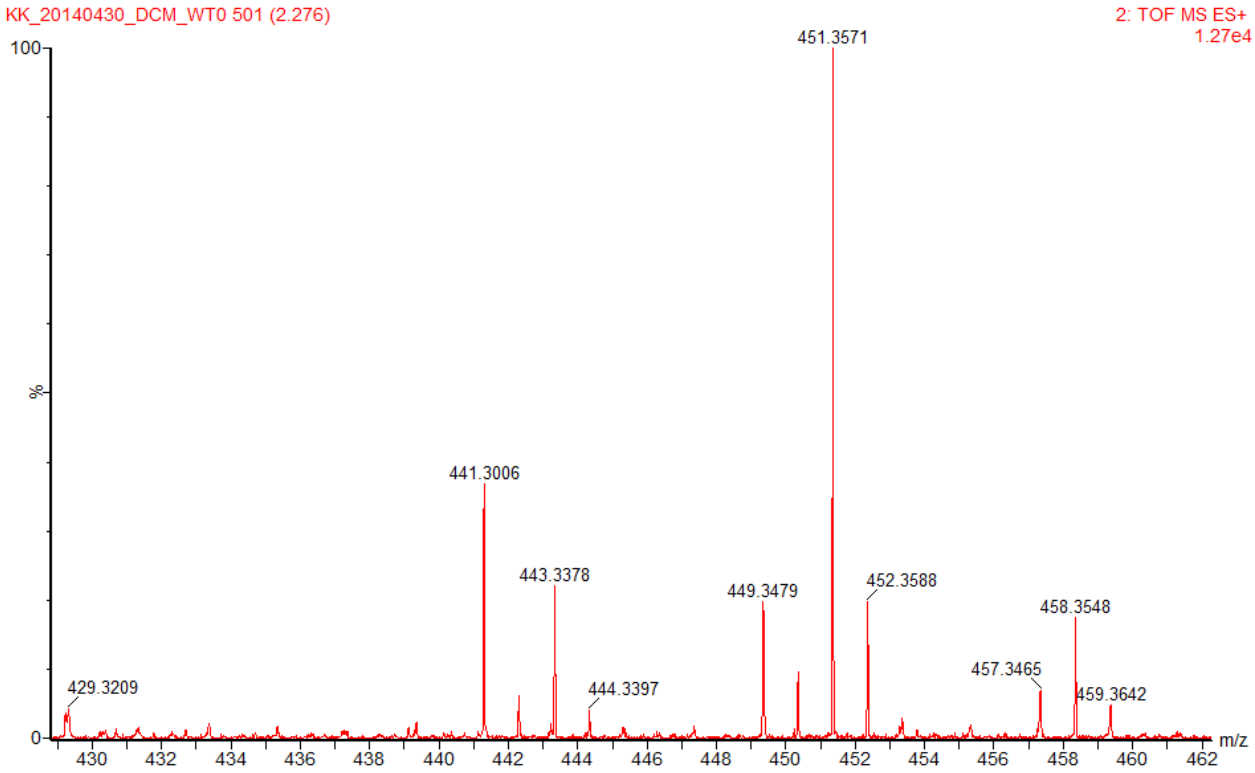

Figure A3.20 – Mass spectrum of phylloquinone extracted from wild-type. A mass of 451.26 was detected for phylloquinone in wild-type extract. This compound could not be detected in the lipid extract from Δ*sll1653* strain. Phylloquinone was eluted after 2.28 min.

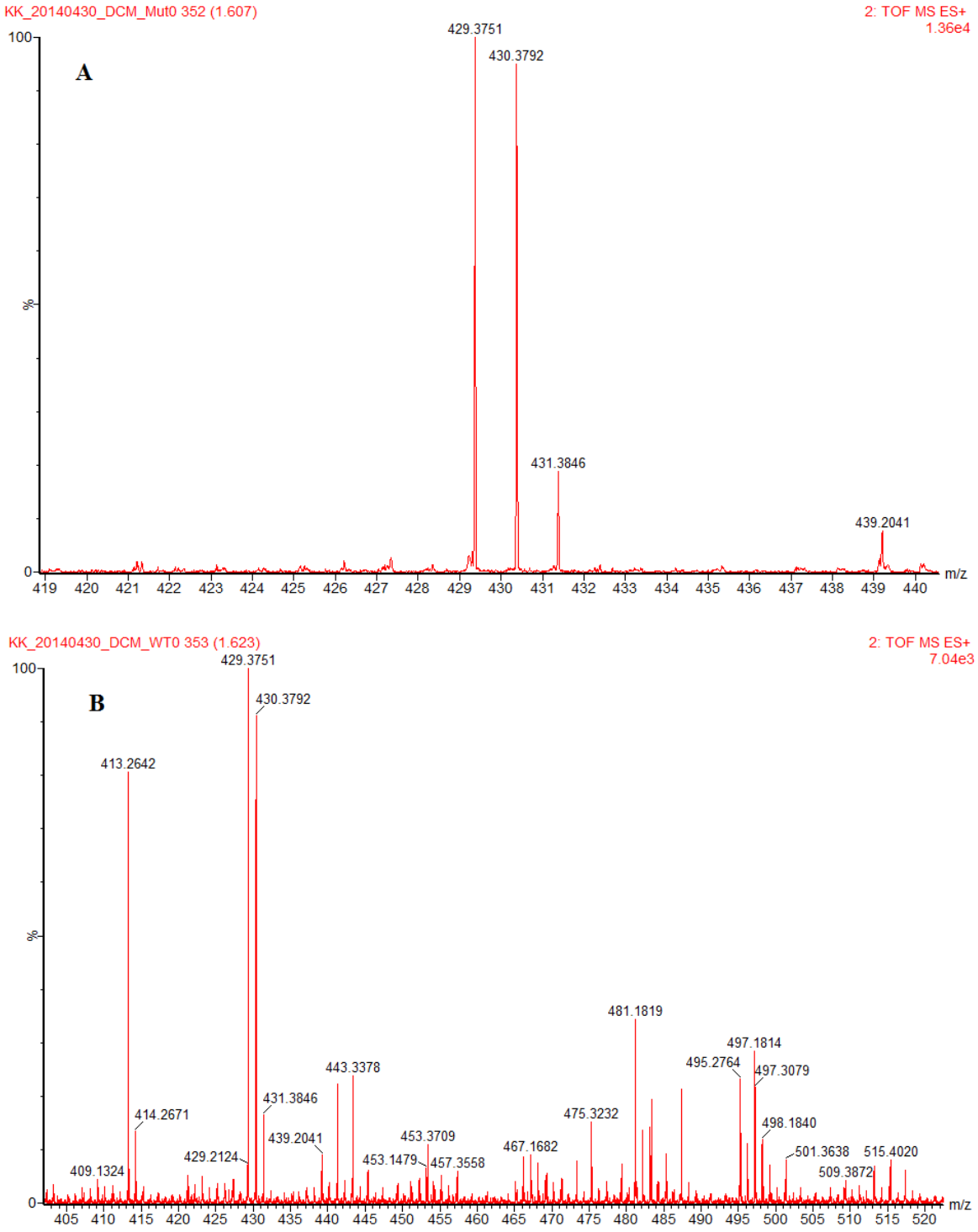

Figure A3.21 – Mass spectrum of α-tocopherol. A mass of 429.38 was detected for the compound identified as α-tocopherol in wild-type (B) and Δ*sll1653* strain (A). The compound was eluted after 1.62 min.

Table A3.1 – Detection signals and masses for identified lipids.

Compound	Mass	Detection signal	
	m/z	WT	Mut
Chlorophyll a	893.54	2,47E+05	1,64E+05
Chlorophyll a ox	907.52	7,12E+05	8,49E+05
Pheophytin a	871.58	8,61E+05	4,75E+05
Chlorophyllide a	614.24	1,02E+05	5,06E+04
b-carotene	536.43	3,37E+05	2,71E+05
Echinenone	550.42	2,97E+05	1,96E+05
Hydroxy-echinenone	566.41	8,17E+04	5,16E+04
Lutein	568.43	1,81E+05	1,68E+05
Myxoxanthophyll	730.52	7,94E+05	4,36E+05
Myxoxanthophyll-fucoside	758.51	6,38E+04	7,95E+04
Plastoquinone ox	749.53	3,45E+05	2,30E+05
Plastoquinone red	751.53	1,18E+06	9,42E+05
Phylloquinone	451.36	1,27E+04	0,00E+00
a-tocopherol	430.38	7,04E+03	1,36E+04